Ruthenium and osmium clusters containing imido and sulfido ligands and their reactions with unsaturated organic molecules

A thesis submitted to the University of London in partial fulfilment of the requirements for the degree of Doctor of Philosophy

By

Shahbano Amjad Ali

Department of Chemistry

University College London

February 2001

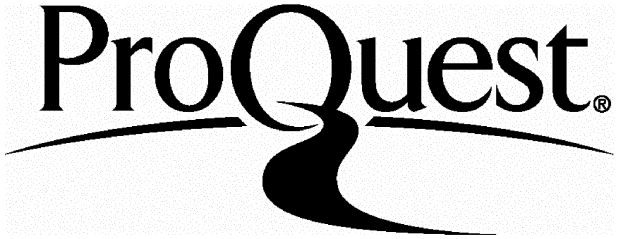

661190

For my mother and in loving memory of my father

ABSTRACT

Chapter **1** is an introduction to our research in triosmium and triruthenium clusters and details the different types of trinuclear clusters and capping ligands available. The uses of clusters in catalysis are then discussed.

Chapter **2** describes the synthesis of amido and imido systems derived from $[M_3(CO)_{12}]$ and NH_2SO_2tolyl. The formation and crystal structure of $[Ru_3(\mu\text{-}H)_2(\mu_3\text{-}NSO_2\text{tolyl})(CO)_9]$ is presented with its thermal decarbonylation to give $[\{Ru_3(\mu\text{-}H)_2(\mu_4\text{-}NSO_2\text{tolyl})(CO)_7\}_2]$ (based on spectroscopic evidence) and protonation to give $[Ru_3(\mu\text{-}H)_3(\mu_3\text{-}NSO_2\text{tolyl})(CO)_9]^+$. The deprotonation of $[Os_3(\mu\text{-}H)(\mu\text{-}NHSO_2\text{tolyl})(CO)_{10}]$ to give the pyramidal μ_2-imido system $[Os_3(\mu\text{-}H)(\mu\text{-}NSO_2\text{tolyl})(CO)_{10}]^-$, which has been crystallographically characterised, is also discussed.

Chapter **3** reports the formation of the MeCN-substituted derivatives by treatment of $[M_3(\mu\text{-}H)_2(\mu_3\text{-}NSO_2\text{tolyl})(CO)_9]$ with $Me_3NO.2H_2O$/MeCN. Important new discoveries on how alkynes are incorporated into these clusters are described, including single insertions into M-H bonds and coupling of alkenyl ligands formed by double insertions to give butadiene clusters. The crystal structures of $[Os_3(\mu\text{-}\textit{trans}\text{-}\sigma,\eta^2\text{-}CH{=}CHBu^t)(\mu_3\text{-}NSO_2\text{tolyl})(CO)_8]$ and $[Ru_3(\mu\text{-}\eta^2,\eta^2\text{-}C_4H_6)(\mu_3\text{-}NSO_2\text{tolyl})(\mu_3\text{-}CO)(CO)_7]$ are given.

Chapter **4** studies the reactions of $[M_3(\mu\text{-}H)_2(\mu_3\text{-}S)(CO)_8(MeCN)]$ (M = Ru or Os) with alkynes. Here evidence for the formation of double insertion products is

presented as well as for single insertion products and butadiene clusters. The mode of coordination for the butadiene ligand in this case was different to those in Chapter **3**. The crystal structure of $[Os_3(\eta^4\text{-PhCH=CHCPh=CH}_2)(\mu_3\text{-S})(CO)_8]$ is discussed. Studies on the reductive coupling of alkynes to give butadienes are described. Comparisons between the different effects of μ_3-NSO_2tolyl compared with μ_3-S and Ru compared with Os are presented.

Chapter **5** focuses on the coupling of high-valent with low-valent transition metal units within a single molecular cluster. For instance, the synthesis and characterisation of the high-low valent clusters $[Ru_3(CO)_{12}MoX_2]$ where MoX_2 is the high-valent fragment is reported. The crystal structure of $[Ru_3(CO)_{12}\{Mo(N\text{-}2,6\text{-}Me_2C_6H_3)_2\}]$ and results on protonating this cluster are presented.

TABLE OF CONTENTS

ACKNOWLEDGEMENTS

I am extremely grateful to my supervisors, Professor Tony Deeming and Dr. Graeme Hogarth, for their support, advice, encouragement and most of all patience throughout my PhD.

My thanks also go to the following people for their invaluable skill and expertise: Dr. Jonathan Steed (KCL) and Dr. Gary Enright (NRC, Ottawa, Canada) for carrying out some of the crystallographic determinations mentioned, Alan Stones and Jill Maxwell for running microanalyses and John Hill for recording the mass spectra reported in this thesis. Special thanks must go to all those involved with the running of the department, in particular Peter Leighton for enduring varying degrees of exasperation when making his daily rounds to the lab. UCL is thanked for financial support and the award of a Thomas Witherden Batt and Momber scholarship (1997-98).

I would also like to thank the various members and visitors of labs 301M and 245 for making life in the lab a very comfortable and pleasant experience: Maria Christofi, Romano Giorgi (for proof reading as well), Anthony Birri, Sameer Bhambri, Despo Speel, Anna Hillier, Venus Lee, Tiz Coffey, Andy Pateman, Jade Prince, Mihaela Pop, Michael Morris, Michael Diego-Castro, Letitia So and anyone else who I have unintentionally forgotten to mention.

I am also very grateful to Sarah Al-Benna and Dharshini Ganeshapillai for their time and friendship throughout my years at UCL.

My final thanks go to my late father and particularly my mother for her love, support and understanding throughout my life, but especially during what has been a very difficult time for both of us.

ABBREVIATIONS

b.p.	Boiling point
br	Broad
Bu^t	*Tert*iary butyl (CMe_3)
Calcd.	Calculated
Cp	Cyclopentadiene (C_5H_5)
Cp*	Pentamethylcyclopentadiene (C_5Me_5)
Cy	Cyclohexyl (C_6H_{11})
d	Doublet
DBU	1,8-diazabicyclo[5.4.0]undec-7-ene
dd	Doublet of doublets
ddd	Doublet of doublet of doublets
DME	Dimethoxyethane
dq	Doublet of quartets
EI	Electron impact
Et	Ethyl (C_2H_5)
FAB	Fast atom bombardment
h	Hour(s)
Hampy	2-Amino-6-methylpyridine (2-NH_2-6-Me-C_5H_3N)
IR	Infrared
m (IR)	Medium
m (NMR)	Multiplet
Me	Methyl (CH_3)
min	Minutes(s)
MO	Molecular orbital

MS	Mass spectrometry
NMR	Nuclear magnetic resonance
Ph	Phenyl (C_6H_5)
ppm	Parts per million
PPN	$[N(PPh_3)_2]^+$
Pr^i	*Iso*-propyl (Me_2CH)
py	Pyridine (C_5H_5N)
q	Quartet
s (IR)	Strong
s (NMR)	Singlet
t	Triplet
THF	Tetrahydrofuran (C_4H_8O)
TLC	Thin-layer chromatography
Tol	Tolyl (4-Me-C_6H_4)
Ts	Tosyl (SO_2Tol)
w	Weak

COMPOUND NUMBERING

1 $[Ru_3(\mu\text{-}H)(\mu\text{-}NHPh)(CO)_{10}]$

2 $[Ru_3(\mu\text{-}H)_2(\mu_3\text{-}NPh)(CO)_9]$

3 $[Ru_3(\mu_3\text{-}NPh)(\mu_3\text{-}CO)(CO)_9]$

4 $[Ru_3(\mu_3\text{-}NPh)_2(CO)_9]$

5 $[Os_3(\mu\text{-}H)(\mu\text{-}NHPh)(CO)_{10}]$

6 $[Os_3(\mu\text{-}H)_2(\mu_3\text{-}NPh)(CO)_9]$

7 $[Os_3(\mu\text{-}H)(\mu\text{-}NHTs)(CO)_{10}]$

8 $[Ru_3(\mu\text{-}H)_2(\mu_3\text{-}NTs)(CO)_9]$

9 $[\{Ru_3(\mu\text{-}H)_2(\mu_4\text{-}NTs)(CO)_7\}_2]$

10 $[Ru_3(\mu\text{-}H)(\mu\text{-}NHTs)(CO)_{10}]$

11 $[Os_3(\mu\text{-}H)_2(\mu_3\text{-}NTs)(CO)_9]$

12a $[Ru_3(\mu\text{-}H)_3(\mu_3\text{-}NPh)(CO)_9][BF_4]$

12b $[Ru_3(\mu\text{-}H)_3(\mu_3\text{-}NPh)(CO)_9][CF_3CO_2]$

13a $[Ru_3(\mu\text{-}H)_3(\mu_3\text{-}NTs)(CO)_9][BF_4]$

13b $[Ru_3(\mu\text{-}H)_3(\mu_3\text{-}NTs)(CO)_9][CF_3CO_2\text{-}H\text{-}CF_3CO_2]$

14a $[Os_3(\mu\text{-}H)_3(\mu_3\text{-}NTs)(CO)_9][BF_4]$

14b $[Os_3(\mu\text{-}H)_3(\mu_3\text{-}NTs)(CO)_9][CF_3CO_2]$

14c $[Os_3(\mu\text{-}H)_3(\mu_3\text{-}NTs)(CO)_9][CF_3CO_2\text{-}H\text{-}CF_3CO_2]$

15 $[PPN][Ru_3(\mu\text{-}H)(\mu_3\text{-}PhNCO)(CO)_9]$

16 $[PPN][Ru_3(\mu\text{-}H)(\mu_3\text{-}NPh)(CO)_9]$

17 $[HDBU][Ru_3(\mu\text{-}H)(\mu_3\text{-}TsNCO)(CO)_9]$

18 $[HDBU][Os_3(\mu\text{-}H)(\mu_3\text{-}PhNCO)(CO)_9]$

19a $[HDBU][Os_3(\mu\text{-}H)(\mu\text{-}NTs)(CO)_{10}]$

19b $[DBU\text{-}H\text{-}DBU][Os_3(\mu\text{-}H)(\mu\text{-}NTs)(CO)_{10}]$

19c $[DBU\text{-}H\ldots OH_2][Os_3(\mu\text{-}H)(\mu\text{-}NTs)(CO)_{10}]$

19d $[HNEt_3][Os_3(\mu\text{-}H)(\mu\text{-}NTs)(CO)_{10}]$

20 $[Ru_3(\mu\text{-}H)_2(\mu_3\text{-}NTs)(CO)_8(MeCN)]$

21 $[Os_3(\mu\text{-}H)_2(\mu_3\text{-}NTs)(CO)_8(MeCN)]$

22 $[Ru_3(\mu\text{-}H)(\mu\text{-}\textit{trans}\text{-}\sigma,\eta^2\text{–}CH{=}CHBu^t)(\mu_3\text{-}NTs)(CO)_8]$

23 $[Ru_3(\mu_3\text{-}NTs)(\mu_3\text{-}CO)(CO)_9]$

24 $[Ru_3(\mu\text{-}\eta^2,\eta^2\text{-}\textit{cis}\text{-}C_4H_6)(\mu_3\text{-}NTs)(\mu_3\text{-}CO)(CO)_7]$

25 $[Ru_3(\mu\text{-}\eta^2,\eta^2\text{-}cis\text{-}PhCH{=}CHCPh{=}CH_2)(\mu_3\text{-}NTs)(\mu_3\text{-}CO)(CO)_7]$

26a $[Ru_3(\mu\text{-}\eta^2,\eta^2\text{-}cis\text{-}PhCH{=}CDCPh{=}CHD)(\mu_3\text{-}NTs)(\mu_3\text{-}CO)(CO)_7]$

26b $[Ru_3(\mu\text{-}\eta^2,\eta^2\text{-}cis\text{-}PhCH{=}CDCPh{=}CDH)(\mu_3\text{-}NTs)(\mu_3\text{-}CO)(CO)_7]$

27 $[Os_3(\mu\text{-}H)(\mu\text{-}trans\text{-}\sigma,\eta^2\text{–}CH{=}CHBu^t)(\mu_3\text{-}NTs)(CO)_8]$

28 $[Os_3(\mu\text{-}H)(\mu\text{-}trans\text{-}CH{=}CHPh)(\mu_3\text{-}NTs)(CO)_8]$

29 $[Ru_3(\mu\text{-}H)_2(\mu_3\text{-}S)(CO)_9]$

30 $[Os_3(\mu\text{-}H)_2(\mu_3\text{-}S)(CO)_9]$

31 $[Os_3(\mu\text{-}H)_2(\mu_3\text{-}S)(CO)_8(MeCN)]$

32 $[Os_3(\mu\text{-}H)(\mu\text{-}\sigma,\eta^2\text{–}PhC{=}CH_2)(\mu_3\text{-}S)(CO)_8]$

33 $[Os_3(\mu\text{-}H)(\mu\text{-}trans\text{-}\sigma,\eta^2\text{–}CH{=}CHPh)(\mu_3\text{-}S)(CO)_8]$

34 $[Os_3(\mu\text{-}trans\text{-}\sigma,\eta^2\text{–}CH{=}CHPh)(\mu\text{-}\sigma,\eta^2\text{–}PhC{=}CH_2)(\mu_3\text{-}S)(CO)_7]$

35 $[Os_3(\mu\text{-}\sigma,\eta^2\text{–}CPh{=}CH_2)_2(\mu_3\text{-}S)(CO)_7]$

36 $[Os_3(\eta^4\text{-}cis\text{-}PhCH{=}CHCPh{=}CH_2)(\mu_3\text{-}S)(CO)_8]$

37 $[Os_3(\mu\text{-}H)(\mu\text{-}\sigma,\eta^2\text{-}CH{=}CH_2)(\mu_3\text{-}S)(CO)_8]$

38 $[Os_3(\mu\text{-}CHCHCHCH_3)(\mu_3\text{-}S)(CO)_8]$

39 $[Os_3(\mu\text{-}\sigma,\eta^2\text{–}CH{=}CH_2)(\mu\text{-}CH{=}CHCH{=}CH_2)(\mu_3\text{-}S)(CO)_8]$

40 $[Os_3(\eta^4\text{-}cis\text{-}C_4H_6)(\mu_3\text{-}S)(CO)_8]$

41 $[Os_3(\mu\text{-}H)_2(\mu_3\text{-}S)(CO)_8(Me_3N)]$

42 $[Ru_3(\eta^4\text{-}cis\text{-}PhCH{=}CHCPh{=}CH_2)(\mu_3\text{-}S)(CO)_8]$

43 $[Ru_3(\eta^4\text{-}cis\text{-}PhCH{=}CHCH{=}CPhH)(\mu_3\text{-}S)(CO)_8]$

44 $[Ru_3(\eta^4\text{-}cis\text{-}PhCH{=}CHCH{=}CHPh)(\mu_3\text{-}S)(CO)_8]$

45 $K_2[Ru_3(CO)_{11}]$

46 $[Mo(N\text{-}2,6\text{-}Me_2C_6H_3)_2Cl_2(dme)]$

47 $[Mo(N\text{-}2,4,6\text{-}Me_3C_6H_2)_2Cl_2(dme)]$

48 $[Mo(N\text{-}2,6\text{-}Me_2\text{–}4\text{-}Br\text{-}C_6H_2)_2Cl_2(dme)]$

49 $[Ru_3(CO)_{12}\{Mo(N\text{-}2,6\text{-}Me_2C_6H_3)_2\}]$

50 $[Ru_3(CO)_{12}\{Mo(N\text{-}2,4,6\text{-}Me_3C_6H_2)_2\}]$

51 $[Ru_3(CO)_{12}\{Mo(N\text{-}2,6\text{-}Me_2\text{-}4\text{-}Br\text{-}C_6H_2)_2\}]$

52 $[Ru_3(CO)_{12}\{MoO_2\}]$

53a $[Ru_3(CO)_{12}\{Mo(NH\text{-}2,6\text{-}Me_2C_6H_3)(N\text{-}2,6\text{-}Me_2C_6H_3)\}][BF_4]$

53b $[Ru_3(CO)_{12}\{Mo(NH\text{-}2,6\text{-}Me_2C_6H_3)(N\text{-}2,6\text{-}Me_2C_6H_3)\}][CF_3CO_2]$

53c $[Ru_3(CO)_{12}\{Mo(NH\text{-}2,6\text{-}Me_2C_6H_3)_2\}][CF_3CO_2]_2$

Chapter 1:

Introduction

PREFACE

The chemistry of transition metal cluster complexes has been extensively studied over the past thirty years or so. Thousands of cluster compounds have been synthesised and characterised. Various aspects of their chemistry have been explored, ranging from structural determination to their catalytic activity.

This thesis describes a small area of the large field of cluster chemistry. Our work is principally concerned with dihydride triruthenium and triosmium clusters, capped with a tosylimido or a sulfido ligand. The emphasis of this project has been to investigate the influence that the capping ligand has on the chemistry carried out at the metal centres. In particular the insertion of alkynes into the metal-hydride bonds of these clusters was explored, which in addition to giving the expected alkenyl complexes also generated butadiene-coordinated clusters. This type of hydrogenative coupling of two alkyne molecules to produce butadiene appears to be unprecedented.

In addition to this, tetranuclear clusters, consisting of a low-valent triruthenium cluster bonded to a high-valent molybdenum bis(imido) moiety, were also prepared. Our approach was to consider the high-valent metal to be an integral part of the cluster with the low-valent cluster fragment acting as a ligand.

1.1 BACKGROUND TO CLUSTER CHEMISTRY

It was during the 1930's and 1940's, with the application of X-ray crystallographic techniques, that the existence of metal-metal bonds was first shown.[1,2] Before this, direct metal-metal bonding was inconceivable and it was assumed metal atoms could

only be joined together by bridging ligands. In the 1960's several metal-metal bonds, unsupported by any bridging atoms or groups, were discovered. Where bridging ligands support metal-metal bonds, there can be uncertainty about the bond order and even doubt as to whether a direct metal-metal bond exists.

The structure of "$CsReCl_4$", the first structurally characterised trinculear cluster, was also deduced in the 1960's, showing that this compound contains a triangular $[Re_3(\mu\text{-}Cl)_3Cl_9]^{3-}$ anion (Fig. 1.1) containing Re-Re double bonds.[1]

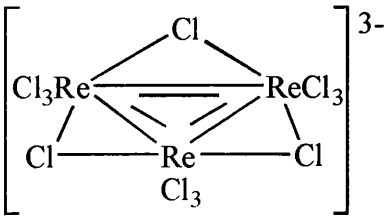

Fig. 1.1 The structure of $[Re_3Cl_{12}]^{3-}$

In 1964 the term "metal atom cluster" was first defined by Cotton[3] to classify "a finite group of metal atoms held together entirely, mainly or at least to a significant extent, by bonds directly between the metal atoms, even though some non-metal atoms may also be intimately associated with the cluster."[4]

The first metal carbonyl cluster, $[Fe_3(CO)_{12}]$, was discovered in the early 1900's,[2,5] but it was not until 1966 that its structure was resolved by Dahl,[6,7] who also structurally characterised the analogous compounds $[Ru_3(CO)_{12}]$ and $[Os_3(CO)_{12}]$.[2]

Higher nuclearity clusters are now known consisting of hundreds or even thousands of metal atoms, being stabilised by an outer shell of ligands.[8] These materials can be considered as intermediates between the smaller metal clusters, metal colloidal

particles and bulk metals. The unusual electrical, magnetic and spectroscopic properties these clusters may possess are of great interest, as they should approach those of a bulk metal with an increasing number of metal atoms.

The other main focus of cluster chemistry is aimed at the potential of using these systems as catalysts, or to gain an insight into the mechanism of the catalytic activity in heterogeneous systems. A wide range of cluster geometries is possible, the cluster framework being generally soft and deformable, the geometry being strongly dependant on the number of electrons. Clusters can act as electron-sinks, as many can be readily oxidised or reduced. Metal-metal bonds can be broken, providing coordination sites for incoming substrates that can bind to more than one atom simultaneously. Ligands are able to adopt unusual coordination modes that would not be found in mononuclear species. Some ligands may only be found in clusters, as they need to be stabilised by bonding to several metal atoms. Clusters also allow migration of coordinated ligands from one metal atom to another, for instance, hydride and carbonyl scrambling is very common.[9] These properties potentially make clusters ideal catalysts, for example, during a catalytic cycle the metal is generally required to change both its oxidation state and coordination geometry.

1.2 TRINUCLEAR CLUSTERS

The maximum binding energies for bulk transition elements occur approximately in the middle of the transition series corresponding to the half-filling of the d and s valence bands. Ligands bind to the metal atoms in a low-valent transition-metal cluster in such a manner to reconstruct this bonding situation and also to obey the 18 valence electron rule. For metal-metal bonding effects to be maximised low formal

oxidation states are necessary. Furthermore the stabilities of clusters increase as a periodic group is descended because of the strengthening of metal-metal bonds following the trend of the bulk metals.[10]

π-Donor ligands generally bind to earlier transition elements, as they donate additional electrons to the metal bonding MO's, especially when in bridging positions. These include ligands such as NR^{2-}, O^{2-}, S^{2-}, Cl^-, Br^-, I^- and OR^-, with the metals usually in the +2 or +3 oxidation states. π-Donor clusters prefer metal atoms with triangular or octahedral geometries. These types of clusters are predominantly formed by Nb, Mo, W and Re, examples include clusters with $[Mo_6X_8]^{4+}$,[11] $[Nb_6X_{12}]^{2+}$,[12] $[Re_3X_9]$[13] cores and their derivatives, and also Mo_3 and W_3 oxide[14] and alkoxide[15] clusters.

π-Acceptor ligands, which withdraw electron density from metal-metal anti-bonding MO's, tend to be associated with later transition metal clusters. The ability of CO to bind in terminal, edge-bridging or face-capping modes results in this being the most widely utilised π-acceptor ligand in low oxidation state cluster compounds. There are many examples of carbonyl clusters, those of the type $[M_3(CO)_{12}]$ (where M = Fe, Ru or Os) being amongst the simplest (Figs. 1.2a and b). Bonding of the CO ligands within the iron compound (Fig. 1.2a) is different to those in the ruthenium (Fig. 1.2b)

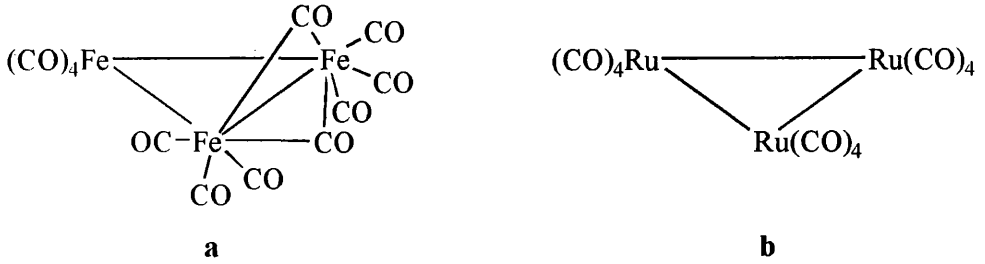

Fig. 1.2 The structures of (a) $[Fe_3(CO)_{12}]$ and (b) $[Ru_3(CO)_{12}]$

and osmium compounds. In the iron compound there are two distinct modes of coordination adopted by the CO ligands (*i.e.* bridging and terminal), whereas in the ruthenium and osmium cases all ligands are terminal. The difference could be due to electronic effects, but steric considerations could also be a factor.[16,17] Examples of other π-acceptor ligands that are also used include nitrous oxide, phosphines and polyenes (in particular cyclopentadienyl and benzene rings).

1.2.1 Electron Counting in Trinuclear Clusters

The vast majority of trinuclear cluster compounds have a total of 48 valence electrons, as predicted by the 18 valence electron rule, if there are three single M-M bonds.[10] However, trinuclear clusters with total valence electron counts below 48 electrons (from 42 electrons) and above 48 electrons (up to 52 electrons) are also known. Clusters with total electron counts below 48 electrons, either have multiple bonds between metal atoms or are formed by the nickel triad, with single metal-metal bonds, since 16 electron complexes are accessible for Ni, Pd and Pt.

An example of a 42-valence electron cluster with three metal-metal double bonds has already been given with $[Re_3(\mu\text{-}Cl)_3Cl_9]^{3-}$ (Fig. 1.1). The cation $[Pd_3(\mu_3\text{-}CO)(\mu\text{-}Ph_2PCH_2PPh_2)_3]^{2+}$ (Fig. 1.3) is also a 42-valence electron cluster, this time with three metal-metal single bonds.[18]

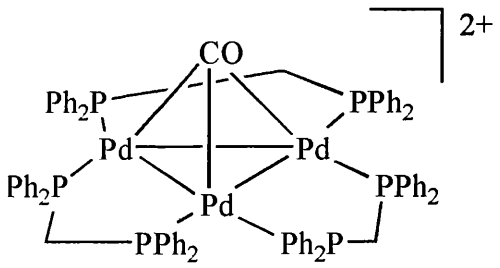

Fig. 1.3 The structure of the $[Pd_3(\mu_3\text{-}CO)(\mu\text{-}Ph_2PCH_2PPh_2)_3]^{2+}$cation

The 46-electron compound $[Os_3(\mu\text{-}H)_2(CO)_{10}]$ (Fig. 1.4) has two metal-metal single bonds and one metal-metal double bond.[19] This unsaturation leads to high reactivity, therefore this cluster is often used as a starting material for the formation of osmium clusters.

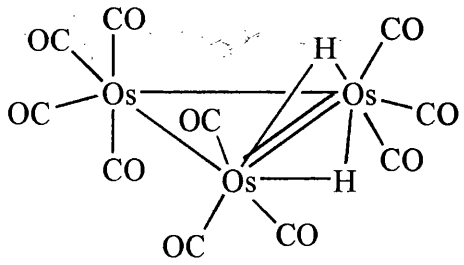

Fig. 1.4 The structure of $[Os_3(\mu\text{-}H)_2(CO)_{10}]$

While the cations $[M_3(\mu_3\text{-}S)_2(PR_3)_6]^{2+}$, where M= Ni, R = Et; M = Pd, R = Me, (Fig. 1.5), both have 48-valence electrons, they cannot be considered to be clusters as the metal-metal distances are too long for direct M-M bonding. Instead they are best described as aggregates of three square-planar 16-electron complexes held together by the sulfur ligands.[20,21]

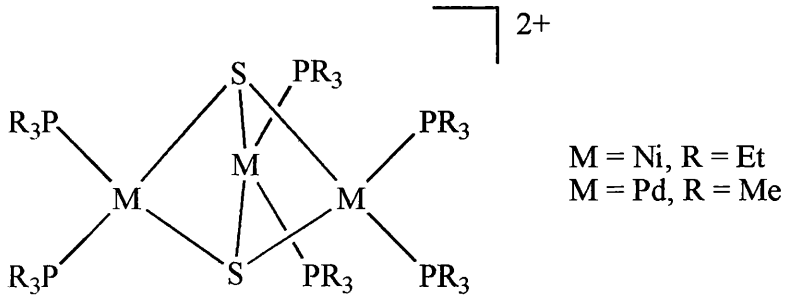

Fig. 1.5 The structure of the$[M_3(\mu_3\text{-}S)_2(PR_3)_6]^{2+}$ cations

In general, clusters with electron counts greater than 48 have fewer than three M-M bonds. An example of this is $[Fe_3(\mu_3\text{-}S)_2(CO)_9]$ (Fig. 1.6) which has a total of 50-valence electrons and two metal-metal bonds.[22]

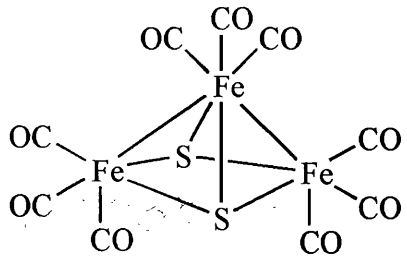

Fig. 1.6 The structure of $[Fe_3(\mu_3\text{-}S)_2(CO)_9]$

Likewise, the 52-electron compound $[Os_3(\mu_3\text{-}S)\{\mu_3\text{-}(PhN)_2SO\}(CO)_9]$ (Fig. 1.7) has only one metal-metal bond, the cluster core being held together by the capping ligands.[23]

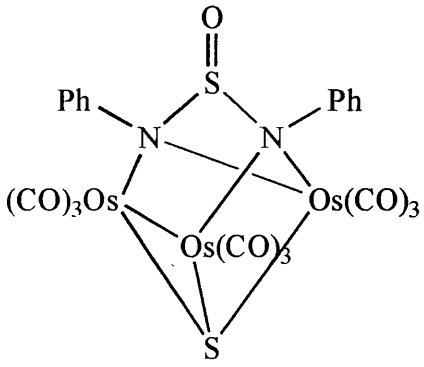

Fig. 1.7 The structure of $[Os_3(\mu_3\text{-}S)\{\mu_3\text{-}(PhN)_2SO\}(CO)_9]$

1.2.2 Trinuclear Ruthenium and Osmium Clusters

The chemistry of transition metal carbonyl clusters has been an important area of organometallic research. In particular ruthenium and osmium clusters have been extensively studied because of their interesting balance of reactivities and stabilities.[24] The role of triruthenium and triosmium clusters in the development of new types of bridging organic and inorganic ligands has been remarkable.[25] There are good reasons for focusing on the chemistry of trinuclear ruthenium and osmium clusters:[25]

- The clusters formed are extremely robust, especially those of osmium.

- Many different organic ligands can be used to tune the properties of these systems, with preservation of cluster nuclearity.
- The clusters are generally air-stable and thus easy to handle.
- Metal-metal bonds can be made or broken, as required by electronic factors, without changing cluster nuclearity.
- There is a vast chemistry with terminal, μ_2 and μ_3 organic and inorganic ligands.
- Ready purification by chromatographic techniques, and the relative ease with which good quality crystals, suitable for X-ray diffraction, can be grown makes analysis straightforward.
- Triosmium clusters can be used as a starting point for understanding ligand chemistry in less robust clusters.[26]

1.3 CAPPING LIGANDS

Ligands that can contribute three orbitals towards bonding are capable of capping a trinuclear cluster.[10] Capped metal clusters offer several real or potential advantages over uncapped ones:

- Thermal durability is commonly improved and cluster breakdown during catalytic and other reactions is suppressed.
- The steric and electronic properties of the cluster can be tuned. Lability at other ligand sites can be enhanced while strengthening the grip of the cap on the metal atoms.
- The provision of chirality to achieve asymmetric induction in reactions at the basal plane is potentially possible.

- The cluster could be bound, *via* the cap, to solid supports (metal oxides or polymers) to produce heterogenised homogeneous catalysts.

The number of electrons donated by a capping ligand can be varied from 1 to 7 electrons, with the cap acting as an inert, non-interfering cluster reinforcement (Fig. 1.9). A review of triosmium clusters with triply bridging ligands is available.[26] Several different caps are accessible[24,27] and this section presents the more recent developments in this area, with various metals.

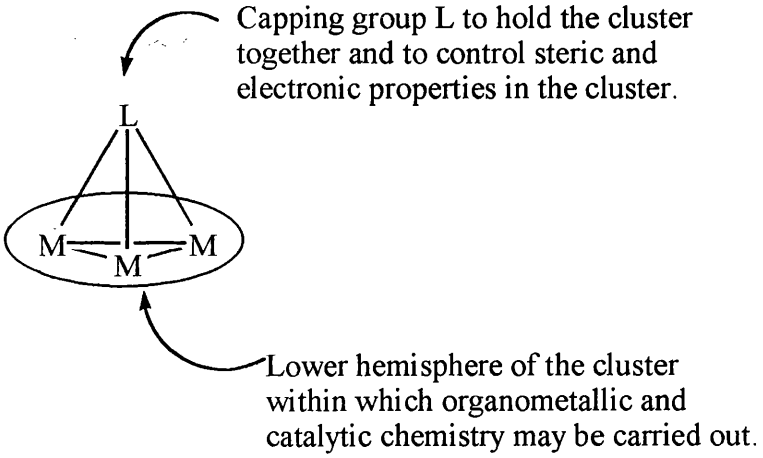

Fig. 1.9 The capping ligand providing cluster reinforcement

1.3.1 One-electron donors

Triply bridging one-electron donors (Fig. 1.10) include the hydride ligand (Fig. 1.10a) as in the cluster $[Ru_3(\mu_3\text{-}H)_2(\mu\text{-}CO)_3(CO)_3(PCy_3)_3]$.[28] This cluster is prepared on treating $[HRu_3(CO)_{11}]^-$ with PCy_3. It is the first reported 44-electron Ru_3 cluster and it contains short Ru-Ru bonds. The $\mu_3\text{-}CH_3$ ligand (Fig. 1.10 b) is found very rarely in transition metal chemistry. The reaction of $[Re_3(\mu\text{-}H)_3(\mu_3\text{-}H)(CO)_9]^-$ with CH_2N_2 gives the first fully characterised cluster of this type, $[Re_3(\mu\text{-}H)_3(\mu_3\text{-}CH_3)(CO)_9]^-$.[29] If the CH_3 group is regarded as a one-electron donor, the cluster would contain 44

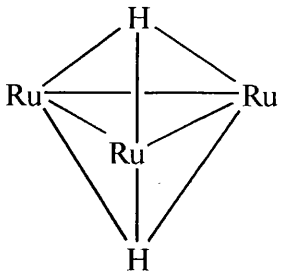

a

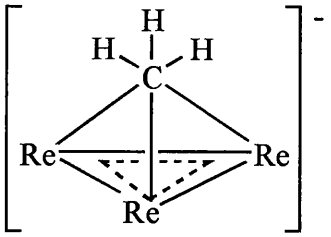

b

Fig. 1.10 One-electron donors (other ligands have been omitted for clarity)

electrons, requiring two Re-Re double bonds delocalised along the three edges. However, it appears the Re-Re bonds are too long to be considered as double bonds. The CH_3 group could be donating more than one electron. There is theoretical evidence for both σ and π donations to the cluster, which could therefore be viewed either as a π-stabilised unsaturated species, or if the CH_3 group is assumed to donate four electrons, then it is saturated. This ligand is also found in methyl lithium, which exists as the tetramer $[LiMe]_4$. The CH_3 group caps the triangular faces of the Li_4 tetrahedron.[30]

1.3.2 Two-electron donors

The most common μ_3 two-electron donor is CO and there are numerous clusters containing this ligand. An example of a cluster containing the CO ligand is $[Ru_3(\mu_3\text{-}NOMe)(\mu_3\text{-}CO)(CO)_9]$ (Fig. 1.11a), which also contains a μ_3-imido ligand, a four-electron donor,[31] this ligand will be discussed in Section 1.3.4. The CS group, being isoelectronic with the CO group, is also a two-electron donor and is found in the cluster $[Fe(CO)_2(PPh_3)Co_2(\eta^5\text{-}Cp)_2(\mu_3\text{-}S)(\mu_3\text{-}CS)]$ (Fig. 1.11b).[32] The $FeCo_2$ core forms an isosceles triangle capped on one face by the CS ligand. The other face is capped by the four-electron donating sulfido ligand (see Section 1.3.4). There are

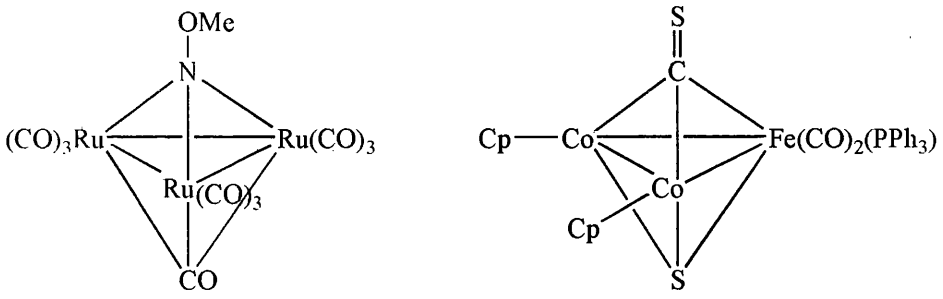

a **b**

Fig. 1.11 Two-electron donors

also η^5-Cp ligands on the two Co atoms, and two CO ligands and a PPh_3 group on the Fe atom. The cluster is prepared by cleaving the η^2-CS_2 ligand in $[Fe(PPh_3)_2(CO)_2(\eta^2\text{-}CS_2)]$ by $[Co(\eta^5\text{-}Cp)(PPh_3)_2]$. The CS ligand in the cluster is nucleophilic and is easily methylated to give $[Fe(CO)_2(PPh_3)Co_2(\eta^5\text{-}Cp)_2(\mu_3\text{-}S)(\mu_3\text{-}CSMe)]^+$.

1.3.3 Three-electron donors

There are several types of μ_3 three-electron donors (Figs. 1.12a - c). Numerous μ_3-alkylidyne (CR) complexes (Fig. 1.12a) are known. Various R groups can be employed such as Me,[33] Cl,[24,34] OMe,[35,36] C≡C-R,[37] pyridine derivatives[24] and $PPh_2CH_2PPh_2$ (dppm).[34] The cluster $[Os_3(\mu\text{-}H)_3(\mu_3\text{-}CMe)(CO)_9]$ can be prepared by the reduction of the ketenylidene group in $[Os_3(\mu\text{-}H)_2(\mu_3\text{-}CCO)(CO)_9]$, with BH_3.THF.[35] Reaction of $[Os_3(\mu\text{-}H)_3(\mu_3\text{-}CCl)(CO)_9]$ with chelating phosphines, such as dppm, gives $[Os_3(\mu\text{-}H)_2(\mu_3\text{-}CPPh_2CH_2PPh_2)(CO)_9]$.[24,34] This compound then undergoes decarbonylation and Os-P bond formation to give the five-membered ring structure $[Os_3(\mu\text{-}H)_2(\mu_3\text{-}CPPh_2CH_2PPh_2)(CO)_8]$.[34] The mixed-metal cluster $[Au_2Ru_3(\mu\text{-}H)(\mu_3\text{-}COMe)(\mu\text{-}dppm)(CO)_9]$ is formed on the reaction of $[Ru_3(\mu\text{-}$

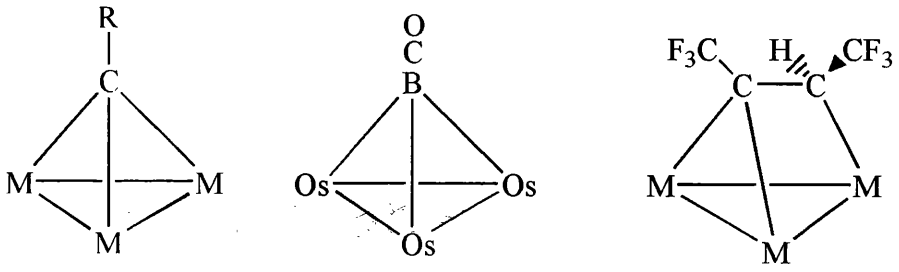

a **b** **c**

Fig. 1.12 Three-electron donors (other ligands have been omitted for clarity)

$H)_3(\mu_3\text{-}COMe)(CO)_9]$ with $[Au_2(\mu\text{-}dppm)Me_2]$. The cluster adopts a square-based pyramid geometry with the two Au atoms and two of the Ru atoms forming the base. The COMe group continues to cap the three Ru atoms.[35] Reaction of the polyynediyldiiron complexes $[(\eta^5\text{-}Cp^*)(CO)_2Fe\text{-}(C{\equiv}C)_n\text{-}Fe(CO)_2(\eta^5\text{-}Cp^*)]$ (where n= 3 or 4) with $[Fe_2(CO)_9]$, results in C≡C bond cleavage to give $[(\eta^5\text{-}Cp^*)(CO)_2Fe\text{-}C{\equiv}C\text{-}\mu_3\text{-}C\text{-}Fe_3(CO)_9\text{-}\mu_3\text{-}C\text{-}(C{\equiv}C)_{n-2}\text{-}Fe(CO)_2(\eta^5\text{-}Cp^*)]$.[37] This is a new type of compound, where a trinuclear cluster is sandwiched by two π-conjugated $(C{\equiv}C)_x$M systems. The cluster $[Os_3(\mu\text{-}H)_2(\mu_3\text{-}CNC_5H_4CH{=}CH_2\text{-}2)(CO)_9]$ reacts with PhC≡CH to give five alkyne-alkylidyne coupled products.[24]

The more unusual carbonyl borylidyne ligand (Fig. 1.12b) in $[Os_3(\mu\text{-}H)_3(\mu_3\text{-}BCO)(CO)_9]$ can be obtained on reaction of $[Os_3(\mu\text{-}H)_2(CO)_{10}]$ with $BH_3S(Me)_2$ at 65 °C.[38] The same reaction carried out at room temperature results in the formation of the cluster $[Os_3(\mu\text{-}H)_2(CO)_9(\mu\text{-}H)_2(\mu_3\text{-}BH)]$, a methylidyne cluster analogue. The $\mu_3\text{-}CF_3CCHCF_3$ ligand (Fig. 1.12c) is an exceptional form of bridging alkenyl ligand. It donates three electrons and is coordinated in a $\mu_3\text{-}\eta^1,\eta^2$-fashion in the complexes $[Os_3(\mu\text{-}H)(\mu_3\text{-}CF_3CCHCF_3)(CO)_{10}]$[39,40] and $[(\eta^5\text{-}Cp^*)WRu_2(\mu_3\text{-}CF_3CCHF_3)(\mu\text{-}NPh)(CO)_7]$.[41]

1.3.4 Four-electron donors

Four-electron μ_3 donor ligands are very common (Figs. 1.13a - f). In Fig. 1.13a, X can be an imido (NR),[23,24,31,42-56] phosphinidene (PR),[44,57-61] oxo,[62] sulfido,[23,43,48,63,64] selenido,[64,65] or a tellurido[64] ligand. There are several examples of μ_3-imido ligands, for instance, the NPh group is perhaps the most studied ligand of this type.[31,42-48] The reaction of $[Ru_3(\mu_3\text{-NPh})(\mu_3\text{-CO})(CO)_9]$ with $[(\eta^5\text{-Cp*})W(O_2)(CCR)]$ (where R = Ph or $CMe{=}CH_2$) results in the formation of the mixed-metal high-valent dioxo tungsten and low-valent ruthenium carbonyl compound $[(\eta^5\text{-Cp*})W(O)(\mu\text{-O})Ru_3(\mu_3\text{-NPh})(CCR)(CO)_8]$. This compound consists of a triruthenium cluster core capped by a μ_3-NPh ligand and a tungsten dioxo fragment, coordinated to the central Ru atom *via* a dative W=O→Ru interaction.[46] Mixed imido and sulfido clusters of the type $[M_3(\mu_3\text{-NPh})(\mu_3\text{-S})(CO)_9]$ have been prepared by reacting thioaniline (PhN=S=O) with $[Ru_3(CO)_{12}]$ or $[Os_3(CO)_{12}]$.[23,48] Another frequently used imido ligand is the NOMe moiety.[24,31,49-52] Studies into the hydrogenation,[49] thermolysis,[24,50] substitution reactions with phosphines[31] and reactions with alkynes[24,51,52] of $[Ru_3(\mu_3\text{-NOMe})(\mu_3\text{-CO})(CO)_9]$ have been investigated. The reaction of $[Ru_3(CO)_{12}]$ with MePhS(O)NH leads to the formation of an interesting imido ligand in the cluster $[Ru_3(\mu\text{-H})(\mu_3\text{-NS(O)MePh})(CO)_9]$. The imido ligand is chiral and the cluster is electron deficient with 46 electrons, as the N=S(O)MePh cap is actually considered as a three-electron donor.[53-55] The X-ray crystallographic data of this compound supports this, as the Ru-Ru bond lengths are shorter than would be associated with a Ru-Ru single bond.[53] The reaction of the azavinylidene cluster $[Ru_3(\mu\text{-H})(\mu\text{-N=CPh}_2)(CO)_{10}]$ with hydrogen leads to the formation of $[Ru_4(\mu\text{-H})_4(CO)_{12}]$ and H_2NCHPh_2, *via* the μ_3-$NCHPh_2$ containing cluster $[Ru_3(\mu\text{-H})_2(\mu_3\text{-NCHPh}_2)(CO)_9]$.[56]

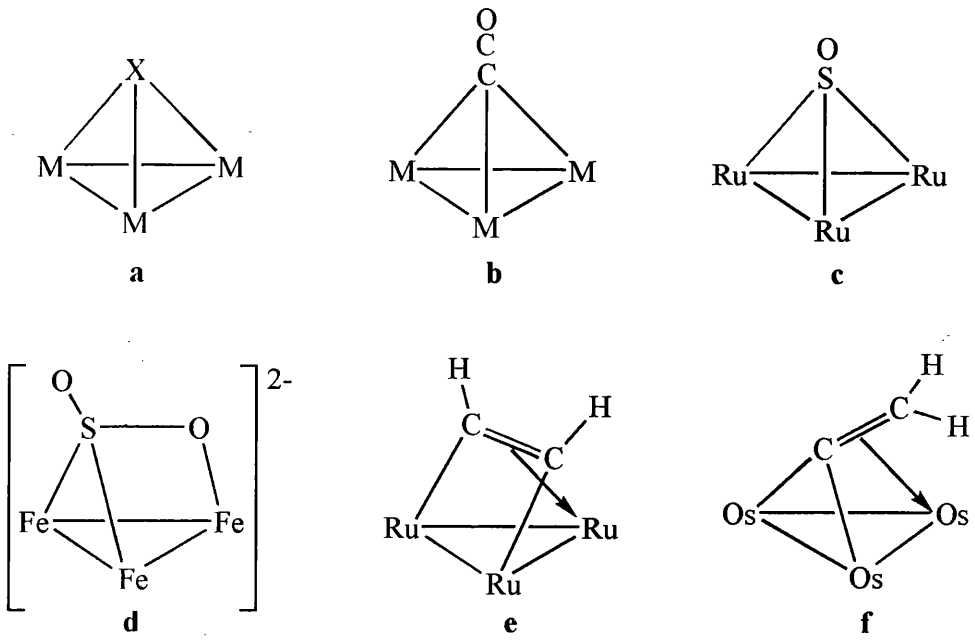

Fig. 1.13 Four-electron donors (other ligands have been omitted for clarity)

Numerous μ_3-phosphinidene clusters bearing different R groups have been characterised,[44] some recent examples are now presented. Reduction of the μ_3-phosphinidene cluster $[Ru_4(\mu_3\text{-PPh})(CO)_{13}]$ with $Co(\eta^5\text{-Cp})_2$ forms $[Ru_4(\mu_3\text{-PPh})(CO)_{12}]^{2-}$. This cluster has a square pyramidal geometry, with three of the four Ru atoms and the PPh ligand forming the basal plane, the fourth Ru atom forming the apex. Reacting this cluster with $Cl_2PNPr^i_2$ forms $[Ru_4(\mu_4\text{-PPh})(\mu_4\text{-PNPr}^i_2)(\mu\text{-CO})(CO)_{10}]$ which now adopts a square bipyramidal geometry, with the four Ru atoms capped by both μ_4-phosphindene ligands.[57] The reaction of $[IrCl(Bu^t_2PH)_3]$ with $[Ru_3(CO)_{12}]$ gives the μ_3-PBu^t capped cluster $[Ru_3(\mu\text{-H})_2(\mu_3\text{-PBu}^t)(CO)_8(Bu^t_2PH)]$.[58] The phosphinidene ligand in $[W(PMe)(CO)_5]$, generated *in situ*, adds across the double bond of $[Os_3(\mu\text{-H})_2(CO)_{10}]$ to form $[Os_3(\mu\text{-H})(\mu\text{-PHMe})(CO)_{10}]$. The H atom on the μ-PHMe ligand subsequently migrates from the phosphorus to the cluster system accompanied by CO loss to give the cluster $[Os_3(\mu\text{-H})_2(\mu_3\text{-PMe})(CO)_9]$.[59] Reaction of $[Ru_3(CO)_{12}]$ with $(PCF_3)_4$ yields the 72-electron

tetranuclear 'cluster' $[\{Ru(CO)_3(\mu_3\text{-}PCF_3)\}_4]$ with no metal-metal bonds. The structure of this compound consists of a distorted cuboid skeleton made up of alternating P and Ru atoms.[61]

Reaction of $[(\eta^6\text{-}C_6Me_6)_2Ru_2(\mu\text{-}H)_3]^+$ with $[(\eta^6\text{-}C_6H_6)Ru(H_2O)_3]^{2+}$ in water forms the trinuclear cluster $[(\eta^6\text{-}C_6H_6)(\eta^6\text{-}C_6Me_6)_2Ru_3(\mu\text{-}H)_3(\mu_3\text{-}O)]^+$, the oxo ligand coming from the water. The X-ray structure of this compound shows the oxo cap is hydrogen bonded to a water molecule.[62] The μ_3-sulfido ligand can be found in many clusters[43] and the mixed sulfido imido clusters $[M_3(\mu_3\text{-}NPh)(\mu_3\text{-}S)(CO)_9]$ (where M = Ru or Os) have already been mentioned.[23,48] The clusters $[Ru_3(\mu_3\text{-}S)\{\eta^1\text{-}CN(Me)SPh\}(CO)_8]$ and $[RuCo_2(\mu_3\text{-}S)\{\eta^1\text{-}CN(Me)SPh\}(CO)_8]$ were prepared by the reaction of 3-methyl-2-benzothiazolinthione (PhN(Me)C(S)S) with $[Ru_4(\mu\text{-}H)_4(CO)_{12}]$ and $[RuCo_3(\mu\text{-}H)(CO)_{12}]$ respectively.[63] The compounds $[Fe_3(\mu_3\text{-}X)(CO)_9]^{2-}$ (where X = S, Se and Te) are all known,[64] and their alkylation reactions will be discussed in Section 1.3.5. Reaction of $[Fe_3(CO)_{12}]$ or $[Ru_3(CO)_{12}]$ with $dppmSe_2$ gives the 50-electron clusters $[M_3(\mu_3\text{-}Se)_2(\mu\text{-}dppm)(CO)_7]$. The two Se ligands cap opposite sides of the clusters and the dppm ligand bridges the open M-M bond.[65]

The ketenylidene ligand (Fig. 1.13b) is positioned vertically in the cluster $[Os_3(\mu\text{-}H)_2(\mu_3\text{-}CCO)(CO)_9]$,[66] but in $[Fe_3(\mu_3\text{-}CCO)(CO)_9]^{2-}$ [67] the linear CCO ligand is at 33.5° from perpendicular to the metal plane and there is only a small energy requirement to switch between these geometries. The reduction of the high nuclearity cluster $[Ru_6C(\mu\text{-}SO_2)(CO)_{15}]^{2-}$ by BF_3 results in the formation of the μ_3-SO containing cluster $[Ru_6C(CO)_{15}(\mu_3\text{-}SO)]$ (Fig. 1.13c). Further reduction of this cluster together

with cleavage of two metal-metal bonds and addition of a CO ligand gives $[Ru_6C(CO)_{16}(\mu_3\text{-}S)]$.[68] The π-acid SO_2 reacts with $[PPN]_2[MFe_3(CO)_{14}]$ (where M = Cr, Mo or W) to give $[PPN]_2[Fe_3(CO)_9(\mu_3,\eta^2\text{-}SO_2)]$ (Fig. 1.13d) and $[PPN]_2[Fe_3(CO)_8(\mu\text{-}SO_2)(\mu_3\text{-}S)]$. Reaction of $[PPN]_2[MFe_3C(CO)_{14}]$ (where M = Cr or W) with SO_2 gives the ketenylidene clusters $[PPN]_2[Fe_3(\mu_3\text{-}CCO)(\mu\text{-}SO_2)(CO)_8]$ and $[PPN]_2[Fe_3(\mu_3\text{-}CCO)(\mu\text{-}SO_2)_2(CO)_7]$.[69]

The cluster $[Ru_3(\eta^1\text{-}C_2H_2)(CO)_{11}]$, formed from $[Ru_3H(\mu\text{-}H)(CO)_{11}]$ and acetylene, can be converted to the μ_3-alkyne cluster $[Ru_3(\mu_3,\eta^2\text{-}C_2H_2)(\mu\text{-}CO)(CO)_9]$ (Fig. 1.13e).[70] Whereas the direct reaction of $[Os_3(CO)_{12}]$ with ethylene forms the 1,1-isomer $[Os_3(\mu\text{-}H)_2(\mu_3\text{-}C{=}CH_2)(CO)_9]$ (Fig. 1.13f), in preference to the 1,2 isomer, $[Os_3(\mu\text{-}H)_2(\mu_3,\eta^2\text{-}C_2H_2)(CO)_9]$, although both compounds are known to be stable enough to isolate.[71]

1.3.5 Five-electron donors

The sulfido capping group in $[Fe_3(\mu_3\text{-}S)(CO)_9]^{2-}$ can be alkylated using methyl triflate or methyl iodide to form $[Fe_3(\mu_3\text{-}SMe)(CO)_9]^-$ (Fig. 1.14a). In contrast to this, the alkylation of the analogous Se and Te cluster occurs at the metal core to give $[Fe_3(\mu_3\text{-}X)(CO)_9(Me)]^-$.[64] Reaction of $[(\eta^5\text{-}Cp)Fe(CO)_2THF][BF_4]$ with $[Fe_3(\mu_3\text{-}S)(CO)_9]^{2-}$ gives the cluster $[Fe_3(CO)_9\{\mu_3\text{-}SFe(\eta^5\text{-}Cp)(CO)_2\}]^-$, consisting of a '$Fe_3(CO)_9(\mu_3\text{-}S)$' fragment coordinated to the Fe atom of $(\eta^5\text{-}Cp)Fe(CO)_2$, which could be considered as the R group in $[Fe_3(\mu\text{-}SR)(CO)_9]^-$ (Fig. 1.14a). The sulfur atom in this cluster adopts a *pseudo* tetrahedral geometry.[72] An example of an alkynyl cap (Fig. 1.14b) is

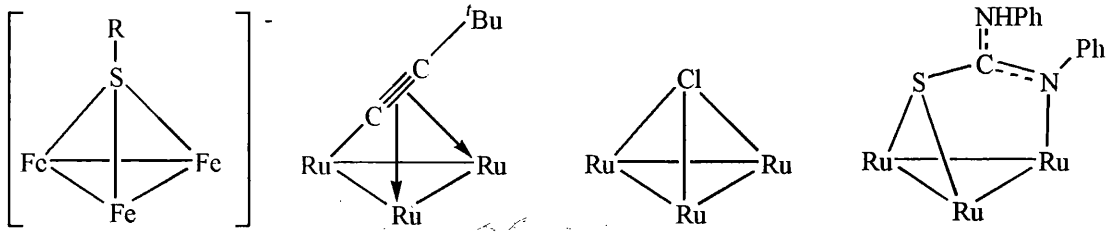

a **b** **c** **d**

Fig. 1.14 Five-electron donors (other ligands have been omitted for clarity)

found in the compound $[Ru_3(\mu\text{-}H)(\mu_3\text{-}CCBu^t)(\mu\text{-}dppm)(CO)_7]$ and this is an extremely common form of alkyne coordination in clusters.[73] In addition to $[Ru_3(\mu\text{-}H)_2(\mu_3\text{-}PBu^t)(CO)_8(Bu^t_2PH)]^-$ mentioned in Section 1.3.4, the reaction of $[IrCl(Bu^t_2PH)_3]$ with $[Ru_3(CO)_{12}]$ also gives the mixed-metal cluster $[Ru_3Ir(\mu_3\text{-}Cl)(\mu\text{-}H)_2(\mu\text{-}PBu^t_2)_2(CO)_7(Bu^t_2PH)(CO)_7]$ which contains a μ_3-Cl ligand (Fig. 1.14c).[58] Reaction of diphenylthiourea $SC(NPh)_2$ with $[Ru_3(CO)_{12}]$ forms $[Ru_3(\mu\text{-}H)(\mu_3,\eta^2\text{-}PhNCSNPhH)(CO)_9]$ (Fig. 1.14d). Reaction of this cluster with PPh_3 at high temperature results in the formation of the μ_3-S containing cluster $[Ru_3(\mu_3\text{-}S)(\mu\text{-}Ph)(\mu\text{-}PPh_2)(CO)_6(PPh_3)]$.[74]

1.3.6 Six-electron donors

Benzene lying parallel to a triangular metal cluster can donate all six of its π-electrons as a $\mu_3\text{-}\eta^2,\eta^2,\eta^2$ capping ligand (Fig. 1.15a) as found in the compound $[Ru_3(\mu\text{-}H)_3(\eta\text{-}C_5Me_5)_3(\mu_3\text{-}\eta^2,\eta^2,\eta^2\text{-}C_6H_6)]$.[75] A two-electron oxidation of this compound results in a 30° rotation of the benzene ring, so one ruthenium atom is η^3 coordinated and there is an η^3 bridge across the other pair of ruthenium atoms (Fig. 1.15b). The ligand can now be described as $\mu_3\text{-}\eta^3,\eta^2,\eta^2$-benzene. This represents a unique example of this

a **b**

Fig. 1.15 The μ_3-benzene ligand (other ligands have been omitted for clarity)

arrangement, while $\mu_3,\eta^2,\eta^2,\eta^2$ coordination is now common, and can also be found in the cluster $[Ru_3(CO)_9(\mu_3\text{-}\eta^2,\eta^2,\eta^2\text{-}C_{60})]$.[76] Another μ_3 six-electron donor is the $(PhN)_2SO$ ligand in the cluster $[Os_3\{\mu_3\text{-}\eta^2\text{-}(PhN)_2S\}(\mu_3\text{-}S)(CO)_9]$, shown in Fig. 1.7, formed from the reaction of $[Os_3(CO)_{10}(MeCN)_2]$ with PhN=S=O.[23]

1.3.7 Seven-electron donors

Triply bridging seven-electron donors are rare, with the examples shown in Figs. 1.16a and 1.16b, being derived from EtC≡CH and PhC≡CPh respectively.[26]

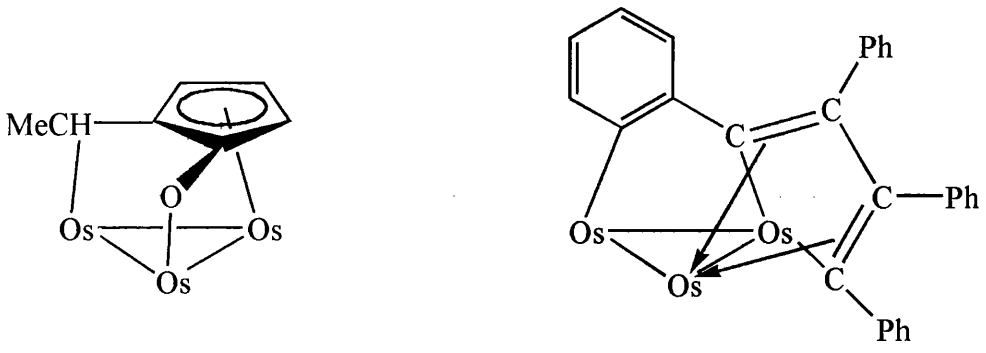

a **b**

Fig. 1.16 Seven-electron donors (other ligands have been omitted for clarity)

1.4 CLUSTERS IN CATALYSIS

Transition metal clusters can be considered to be at the interface between simple molecular complexes and metal surfaces. Mononuclear complexes used in most

homogeneous catalysis can be tuned, through choice of ligands, to achieve favourable reactivity and selectivity. Heterogeneous catalysts, whilst they cannot be tuned so easily, offer the advantage of being thermally stable, with products being easily separated from the catalyst. They also permit catalysis requiring the presence of several metal atoms, this not being possible with a mononuclear homogeneous catalyst. Thus, in principle, homogeneous cluster catalysis offers the advantages of both systems. It is possible to tune the catalyst by choice of ligands, while allowing substrate interactions with several metal atoms.[77] Novel bonding modes could lead to different or lower energy reaction pathways.[78] Clusters, being molecular compounds, are usually soluble in organic solvents and can be characterised in solution using spectroscopic techniques. Clusters may also be intermediate complexes, formed during homogeneous catalysis with mononuclear species. The analogies between ligands bound to clusters and those bound to surfaces was recognised by Muetterties.[79,80] Clusters can act as models for structures and reactivities of organic or other substrates that are known to bind to a metal surface during heterogeneous catalysis. However, the electronic structures of clusters and metal surfaces are very different and reaction rates and energetics of processes are unlikely to be related.

To stabilise clusters for catalysis, bridging ligands can be used to lock the metals together and inhibit cluster fragmentation, especially if metal-metal bonds are broken. This can then prevent ambiguity with regards to identifying the active complex.

An example of homogenous catalysis, carried out by a capped cluster, is the hydrogenation of alkynes by ruthenium clusters containing a bridge, derived from the deprotonation of 2-amino-6-methylpyridine (Hampy).[81] A catalytic cycle is shown in Scheme 1.1.

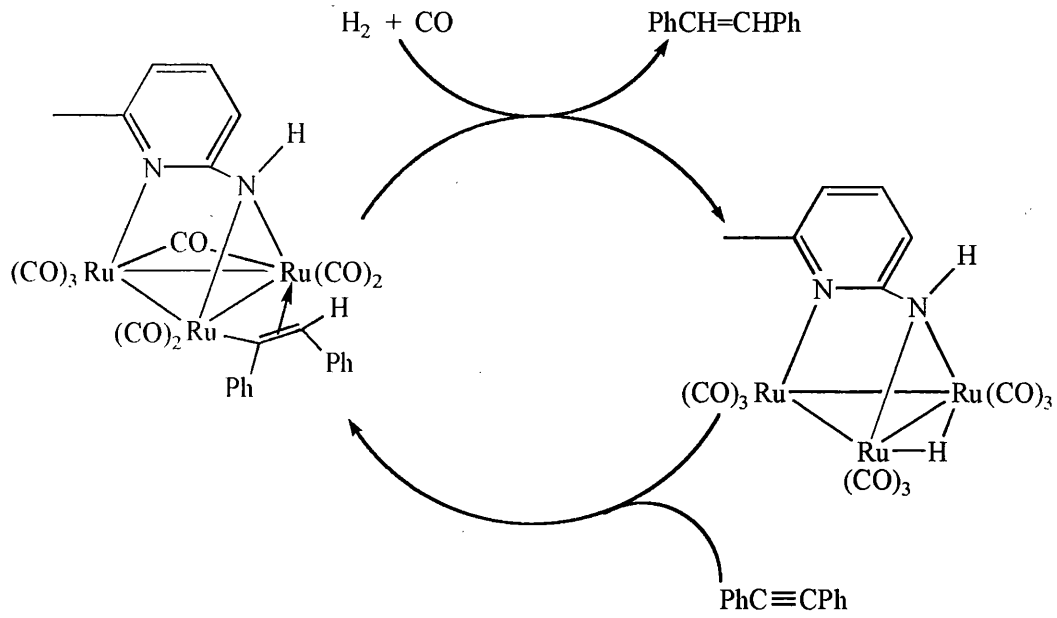

Scheme 1.1 The catalytic hydrogention of diphenylethyne

The alkenyl cluster $[Ru_3(\mu_3\text{-ampy})(\mu\text{-PhC=CHPh})(\mu\text{-CO})(CO)_7]$ is an intermediate in this cycle. This cluster was investigated for its catalytic properties, and was found to be more efficient as a catalyst precursor for the hydrogenation of phenylethyne, than the parent compound $[Ru_3(\mu\text{-H})(\mu_3\text{-ampy})(CO)_9]$. The cationic hydrido derivative $[Ru_3(\mu\text{-H})(\mu_3\text{-ampy})(\mu\text{-PhC=CHPh})(CO)_8][BF_4]$ was also used as a catalyst precursor. As both of the alkenyl clusters are coordinatively saturated it follows that vacant sites are required for hydrogenation. This can be achieved by the decoordination of the alkenyl group, from bridging to terminal mode. Addition of hydrogen, to give a di- and a trihydride intermediate respectively, would then lead to elimination of stilbene and formation of an unsaturated species, which would rapidly add diphenylethyne and regenerate the catalyst precursor.[81,82]

1.5 TARGETS, AIMS AND OBJECTIVES IN THIS THESIS

Our research required robust cluster systems and to this end ruthenium and osmium carbonyl clusters with capping ligands, which could be varied, were employed. To

facilitate the chemistry to be carried out at the basal plane, bridging hydrido ligands and labile terminal ligand sites for incoming organic substrates to bind, were also incorporated.

Chapter 2 describes the synthesis of hydrido μ_3-tosylimido and μ-tosylamido clusters. This particular ligand was chosen on the basis that the tosyl group is a poorer electron donor than the phenyl group, resulting in less electron density being available at the cluster core. To test this, the reactivity of the tosylimido and tosylamido clusters was compared with their phenylimido and phenylamido counterparts. Chapter 3 details the chemistry on replacing CO with MeCN, to create the required labile sites at the basal plane, for the insertion of terminal alkynes into the metal-hydride bonds of the tosylimido clusters. Our initial aim to couple the imido group with alkynes to provide new routes to nitrogen heterocyclic compounds proved unsuccessful, although new types of chemistry at basal sites in capped clusters were established. In addition to alkyne hydrogenation, double insertion can occur to give two alkenyl ligands, which couple to generate butadiene-coordinated clusters. Chapter 4 reports parallel chemistry with analogous clusters containing the capping sulfido ligand, which is less bulky and a better electron donor than the tosylimido ligand. Comparisons between the two systems are made. Chapter 5 describes an entirely new class of transition metal system, in which a low-valent ruthenium cluster coordinates as a ligand at high-valent molybdenum complexes, such that metal-metal bonds are formed between metals as much as six oxidation states apart.

Chapter 2:

The synthesis, protonation and deprotonation of tosylimido and tosylamido clusters

2.1 INTRODUCTION

The imido (NR) ligand is very versatile and coordinates to both high and low valent metal centres (Figs. 2.1a - e).[83-86] The terminal modes (Figs. 2.1a and b) are

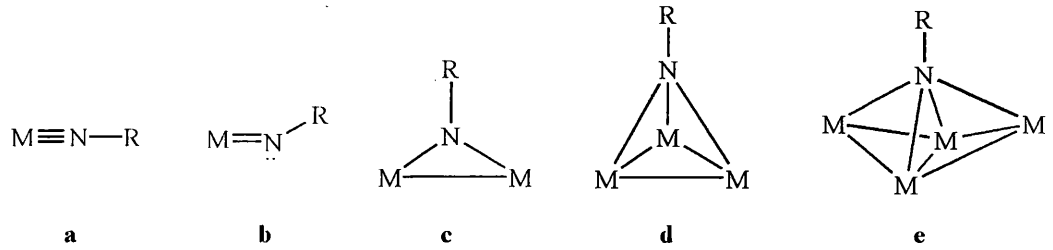

Fig. 2.1 The coordination modes of the imido ligand

associated with electron-poor early transition metals, whereas the bridging modes (Figs. 2.1d and e) are associated with the more electron-rich late transition metals.[86]

The chemistry of transition metal clusters with μ_3-imido ligands has been the subject of great interest due to their involvement as intermediates in the catalytic reductive carbonylation of nitroaromatics to form aryl isocyanates in the presence of $[Ru_3(CO)_{12}]$.[52,87-93] Aryl isocyanates are used in the formation of pesticides such as carbamates (Scheme 2.1).[83,91]

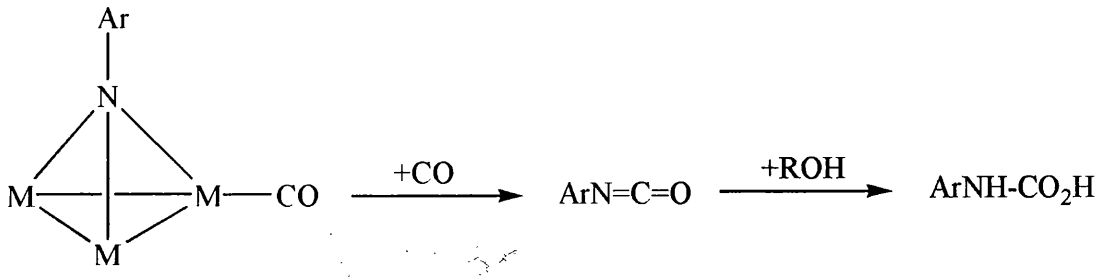

Scheme 2.1 The formation of carbamates from aryl isocyanates

The reaction of aniline with $[Ru_3(CO)_{12}]$ forms four products (Scheme 2.2).[94] The amido species $[Ru_3(\mu\text{-}H)(\mu\text{-}NHPh)(CO)_{10}]$ **1** can be converted to the imido compound

$[Ru_3(\mu\text{-}H)_2(\mu_3\text{-}NPh)(CO)_9]$ **2** by the oxidative addition of the N-H bond to the metal core and loss of CO. Carbonylation of **2** results in H_2 elimination to give the complex $[Ru_3(\mu_3\text{-}NPh)(\mu_3\text{-}CO)(CO)_9]$ **3** which can be converted to $[Ru_3(\mu_3\text{-}NPh)_2(CO)_9]$ **4** on further addition of aniline.

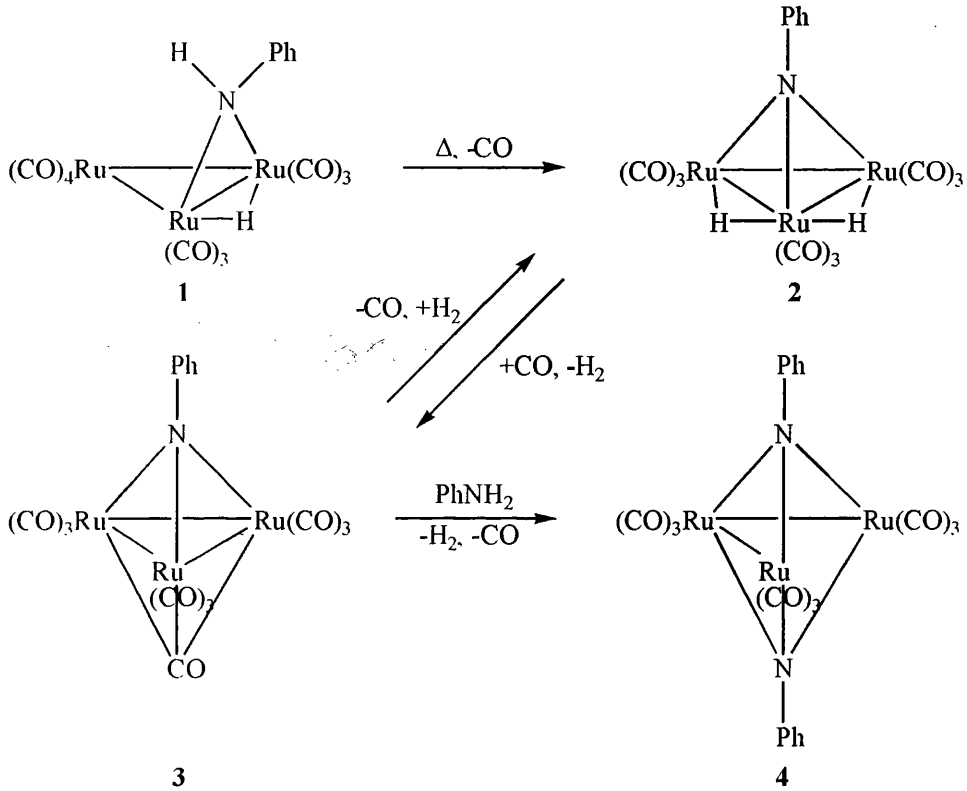

Scheme 2.2 The products formed on the reaction of aniline with $[Ru_3(CO)_{12}]$

The analogous reaction of aniline with $[Os_3(CO)_{12}]$ initially forms the amido compound $[Os_3(\mu\text{-}H)(\mu\text{-}NHPh)(CO)_{10}]$ **5** (Scheme 2.3), which loses CO thermally to

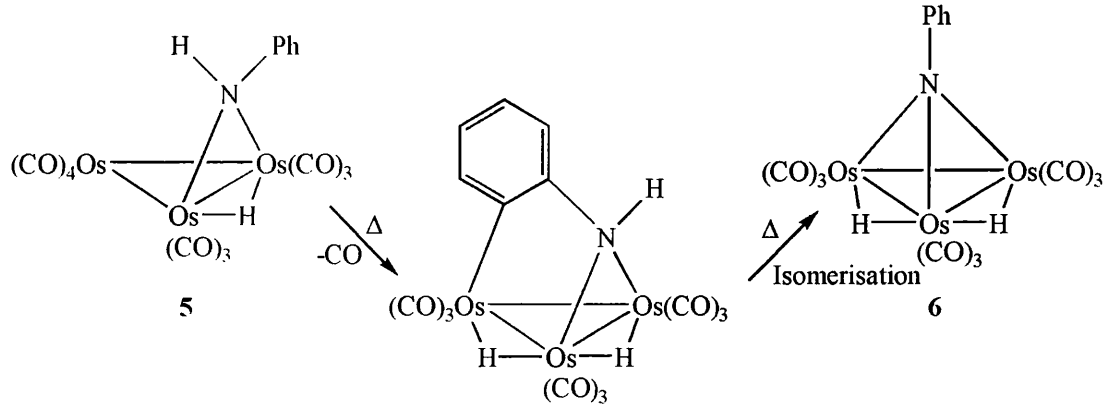

Scheme 2.3 The products formed on the reaction of aniline with $[Os_3(CO)_{12}]$

form the orthometallated species $[Os_3(\mu\text{-}H)_2(HNC_6H_4)(CO)_9]$.[95] Room temperature photolysis of **5** or thermolysis of $[Os_3(\mu\text{-}H)_2(HNC_6H_4)(CO)_9]$ gives the imido compound $[Os_3(\mu\text{-}H)_2(\mu_3\text{-}NPh)(CO)_9]$ **6**.[95,96] The compounds $[Os_3(\mu_3\text{-}NPh)(\mu_3\text{-}CO)(CO)_9]$ and $[Os_3(\mu_3\text{-}NPh)_2(CO)_9]$ have also been prepared from the reaction of nitrobenzene with $[Os_3(CO)_{12}]$.[97]

High-valent tosylimido-metal (M=NTs) species are believed to be active intermediates in metal-mediated alkene aziridination (Scheme 2.4).[98-100]

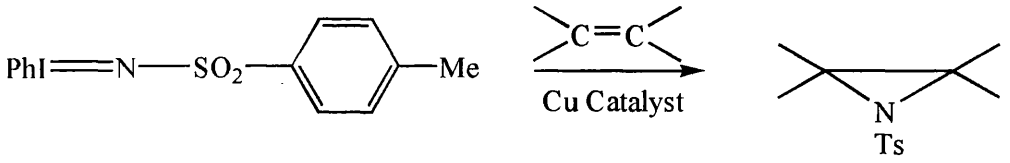

Scheme 2.4 The aziridination reaction

A few high-valent tosylimido-metal complexes have been isolated,[101,102] but the use of the tosylimido (4-tolylSO$_2$N) ligand in low-valent cluster compounds has not been explored, except for the preparation of the tosylamido cluster $[Os_3(\mu\text{-}H)(\mu\text{-}NHTs)(CO)_{10}]$ **7** from $[Os_3(\mu\text{-}H)_2(CO)_{10}]$ and tosylazide.[103] The tosylimido ligand is a poorer electron donor than alkyl or aryl imido ligands, due to the electron-withdrawing influence of the tolylSO$_2$ group. It is therefore expected that M-CO bonds in tosylimido metal carbonyl cluster compounds will be weaker than those in the corresponding phenylimido compounds, giving rise to differences in reactivity.

2.2 TARGETS, AIMS AND OBJECTIVES IN THIS CHAPTER

- To synthesise tosylimido and tosylamido cluster compounds.
- To investigate the reactivity of these systems.

- To compare these results with the known phenylimido and phenylamido analogues.

2.3 RESULTS AND DISCUSSION

2.3.1 Reaction of $[Ru_3(CO)_{12}]$ with *p*-toluenesulfonamide

Direct thermal reaction of $[Ru_3(CO)_{12}]$ with *p*-toluenesulfonamide (4-$MeC_6H_4SO_2NH_2$), in refluxing toluene over 8 hours, formed $[Ru_3(\mu\text{-}H)_2(\mu_3\text{-}NTs)(CO)_9]$ **8** as a yellow solid in 51% yield along with seven other products, three of which have been identified. The known compound $[Ru_4(\mu\text{-}H)_4(CO)_{12}]$, characterised from spectroscopic data,[104] is formed in 4% yield. The second compound is $[Ru_6(\mu_6\text{-}C)(\mu\text{-}CO)(CO)_{13}(\eta^6\text{-toluene})]$[105] isolated in 1% yield and is known to be formed from $[Ru_3(CO)_{12}]$ in refluxing toluene, and the third compound is believed to be $[\{Ru_3(\mu\text{-}H)_2(\mu_4\text{-}NTs)(CO)_7\}_2]$ **9**, a red solid formed in 5% yield. Compound **9** will be discussed later in the chapter. The remaining four compounds - a pale orange solid, a dark red/brown solid, a dark brown solid and a yellow/brown solid have not been identified and were not investigated further.

The cluster **8** is formed by loss of CO and oxidative addition of the N-H bond in the conversion of the intermediate $[Ru_3(\mu\text{-}H)(\mu\text{-}NHTs)(CO)_{10}]$ **10**. The decacarbonyl cluster is isolated in small quantities when the reaction is carried out under milder conditions, for instance at slightly lower temperature or if the reaction is carried out for a shorter period of time. A good synthesis of **10** has not been possible because it is only observed when there is only partial conversion of $[Ru_3(CO)_{12}]$. Under more

vigorous conditions, with high conversion of $[Ru_3(CO)_{12}]$, **10** could not be isolated. This observation is consistent with those for the formation of the analogous phenylimido compounds.[94]

As expected the CO absorptions in the IR spectra of the clusters **8** and **10** show a shift to higher wavenumber, when compared to those of the phenylimido compounds, due to the electron-withdrawing effects of the SO_2 group in the NTs moiety. There is less electron density available for donation to the CO π^*-orbitals in the NHTs and NTs clusters.

The ^1H NMR spectrum of **8** shows a singlet at δ -17.26 assigned to the hydride ligands, a singlet at δ 2.44 for the Me group of the NTs ligand, and an AA'BB' pattern for the tolyl ring at δ 7.33 and 7.82. The positive FAB mass spectrum displayed a molecular ion peak at m/z 726 and daughter ions due to successive loss of nine carbonyl ligands.

Single crystals of **8** were grown by slow evaporation of a heptane solution and the structure determined by X-ray diffraction is shown in Fig. 2.2. Selected bond lengths and angles are given in Table 2.1.

The three ruthenium atoms form a closed isosceles triangle [Ru(1)-Ru(2) 2.847(2); Ru(1)-Ru(3) 2.751(2); Ru(2)-Ru(3) 2.859(2) Å]. Each ruthenium atom is bonded to three terminal CO ligands and also to the nitrogen cap. The hydride ligands could not be located. However, one of the Ru-Ru bonds is shorter than the other two, confirming the presence of two bridging hydride ligands on the longer Ru-Ru edges.

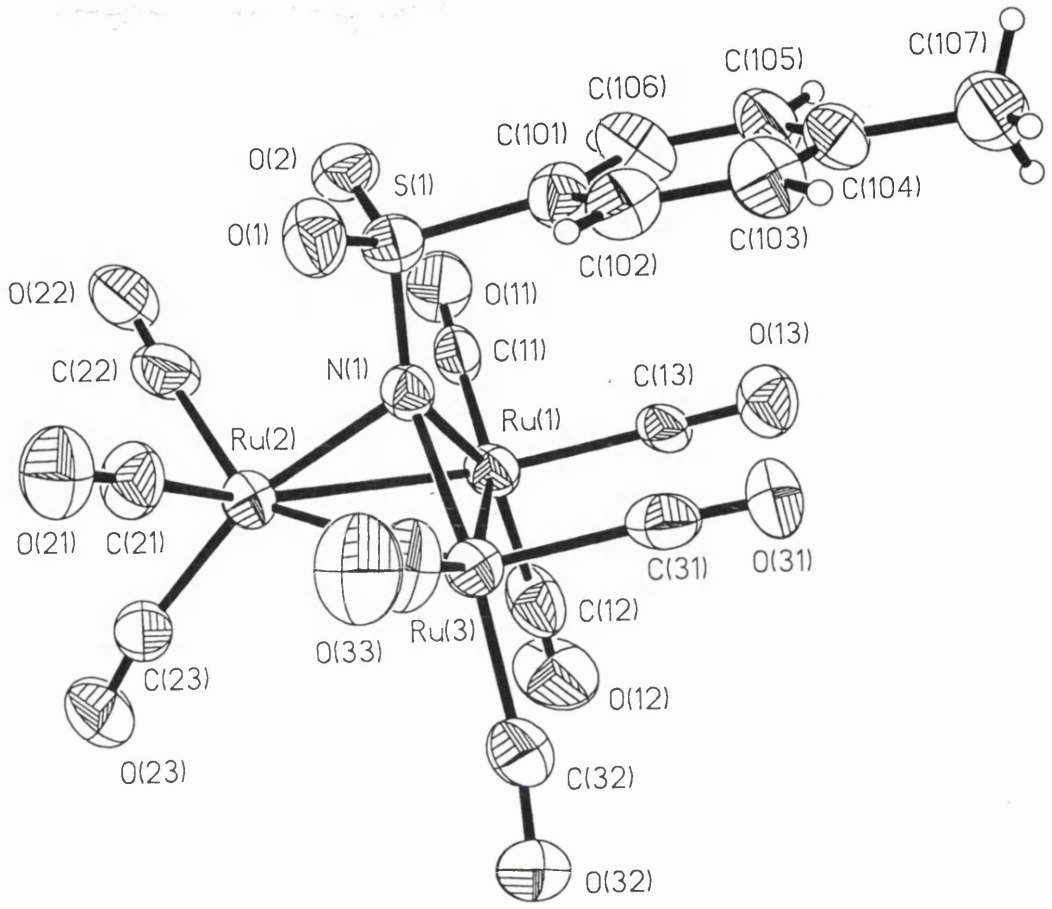

Fig. 2.2 The X-ray structure of $[Ru_3(\mu\text{-}H)_2(\mu_3\text{-}NTs)(CO)_9]$ 8

Table 2.1 Selected bond lengths (Å) and angles (°) for 8

Ru(1)-N(1)	2.109(13)	Ru(3)-N(1)	2.104(12)
Ru(1)-Ru(3)	2.751(2)	N(1)-S(1)	1.634(13)
Ru(1)-Ru(2)	2.847(2)	S(1)-O(2)	1.466(13)
Ru(2)-N(1)	2.116(12)	S(1)-O(1)	1.473(13)
Ru(2)-Ru(3)	2.859(2)	S(1)-C(101)	1.78(2)
N(1)-Ru(1)-Ru(3)	49.2(3)	Ru(3)-N(1)-Ru(1)	81.5(5)
N(1)-Ru(1)-Ru(2)	47.7(3)	S(1)-N(1)-Ru(2)	121.6(7)
Ru(3)-Ru(1)-Ru(2)	61.38(5)	Ru(3)-N(1)-Ru(2)	85.3(5)
N(1)-Ru(2)-Ru(1)	47.5(3)	Ru(1)-N(1)-Ru(2)	84.8(5)
N(1)-Ru(2)-Ru(3)	47.2(3)	O(2)-S(1)-O(1)	118.5(8)
Ru(1)-Ru(2)-Ru(3)	57.65(5)	O(2)-S(1)-N(1)	107.6(7)
N(1)-Ru(3)-Ru(1)	49.3(4)	O(1)-S(1)-N(1)	108.7(7)
N(1)-Ru(3)-Ru(2)	47.5(3)	O(2)-S(1)-C(101)	108.8(8)
Ru(1)-Ru(3)-Ru(2)	60.97(5)	O(1)-S(1)-C(101)	109.1(8)
S(1)-N(1)-Ru(3)	133.3(7)	N(1)-S(1)-C(101)	103.1(7)
S(1)-N(1)-Ru(1)	133.4(7)		

Consistent with this argument, the Ru-Ru-C angles to equatorial CO ligands are larger when there is a hydride on that Ru-Ru edge. The tolyl ring of the Ts group is bent over one of the Ru-Ru bonds, that with no bridging hydride. The Ru-N bonds are slightly (about 0.04 Å) longer in the NTs compound **8** than in the analogous NPh cluster **2** (Table 2.2),[106] which could be due to the electron-withdrawing effect of the SO_2 group making the Ru-N bond in the NTs cluster slightly weaker.

Table 2.2 Comparison of Ru-N bond lengths (Å) between 2 and 8

	$[Ru_3(\mu\text{-}H)_2(\mu_3\text{-}NPh)(CO)_9]$[106] **2**	*$[Ru_3(\mu\text{-}H)_2(\mu_3\text{-}NTs)(CO)_9]$* **8**
Ru(1)-N(1)	2.072(4)	2.109(13)
Ru(2)-N(1)	2.074(4)	2.116(12)
Ru(3)-N(1)	2.059(4)	2.104(12)

The ^{1}H NMR spectrum of **10** shows a doublet at δ -14.39 assigned to the hydride ligand coupled to the NH proton (J = 1.3 Hz), a singlet at δ 2.48 for the Me group of the NTs ligand, a broad signal at δ 5.73 for the NH group and an AA'BB' pattern for the tolyl ring at δ 7.41 and 7.81. The positive ion FAB mass spectrum showed a molecular ion peak at m/z 754 and daughter ions due to the successive loss of 10 CO ligands.

2.3.2 Reaction of $[Os_3(CO)_{12}]$ with *p*-toluenesulfonamide

Treatment of $[Os_3(CO)_{12}]$ with *p*-toluenesulfonamide in refluxing octane for 7 days gave four isolable products, two of which remain unidentified, a pale brown solid and a yellow solid. The other two compounds were found to be $[Os_3(\mu\text{-}H)(\mu\text{-}$

NHTs)$(CO)_{10}$] **7**, a yellow solid obtained in 4% yield, and [$Os_3(\mu\text{-}H)_2(\mu_3\text{-}NTs)(CO)_9$] **11** a cream solid formed in 56% yield. The cluster **7** has been prepared previously by Churchill *et al.*,[103] although it was prepared following a different procedure. As stated earlier the IR spectra of these clusters in the CO region show a shift to higher wavenumber when compared to the phenylimido and amido clusters. The ^{1}H NMR spectrum of **11** shows a singlet at δ -18.74 for the hydride ligands, a singlet at δ 2.46 assigned to the Me group of the NTs ligand and an AA'BB' pattern for the tolyl ring at δ 7.35 and 7.79. The positive FAB mass spectrum showed a molecular ion peak at m/z 995 and daughter ions due to the successive loss of 9 CO ligands.

2.3.3 Thermolysis of [$Ru_3(\mu\text{-}H)_2(\mu_3\text{-}NTs)(CO)_9$] 8

One method to form higher nuclearity carbonyl clusters is by the simple pyrolysis of a lower nuclearity cluster in a high boiling solvent. The cluster **8** was refluxed in octane for $7^1/_2$ hours. The reaction was monitored by IR spectroscopy, which showed complete conversion of **8** to a cluster of apparent formula [{$Ru_3(\mu\text{-}H)_2(\mu_4\text{-}NTs)(CO)_7$}$_2$] **9**. This was identified from its elemental analysis, and the positive FAB mass spectrum exhibits a molecular ion peak at m/z 1341 and daughter ions due to the successive loss of fourteen CO ligands. This compound is also formed during the preparation of **8** after prolonged reaction (Section 2.3.1). The ^{1}H NMR spectrum of **9** shows the presence of isomers; an attempt to separate them by TLC proved unsuccessful. The hydride region of the spectrum shows eight hydride doublets (Fig. 2.3a) and there are also four sets of Me and tolyl signals (Fig. 2.3b). The loss of four CO ligands results in an electron deficient cluster; the donation of electrons from the oxygen atoms of the SO_2 group or metal-metal bonding are two ways in which the

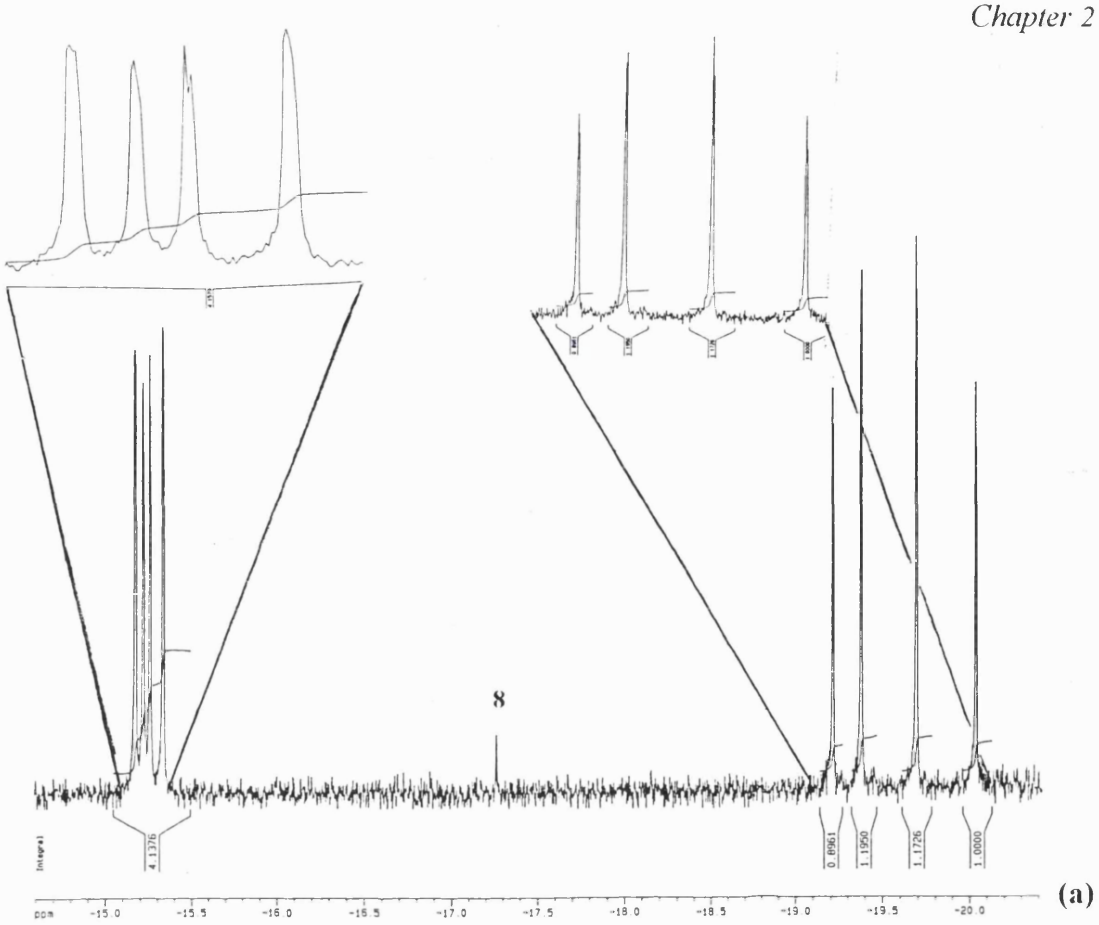

Fig. 2.3 The ^{1}H NMR spectrum of [{$Ru_3(\mu\text{-}H)_2(\mu_4\text{-}NTs)(CO)_7$}$_2$] 9 in (a) the hydride region and (b) at δ = 2 – 8 ppm

deficit could be rectified. The ν(S=O) absorptions in the IR spectrum occur at 1146 (m) and 1086 (m) cm^{-1} in **8** and at 1105 (m), 1030 (m) and 1012 (m) cm^{-1} for **9**, suggesting that **9** is less symmetrical than **8**, and that the S=O bonds have been weakened by electron donation as shown by the decrease in wavenumber. The isomerism could arise from the different modes of coordination of the oxygen atoms of the SO_2 group (Figs. 2.4a and b). If one oxygen atom is the electron donor

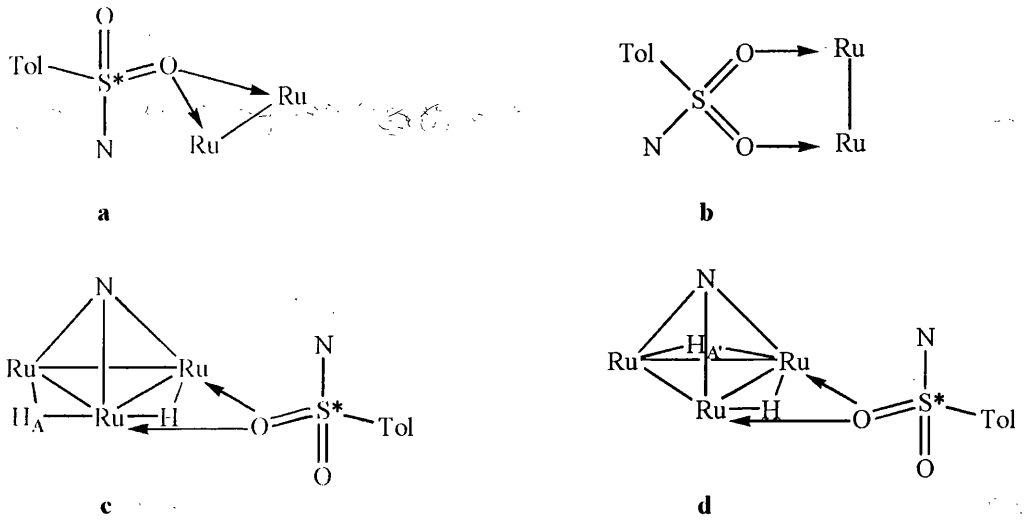

Fig. 2.4 The different possible isomers of 9

(Fig. 2.4a), a chiral sulfur atom and also chiral cluster units result, which could give rise to a number of isomers. Alternatively, both oxygen atoms could coordinate to the ruthenium atoms as shown in Fig. 2.4b, but this gives a symmetrical cluster and is not consistent with the ^1H NMR spectrum. Isomerism can also arise from the position of the bridging hydride ligands (Figs. 2.4c and d). From the ^1H NMR spectrum it appears that there are two isomers, in an approximate 1:1 ratio, in which the four hydride ligands and the two triruthenium units in each isomer are inequivalent. Alternatively there may be four isomers, in an approximate 1:1:1:1 ratio, which have two pairs of hydride ligands and two triruthenium units in each isomer that are equivalent. The nature of bonding in these isomers is extremely speculative.

Unfortunately, no single crystals were obtained, even after many crystallisation attempts, and without a single-crystal determination we believe it will not be possible to establish the structure.

2.3.4 Protonation reactions

We carried out protonation and deprotonation studies to test the difference between Ph and Ts as substituents. Our expectation was that the ability to protonate NR containing clusters at the metal should be inversely related to the ability to deprotonate the NHR clusters. Likewise, the more difficult to deprotonate the NHR clusters the more nucleophilic would be the NR ligand so generated. Our results presented in the following sections largely support these ideas.

The cluster $[Ru_3(\mu\text{-}H)_2(\mu_3\text{-}NPh)(CO)_9]$ **2** was prepared using literature procedures, in 98% yield, by hydrogenation of $[Ru_3(\mu_3\text{-}NPh)(\mu_3\text{-}CO)(CO)_9]$ **3**, itself formed from $[Ru_3(CO)_{12}]$ and nitrosobenzene.[97,106] The compounds **2**, **8**, and $[Os_3(\mu\text{-}H)_2(\mu_3\text{-}NTs)(CO)_9]$ **11** in solutions of dichloromethane were treated with an excess of tetrafluoroboric acid ($HBF_4.Et_2O$). Immediate reactions occurred in all cases, which was confirmed by the change in the IR spectra with shifts of ν(CO) to higher wavenumbers indicative of the formation of cations. All IR spectra simplified upon protonation (Table 2.3), consistent with the formation of the trihydride clusters $[M_3(\mu\text{-}H)_3(\mu_3\text{-}NR)(CO)_9][BF_4]$ (where M = Ru, R = Ph **12a** or Ts **13a**, M = Os, R = Ts **14a**) with local C_{3v} symmetry.

The clusters **2**, **8** and **11**, in $CDCl_3$ were treated with an excess of trifluoroacetic acid. The reactions were monitored by ^1H NMR spectroscopy, again rapid conversion to a

new product being observed. The ^{1}H NMR spectra in all cases confirm the formation of trihydride products, as a new hydride singlet appears with an integral ratio of three in each case (Table 2.3). As **2** and **8** were protonated, the signals in the ^{1}H NMR spectrum for the starting materials gradually decreased on addition of acid, while the signals for the protonated complex increased in intensity.

Table 2.3 A comparison of IR and ^{1}H NMR spectroscopy data for the protonated complexes

Protonated Compound	*ν(CO)/cm^{-1}*	*δ(^{1}H NMR)*
$[Ru_3(\mu\text{-}H)_3(\mu_3\text{-}NPh)(CO)_9]^+$ **12a and 12b from 2**	2126 (s), 2077 (m).	-17.43 (s, 3H, Ru-*H*), 7.29-7.39 (m, 5H, Ph).
$[Ru_3(\mu\text{-}H)_3(\mu_3\text{-}NTs)(CO)_9]^+$ **13a and 13b from 8**	2136 (s), 2092 (m).	–17.88 (s, 3H, Ru-*H*), 2.51 (s, 3H, C*H*$_3$), 7.53 (d, 2H, *J* = 8.1 Hz, Ar), 7.95 (d, 2H, *J* = 8.1 Hz, Ar).
$[Os_3(\mu\text{-}H)_3(\mu_3\text{-}NTs)(CO)_9]^+$ **14a and 14c from 11**	2155 (w), 2133 (s), 2082 (m).	-18.65 (s, 3H, Os-*H*), 2.53 (s, 3H, Me), 7.54 (d, 2H, *J* = 8.2 Hz, Ar), 7.95 (d, 2H, *J* = 8.1Hz, Ar).

The cluster **11** protonates slowly, with the ^{1}H NMR signals for **11** broadening, and broad signals corresponding to an intermediate are observed to overlap with these signals. In addition, signals due to the final protonated cluster were also observed (Fig. 2.5b). On further addition of acid, the signals for the intermediate complex sharpened, with chemical shifts very similar to those for **11**. The peaks for **11**

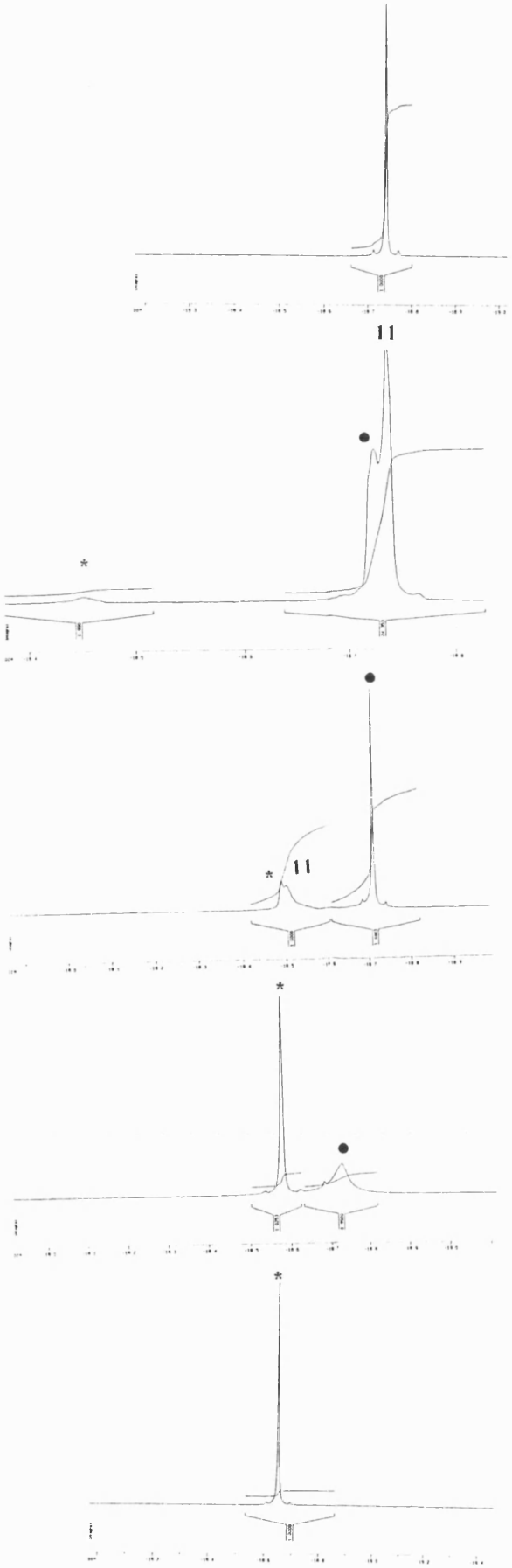

(a) ^{1}H NMR spectrum of 11

(b) 5 equivalents of CF_3CO_2H

(c) 2 drops of CF_3CO_2H

(d) 3 drops of CF_3CO_2H

● = Intermediate

* = Final product

(e) Several drops of CF_3CO_2H

Fig. 2.5 ^{1}H NMR spectra obtained on protonation of 11 (in the hydride region)

broadened and shifted, overlapping the signals for the final product (Fig. 2.5c). The peaks for the intermediate complex then broadened and the signals for the final product increased in intensity on addition of excess acid (Fig. 2.5d), until the peaks for the intermediate complex disappeared and there was clean formation of the final trihydride cluster (Fig. 2.5e). ^{1}H NMR experiments indicate that the tosylimido clusters require more acid for complete protonation than the phenylimido cluster. This is expected because of the electron-withdrawing effect of the tosyl group, which makes the metal atoms less basic and less susceptible to electrophilic attack.

The compound formed on protonation of **2** is likely to be $[Ru_3(\mu\text{-}H)_3(\mu_3\text{-}NPh)(CO)_9][CF_3CO_2]$ **12b**, but on protonation of **8,** as there is such an excess of acid present, the compound formed may be $[Ru_3(\mu\text{-}H)_3(\mu_3\text{-}NTs)(CO)_9][CF_3CO_2\text{-}H\text{-}O_2CCF_3]$ **13b**.

It is tentatively suggested that the intermediate cluster formed on protonation of **11** is of the form $[Os_3(\mu\text{-}H)_3(\mu_3\text{-}NTs)(CO)_9][CF_3CO_2]$ **14b**, which is initially in equilibrium with **11** (Scheme 2.5). Addition of excess acid could then result in an equilibrium between **14b** and the final product $[Os_3(\mu\text{-}H)_3(\mu_3\text{-}NTs)(CO)_9][CF_3CO_2\text{-}H\text{-}O_2CCF_3]$ **14c**.

2.3.5 Deprotonation reactions

Bhaduri *et al.*[107] studied the deprotonation of the cluster $[Ru_3(\mu\text{-}H)(\mu\text{-}NHPh)(CO)_{10}]$ **1**. They found that deprotonation occurs at the nitrogen atom to leave a lone pair of

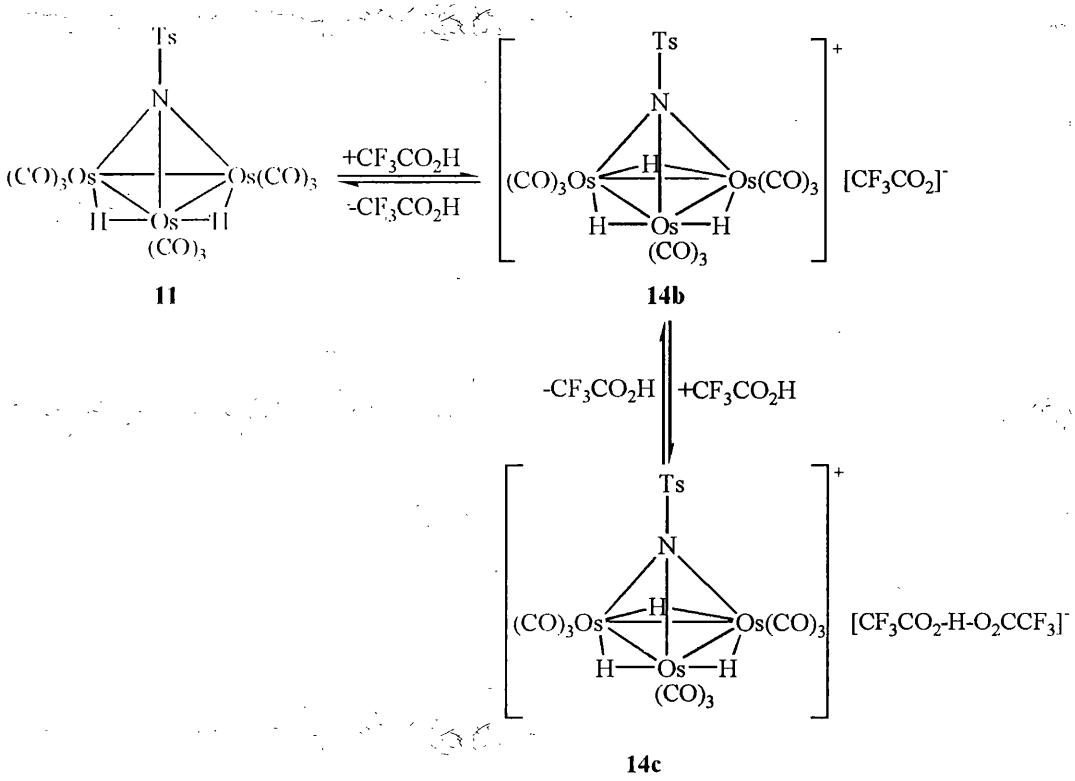

11 **14b** **14c**

Scheme 2.5 The protonation of 11

electrons that attacks an axial CO ligand on the adjacent ruthenium atom, to form a cluster with a μ_3-bound phenyl isocyanate **15** (Scheme 2.6). In solution **15** undergoes irreversible loss of CO to form $[Ru_3(\mu\text{-}H)(\mu_3\text{-}NPh)(CO)_9]^-$ **16**.

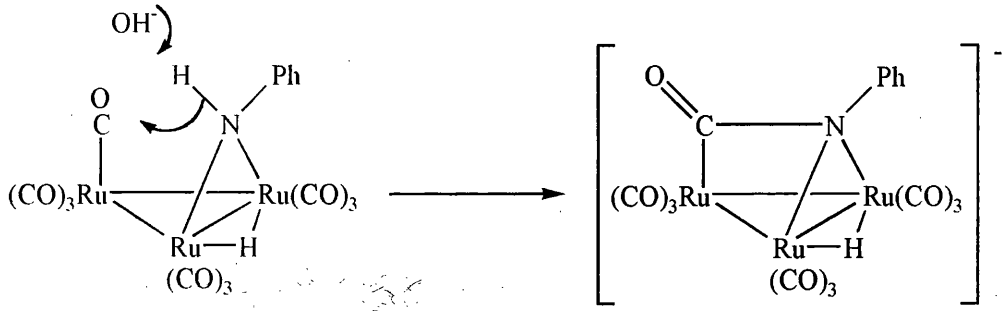

1 **15**

Scheme 2.6 The deprotonation of 1

The cluster $[Os_3(\mu\text{-}H)(\mu\text{-}NHPh)(CO)_{10}]$ **5** was prepared using a literature procedure, by direct thermal reaction of $[Os_3(CO)_{12}]$ with aniline, in 66% yield.[95] Deprotonation

experiments were then carried out on this cluster along with $[Os_3(\mu\text{-}H)(\mu\text{-}NHTs)(CO)_{10}]$ **7** and $[Ru_3(\mu\text{-}H)(\mu\text{-}NHTs)(CO)_{10}]$ **10**.

Dichloromethane solutions of the compounds **10**, **5** and **7** were treated with an excess of DBU (1,8-diazabicyclo[5.4.0]undec-7-ene). Immediate reactions occurred in all cases, apparent from changes in the IR spectra. The IR spectra of the deprotonated compounds formed from **10** and **5** are similar to that of the isocyanate **15** (Table 2.4).

Table 2.4 A comparison of IR spectroscopy data for the deprotonated complexes

Deprotonated Compound	*ν(CO)/cm^{-1}*
$[PPN][Ru_3(\mu\text{-}H)(\mu_3\text{-}PhNCO)(CO)_9]$[107] **15**	2066 (w), 2034 (s), 2006 (s), 1980 (s, br), 1928 (w, sh), 1610 (m, br).
$[PPN][Ru_3(\mu\text{-}H)(\mu_3\text{-}NPh)(CO)_9]$[107] **16**	2054 (w), 2026 (s), 1994 (s), 1966 (s, br), 1915 (w, sh)
$[HDBU][Ru_3(\mu\text{-}H)(\mu_3\text{-}TsNCO)(CO)_9]$ **17 from 10**	2070 (w), 2043 (s), 2011 (s), 1976 (s), 1942 (m, sh).
$[HDBU][Os_3(\mu\text{-}H)(\mu_3\text{-}PhNCO)(CO)_9]$ **18 from 5**	2069 (s), 2046 (s), 2036 (m, sh), 2007 (s), 1982 (s), 1938 (w), 1916 (w).
$[HDBU][Os_3(\mu\text{-}H)(\mu\text{-}NTs)(CO)_{10}]$ **19a from 7**	2095 (w), 2053 (s), 2042 (m, sh), 2005 (s), 1980 (m, sh), 1959 (m, sh).

However, the IR spectrum of the deprotonated compound formed from **7** is very different to that of the isocyanate compound. This cannot simply be accounted for by the increase in wavenumber in the CO region of the IR spectrum for the tosylimido clusters relative to those for the phenylimido clusters.

The clusters **5** and **7**, in $CDCl_3$, were each treated with a ten-fold excess of DBU. The reactions were monitored by ^1H NMR spectroscopy. The ^1H NMR spectra obtained in the deprotonation studies on the osmium clusters show, in both cases, deprotonation at nitrogen, with the gradual loss of the NH signal and the appearance of a new hydride peak as well as new signals in the aromatic region (Table 2.5).

Table 2.5 A comparison of ^1H NMR data for 18 and 19c

Deprotonated Compound	*δ (^1H NMR)*
[HDBU][Os_3(μ-H)(μ$_3$-PhNCO)(CO)$_9$] **18 from 5**	-15.21 (s, 1H, Os-*H*), 6.65 (d, 2H, *J* = 7.0 Hz, *o*-$H_2C_6H_3$), 7.03 (t, 1H, *J* = 6.6 Hz, *p*-HC_6H_4), 7.12 (m, 2H, *J* = 6.5 Hz, *m*-$H_2C_6H_3$).
[DBUH...OH_2][Os_3(μ-H)(μ-NTs)(CO)$_{10}$] **19c from 7**	-15.51 (s, 1H, Os-*H*), 2.33 (s, 3H, CH_3), 7.13 (d, 2H, *J* = 8.0 Hz, Ar), 7.71 (d, 2H, *J* = 8.2 Hz, Ar).

As cluster **5** is deprotonated, the signals in the ^1H NMR spectrum for the starting material gradually decrease on addition of base, while the signals for the deprotonated complex increase in intensity. However, this observation does not confirm whether or not attack at the CO ligand has occurred.

On addition of 1 equivalent of DBU to **7**, the hydride doublet in the ^1H NMR spectrum becomes a singlet and the NH signal disappears, but there is little deviation of chemical shift when compared to those for **7** (Fig. 2.6b). A further 4 equivalents of DBU were added resulting in another two sets of signals appearing, one very broad

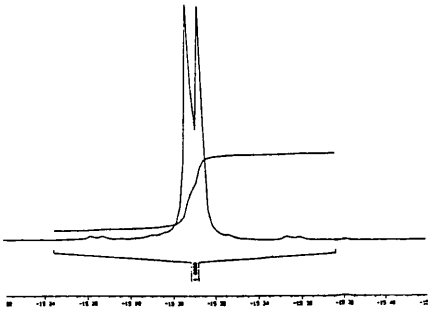

(a) ^{1}H NMR spectrum of 7

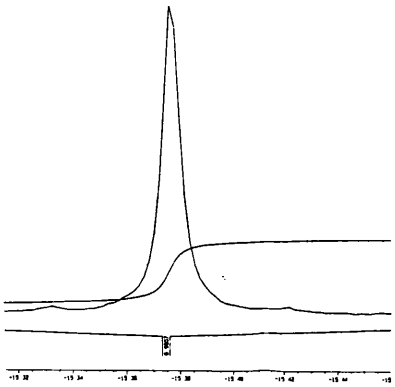

(b) 1 equivalent of DBU

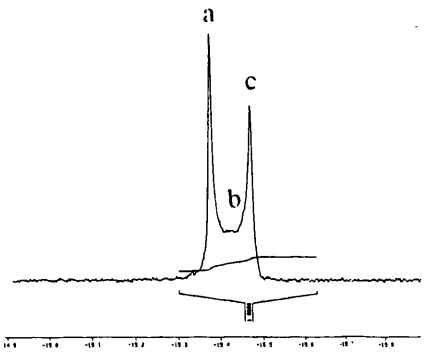

(c) 5 equivalents of DBU

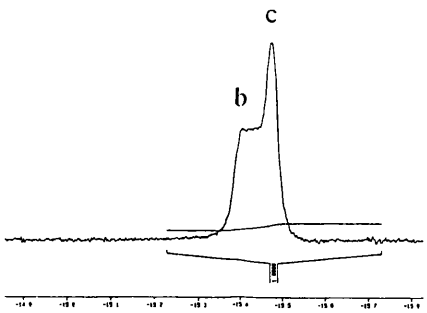

(d) 10 equivalents of DBU

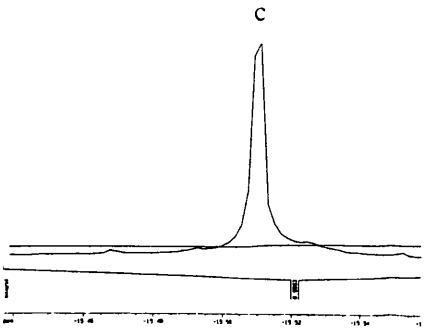

a = **19a**

b = **19b**

c = **19c**

(e) After 10 days

Fig. 2.6 ^{1}H NMR spectra obtained on deprotonation of 7 (in the hydride region).

set and the other very sharp (Fig. 2.6c). After a total of 10 equivalents of DBU had been added, the initial signals formed on addition of 1 equivalent of DBU had disappeared, leaving only the second set of signals (Fig. 2.6d). On leaving the solution for 10 days, the broad set of signals had disappeared, leaving only the sharp signals. The IR spectrum of this product was identical to that of **19a** (Fig. 2.6e).

On deprotonation with 1 equivalent of DBU there is evidence for deprotonation at the nitrogen atom and it is likely that this is the hydrogen bonded compound **19a** (see later) in equilibrium with 7 (Scheme 2.7). Addition of excess DBU forms another two

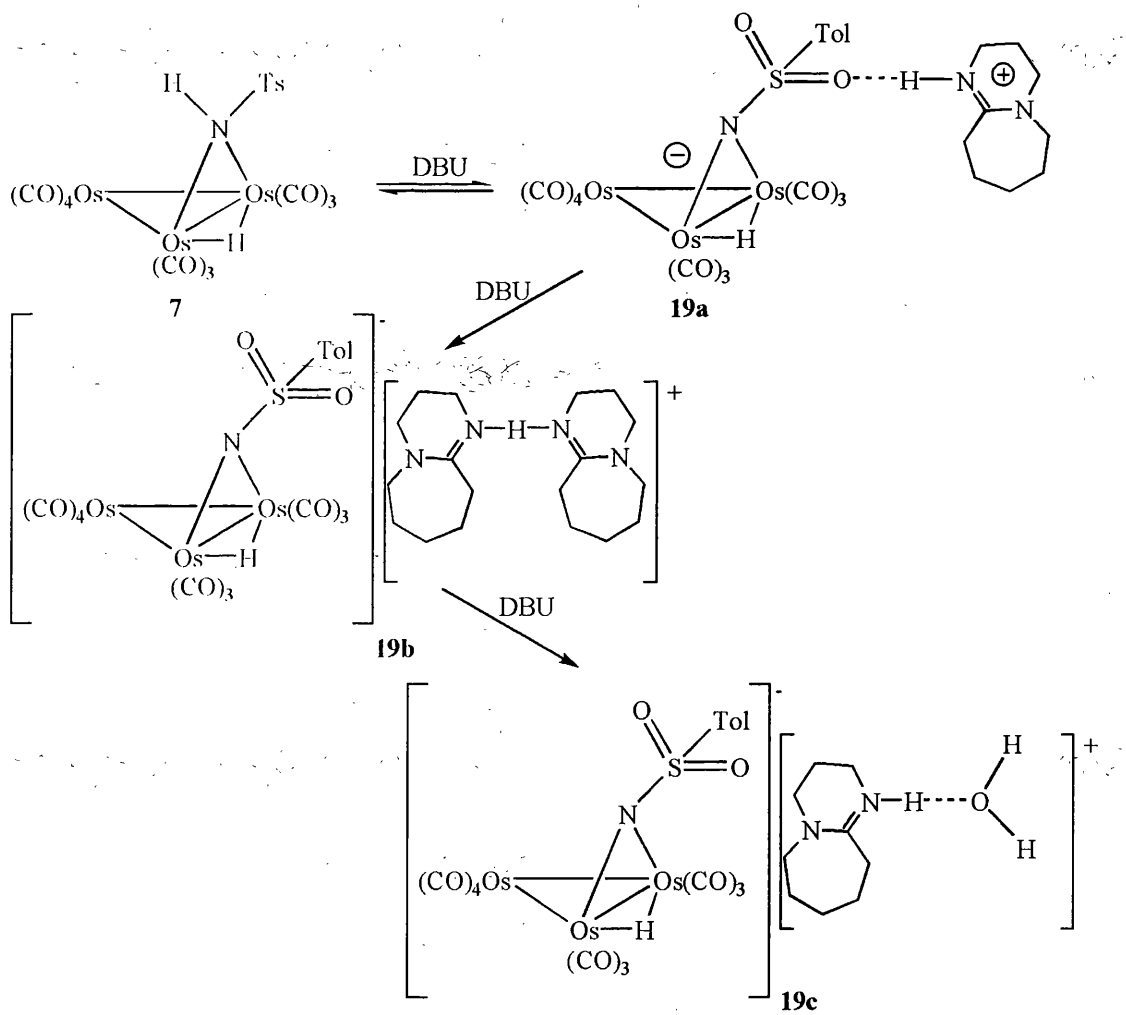

Scheme 2.7 The deprotonation of 7

complexes. The first is speculated to be the non-hydrogen bonded complex [DBU-H-DBU][$Os_3(\mu\text{-}H)(\mu\text{-}NTs)(CO)_{10}$] **19b**. The second is believed to be a complex with the cation hydrogen bonded to water [DBUH...OH_2][$Os_3(\mu\text{-}H)(\mu\text{-}NTs)(CO)_{10}$] **19c**, which could be formed over a period of time as the NMR sample absorbed water. Changes in the cation are not likely to affect the cluster core, consistent with no change in the IR spectrum.

Single crystals of the deprotonated cluster formed from **7** were grown by deprotonating this cluster with triethylamine in a diethyl ether solution, which was then layered with hexane and the diethyl ether allowed to evaporate. An IR spectrum of the crystals obtained showed a mixture of the starting material and the deprotonated cluster. Re-dissolving the crystals in dichloromethane and running an IR spectrum showed complete conversion of the deprotonated complex to the starting material. However, a crystal structure of the deprotonated cluster [$HNEt_3$][$Os_3(\mu\text{-}H)(\mu\text{-}NTs)(CO)_{10}$] **19d** was obtained, which is shown in Fig. 2.7, with selected bond lengths and angles given in Table 2.6.

The structure shows attack at CO has not occurred, consistent with the nucleophilicity of the nitrogen atom of the tosylimido group being less than that of the phenylimido group. A hydrogen bond is formed between one of the oxygen atoms of the SO_2 group and the proton on $[HNEt_3]^+$. Comparison with the structure of the starting material (Fig. 2.8), obtained by Churchill *et al.*[103] shows the distance between the nitrogen atom and the axial CO ligand on Os(3) has decreased upon deprotonation (Table 2.7).

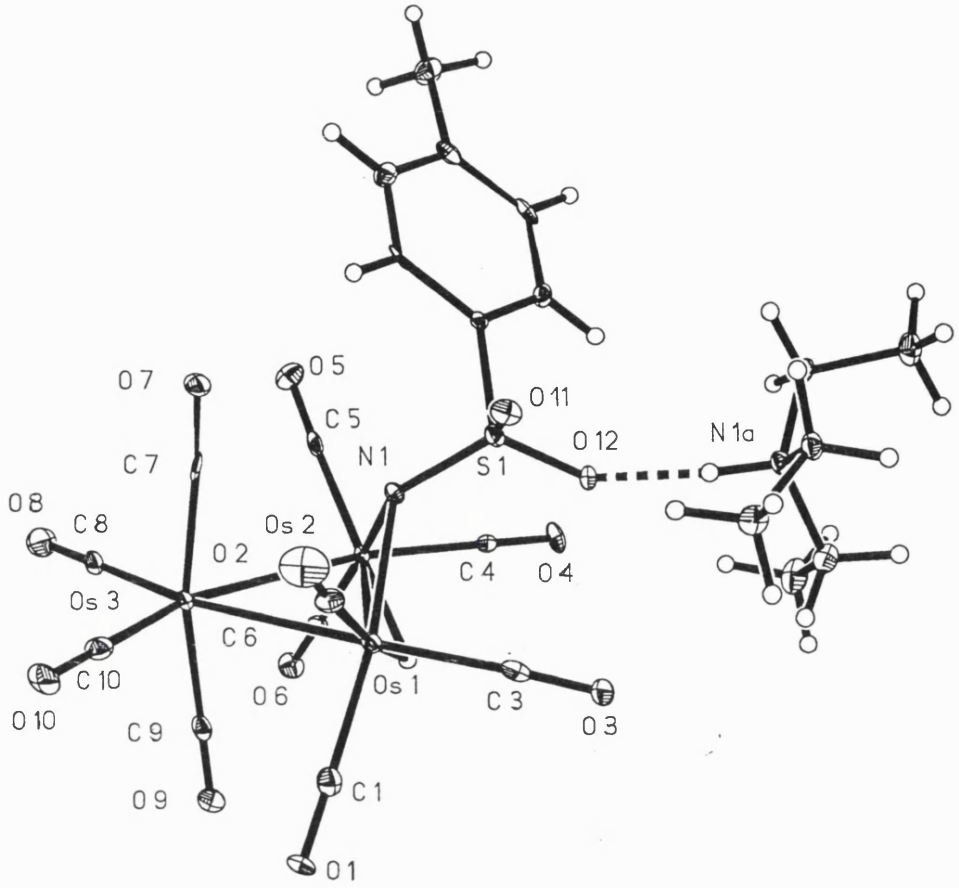

Fig. 2.7 The X-ray structure of $[HNEt_3][Os_3(\mu\text{-}H)(\mu\text{-}NTs)(CO)_{10}]$ 19d

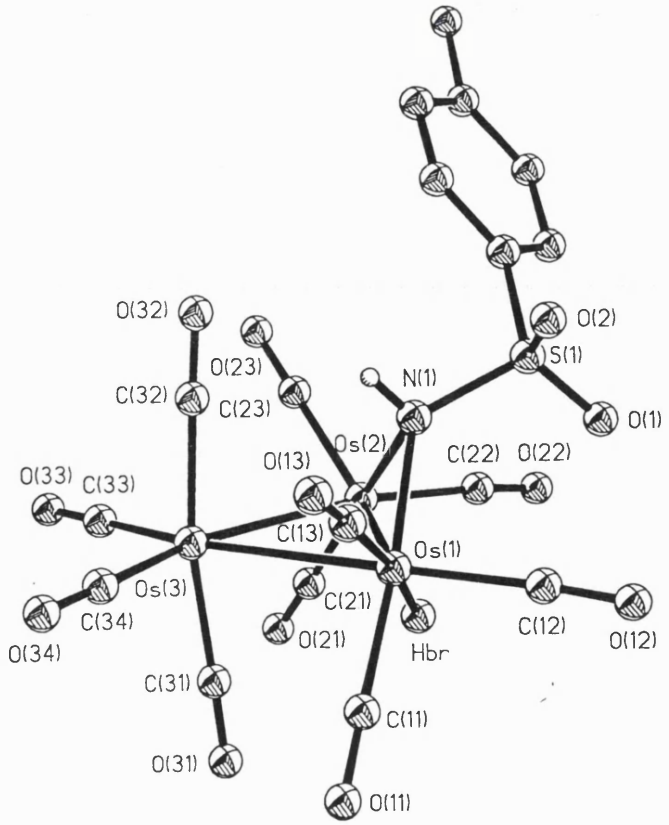

Fig. 2.8 The structure of $[Os_3(\mu\text{-}H)(\mu\text{-}NHTs)(CO)_{10}]$ 7

Table 2.6 Selected bond lengths (Å) and angles (°) for 19d

Os(1)-N(1)	2.118(5)	S(1)-O(11)	1.460(4)
Os(1)-Os(2)	2.8113(3)	S(1)-O(12)	1.473(4)
Os(1)-Os(3)	2.8437(4)	S(1)-N(1)	1.557(5)
Os(2)-N(1)	2.106(5)	S(1)-C(11)	1.781(6)
Os(2)-Os(3)	2.8496(3)		
N(1)-Os(1)-Os(2)	48.10(12)	O(11)-S(1)-C(11)	107.4(2)
N(1)-Os(1)-Os(3)	79.79(14)	O(12)-S(1)-C(11)	104.6(3)
C(5)-Os(2)-N(1)	95.6(2)	N(1)-S(1)-C(11)	104.3(3)
C(6)-Os(2)-N(1)	167.0(2)	S(1)-N(1)-Os(2)	125.5(3)
C(4)-Os(2)-N(1)	96.7(2)	S(1)-N(1)-Os(1)	120.0(3)
N(1)-Os(2)-Os(1)	48.46(13)	Os(2)-N(1)-Os(1)	83.4(2)
N(1)-Os(2)-Os(3)	79.83(14)	C(5A)-N(1A)-C(1A)	111.4(5)
O(11)-S(1)-O(12)	112.1(3)	C(5A)-N(1A)-C(3A)	111.6(5)
O(11)-S(1)-N(1)	111.0(3)	C(1A)-N(1A)-C(3A)	113.5(5)
O(12)-S(1)-N(1)	116.6(3)		

Table 2.7 Comparison of bond lengths (Å) and angles (°) of clusters 7 and 19d

	$Os_3(\mu\text{-}H)(\mu\text{-}NHTs)(CO)_{10}$[103] **7**	*$[Os_3(\mu\text{-}H)(\mu\text{-}NTs)(CO)_{10}]^-$* **19d**
Os-Os	2.814(1), 2.858(1), 2.847(1)	2.8113(3), 2.8437(4), 2.8496(3)
Os-N	2.162(7), 2.145(7)	2.118(5), 2.106(5)
N-S	1.679(7)	1.557(5)
S-O	1.434(6), 1.420(7)	1.460(4), 1.473(4)
Os-N-Os	81.6(2)	83.4(2)
Os-N-S	120.1(4), 125.3(4)	120.0(3), 125.5(3)
N...CO	2.937	2.687
Dihedral angle Os(1)Os(2)Os(3)-Os(1)Os(2)N(1)	108.2	103.5

The Os-N and N-S distances have decreased on deprotonation, while the S-O distances have increased as would be expected with the increased π-delocalisation on to the SO anti-bonding orbitals.

The dihedral angle Os(1)Os(2)Os(3)-Os(1)Os(2)N(1) decreases on deprotonation from 108.2° to 103.5° again indicating slight movement of the nitrogen atom towards the carbonyl ligand. If the N atom had become planar on deprotonation, the sum of the Os-N-Os and Os-N-S angles would be 360°, as in the high-valent compound $[\{Mo(\eta\text{-}C_5H_4Me)(NPh)(\mu\text{-}NPh)\}_2]$ where the angles around the N atom of the μ-NPh ligands total 359.8° implying the imido moiety has significant π-donor character.[108] The sum of these angles in the starting material is 327.0° and this changes to 328.9° for the deprotonated cluster. Therefore the N atom remains pyramidal as this is a low valent cluster and there are no suitable π-acceptor orbitals on the osmium atoms to accommodate the negative charge at nitrogen formed on deprotonation. The torsional angles along the N-S bond have not changed significantly upon deprotonation (Table 2.8), again indicating the hybridisation at the N atom remains substantially unchanged.

Table 2.8 Comparison of torsional (°) angles along the N-S bond of clusters 7 and 19d

	$[Os_3(\mu\text{-}H)(\mu\text{-}NHTs)(CO)_{10}]$ **7**	$[Os_3(\mu\text{-}H)(\mu\text{-}NTs)(CO)_{10}]^-$ **19d**
Os(1)N(1)S(1)O	61.9, 68.7	64.7, 65.2
Os(1)N(1)S(1)C(tol)	176.7	179.4
Os(2)N(1)S(1)O	39.8, 170.4	39.8, 169.7
Os(2)N(1)S(1)C(tol)	75.0	74.9

The results of the protonation and deprotonation studies highlight the different influences that the Ph and Ts groups have on the nucleophilicity and acidity of the clusters. The compound $[Ru_3(\mu\text{-}H)_2(\mu_3\text{-}NPh)(CO)_9]$ **2** is protonated much more easily

than either $[Ru_3(\mu\text{-}H)_2(\mu_3\text{-}NTs)(CO)_9]$ **8** or $[Os_3(\mu\text{-}H)_2(\mu_3\text{-}NTs)(CO)_9]$ **11**. In all cases protonation occurs at the metal-metal bond that is not bridged by a hydride ligand. However when NTs was the ligand, a greater concentration of acid was required during the NMR study indicating that the NTs ligand makes the cluster less nucleophilic at the metal core than the NPh ligand does. These observations are totally consistent with the accepted view that the $MeC_6H_4SO_2$ group is strongly electron withdrawing.

Deprotonation studies show that $[Ru_3(\mu\text{-}H)(\mu\text{-}NHPh)(CO)_{10}]$ **1** and $[Os_3(\mu\text{-}H)(\mu\text{-}NHPh)(CO)_{10}]$ **5** lead to NPh ligands which nucleophilically attack an axial CO ligand on an adjacent metal atom, generating μ_3-PhNCO systems. This also appears to be the case for $[Ru_3(\mu\text{-}H)(\mu\text{-}NHTs)(CO)_{10}]$ **10**, although for the osmium analogue **7**, the X-ray structure of $[HNEt_3][Os_3(\mu\text{-}H)(\mu\text{-}NTs)(CO)_{10}]$ **19d** shows that nucleophilic attack at the CO ligand has not occurred. This is consistent with the negative charge being delocalised onto the Ts group, making the nitrogen atom more acidic than is the case with the Ph group. This final result also indicates that the nucleophilicity of the μ-NR groups is greater for ruthenium than osmium.

2.4 CONCLUSIONS

- The new clusters $[M_3(\mu\text{-}H)_2(\mu_3\text{-}NTs)(CO)_9]$ (M = Ru or Os) and $[Ru_3(\mu\text{-}H)(\mu\text{-}NHTs)(CO)_{10}]$, may be prepared by thermal treatment of the parent clusters $[Ru_3(CO)_{12}]$ and $[Os_3(CO)_{12}]$ with *p*-toluenesulfonamide.
- The cluster $[Ru_3(\mu\text{-}H)_2(\mu_3\text{-}NTs)(CO)_9]$ can be decarbonylated thermally to form an aggregate of two clusters.

- The clusters $[M_3(\mu\text{-H})_2(\mu_3\text{-NTs})(CO)_9]$ are less susceptible to electrophilic attack than the corresponding phenylimido clusters.
- Deprotonation of $[Os_3(\mu\text{-H})(\mu\text{-NHPh})(CO)_{10}]$ and $[Ru_3(\mu\text{-H})(\mu\text{-NHTs})(CO)_{10}]$ give anionic μ_3-RNCO species as with $[Ru_3(\mu\text{-H})(\mu\text{-NHPh})(CO)_{10}]$. In contrast, the tosylamido complex $[Os_3(\mu\text{-H})(\mu\text{-NHTs})(CO)_{10}]$ is easily deprotonated to give an anionic cluster with a pyramidal μ-imido ligand. The anionic charge being delocalised on to the $CH_3C_6H_4SO_2$ group, decreasing the nucleophilicity of the imido nitrogen atom.

2.5 EXPERIMENTAL

2.5.1 Materials and Instrumentation

All thermal reactions were carried out under N_2 using standard Schlenk line techniques unless otherwise specified. All solvents and reagents were obtained were obtained from commercial sources and used without further purification except for $[Os_3(CO)_{12}]$, which was prepared by treating a solution of $[OsO_4]$ in ethanol with CO (75 bar) at 230 °C. Column chromatography was carried out using BDH Kieselgel (40-63 μm) silica; TLC was carried out on Merck pre-coated Kieselgel 60 F_{254} silica plates.

All IR spectra were recorded using a CaF_2 solution cell on a Nicolet 205 FTIR spectrometer, using light petroleum spirit (b.p. 40-60 °C) as the reference solvent, unless otherwise stated. NMR spectra were recorded on a Bruker AC300 or AMX400 spectrometer using deuterated chloroform $CDCl_3$ (δ 7.27) as the internal reference. FAB mass spectra were acquired by the departmental service at University College

London (UCL) on a VG ZAB-SE spectrometer (*m*-nitrobenzyl alcohol matrix). Elemental analyses were carried out by the departmental service at UCL. The X-ray structure of $[Ru_3(\mu\text{-}H)_2(\mu_3\text{-}NTs)(CO)_9]$ was obtained by Professor A. J. Deeming at UCL. X-ray data were collected at room temperature using a Nicolet R3v/m diffractometer, with crystals mounted in air. The structure was solved by direct methods and refined using (SHELXL-97) with all non-hydrogen atoms anisotropic and with hydrogen atoms included using a riding model. The X-ray structure of $[HEt_3N][Os_3(\mu\text{-}H)(\mu\text{-}NTs)(CO)_{10}]$ was obtained by Dr. J. W. Steed at King's College London using a Nonius Kappa CCD equipped area detector diffractometer. A suitable crystal was mounted in an oil droplet solidified at $T = 100(2)$ K. The Nonius 'Collect' software was used for indexing and data collection. The structure was solved by direct methods and refined (SHELXL-97) with all non-hydrogen atoms anisotropic and with hydrogen atoms included using a riding model. Crystal parameters and bond lengths and angles are reported in the appendices.

2.5.2 Reaction of $[Ru_3(CO)_{12}]$ with *p*-toluenesulfonamide

A solution of $[Ru_3(CO)_{12}]$ (508 mg, 0.795 mmol) and *p*-toluenesulfonamide (670 mg, 3.915 mmol) in toluene (70 cm^3) was refluxed gently, while monitoring by IR spectroscopy. After 8 h all $[Ru_3(CO)_{12}]$ was consumed and the orange solution had turned dark brown. After cooling to room temperature, the solvent was removed under reduced pressure. Flash chromatography on silica gel [light petroleum/CH_2Cl_2 eluent with a gradual increase in CH_2Cl_2 from 0% to ~ 65%] followed by removal of solvent under reduced pressure, yielded 8 bands. A bright yellow band yielded $[Ru_4(\mu\text{-}H)_4(CO)_{12}]$ as a bright yellow solid (24 mg, 4%),[104] a pale orange band gave a pale orange solid (trace amount), a dark brown band gave a dark red/brown solid (20

mg), a dark red band yielded $[Ru_6(\mu_6\text{-}C)(\mu\text{-}CO)(CO)_{13}(\eta^6\text{-toluene})]$ as a dark red/brown solid (14 mg, 1%),[105] a dark brown band gave a dark brown solid (25 mg), an orange band yielded an inseparable mixture of isomers of $[\{Ru_3(\mu\text{-}H)_2(\mu_4\text{-}NTs)(CO)_7\}_2]$ **9** as a red solid (57 mg, 5%), a large orange/yellow band yielded $[Ru_3(\mu\text{-}H)_2(\mu_3\text{-}NTs)(CO)_9]$ **8** as a yellow crystalline solid (293 mg, 51%), an orange band gave an unstable mixture of compounds as a yellow/brown solid (84 mg). The cluster $[Ru_3(\mu\text{-}H)(\mu\text{-}NHTs)(CO)_{10}]$ **10** was isolated as an orange/red solid (15 mg, 5%) when the above reaction is warmed gently for 10 h, with high recovery of $[Ru_3(CO)_{12}]$ (272 mg, 54%). The compounds **9** and **8** were recrystallised by dissolving in the minimum amount of CH_2Cl_2, adding hexane (~ 15 cm^3), removing solvent under reduced pressure until precipitation occurred and isolating the solid by filtration. Crystallographic quality crystals of **8** were grown by dissolving the solid in the minimum amount of heptane, with gentle warming to aid dissolution, and allowing the heptane to slowly evaporate at room temperature to give plates.

Pale orange solid: IR ν(CO): 2119 (w), 2052 (m), 2025 (m), 2019 (w, sh), 2011 (m), 2003 (w) cm^{-1}.

Dark red/brown solid: IR ν(CO): 2101 (w), 2091 (w, sh), 2077 (s), 2067 (w), 2059 (s), 2041 (s), 2032 (m, sh), 2018 (w), 2011 (m), 2004 (w, sh), 1992 (w), 1984 (w), 1973 (w), 1963 (w), 1879 (m), 1872 (w, sh), 1847 (w) cm^{-1}. ^1H NMR: δ -16.95 (d, 1H, *J* = 2.4 Hz, Ru-*H*), -11.62 (d, 1H, *J* = 2.0 Hz, Ru-*H*), 2.41 (s, 3H, C*H*$_3$), 6.87 – 7.32 (m, 5H, tolyl). MS (FAB): *m/z* 1228 (M^+).

Dark brown solid: IR ν(CO): 2080 (w), 2049 (m), 2036 (m, sh), 2029 (s), 2011 (w), 1999 (w), 1991 (w), 1985 (w), 1975 (w), 1973 (w), 1967 (w) cm^{-1}. ^1H NMR: δ – 17.44 (d, br, 1H, Ru-*H*), -13.81 (d, 1H, Ru-*H*), 2.13 (s, 3H, C*H*$_3$), 2.36 (s, 3H, C*H*$_3$), 4.96 (t, 1H, *J* = 5.5 Hz, tolyl), 5.07 (t, 1H, *J* = 5.4 Hz, tolyl), 5.16 (t, 1H, *J* = 5.4 Hz,

tolyl), 5.24 (d, 2H *J* = 5.7 Hz, tolyl), 7.01 (br, 2H, Ar), 7.18 (br, 2H, Ar). MS (FAB): *m/z* 1236 (M^+).

[{$Ru_3(\mu\text{-}H)_2(\mu_4\text{-}NTs)(CO)_7$}$_2$] 9: IR ν(CO): 2106 (w), 2092 (s), 2077 (w, sh), 2066 (w), 2058 (w, sh), 2054 (m), 2041 (m) 2022(m), 2006 (w), 1999 (w), 1992 (w), 1988 (w), 1980 (w), 1973 (w), 1965 (w), 1953 (w) cm^{-1}, IR (KBr) ν(S=O): 1105 (m), 1030 (m), 1012 (m) cm^{-1}. ^1H NMR: δ –20.03 (d, 1H, *J* = 1.6 Hz, Ru-*H*), -19.69 (d, 1H, *J* = 2.0 Hz, Ru-*H*), -19.38 (d, 1H, *J* = 1.6 Hz, Ru-*H*), -19.21 (d, 1H, *J* = 1.6 Hz, Ru-*H*), -15.33 (d, 1H, Ru-*H*), -15.26 (d, 1H, *J* = 1.6 Hz, Ru-*H*), -15.21 (d, 1H, Ru-*H*), -15.17 (d, 1H, *J* = 2.4 Hz, Ru-*H*), 2.40 (s, 3H, C*H*$_3$), 2.44 (s, 3H, C*H*$_3$) 2.51 (s, 3H, C*H*$_3$), 2.54 (s, 3H, C*H*$_3$), 7.19 (d, 2H, *J* = 8.0 Hz, Ar), 7.28 (d, 2H, *J* = 5.8 Hz, Ar), 7.35 (d, 2H, *J* = 8.3 Hz, Ar), 7.46 (d, 2H, *J* = 8.1 Hz, Ar), 7.72 (d, 2H, *J* = 8.1 Hz, Ar), 7.73 (d, 2H, *J* = 8.5 Hz, Ar), 7.88 (d, 2H, *J* = 8.2 Hz, Ar), 7.99 (d, 2H, *J* = 8.2 Hz, Ar). MS (FAB): *m z* 1341 (M^+). Anal. Calcd for $C_{28}H_{18}N_2O_{18}S_2Ru_6$: C, 25.08, H, 1.35, N, 2.09%. Found: C, 24.69, H, 1.80, N, 1.90%.

[$Ru_3(\mu\text{-}H)_2(\mu_3\text{-}NTs)(CO)_9$] 8: IR (hexane) ν(CO): 2128 (m), 2089 (s), 2078 (s), 2071 (m), 2063 (m), 2052 (s), 2029 (m), 2021 (m) 2015 (s), 2008 (m), 2000 (w) cm^{-1}. IR (CH_2Cl_2) ν(CO): 2128 (m), 2091 (s), 2072 (s), 2063 (m, sh), 2014 (m) cm^{-1}, IR (KBr) ν(S=O): 1146 (m), 1086 (m) cm^{-1}. ^1H NMR: δ -17.26 (s, 2H, Ru-*H*), 2.44 (s, 3H, C*H*$_3$), 7.33 (d, 2H, *J* = 7.6 Hz, Ts), 7.82 (d, 2H, *J* = 7.9 Hz, Ts),. MS (FAB): *m/z* 726 (M^+). Anal. Calcd for $C_{16}H_9NO_{11}SRu_3$: C, 26.45; H, 1.25; N, 1.93%. Found: C, 26.64; H, 1.11; N, 1.90%.

Yellow/brown solid: IR ν(CO): 2123 (m), 2085 (s), 2064 (s), 2054 (s), 2043 (w), 2028 (s), 2009 (s), 1998 (w), 1995 (w), 1969 (w) cm^{-1}. ^1H NMR: δ –12.55 (s, br 1H, Ru-*H*), -11.27 (s, br, 1H, Ru-*H*), 2.38 - 2.52 (6s, C*H*$_3$), 7.27 – 7.95 (m, Ar).

$[Ru_3(\mu\text{-}H)(\mu\text{-}NHTs)(CO)_{10}]$ 10: IR ν(CO): 2108 (w), 2079 (s), 2063 (s), 2029 (m), 2022 (m, sh), 2008 (m), 2000 (w, sh), 1979 (w) cm^{-1}. IR (CH_2Cl_2) ν(CO): 2109 (m), 2077 (s), 2062 (s), 2028 (s), 2008 (s), 1981 (m) cm^{-1}. ^1H NMR: δ -14.39 (d, 1H, J = 1.3 Hz, Ru-*H*), 2.48 (s, 3H, C*H*$_3$), 5.73 (s, 1H, N*H*), 7.41 (d, 2H, J = 8.3 Hz, Ts), 7.81 (d, 2H, J = 8.3 Hz, Ts). MS (FAB): *m/z* 754 (M^+). Anal. Calcd for $C_{17}H_9NO_{12}SRu_3$: C, 27.06, H, 1.20, N, 1.86%. Found: C, 26.82, H, 1.22, N, 1.75%.

2.5.3 Reaction of $[Os_3(CO)_{12}]$ with *p*-toluenesulfonamide

A solution of $[Os_3(CO)_{12}]$ (500 mg, 0.551 mmol) and *p*-toluenesulfonamide (472 mg, 2.758 mmol) in octane (70 cm^3) was refluxed gently, while monitoring by IR spectroscopy. After 7 days all $[Os_3(CO)_{12}]$ was consumed and the yellow solution had turned dark brown. After cooling to room temperature, the solvent was removed under reduced pressure. Flash chromatography on silica gel [light petroleum/CH_2Cl_2 eluent with a gradual increase in CH_2Cl_2 from 0% to ~100%] followed by removal of solvent under reduced pressure, yielded 4 bands. A light brown band gave a light brown solid (35 mg), a yellow band yielded $[Os_3(\mu\text{-}H)(\mu\text{-}NHTs)(CO)_{10}]$ **7** as a yellow crystalline solid (24 mg, 4%),[103] a light yellow band yielded $[Os_3(\mu\text{-}H)_2(\mu_3\text{-}NTs)(CO)_9]$ **11** as a cream crystalline solid (307 mg,56 %) and a yellow band gave a yellow solid (26 mg). The compounds **7** and **11** were recrystallised by dissolving in the minimum amount of CH_2Cl_2, adding hexane (~ 15 cm^3) removing solvent under reduced pressure until precipitation occurred and isolating the solid by filtration.

Light brown solid: IR ν(CO): 2119 (w), 2106 (w), 2087 (w), 2076 (s), 2068 (m, sh), 2063 (s), 2040 (m), 2026 (m), 2010 (w), 2004 (w), 1999 (w), 1980 (w), 1973 (w), 1968 (w), 1960 (w) cm^{-1}.

$[Os_3(\mu\text{-}H)(\mu\text{-}NHTs)(CO)_{10}]$ 7: IR (hexane) ν(CO): 2111 (w), 2079 (s), 2061 (s), 2026 (s), 2011 (m), 2005 (s), 1990(m), 1974 (m) cm^{-1}. IR ($CHCl_2$) ν(CO): 2111 (m), 2077 (s), 2060 (s), 2025 (s), 2003 (s, sh), 1986 (m, sh) cm^{-1}. ^1H NMR: δ -15.31 (d, 1H, *J* = 1.4 Hz, Os-*H*), 2.49 (s, 3H, C*H*$_3$), 5.82 (s, 1H, N*H*), 7.42 (d, 2H, *J* = 8.2 Hz, Ar), 7.79 (d, 2H, *J* = 8.1 Hz, Ar). MS (EI): *m/z* 1021 (M). Anal. Calcd for $C_{17}H_9NO_{12}SOs_3$: C, 19.98; H, 0.89; N, 1.37%. Found: C, 20.11; H, 0.72; N, 1.30%.

$[Os_3(\mu\text{-}H)_2(\mu_3\text{-}NTs)(CO)_9]$ 11: IR (hexane) ν(CO): 2128 (m), 2089 (m), 2068 (s), 2041 (m), 2021 (w), 2012 (m), 2005 (m), 1997 (w), 1989 (w, br) cm^{-1}. IR ($CHCl_2$) ν(CO): 2128 (m), 2090 (m), 2066 (s), 2043 (m), 2012 (m), 2001 (m, sh), 1990 (m) cm^{-1}. ^1H NMR: δ -18.74 (s, 2H, Os-*H*), 2.46 (s, 3H, C*H*$_3$), 7.35 (d, 2H, *J* = 8.2 Hz, Ar), 7.79 (d, 2H, *J* = 8.2 Hz, Ar). MS (FAB): *m/z* 995 (M^+). Anal. Calcd for $C_{16}H_9NO_{11}SOs_3$: C, 19.33; H, 0.91; N, 1.41%. Found: C, 19.88; H, 0.64; N, 1.32%.

Yellow solid: IR ν(CO): 2121 (m), 2086 (s), 2049 (s), 2041 (s, sh), 2035 (w, sh), 2027 (w), 2016 (m), 2007 (m, sh), 1999 (m, sh), 1985 (w), 1978 (m, sh), 1958 (m), 1944 (w) cm^{-1}. MS (FAB): *m/z* 1383 (M^+).

2.5.4 Thermolysis of $[Ru_3(\mu\text{-}H)_2(\mu_3\text{-}NTs)(CO)_9]$ 8

A solution of **8** (30 mg, 0.041 mmol) in octane (25 cm^3) was refluxed, while monitoring by IR spectroscopy. After $7^1/_2$ h all **8** had been consumed and the yellow solution had turned dark brown. After cooling to room temperature, the solvent was removed under reduced pressure. Preparative TLC using 50%CH_2Cl_2: 50% light petroleum as eluent yielded **9** (8 mg, 14%) as the only product.

2.5.5 Protonation of $[Ru_3(\mu\text{-}H)_2(\mu_3\text{-}NPh)(CO)_9]$ 2

The compound **2** was prepared using literature procedures.[97,106] A solution of $[Ru_3(CO)_{12}]$ (152 mg, 0.238 mmol) and nitrosobenzene (113 mg, 1.055 mmol) in dry THF was heated at 57 °C while monitoring by IR spectroscopy. After 4 h the orange solution had turned dark brown. After cooling to room temperature, the solvent was removed under reduced pressure. Flash chromatography on silica gel using light petroleum as eluent, followed by removal of solvent under reduced pressure, yielded 2 bands. A bright yellow band which yielded $[Ru_3(CO)_{12}]$ (57 mg, 0.089 mmol) and a yellow band which yielded $[Ru_3(\mu_3\text{-}NPh)(\mu_3\text{-}CO)(CO)_9]$ **3** (73 mg, 73%). A solution of **3** (73 mg, 0.108 mmol) in heptane (50 cm^3) was placed in a 2-neck 100 cm^3 round bottomed flask, equipped with a magnetic stirrer bar, a condenser with an oil bubbler attached and a gas-inlet adaptor. The solution was refluxed under a flow of H_2 gas, while monitoring by IR spectroscopy. After $3^1/_2$ h all of **3** was consumed and the bright yellow solution had turned bright orange. After cooling to room temperature, the solvent was removed under reduced pressure. Preparative TLC using light petroleum as eluent yielded **2** as a yellow solid (69 mg, 98% based on $[Ru_3(\mu_3\text{-}NPh)(\mu_3\text{-}CO)(CO)_9]$)

Compound 2: IR (CH_2Cl_2) ν(CO): 2116 (m), 2078 (s), 2055 (s), 2029 (w, sh), 2008 (m), 1998 (m, sh) cm^{-1}. ^1H NMR: δ -16.91 (s, 2H, Ru-*H*), 6.99 – 7.21 (m, 5H, Ph).

(a) IR Experiment: To a yellow solution of **2** (~ 5 mg, 0.008 mmol) in CH_2Cl_2 (2 cm^3) was added HBF_4 (1 drop), the solution turned light yellow immediately, and an IR spectrum was run, which was consistent with the formation of $[Ru_3(\mu\text{-}H)_3(\mu_3\text{-}NPh)(CO)_9][BF_4]$ **12a**.

$[Ru_3(\mu\text{-}H)_3(\mu_3\text{-}NPh)(CO)_9][BF_4]$ 12a: IR (CH_2Cl_2) ν(CO): 2126 (s), 2077 (m) cm^{-1}.

(b) ^{1}H NMR Experiment: To a yellow solution of **2** (17 mg, 0.027 mmol) in $CDCl_3$ was added CF_3CO_2H (3 drops in total), the solution turned light yellow immediately, and an NMR spectrum obtained, which was consistent with the formation of $[Ru_3(\mu\text{-}H)_3(\mu_3\text{-}NPh)(CO)_9][CF_3CO_2]$ **12b**.

$[Ru_3(\mu\text{-}H)_3(\mu_3\text{-}NPh)(CO)_9][CF_3CO_2]$ 12b: ^{1}H NMR: δ -17.43 (s, 3H, Ru-*H*), 7.29 – 7.37 (m, 5H, Ph).

2.5.6 Protonation of $[Ru_3(\mu\text{-}H)_2(\mu_3\text{-}NTs)(CO)_9]$ 8

(a) IR Experiment: To a yellow solution of **8** (~ 5 mg, 0.007 mmol) in CH_2Cl_2 (2 cm^3) was added HBF_4 (1 drop), the solution turned light yellow immediately, and an IR spectrum was run, which was consistent with the formation of $[Ru_3(\mu\text{-}H)_3(\mu_3\text{-}NTs)(CO)_9][BF_4]$ **13a**.

$[Ru_3(\mu\text{-}H)_3(\mu_3\text{-}NTs)(CO)_9][BF_4]$ 13a: IR (CH_2Cl_2) ν(CO): 2136 (s), 2092 (m) cm^{-1}.

(b) ^{1}H NMR Experiment: To a yellow solution of **8** (15 mg, 0.021 mmol) in $CDCl_3$ was added CF_3CO_2H (several drops in total), the solution turned light yellow immediately, and an NMR spectrum obtained, which was consistent with the formation of $[Ru_3(\mu\text{-}H)_3(\mu_3\text{-}NTs)(CO)_9][CF_3CO_2\text{-}H\text{-}O_2CCF_3]$ **13b**.

$[Ru_3(\mu\text{-}H)_3(\mu_3\text{-}NTs)(CO)_9][CF_3CO_2\text{-}H\text{-}O_2CCF_3]$ 13b: ^{1}H NMR: δ –17.88 (s, 3H, Ru-*H*), 2.51 (s, 3H, C*H*$_3$), 7.53 (d, 2H, *J* = 8.1 Hz, Ar), 7.95 (d, 2H, *J* = 8.1 Hz, Ar).

2.5.7 Protonation of $[Os_3(\mu\text{-}H)_2(\mu_3\text{-}NTs)(CO)_9]$ 11

(a) IR Experiment: To a very pale yellow solution of **11** (~ 5 mg, 0.005 mmol) in CH_2Cl_2 (2 cm^3) was added HBF_4 (1 drop), the solution turned virtually colourless

immediately, and an IR spectrum was run, which was consistent with the formation of $[Os_3(\mu\text{-}H)_3(\mu_3\text{-}NTs)(CO)_9][BF_4]$ **14a**.

$[Os_3(\mu\text{-}H)_3(\mu_3\text{-}NTs)(CO)_9][BF_4]$ 14a: IR (CH_2Cl_2) ν(CO): 2155 (w), 2133 (s), 2082 (m) cm^{-1}.

(b) ^1H NMR Experiment: To a very pale yellow solution of **11** (10 mg, 0.010 mmol) in $CDCl_3$ was added CF_3CO_2H (several drops in total), the solution turned virtually colourless immediately, and an NMR spectrum obtained, which was consistent with the formation of $[Os_3(\mu\text{-}H)_3(\mu_3\text{-}NTs)(CO)_9][CF_3CO_2\text{-}H\text{-}O_2CCF_3]$ **14c**.

$[Os_3(\mu\text{-}H)_3(\mu_3\text{-}NTs)(CO)_9][CF_3CO_2\text{-}H\text{-}O_2CCF_3]$ 14c: ^1H NMR δ: -18.65 (s, 3H, Os-*H*), 2.53 (s, 3H, C*H*$_3$), 7.54 (d, 2H, *J* = 8.2 Hz, Ar), 7.95 (d, 2H, *J* = 8.1 Hz, Ar).

2.5.8 Deprotonation of $[Ru_3(\mu\text{-}H)(\mu\text{-}NHTs)(CO)_{10}]$ 10

IR Experiment: To a yellow/orange solution of **10** (~ 5 mg, 0.006 mmol) in CH_2Cl_2 (2 cm^3) was added DBU (1 drop), the solution turned light yellow immediately, and an IR spectrum was run, which was consistent with the formation [HDBU][$Ru_3(\mu$-H)(μ_3-TsNCO)$(CO)_9$] **17**.

[HDBU][$Ru_3(\mu$-H)(μ_3-TsNCO)$(CO)_9$] 17: IR (CH_2Cl_2) ν(CO): 2070 (w), 2043 (s), 2011 (s), 1976 (s), 1942 (m, sh) cm^{-1}.

2.5.9 Deprotonation of $[Os_3(\mu\text{-}H)(\mu\text{-}NHPh)(CO)_{10}]$ 5

The compound **5** was prepared using literature procedures.[95] In a 3-neck 50 cm^3 round bottomed flask, equipped with a magnetic stirrer bar, condenser with an oil bubbler attached and a gas-inlet adapter was placed $[Os_3(CO)_{12}]$ (150 mg, 0.165 mmol) and distilled aniline (20 cm^3) to form a suspension which was refluxed. After

$3^1/_2$ h all $[Os_3(CO)_{12}]$ had dissolved and the solution had turned dark brown. The solution was refluxed for a further 3 h under a flow of CO gas (1 atm). The aniline was removed under reduced pressure. Flash chromatography on silica gel using light petroleum as eluent followed by removal of solvent under reduced pressure yielded **5** as a yellow solid (103 mg, 66%).

Compound 5: IR (CH_2Cl_2) ν(CO): 2105 (m), 2068 (s), 2052 (s), 2035 (m, sh), 2020 (s), 2003 (s), 1993 (s, sh) cm^{-1}. ^1H NMR δ: -14.09 (d, 1H, J = 2.8Hz, Os-*H*), 5.81 (s, br, 1H, N*H*), 6.79 – 7.25 (m, 5H, Ph).

(a) IR Experiment: To a yellow solution of **5** (~ 5 mg, 0.005 mmol) in CH_2Cl_2 (2 cm^3) was added DBU (1 drop), the solution turned light yellow immediately, and an IR spectrum was run, which was consistent with the formation of [HDBU][Os_3(μ-H)(μ$_3$-PhNCO)(CO)$_9$] **18**.

[HDBU][Os_3(μ-H)(μ$_3$-PhNCO)(CO)$_9$] 18: IR (CH_2Cl_2) ν(CO): 2069 (s), 2046 (s), 2036 (m, sh), 2007 (s), 1982 (s), 1938 (w), 1916 (w) cm^{-1}.

(b) ^{1}H NMR Experiment: To a yellow/orange solution of **5** (9 mg, 0.010 mmol) in $CDCl_3$ was added a solution of DBU (15 mg, 0.098 mmol in total) in $CDCl_3$, the solution turned light yellow, and an NMR spectrum of **18** obtained.

[HDBU][Os_3(μ-H)(μ$_3$-PhNCO)(CO)$_9$] 18: ^{1}H NMR: δ -15.21 (s, 1H, Os-*H*), 6.65 (d, 2H, J = 7.0 Hz, *o*-$H_2C_6H_3$), 7.03 (t, 1H, J = 6.6 Hz, *p*-HC_6H_4), 7.12 (m, 2H, J = 6.5 Hz, *m*-$H_2C_6H_3$).

2.5.10 Deprotonation of [Os_3(μ-H)(μ-NHTs)(CO)$_{10}$] 7

(a) IR Experiment: To a yellow/orange solution of **7** (~ 5 mg, 0.005 mmol) in CH_2Cl_2 (2 cm^3) was added DBU (1 drop), no colour change was observed, and an IR

spectrum was run, which was consistent with the formation of $[Os_3(\mu\text{-}H)(\mu\text{-}NTs)(CO)_{10}][HDBU]$ **19a**.

$[HDBU][Os_3(\mu\text{-}H)(\mu\text{-}NTs)(CO)_{10}]$ 19a: IR (CH_2Cl_2) ν(CO): 2095 (w), 2053 (s), 2042 (m, sh), 2005 (s), 1980 (m, sh), 1959 (m, sh) cm^{-1}.

(b) ^{1}H NMR Experiment: To a very pale yellow solution of **7** (12 mg, 0.012 mmol) in $CDCl_3$ was added a solution of DBU (18 mg, 0.121 mmol in total) in $CDCl_3$, no colour change was observed, and an NMR spectrum of $[Os_3(\mu\text{-}H)(\mu\text{-}NTs)(CO)_{10}][DBUH\ldots OH_2]$ **19c** obtained.

$[DBUH\ldots OH_2][Os_3(\mu\text{-}H)(\mu\text{-}NTs)(CO)_{10}]$ 19c: ^{1}H NMR: δ -15.51 (s, 1H, Os-*H*), 2.33 (s, 3H, C*H*$_3$), 7.13 (d, 2H, J = 8.0 Hz, Ar), 7.71 (d, 2H, J = 8.2 Hz, Ar).

To a yellow solution of **7** (8 mg, 0.008 mmol) in the minimum volume of diethyl ether (~ 0.5 cm^3), was added Et_3N (1 small drop), no colour change was observed. This solution was layered with hexane (~ 1 cm^3) and left in the dark to allow the diethyl ether to evaporate. The colourless hexane solution was removed to leave a yellow crystalline solid, a mixture of **7** and crystals suitable for X-ray crystallography of $[HEt_3N][Os_3(\mu\text{-}H)(\mu\text{-}NTs)(CO)_{10}]$ **19d**.

Chapter 3:

Alkyne insertion into metal-hydrogen bonds of tosylimido capped clusters

3.1 INTRODUCTION

Coordination site vacancies are often required for metal carbonyl complexes to react. Traditionally, harsh thermal and photochemical techniques have been used to create vacancies, but problems arise from these techniques when trying to isolate reaction intermediates. A milder method is to displace a CO ligand using the oxidant trimethylamine-*N*-oxide combined with other reagents, ligands or weakly coordinating solvents such as acetonitrile, which can then be easily replaced by a more strongly coordinating ligand (Scheme 3.1). The high volatility of trimethylamine allows it to be removed easily from reaction mixtures. This method also allows isolation of compounds that would otherwise be inaccessible by harsher techniques.

$$M(CO)_n + x\,MeCN + xMe_3NO \longrightarrow M(CO)_{n-x}(MeCN)_x + x\,CO_2 + xMe_3N$$

$$M(CO)_{n-x}(MeCN)_x + xL \longrightarrow M(CO)_{n-x}(L)_x + xMeCN$$

Scheme 3.1 The substitution of CO for MeCN

Alkynes can insert into the M-H bond of a hydrido cluster to form μ-σ,η^2-alkenyl containing clusters. For example, the unsaturated cluster $[Os_3(\mu\text{-}H)_2(CO)_{10}]$ reacts with ethyne to form the alkenyl complex $[Os_3(\mu\text{-}H)(\mu\text{-}\sigma,\eta^2\text{-}CH{=}CH_2)(CO)_{10}]$ (Fig. 3.1).[109,110] Analogous compounds have been formed from the phosphine derivative

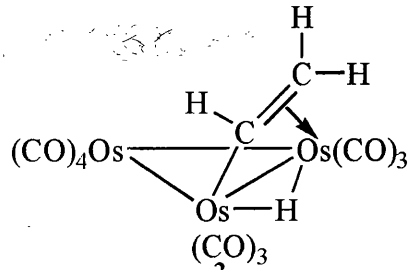

Fig. 3.1 The structure of $[Os_3(\mu\text{-}H)(\mu\text{-}\sigma,\eta^2\text{-}CH{=}CH_2)(CO)_{10}]$

$[Os_3(\mu\text{-}H)_2(CO)_9(L)]$ (where L = PPh_3, PPh_2Et, $P(OMe)_3$, PEt_3, $P(p\text{-}MeOC_6H_4)_3$, P(tolyl)$_3$ and P(Cy)$_3$).[111-113] Two isomers are formed in the solid state when L = PPh_3, the structures of which have been deduced (Figs. 3.2a and b).[113] In solution the

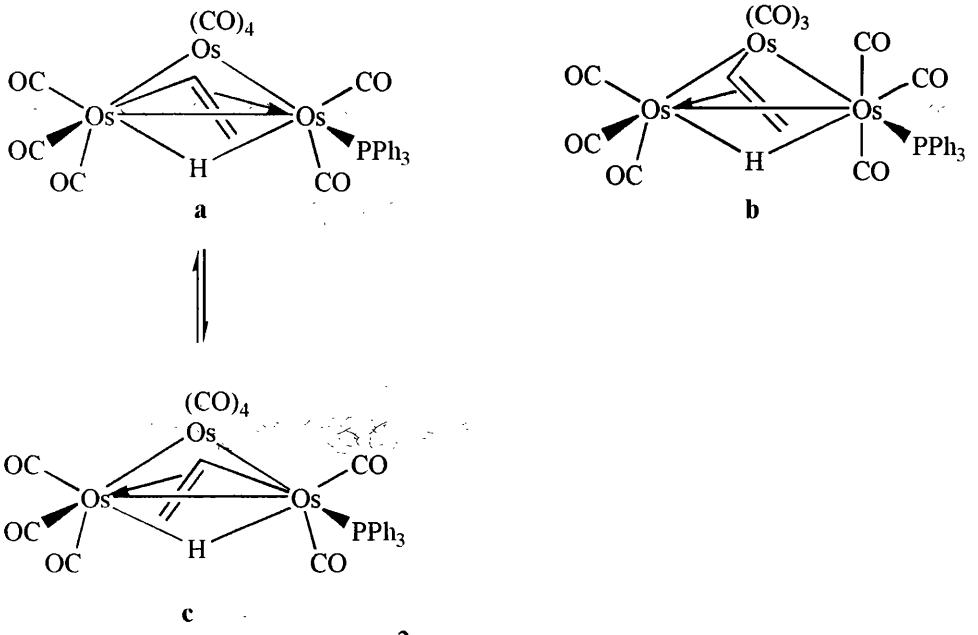

Fig. 3.2 The isomers of $[Os_3(\mu\text{-}H)(\mu\text{-}\sigma,\eta^2\text{-}CH{=}CH_2)(CO)_9(PPh_3)]$

isomer in Fig. 3.2a is also in equilibrium with a third isomer (Fig. 3.2c). These examples have shown that single insertion of an alkyne into a dihydride cluster has occurred. Double insertion can also occur, for instance, the reaction of the acetonitrile complex $[Os_3(\mu\text{-}H)_2(\mu_3\text{-}C_6H_4)(MeCN)_2(CO)_7]$ with diphenylacetylene forms the dialkenyl cluster $[Os_3(\mu_3\text{-}C_6H_4)(\mu\text{-}\sigma,\eta^2\text{-}PhC{=}CHPh)_2(CO)_7]$ (Fig. 3.3).[114] In most

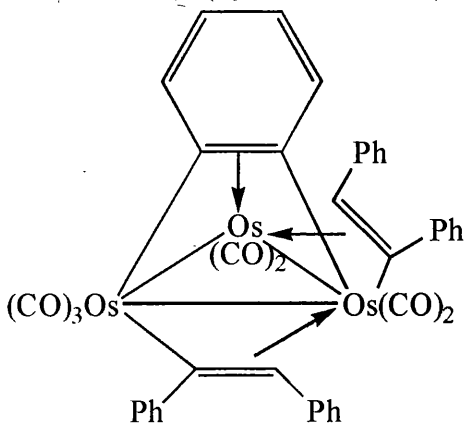

Fig. 3.3 The structure of $[Os_3(\mu_3\text{-}C_6H_4)(\mu\text{-}\sigma,\eta^2\text{-}PhC{=}CHPh)_2(CO)_7]$

organometallic reactions concerned with dihydrido clusters, both hydride ligands are transferred to the same organic group leading to simple hydrogenation, for example from alkyne to alkene. However, two organyl ligands formed by double insertion could couple to form new organic ligands. This chapter describes some new 1,3-diene-containing clusters formed by double insertion of alkynes into two M-H bonds, followed by coupling of the two alkenyl ligands. The formation of 1,3-dienes by reductive coupling of alkynes is extremely unusual. Catalytic hydrodimerisation of alkyne leading to 1,3-dienes have only been reported by Tani *et al.* (Scheme 3.2).[115]

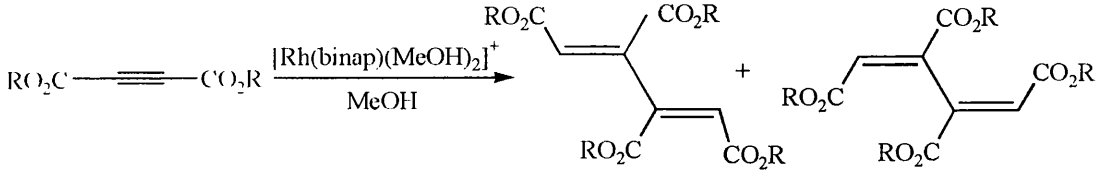

Scheme 3.2 The catalytic hydrodimerisation of $RO_2C-C\equiv C-CO_2R$

Before this example, only stoichiometric syntheses of 1,3-dienes from alkynes were known, such as *via* hydrocupration of terminal alkynes,[116] through the reduction of dimethyl acetylenedicarboxylate with Cu(II)/hydrosilanes which forms 1,3-dienes as by-products.[117] 1,3-dienes are also produced during the reduction of terminal alkynes with $[CoHCl(PPh_3)_2]$[118] and in the reaction of dimethyl acetylenedicarboxylate with $[(\eta^5\text{-Cp})RuX(PPh_3)_2]$ (where X = Cl or I).[119] In spite of these examples, it does not seem that a 1,3-butadiene cluster has been formed previously by an alkenyl-alkenyl coupling process, although C-C coupling of an alkenyl species with a surface-bound methylene is implicated in Fischer-Tropsch synthesis.[120]

The butadiene ligand has several modes of coordination. In monomeric complexes butadiene can coordinate in an η^4-cisoid fashion as in the complex $[Fe(CO)_3(\eta^4\text{-}cis\text{-}$

C_4H_6)] (Fig.3.4), this being the most common mode.[121] It can also adopt the η^4-

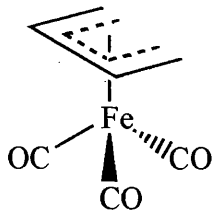

Fig. 3.4 The structure of $[Fe(CO)_3(\eta^4\text{-}cis\text{-}C_4H_6)]$

transoid coordination mode in compounds such as $[ZrCp_2(\eta^4\text{-}s\text{-}trans\text{-}C_4H_6)]$ (Fig. 3.5a),[122] which can slowly interconvert to the cisoid isomer (Fig. 3.5b).[123] The two

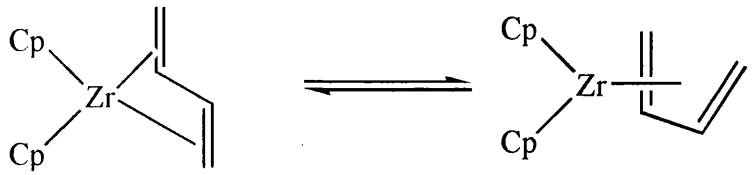

a **b**

Fig. 3.5 The isomers of $[ZrCp_2(\eta^4\text{-}C_4H_6)]$

Cp rings in the cisoid isomer are exchanged by a rapid movement of the diene, possibly through a di-σ-bonded 16-electron intermediate (Scheme 3.3).

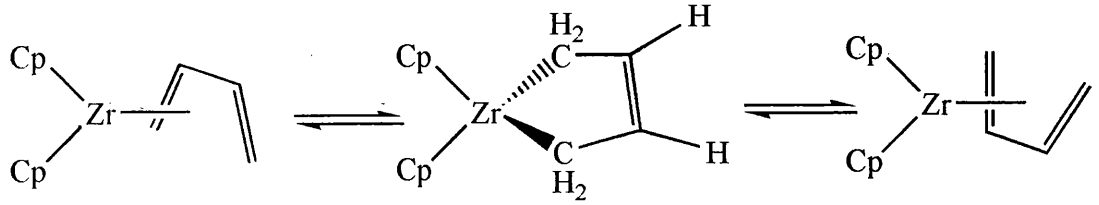

Scheme 3.3 The exchange of the two Cp rings in $[ZrCp_2(\eta^4\text{-}s\text{-}cis\text{-}C_4H_6)]$

In polynuclear compounds, butadiene can have several modes of coordination in addition to the above. It can be attached to one metal centre as in the cluster $[Os_3(CO)_{10}(\eta^4\text{-}s\text{-}cis\text{-}C_4H_6)]$ (Fig. 3.6a), where the butadiene is coordinated at axial and equatorial sites of a single osmium atom. This compound has another isomer

$[Os_3(CO)_{10}(\mu\text{-}\eta^2,\eta^2\text{-}s\text{-}trans\text{-}C_4H_6)]$ in which the butadiene is bridging an Os-Os bond and coordinates at equatorial positions of the two osmium atoms (Fig. 3.6b).[124,125]

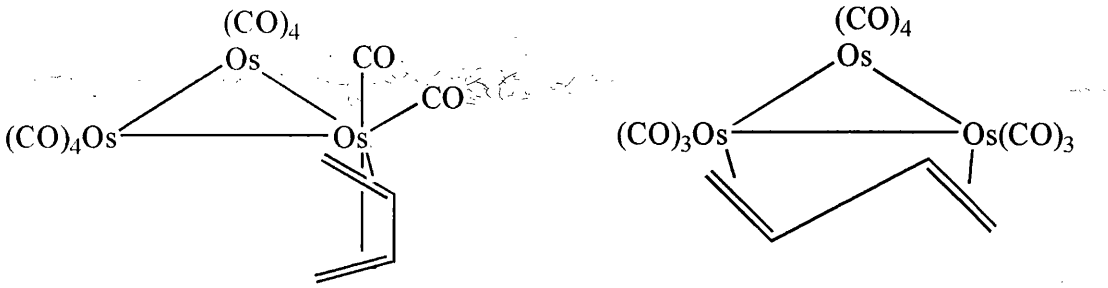

a b

Fig. 3.6 The isomers of $[Os_3(CO)_{10}(C_4H_6)]$

The $\mu\text{-}\eta^2,\eta^2\text{-}s\text{-}trans$-butadiene coordination mode is also found in the dinuclear palladium complex $[Pd_2Cl(\mu\text{-}Cl)(PPh_3)(\mu\text{-}\eta^2,\eta^2\text{-}s\text{-}trans\text{-}C_4H_6)]$ (Fig. 3.7).[126]

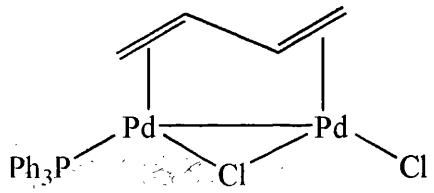

Fig. 3.7 The structure of $[Pd_2Cl(\mu\text{-}Cl)(PPh_3)(\mu\text{-}\eta^2,\eta^2\text{-}s\text{-}trans\text{-}C_4H_6)]$

The anion $[Pt_2Cl_6(C_4H_6)]^{2-}$ also contains a bridging *trans*-butadiene which links two ($PtCl_3$) groups (Fig 3.8a) but in this case there is no metal-metal bond.[127] The

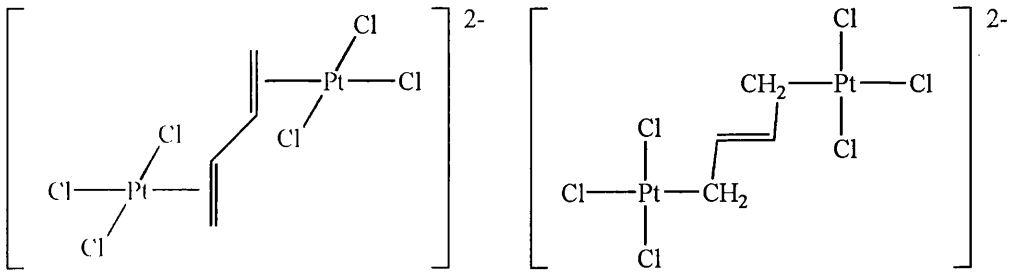

a b

Fig. 3.8 The two representations of $[Pt_2Cl_6(C_4H_6)]^{2-}$

two terminal C-C bonds are longer than the central C-C bond and the compound is better represented by Fig. 3.8b than Fig. 3.8a.

The butadiene-lanthanoid complex $[(\eta^5\text{-Cp}^*)_2\text{La(thf)}(\mu\text{-}\eta^1,\eta^3\text{-C}_4\text{H}_6)\text{La}(\eta^5\text{-Cp}^*)_2]$ contains a $\mu\text{-}\eta^1,\eta^3$-*s-cis*-butadiene ligand (Fig. 3.9).[128] The atoms C(2), C(3) and C(4) are η^3-coordinated to La(2), in an allyl type formation, while C(1) is σ-bonded to La(1).

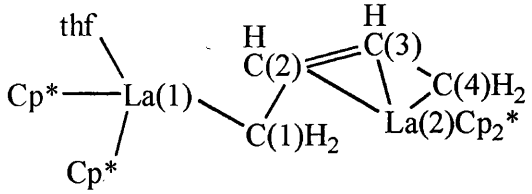

Fig. 3.9 The structure of $[Cp^*_2La(thf)(\mu\text{-}\eta^1,\eta^3\text{-}C_4H_6)LaCp^*_2]$

The unusual $\mu\text{-}\eta^1,\eta^4$-*s-cis*-1,3-diene coordination is found in the complex $[W_2(OCH_2{}^tBu)_6(1,3\text{-butadiene})(py)]$ (Fig. 3.10).[129] Electron counting requires the

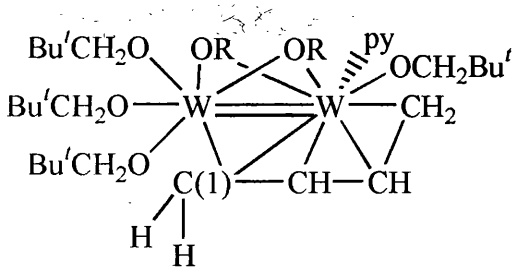

Fig. 3.10 The structure of $[W_2(OCH_2{}^tBu)_6(1,3\text{-butadiene})(py)]$

diene to be a dianionic ligand, and the C-C distances in the coordinated diene are consistent with this. The carbon atom C(1) is considered to be hypervalent, being bonded to two H atoms, one C atom and two W atoms.

The $\mu\text{-}\eta^2,\eta^2$-*s-cis*-1,3-diene coordination mode is known in several cases, for example in the compounds $[(\eta^5\text{-Cp}^*\text{Rh})_2\{\mu\text{-}\eta^2,\eta^2\text{-}s\text{-}cis\text{-}CH_2{=}C(CO_2Me)C(CO_2Me){=}CH_2\}\{\mu\text{-}SC(CO_2Me){=}CH(CO_2Me)\}][BPh_4]$ (Fig. 3.11a)[130] and $[(\eta^5\text{-CpCo})_2(\mu\text{-}\eta^2,\eta^2\text{-}s\text{-}cis\text{-}C_4H_6)(\mu\text{-CO})]$ (Fig. 3.11b).[131]

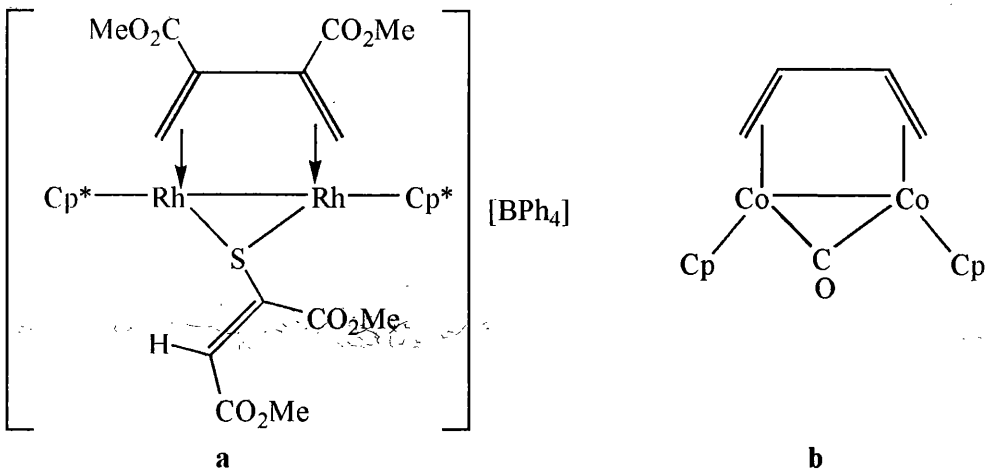

a **b**

Fig. 3.11 The structures of two compounds with a 1,3-butadiene ligand in the μ-η^2,η^2-*s-cis*-coordination mode

3.2 TARGETS, AIMS AND OBJECTIVES IN THIS CHAPTER

- To replace CO by the more labile MeCN ligand in the tosylimido capped clusters $[Ru_3(\mu\text{-}H)_2(\mu_3\text{-}NTs)(CO)_9]$ **8** and $[Os_3(\mu\text{-}H)_2(\mu_3\text{-}NTs)(CO)_9]$ **11**, which contain two basal hydrido bridges, thereby creating terminal ligand sites for incoming organic substrates to bind.
- To react these MeCN clusters with alkynes and induce single and double insertions into the M-H bonds of the clusters, followed by coupling to form butadiene clusters.
- To form the basis of a new type of organometallic cluster chemistry and potentially cluster catalysis.

3.3 RESULTS AND DISCUSSION

3.3.1 Preparation of $[Ru_3(\mu\text{-}H)_2(\mu_3\text{-}NTs)(CO)_8(MeCN)]$ 20

Treatment of $[Ru_3(\mu\text{-}H)_2(\mu_3\text{-}NTs)(CO)_9]$ **8** in CH_2Cl_2 with a $Me_3NO.2H_2O$/MeCN

solution at room temperature resulted in an immediate reaction, as shown by changes in the IR spectrum, to form $[Ru_3(\mu\text{-}H)_2(\mu_3\text{-}NTs)(CO)_8(MeCN)]$ **20**. The solution was filtered through silica gel to remove any unreacted $Me_3NO.2H_2O$. Any Me_3N produced would have been removed under reduced pressure. CO absorptions in the IR spectrum of **20** showed a shift to lower wavenumber, when compared to **8**, as there are fewer CO ligands and a better donor ligand has been introduced. The room temperature ^1H NMR spectrum of **20** (Fig. 3.12a) shows two broad signals at δ -22.34

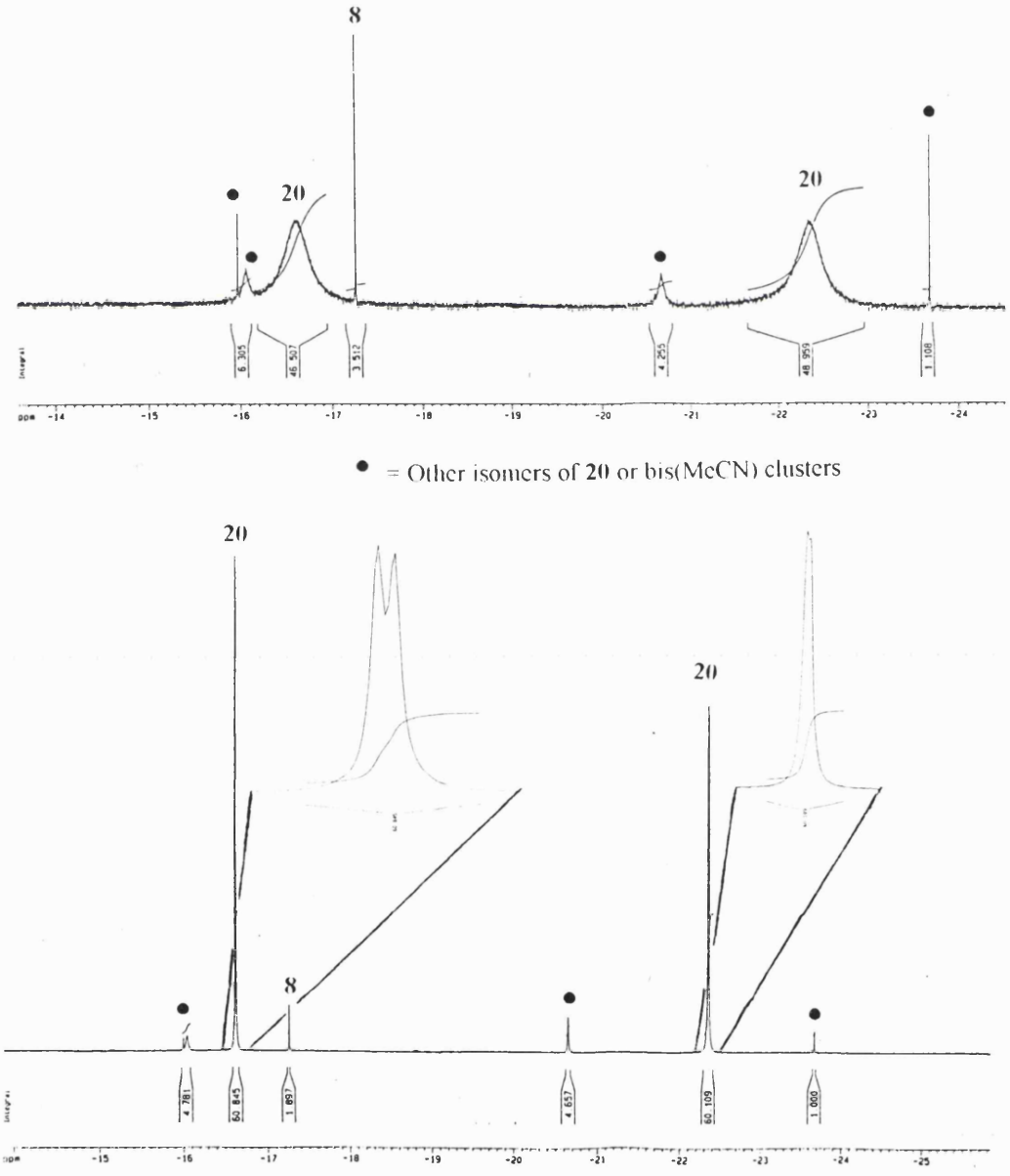

Fig. 3.12 Part of the ^1H NMR spectrum (hydride region) of $[Ru_3(\mu\text{-}H)_2(\mu_3\text{-}NTs)(CO)_8(MeCN)]$ 20 at (a) room temperature and (b) –25 °C

and –16.59 for the hydride ligands, a singlet at δ 2.31 for the Me group of the MeCN ligand, another singlet at δ 2.42 for the Me group of the NTs ligand, and an AA'BB' pattern for the tolyl ring at δ 7.29 and 7.86. At –25 °C the broad hydride signals sharpen to two doublets at δ -22.37 and –16.63 (Fig. 3.12b), confirming the inequivalence of the hydride ligands. NMR integrals confirm the formation of the monoacetonitrile complex.

As the MeCN ligand is most likely to coordinate at an equatorial site *cis* to the capping atom N, there are three possible isomers for this compound (Fig. 3.13). The

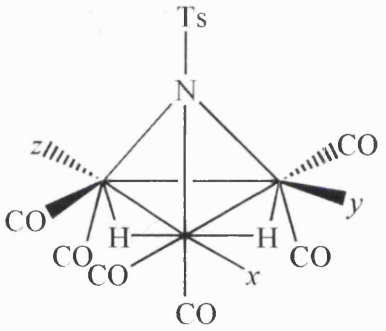

Fig. 3.13 The possible coordination sites for the MeCN ligand

MeCN ligand could bind at sites *x*, *y* or *z*, each of which would result in inequivalent hydride ligands. The most likely binding site for the MeCN ligand is position *x* as hydride ligands are both more likely to bind to the most electron-rich metal. The ^{1}H NMR spectrum also shows small traces of other compounds, one of which being unreacted **8**, and the other peaks may be due to other isomers being present or maybe small quantities of the bis-MeCN complex. The broadness of the hydride signals at room temperature could be due to the onset of hydride exchange either by hydride motion (Fig. 3.14a) or by a 'turnstile' mechanism involving the carbonyl and MeCN ligands (Fig. 3.14b).

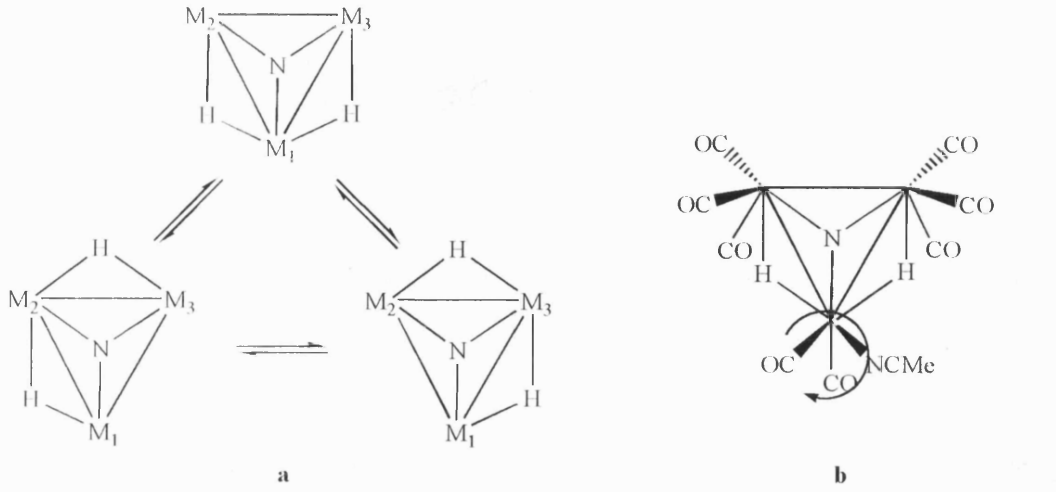

Fig. 3.14 The two possible mechanisms that may cause the broadness of the ^{1}H NMR spectrum of 20; (a) hydride migration and (b) the "turnstile mechanism"

The positive ion FAB mass spectrum displayed a molecular ion peak at *m/z* 740 and daughter ions due to successive loss of eight carbonyl ligands. There were also low intensity peaks consistent with those of **8**. However, this would be expected as the ^{1}H NMR spectrum also shows traces of **8**. It is likely that full conversion may not take place as CO, released during the reaction, could in principle reconvert some of **20** back to **8**.

3.3.2 Preparation of $[Os_3(\mu\text{-}H)_2(\mu_3\text{-}NTs)(CO)_8(MeCN)]$ 21

A dichloromethane solution of $[Os_3(\mu\text{-}H)_2(\mu_3\text{-}NTs)(CO)_9]$ **11** was treated with a $Me_3NO.2H_2O$/MeCN, solution at room temperature, resulting in an immediate reaction, as shown by changes in the IR spectrum, to form $[Os_3(\mu\text{-}H)_2(\mu_3\text{-}NTs)(CO)_8(MeCN)]$ **21**. As in the ruthenium case, the solution was filtered through silica gel to remove any unreacted $Me_3NO.2H_2O$. The IR spectrum of **21** was very similar to that of **20**. The room temperature ^{1}H NMR of **21** (Fig. 3.15) shows two hydride doublets at δ -17.48 and –16.92, a singlet at δ 2.44 for the Me group of the

NTs ligand, another singlet at δ 2.57 for the Me group of the MeCN ligand, and an AA'BB' pattern for the tolyl ring of the NTs ligand at δ 7.31 and 7.81.

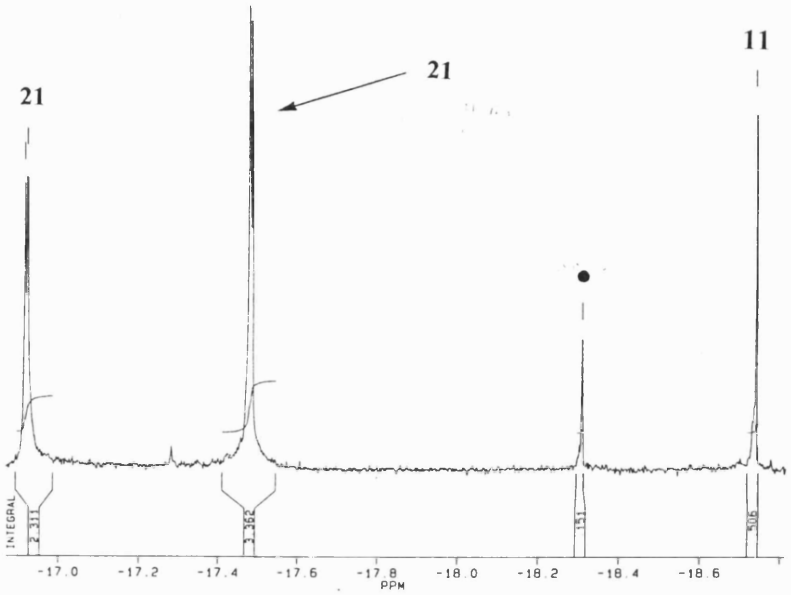

Fig. 3.15 Part of the room temperature ^{1}H NMR spectrum (hydride region) of $[Os_3(\mu\text{-}H)_2(\mu_3\text{-}NTs)(CO)_8(MeCN)]$ 21 • = Other isomer of **21** or bis(MeCN) cluster

This spectrum is analogous to the ^{1}H NMR spectrum of **20**, at –25 °C, consistent with the MeCN ligand being in site *x* (Fig. 3.13). However, this time there is no indication of fluxionality even at room temperature. There is an extra peak in the hydride region of the ^{1}H NMR spectrum, again perhaps due to another isomer of the monoacetonitrile derivative or a small amount of the bis-MeCN compound being present. There is also a weak peak consistent with a small amount of **11**. The positive ion FAB mass spectrum displayed a molecular ion peak at *m/z* 1008 and daughter ions due to successive loss of eight carbonyl ligands. There were also weak peaks consistent with **11**.

3.3.3 Re-carbonylation of $[Ru_3(\mu\text{-}H)_2(\mu_3\text{-}NTs)(CO)_8(MeCN)]$ 20

Treatment of **20** with CO in CH_2Cl_2 at room temperature resulted in the immediate reformation of **8** as shown by IR spectroscopy.

3.3.4 Re-carbonylation of $[Os_3(\mu\text{-}H)_2(\mu_3\text{-}NTs)(CO)_8(MeCN)]$ 21

No reaction occurred when treating **21** with CO, in CH_2Cl_2 at room temperature, for $1^1/_2$ hours (monitored by IR spectroscopy). The CH_2Cl_2 was replaced with THF and the solution refluxed under a CO atmosphere for 2 hours, after which time IR spectroscopy showed complete conversion to **11**. The cluster **21** is re-carbonylated at a much slower rate than **20**, emphasising the greater reactivity of ruthenium as compared to osmium. This observation encouraged us to carry out reactions of **20** at room temperature, and of **21** in refluxing THF.

3.3.5 Reaction of $[Ru_3(\mu\text{-}H)_2(\mu_3\text{-}NTs)(CO)_8(MeCN)]$ 20 with $Bu^tC{\equiv}CH$

Treatment of **20** with a six-fold excess of $Bu^tC{\equiv}CH$, in CH_2Cl_2 at room temperature, for $1^1/_2$ hours resulted in the reversible formation of the mono-insertion alkenyl product $[Ru_3(\mu\text{-}H)(\mu\text{-}\textit{trans}\text{-}CH{=}CHBu^t)(\mu_3\text{-}NTs)(CO)_8]$ **22**. This cluster did not appear to be stable and could not be purified by TLC due to decomposition and reformation of **8**. The ^1H NMR spectrum of the crude product **22** showed signals for **8**, signals for the NTs ligand as well as singlets at δ -13.64 and 1.22 due to the hydride ligand and the nine protons of the Bu^t group respectively, and doublets at δ 6.17 and 9.82 due to the β-carbon and α-carbon protons of the alkenyl group, respectively. The NMR integrals showed that compounds **22** and **8** were formed in an approximate 9:1 ratio.

There are three possible isomers for the alkenyl ligand (Figs. 3.16a - c).

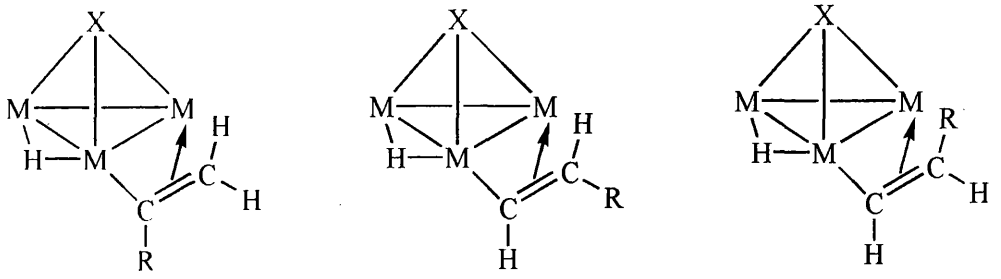

α-isomer a | β-isomer b | β'-isomer c

Fig. 3.16 The possible isomers of hydrido-alkenyl clusters

The coupling constant (12.3 Hz) for the doublets, due to the alkenyl ligands, is consistent with the β-isomer being formed. The positive ion FAB mass spectrum displayed a molecular ion peak at *m/z* 779 and daughter ions due to successive loss of eight carbonyl ligands. There were also weak peaks at *m/z* 834 and 860 which may correspond to the dialkenyl cluster $[Ru_3(\mu\text{-}\textit{trans}\text{-}CH{=}CHBu^t)_2(\mu_3\text{-}NTs)(CO)_7]$ and the butadiene cluster $[Ru_3(\mu\text{-}C_4H_4Bu^t_2)_2(\mu_3\text{-}NTs)(CO)_8]$ respectively. However, these clusters were not isolated or observed in the ^1H NMR spectrum of the crude reaction mixture, so there is no additional proof that they have been formed in this case. It is possible that these clusters may have been formed in very small quantities, and therefore, further work needs to be carried out to optimise reaction conditions in order to isolate these compounds

3.3.6 Carbonylation of $[Ru_3(\mu\text{-}H)(\mu\text{-}\textit{trans}\text{-}CH{=}CHBu^t)(\mu_3\text{-}NTs)(CO)_8]$ 22

A solution of **22** in $CDCl_3$ was treated with CO at room temperature and pressure for 5 minutes. A ^1H NMR spectrum of this crude mixture showed signals for compounds

8 and **22**, indicating an incomplete reaction, and also signals for free $Bu^tCH=CH_2$. The $CDCl_3$ was replaced with CH_2Cl_2 and this solution was treated with CO at room temperature for 30 minutes, after which time IR spectroscopy indicated the reaction was complete. After purification, five compounds were obtained, the major component of these being $[Ru_3(\mu_3\text{-NTs})(\mu_3\text{-CO})(CO)_9]$ **23**, a yellow solid formed in 28% yield. The remaining four solids, three of which were yellow and one was pale brown, were obtained in such low yield that they could not be conclusively characterised from spectroscopic data.

The IR spectrum of **23** was simple, consistent with a compound of C_{3v} symmetry and the ν(CO) frequencies showed a shift to higher wavenumber when compared to those of the analogous phenylimido cluster **3**. The ^1H NMR spectrum displayed a singlet at δ 2.43 due to the Me group of the NTs ligand and an AA'BB' pattern at δ 7.34 and 7.78 due to the tolyl ring. The positive ion FAB mass spectrum displayed a molecular ion peak at *m z* 755 and daughter ions due to successive loss of ten carbonyl ligands. There are also other weak peaks in the mass spectrum, although the sample of **23** by other criteria was very pure.

3.3.7 Hydrogenation of $[Ru_3(\mu_3\text{-NTs})(\mu_3\text{-CO})(CO)_9]$ 23

A solution of **23** in refluxing heptane was treated with H_2 for $2^1/_2$ hours. IR and ^1H NMR spectroscopy showed complete conversion to **8**. These results show that **20** could, in principle, catalyse the hydrogenation of $Bu^tC\equiv CH$ to form $Bu^tCH=CH_2$ (Scheme 3.4). We did not carry out the reaction of **22** with H_2 to develop these ideas further.

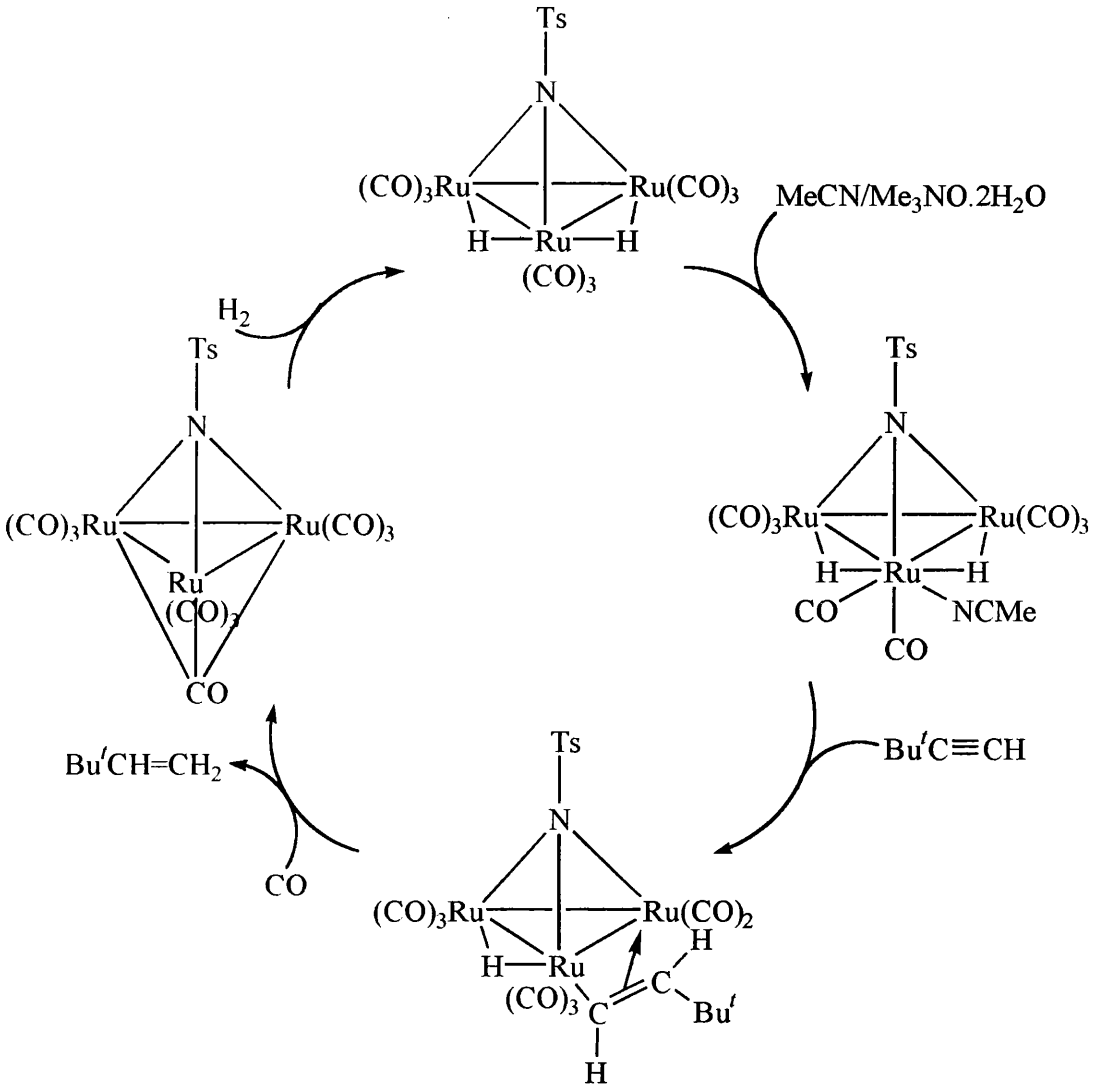

Scheme 3.4 The stepwise hydrogenation of $Bu^tC{\equiv}CH$ to $Bu^tCH{=}CH_2$

3.3.8 Reaction of $[Ru_3(\mu\text{-}H)_2(\mu_3\text{-}NTs)(CO)_8(MeCN)]$ 20 with CH≡CH

Treatment of **20** with CH≡CH (1 atm) in CH_2Cl_2, at room temperature, for 45 minutes gave a mixture from which $[Ru_3(\mu\text{-}\eta^2,\eta^2\text{-}C_4H_6)(\mu_3\text{-}NTs)(\mu_3\text{-}CO)(CO)_7]$ **24**, a yellow solid was isolated in 8% yield. A small amount of **8** was also recovered along with two other compounds, a yellow/brown oil and a yellow solid, which were obtained in very small quantities and could not be identified. The IR spectrum of **24** showed a peak at 1758 cm^{-1} indicating the presence of a μ_3-CO ligand. The ^1H NMR spectrum

shows signals for the NTs ligand. The butadiene ligand gave a doublet at δ 2.90 with a coupling constant of 13.4 Hz, due to the geminal protons *trans* to the vicinal protons, a doublet at δ 3.98, with a coupling constant of 9.5 Hz, due to the geminal protons *cis* to the vicinal protons, and a multiplet at δ 4.58 for the vicinal protons. This last signal also displays ^{4}J coupling. This spectrum also confirmed a *cis*-butadiene configuration. The positive FAB mass spectrum displayed a molecular ion peak at *m z* 752 and daughter ions due to successive loss of eight carbonyl ligands. To confirm the molecular structure of **24**, single crystals were grown by diffusion of CH_2Cl_2 into heptane and the structure determined crystallographically as shown in Fig. 3.17. Selected bond lengths and angles are given in Table 3.1. The three ruthenium atoms form a closed isosceles triangle [Ru(1)-Ru(2) 2.7560(3); Ru(1)-Ru(3) 2.7416(4); Ru(2)-Ru(3) 2.7554(3) Å]. Each ruthenium atom is bonded to the nitrogen cap and also to the μ_3-CO ligand. The Ru-N bonds are within the expected range. Two ruthenium atoms, Ru(1) and Ru(2), are bonded to two terminal CO groups and Ru(3) is bonded to three terminal CO groups. The Ru(1)-Ru(2) edge is bridged by the μ-η^2,η^2-*s*-*cis*-butadiene ligand, the termini of which are pointing up towards the NTs ligand. One of the carbon-carbon bonds, the central C(10)-C(11) bond, is longer (1.461(4) Å) than the other two C-C bonds C(9)-C(10) and C(11)-C(12) (both 1.393(5) Å) as expected for a butadiene ligand. The tolyl ring of the NTs group is bending over Ru(3), which is not attached to the butadiene ligand. This compound can be thought of as $[Ru_3(\mu_3\text{-NTs})(\mu_3\text{-CO})(CO)_9]$ **23**, with two of the equatorial CO ligands having been replaced by the butadiene ligand.

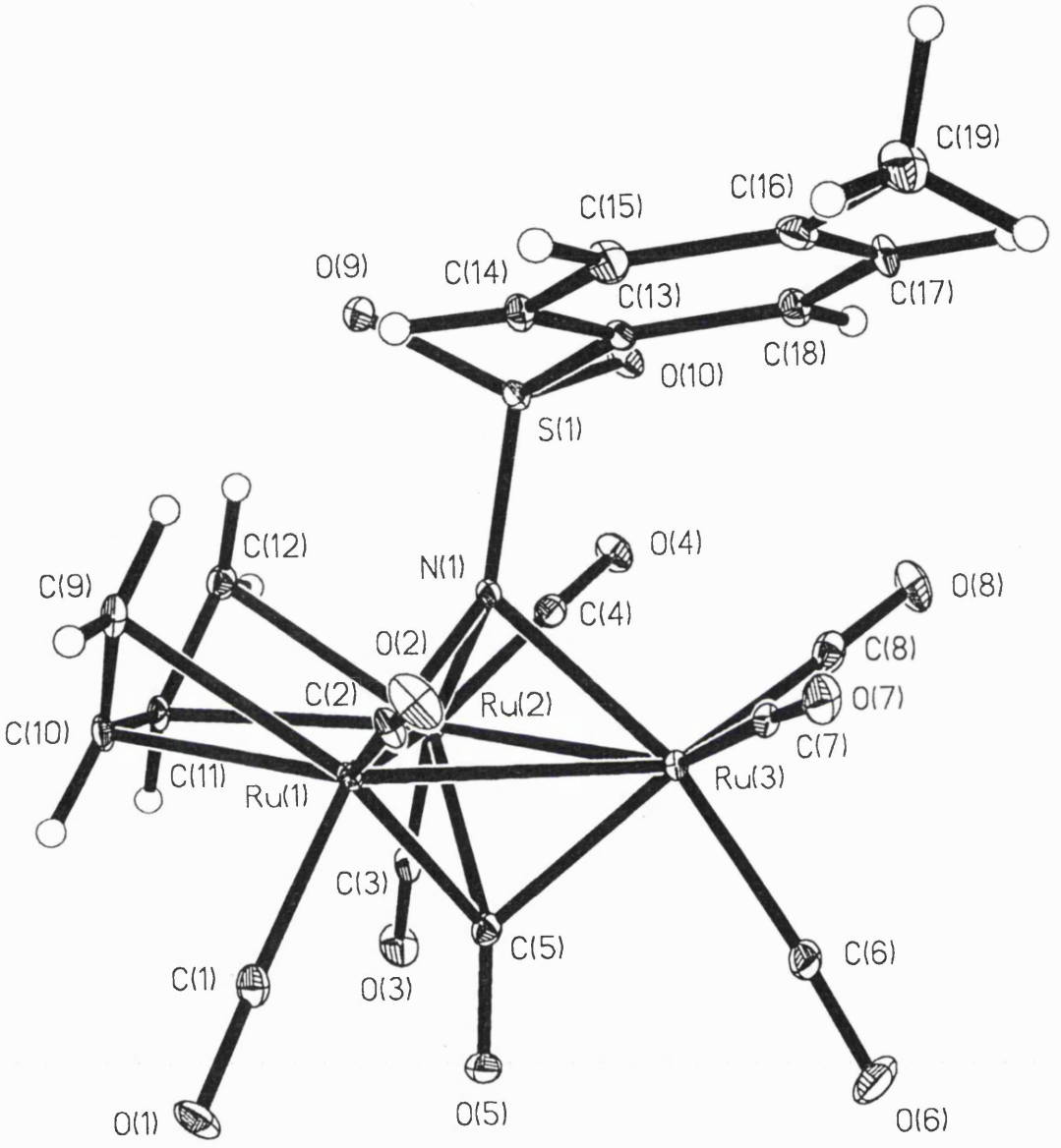

Fig. 3.17 The X-ray structure of $[Ru_3(\mu\text{-}\eta^2,\eta^2\text{-}C_4H_6)(\mu_3\text{-}NTs)(\mu_3\text{-}CO)(CO)_7]$ 24

Table 3.1 Selected bond lengths (Å) and angles (°) for 24

Ru(1)-Ru(2)	2.7560(3)	Ru(2)-C(11)	2.338(3)
Ru(1)-Ru(3)	2.7416(4)	Ru(2)-C(12)	2.246(3)
Ru(2)-Ru(3)	2.7554(3)	C(9)-C(10)	1.393(5)
Ru(1)-C(9)	2.258(3)	C(10)-C(11)	1.461(4)
Ru(1)-C(10)	2.304(3)	C(11)-C(12)	1.393(5)
C(9)-C(10)-C(11)	127.5(3)	C(10)-C(11)-C(12)	127.6(3)

3.3.9 Reaction of $[Ru_3(\mu\text{-}H)_2(\mu_3\text{-}NTs)(CO)_8(MeCN)]$ 20 with PhC≡CH

Treatment of a solution of **20** in CH_2Cl_2 with a three-fold excess of PhC≡CH, at room temperature, for 45 minutes resulted in a mixture of compounds. After purification, eight compounds were isolated including **8** and $[Ru_3(\mu\text{-}\eta^2,\eta^2\text{-}C_4H_4Ph_2)(\mu_3\text{-}NTs)(\mu_3\text{-}CO)(CO)_7]$ **25**, a yellow solid in 16% yield. The remaining six compounds, two orange oily solids, two red solids, an orange oil and an orange solid, were obtained in low yield and could not be identified from spectroscopic data. The IR spectrum of **25** is very similar to that of **24**, indicating that **25** has a similar structure to **24**. However, because of the Ph substituents there are possibilities of isomers for the butadiene ligand. From the ^{1}H NMR spectrum of **25** the isomer formed was deduced, and head-to-tail coupling of PhC≡CH, to give the isomer shown in Fig. 3.18a, is confirmed. The ^{1}H NMR spectrum (see later Fig. 3.20a) shows signals for the NTs and Ph groups, as well as a doublet at δ 2.98 (J = 1.0 Hz) for H^c (Fig. 3.18b), which couples

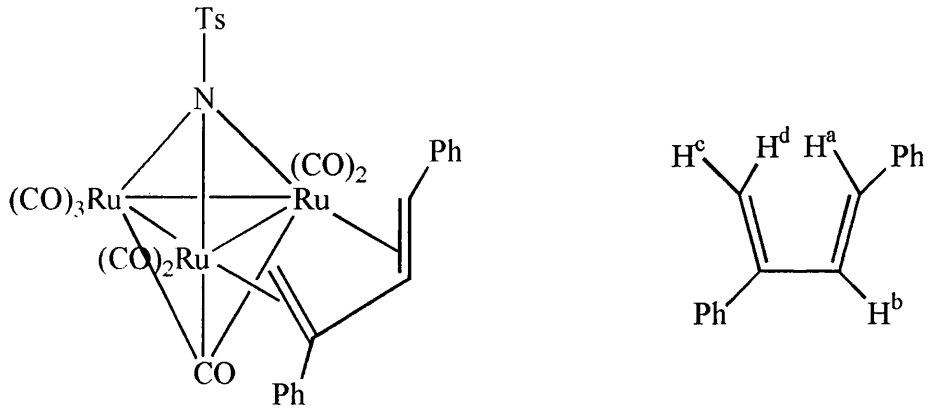

a **b**

Fig. 3.18 The isomer of the butadiene formed on reaction of 20 with PhC≡CH (a) Coordinated to the cluster and (b) Uncoordinated

to H^b, a singlet at δ 4.72 for H^d, a doublet at δ 5.53 (J = 13.5 Hz) for H^a which also couples to H^b, and a doublet of doublets (J = 1.5 and 13.4 Hz) at δ 5.82 for H^b. The

positive ion FAB mass spectrum displayed a molecular ion peak at *m/z* 904 and daughter ions due to successive loss of eight carbonyl ligands, and also due to the additional loss of the butadiene ligand.

The formation of 1,3-diene clusters from hydrogenative coupling of alkynes is unprecedented. Intermediate alkenyl complexes were not observed in the formation of **24** and **25**, although the formation of $[Ru_3(\mu\text{-}H)(\mu\text{-}trans\text{-}CH{=}CHBu^t)(\mu_3\text{-}NTs)(CO)_8]$ **22** suggests they are involved. The reaction is also regioselective, with only *trans*-1,3-diphenylbutadiene being isolated. It is possible that alkenyl clusters and other butadiene isomers were formed in very low yield and could not be identified. In contrast to these results with PhC≡CH, the bulkiness of the Bu^t group in $Bu^tC{\equiv}CH$ could prevent the formation of a butadiene, with only the single insertion compound **22** being observed.

3.3.10 Reaction of $[Ru_3(\mu\text{-}H)_2(\mu_3\text{-}NTs)(CO)_8(MeCN)]$ 20 with PhC≡CD

To establish where hydride insertion was taking place, a solution of **20** in CH_2Cl_2 was treated with a four-fold excess of PhC≡CD, at room temperature, for $1^1/_2$ hours resulting in a mixture of compounds. After purification, five compounds were isolated including **8** and $[Ru_3(\mu\text{-}\eta^2,\eta^2\text{-}C_4H_2D_2Ph_2)(\mu_3\text{-}NTs)(\mu_3\text{-}CO)(CO)_7]$ obtained as an isomeric mixture of **26a** and **26b**, a yellow solid in 21% yield. The remaining three compounds, two orange solids and a red solid were obtained in low yield and could not be identified. However, this reaction corresponded closely to that of the reaction of **20** with PhC≡CH. The IR spectrum of the mixture of **26a** and **26b**, as

expected, is very similar to the spectra of **24** and **25**. The possible isomers of the butadiene ligand in $[Ru_3(\mu\text{-}\eta^2,\eta^2\text{-}C_4H_2D_2Ph_2)(\mu_3\text{-}NTs)(\mu_3\text{-}CO)(CO)_7]$ are shown in Fig. 3.19. The ^1H NMR spectrum (Fig. 3.20b) shows signals for the NTs and Ph groups, a singlet at δ 2.97 for H^c, a singlet at δ 4.70 for H^d, and a singlet at δ 5.51 for H^a. From the intensity of the signals, the isomer in Fig. 3.19a, where H^c was from the hydride ligand, was found to be the predominant isomer (*ca.* 90%). As predicted, there is no signal at δ 5.81 for H^b. However, we would expect the isomer in Fig. 3.19b to be the predominant one, formed from *cis* addition to both alkyne ligands. This suggests that there may be *cis* addition to one alkyne and *trans* addition to the other, or there could be rotation about the C=CHD bond. The positive ion FAB mass spectrum displayed a molecular ion peak at *m/z* 906 and daughter ions due to successive loss of eight carbonyl ligands, and also due to the additional loss of the butadiene ligand.

a **b**

Fig. 3.19 The two possible butadiene isomers found in 26a and 26b

3.3.11 Reaction of $[Ru_3(\mu\text{-}H)_2(\mu_3\text{-}NTs)(CO)_8(MeCN)]$ 20 with 1,3-Butadiene

Treatment of **20** with 1,3-butadiene, at room temperature, for 7 hours resulted in a mixture of compounds. Following purification, five bands were isolated including $[Ru_3(\mu\text{-}H)_2(\mu_3\text{-}NTs)(CO)_9]$ **8** (4%) and $[Ru_3(\mu\text{-}\eta^2,\eta^2\text{-}C_4H_6)(\mu_3\text{-}NTs)(\mu_3\text{-}CO)(CO)_7]$ **24** (22%), identified from spectroscopic data. Of the remaining three compounds, all

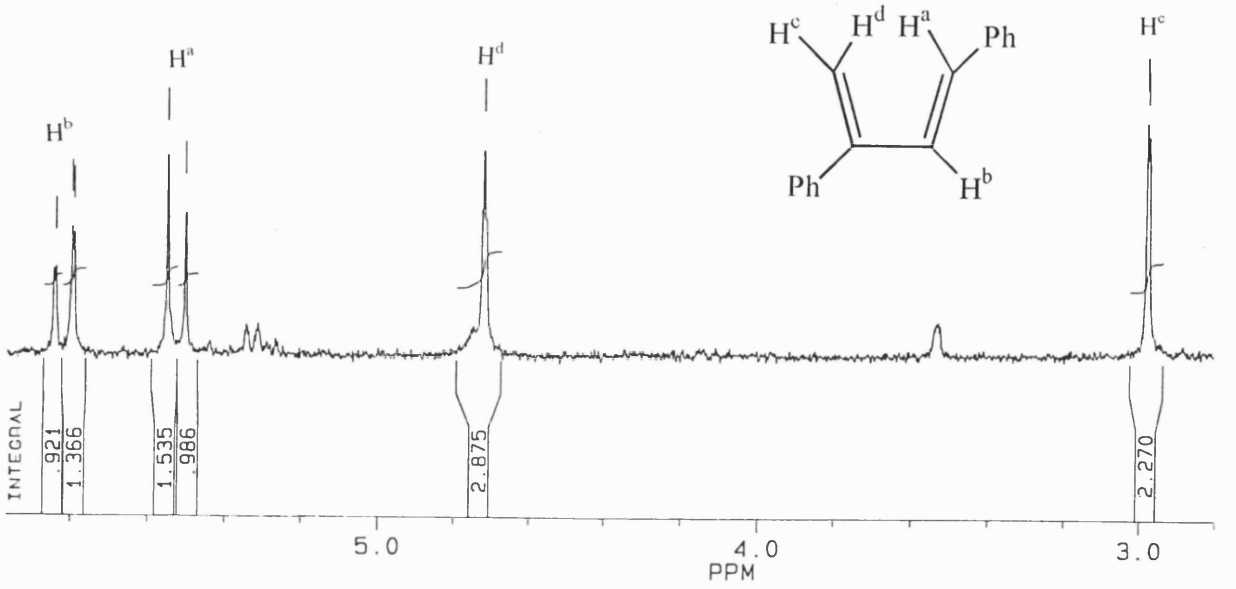

(a)

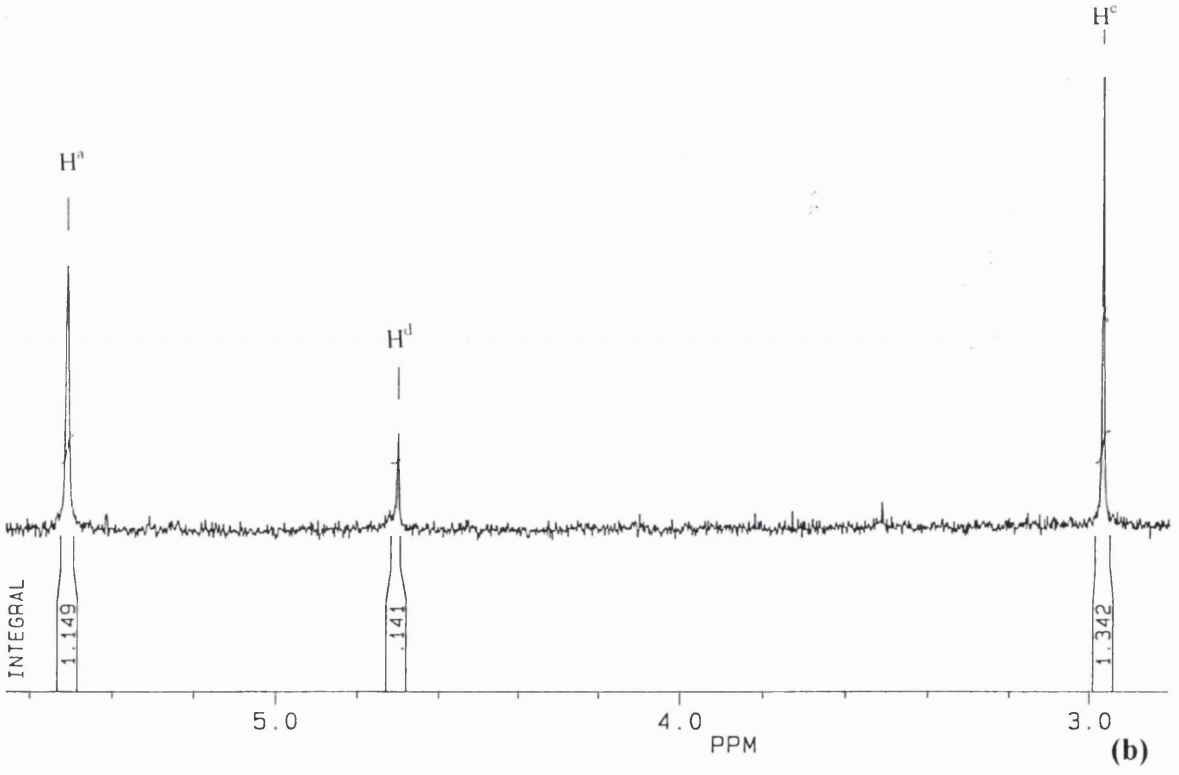

(b)

Fig. 3.20 Part of the ^{1}H NMR spectra of (a) [$Ru_3(\mu\text{-}\eta^2,\eta^2\text{-}C_4H_4Ph_2)(\mu_3\text{-}NTs)(\mu_3\text{-}CO)(CO)_7$] 25 and (b) [$Ru_3(\mu\text{-}\eta^2,\eta^2\text{-}C_4H_2D_2Ph_2)(\mu_3\text{-}NTs)(\mu_3\text{-}CO)(CO)_7$] 26a and b

yellow solids, two were formed in very low yield. The IR spectrum of the third compound showed a very weak signal at 1748 cm^{-1} assigned to a μ_3-CO ligand, and what appear to be four doublets, in the weak ^1H NMR spectrum, each with an integral of two protons. This would be consistent with a C_4H_8 ligand with the additional two protons coming from the hydride ligands. There were also signals for the NTs group. The EI mass spectrum displayed a weak molecular ion peak at *m/z* 750, a compound with the formulation $[Ru_3(C_4H_8)(\mu_3\text{-NTs})(CO)_8]$ would have a molecular mass of 752. However, a structure for the ligand consistent with the ^1H NMR data could not be deduced.

3.3.12 Reaction of $[Os_3(\mu\text{-}H)_2(\mu_3\text{-NTs})(CO)_8(MeCN)]$ 21 with $Bu^tC{\equiv}CH$

Treatment of **21** with four equivalents of $Bu^tC{\equiv}CH$ in THF, at 65 °C, for 12 hours resulted in the clean formation of $[Os_3(\mu\text{-}H)(\mu\text{-}\textit{trans}\text{-}CH{=}CHBu^t)(\mu_3\text{-NTs})(CO)_8]$ **27**, as a yellow solid in 73% yield. The IR spectrum of this compound was similar to that of the analogous ruthenium compound **22**. The ^1H NMR spectrum showed signals for the NTs group, singlets at δ -12.89 and 1.28 due to the hydride ligand and the nine protons of the Bu^t group respectively, and doublets at δ 5.99 and 9.48 (J = 12.4 Hz) for the coupled protons on the β- and α-carbons of the alkenyl ligand, respectively. The positive ion FAB mass spectrum displayed a molecular ion peak at *m/z* 1049 and daughter ions resulting from successive loss of eight carbonyl ligands. To confirm the molecular structure of **27**, single crystals were grown, by evaporation of a hexane solution and the structure determined crystallographically (Fig. 3.21). Selected bond lengths and angles are presented in Table 3.2.

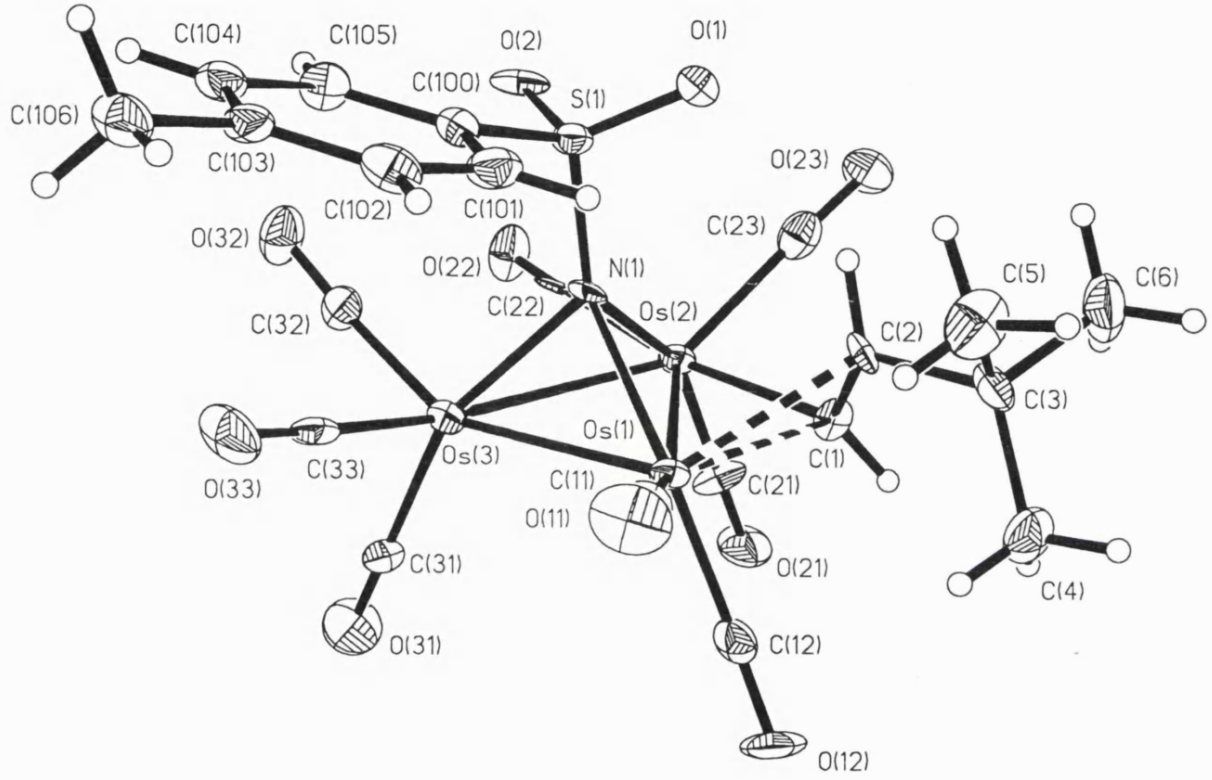

Fig. 3.21 The X-ray structure of $[Os_3(\mu\text{-}H)(\mu\text{-}CH{=}CHBu^t)(\mu_3\text{-}NTs)(CO)_8]$ 27

Table 3.2 Selected bond lengths (Å) and angles (°) for 27

Os(1)-Os(2)	2.7513(11)	Os(1)-C(2)	2.333(14)
Os(1)-Os(3)	2.7859(12)	Os(2)-C(1)	2.203(14)
Os(2)-Os(3)	2.8417(12)	C(1)-C(2)	1.47(2)
Os(1)-C(1)	2.16(2)		
Os(1)-Os(2)-Os(3)	59.72(3)	C(1)-Os(1)-C(2)	37.8(6)
Os(1)-Os(3)-Os(2)	58.53(3)	C(2)-Os(1)-Os(2)	77.4(4)
Os(2)-Os(1)-Os(3)	61.75(3)	C(2)-C(1)-Os(1)	77.5(9)
Os(1)-C(1)-Os(2)	78.2(5)	C(2)-C(1)-Os(2)	119.8(11)

The three osmium atoms form a closed isosceles triangle [Os(1)-Os(2) 2.7513(11); Os(1)-Os(3) 2.7859(12); Os(2)-Os(3) 2.8417(12) Å]. Each osmium atom is bonded to the nitrogen cap. Two osmium atoms, Os(2) and Os(3) are bonded to three terminal CO ligands, while Os(1) is bonded to two. The hydride ligand could not be located. The Os(2)-Os(3) edge is the longest Os-Os bond in the molecule, on this basis, it could be speculated that this edge is bridged by the hydride ligand. However, the Os-Os-C angles to equatorial CO ligands do not support this assumption. These angles should be large if a hydride ligand is present along that Os-Os edge. The Os(2)-Os(3)-C(32) angle of 102.5(6) ° is quite small, and the Os(3)-Os(2)-C(22) angle of 75.9(5) ° suggests the carbonyl ligand, C(22)O(22), is nearly semi-bridging. The Os-Os-C angles along the Os(1)-Os(3) edge [Os(3)-Os(1)-C(11) 111.7(6); Os(1)-Os(3)-C(33) 101.3(8) °] are relatively large. This could mean the hydride ligand is bridging the Os(1)-Os(3) edge. The Os(1)-Os(2) edge is the shortest metal-metal bond and is bridged by the β-alkenyl ligand which acts as a 3-electron donor. The carbon atom C(1) occupies an equatorial site and is σ-bonded to Os(2), and there is a π-interaction between C(1)-C(2) and Os(1). The tolyl ring of the NTs ligand is bending over the Os(1)-Os(3) edge. The C(1)-C(2) distance in the alkenyl moiety is 1.47(2) Å is significantly longer than for a free carbon-carbon double bond.

3.3.13 Reaction of $[Os_3(\mu\text{-}H)_2(\mu_3\text{-}NTs)(CO)_8(MeCN)]$ 21 with PhC≡CH

The cluster **21** was treated with a four-fold excess of PhC≡CH in refluxing THF for 10 hours. This resulted in the reversible formation of $[Os_3(\mu\text{-}H)(\mu\text{-}\textit{trans}\text{-}CH{=}CHPh)(\mu_3\text{-}NTs)(CO)_8]$ **28**. As with **22**, the cluster **28** could not be purified by

TLC. The IR spectrum of **28** is similar to that of **22** and **27**. The ^{1}H NMR spectrum of the crude material, **28**, showed signals for **11**, the NTs and Ph groups, along with a singlet at δ -12.82 for the hydride ligand, and doublets at δ 6.63 and 9.97 (J = 12.1 Hz) due to the coupled protons on the β- and α-carbon atoms of the alkenyl ligand, respectively.

Osmium being less reactive than ruthenium not only requires higher temperatures for reaction to occur, but only the hydrido-alkenyl clusters are isolated, with no evidence of butadiene formation. From these results it seems that the β-isomer of the hydrido-alkenyl clusters is formed regioselectively. However, it is possible that the α-isomer could be involved with formation of the *trans*-1,3-diphenylbutadiene, which could be thought of as a β-alkenyl coupled to an α-alkenyl ligand (Scheme 3.5).

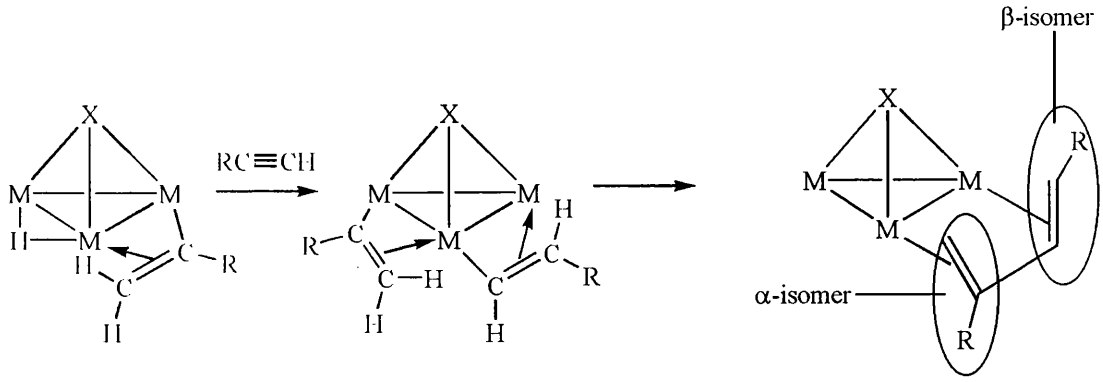

Scheme 3.5 The coupling of two alkenyl ligands to form a butadiene ligand

Further investigation into the possible mechanism for butadiene formation is given in Chapter 4. Potentially the catalytic formation of butadiene from alkynes is possible, which, if achieved would be a totally new type of catalysis.

3.4 CONCLUSIONS

- A carbonyl ligand in the clusters $[Ru_3(\mu\text{-}H)_2(\mu_3\text{-}NTs)(CO)_9]$ and $[Os_3(\mu\text{-}H)_2(\mu_3\text{-}NTs)(CO)_9]$ can be easily displaced to form the acetonitrile clusters of the type $[M_3(\mu\text{-}H)_2(\mu_3\text{-}NTs)(CO)_8(MeCN)]$.
- Insertion of alkynes into the M-H bonds of the acetonitrile clusters can occur to give (a) single insertion alkenyl clusters and (b) hydrogenative coupling of alkynes to give butadiene-containing clusters. In the case of $[Ru_3(\mu\text{-}H)(\mu\text{-}\textit{trans}\text{-}CH{=}CHBu^t)(\mu_3\text{-}NTs)(CO)_8]$, reductive elimination of $Bu^tCH{=}CH_2$ is observed on reaction with CO.
- These reactions appear to be regioselective with only the β-isomer of the hydrido-alkenyl clusters and the 1,3-*trans*-diphenylbutadiene being observed.
- The catalytic regioselective formation of butadienes from alkynes may be possible using capped clusters.

3.5 EXPERIMENTAL

3.5.1 Materials and Instrumentation

All materials and instrumentation are as described in Chapter 2 (Section 2.5.1). In addition to this all reactions were carried out under N_2 using standard Schlenk techniques unless otherwise specified. Solvents were distilled prior to use under an atmosphere of nitrogen over drying agents except those used for TLC or crystallisations. Acetonitrile and dichloromethane were distilled over CaH_2 and THF and heptane over sodium wire.

Some NMR spectra were recorded on a Bruker AC300 or Avance 500 spectrometer using deuterated chloroform $CDCl_3$ (δ 7.27) as an internal reference. EI mass spectra were acquired by the departmental service at University College London (UCL) on a VG ZAB-SE spectrometer. The X-ray structure of $[Ru_3(\mu\text{-}\eta^2,\eta^2\text{-}C_4H_6)(\mu_3\text{-}NTs)(\mu_3\text{-}CO)(CO)_7]$ was obtained by Dr. J. W. Steed at King's College London using a Nonius Kappa CCD equipped area detector diffractometer (as described in Chapter 2). The X-ray structure of $[Os_3(\mu\text{-}H)(\mu\text{-}\textit{trans}\text{-}CH{=}CHBu^t)(\mu_3\text{-}NTs)(CO)_8]$ was obtained by Professor A. J. Deeming at UCL. X-ray data were collected at room temperature using a Nicolet R3v/m diffractometer (as described in Chapter 2).

3.5.2 Preparation of $[Ru_3(\mu\text{-}H)_2(\mu_3\text{-}NTs)(CO)_8(MeCN)]$ 20

$[Ru_3(\mu\text{-}H)_2(\mu_3\text{-}NTs)(CO)_9]$ **8** (50 mg, 0.069 mmol) was placed in a Schlenk tube, and CH_2Cl_2 (15 cm^3) added. In another Schlenk tube was placed $Me_3NO.2H_2O$ (8 mg, 0.070 mmol) and MeCN (15 cm^3). The $Me_3NO.2H_2O$/MeCN solution was then added, dropwise, to the solution of **8** in CH_2Cl_2 *via* a cannula. The resulting yellow solution was left to stir at room temperature, while monitoring by IR spectroscopy, until all **8** had been consumed (10 min). Silica gel was added to the stirring solution, which was then filtered into another Schlenk tube. The silica gel was washed with dry CH_2Cl_2 (3 × 10 cm^3) and the washings added to the filtrate. The solvent was then removed from the filtrate under reduced pressure, to yield $[Ru_3(\mu\text{-}H)_2(\mu_3\text{-}NTs)(CO)_8(MeCN)]$ **20** as an oily yellow solid.

Compound 20: IR (CH_2Cl_2) ν(CO): 2092 (m), 2065 (s), 2057 (s, sh), 2013 (s), 1936 (w) cm^{-1}. ^1H NMR (+22 °C): δ -22.34 (br, 1H, Ru-*H*), -16.59 (br, 1H, Ru-*H*), 2.31 (s, 3H, C*H*$_3$CN), 2.42 (s, 3H, C*H*$_3$), 7.29 (d, 2H, *J* = 8.1 Hz), 7.86 (d, 2H, *J* = 8.1 Hz). ^1H NMR (-25 °C): δ -22.37 (d, 1H, *J* = 2.0 Hz, Ru-*H*), -16.63 (d, 1H, *J* = 3.0 Hz, Ru-*H*),

2.32 (s, 3H, C*H*$_3$CN), 2.41 (s, 3H, C*H*$_3$), 7.29 (d, 2H, *J* = 8.1 Hz, Ar), 7.83 (d, 2H, *J* = 8.1 Hz, Ar). MS (FAB): *m/z* 740 (M^+).

3.5.3 Preparation of [$Os_3(\mu\text{-}H)_2(\mu_3\text{-}NTs)(CO)_8(MeCN)$] 21

[$Os_3(\mu\text{-}H)_2(\mu_3\text{-}NTs)(CO)_9$] **11** (53 mg, 0.053 mmol) was placed in a Schlenk tube, and CH_2Cl_2 (15 cm^3) added. In another Schlenk tube was placed $Me_3NO.2H_2O$ (8 mg, 0.070 mmol) and MeCN (15 cm^3). The $Me_3NO.2H_2O$/MeCN solution was then added, dropwise, to the solution of **11** in CH_2Cl_2 *via* a cannula. The resulting pale yellow solution was left to stir at room temperature, while monitoring by IR spectroscopy until all **11** had been consumed (10 min). Silica gel was added to the stirring solution, which was then filtered into another Schlenk tube. The silica gel was washed with dry CH_2Cl_2 (3 × 10 cm^3) and the washings added to the filtrate. The solvent was then removed from the filtrate, under reduced pressure, to leave an oily yellow solid of [$Os_3(\mu\text{-}H)_2(\mu_3\text{-}NTs)(CO)_8(MeCN)$] **21.**

Compound 21: IR (CH_2Cl_2) ν(CO): 2091 (m), 2058 (s), 1999 (s) cm^{-1}. ^{1}H NMR: δ -17.48 (d, 1H, *J* = 1.8 Hz, Os-*H*), -16.92 (d, 1H, *J* = 1.8 Hz, Os-*H*), 2.44 (s, 3H, C*H*$_3$), 2.57 (s, 3H, C*H*$_3$CN), 7.31 (d, 2H, *J* = 8.2 Hz, Ar), 7.81 (d, 2H, *J* = 8.3 Hz, Ar). MS (FAB): *m/z* 1008 (M^+). Anal. Calcd for $C_{17}H_{12}N_2O_{10}SOs_3$: C, 20.28, H, 1.20, N, 2.78%. Found: C, 20.63, H, 1.25, N, 2.66%.

3.5.4 Re-carbonylation of [$Ru_3(\mu\text{-}H)_2(\mu_3\text{-}NTs)(CO)_8(MeCN)$] 20

The compound **20** (51 mg, 0.069 mmol) was dissolved in CH_2Cl_2 (~ 60 cm^3) and transferred to a 3-necked 100 cm^3 round bottomed flask, equipped with an oil bubbler, a stopper, a gas-inlet adaptor and a magnetic stirrer bar. Carbon monoxide was bubbled through the stirring solution at room temperature for 10 min, after which time

an IR spectrum was run in CH_2Cl_2 that showed all **20** had been converted back to **8** quantitatively.

3.5.5 Re-carbonylation of $[Os_3(\mu\text{-}H)_2(\mu_3\text{-}NTs)(CO)_8(MeCN)]$ 21

The compound **21** (49 mg, 0.049 mmol) was dissolved in THF (~ 25 cm^3) and transferred to a 3-necked 50 cm^3 round bottomed flask, equipped with a condenser attached to an oil bubbler, a stopper, a gas-inlet adaptor and a magnetic stirrer bar. Carbon monoxide was bubbled through the stirring solution at reflux for 2 h, after which time an IR spectrum was run in CH_2Cl_2, this showed all of **21** had been converted back to **11** quantitatively.

3.5.6 Reaction of $[Ru_3(\mu\text{-}H)_2(\mu_3\text{-}NTs)(CO)_8(MeCN)]$ 20 with $Bu^tC{\equiv}CH$

The compound **20** (52 mg, 0.070 mmol) was dissolved in CH_2Cl_2 (20 cm^3) and to this was added a solution of $Bu^tC{\equiv}CH$ (37 mg, 0.450 mmol) in CH_2Cl_2 (5 cm^3). The solution was stirred at room temperature while monitoring by IR spectroscopy. After $1^1/_2$ h all **20** was consumed and the solution turned from yellow/orange to orange. The CH_2Cl_2 and $Bu^tC{\equiv}CH$ were removed under reduced pressure to leave a dark orange/red oily solid mixture of $[Ru_3(\mu\text{-}H)(\mu\text{-}\textit{trans}\text{-}CH{=}CHBu^t)(\mu_3\text{-}NTs)(CO)_8]$ **22** and **8** (in an approximate 9:1 ratio).

$[Ru_3(\mu\text{-}H)(\mu\text{-}\textit{trans}\text{-}CH{=}CHBu^t)(\mu_3\text{-}NTs)(CO)_8]$ 22: Crude IR (CH_2Cl_2) ν(CO): 2105 (m), 2089 (w, sh), 2075 (m), 2058 (m, sh), 2040 (s), 1991 (m, sh), 1983 (m) cm^{-1}. Crude ^1H NMR: δ -13.64 (s, 1H, Ru-*H*), 1.22 (s, 9H, Bu^t), 2.41 (s, 3H, CH_3), 6.17

(d, 1H, J = 12.2 Hz, CH=C*H*Bu^t), 7.28 (d, 2H, J = 7.8 Hz, Ar), 7.66 (d, 2H, J = 8.3 Hz, Ar), 9.82 (d, 1H, J = 12.2 Hz, C*H*=CHBu^t).

3.5.7 Carbonylation of $[Ru_3(\mu\text{-H})(\mu\text{-}\textit{trans}\text{-CH=CHBu}^t)(\mu_3\text{-NTs})(CO)_8]$ 22

The crude mixture of **8** and **22** was re-dissolved in $CDCl_3$ and placed in an NMR tube. Carbon monoxide was bubbled through this solution at room temperature for 5 min. A ^{1}H NMR spectrum of this crude mixture was obtained. The solution was transferred to a Schlenk tube and the solvent removed under reduced pressure to leave an orange/brown oily solid. This was re-dissolved in CH_2Cl_2 (15 cm^3) and carbon monoxide was bubbled through the solution while monitoring by IR spectroscopy. After 30 min all **22** was consumed, the solvent was removed under reduced pressure. This crude mixture was purified by TLC using 50% CH_2Cl_2: 50% light petroleum as eluent. Extraction with CH_2Cl_2, followed by removal of solvent under reduced pressure yielded 5 bands. A yellow band gave a yellow solid (6 mg); a yellow band gave a yellow solid (7 mg); a yellow band gave a pale brown solid (3 mg); a yellow band yielded $[Ru_3(\mu_3\text{-NTs})(\mu_3\text{-CO})(CO)_9]$ **23** as a yellow crystalline solid (15 mg, 28% based on $[Ru_3(\mu\text{-H})_2(\mu_3\text{-NTs})(CO)_9]$) and a yellow band gave a pale yellow solid (3 mg).

1st yellow solid: IR ν(CO): 2074 (m), 2040 (s), 1998 (s) cm^{-1}. ^{1}H NMR: δ 6.62 (s, 1H), 6.98 (d, 2H, J = 8.7 Hz, Ar), 7.25 (d, 2H, J = 8.7 Hz, Ar).

2nd yellow solid: IR ν(CO): 2039 (w), 2021 (s), 2006 (w), 2002 (m, sh), 1982 (w), 1972 (w), 1966 (w), 1938 (w), 1935 (w, sh) cm^{-1}. MS (FAB): *m/z* 890 (M^+).

Pale brown solid: IR ν(CO): 2101 (m), 2076 (s), 2072 (m, sh), 2050 (w), 2040 (m), 2029 (m), 2014 (m), 2004 (m), 1729 (w) cm^{-1}. ^{1}H NMR: δ 2.43 (s, 3H, C*H*$_3$), 7.32

(d, 2H, J = 8.2 Hz Ar), 7.89 (d, 2H, J = 8.3 Hz, Ar), 8.48 (s, 1H). MS (FAB): *m/z* 943 (M^+).

$[Ru_3(\mu_3\text{-NTs})(\mu_3\text{-CO})(CO)_9]$ 23: IR (heptane): ν(CO) 2112 (w), 2081 (s), 2052 (w), 2041 (m), 2031 (m), 2014 (w), 1748 (w) cm^{-1}. 1H NMR: δ 2.45 (s, 3H, CH_3), 7.34 (d, 2H, J = 8.1 Hz, Ar), 7.78 (d, 2H, J = 8.2 Hz, Ar). MS (FAB): *m/z* 755 (M^+). Anal. Calcd for $C_{17}H_7NO_{12}SRu_3$: C, 27.13, H, 0.94, N, 1.86%. Found: C, 27.15, H, 0.83, N, 1.83%.

Pale yellow solid: IR ν(CO): 2128 (w), 2090 (m), 2082 (s), 2073 (m), 2062 (m), 2039 (m), 2014 (m) cm^{-1}. MS (FAB): *m/z* 861 or 730 (M^+).

3.5.8 Hydrogenation of $[Ru_3(\mu_3\text{-NTs})(\mu_3\text{-CO})(CO)_9]$ 23

In a 3-necked 50 cm^3 round-bottomed flask equipped with a condenser attached to an oil bubbler, a stopper, a gas-inlet adaptor and a magnetic stirrer bar, was placed a solution of **23** (5 mg, 0.007 mmol) in heptane (20 cm^3). Hydrogen was bubbled through the refluxing solution, while monitoring by IR spectroscopy. After $2^1/_2$ h all **23** was consumed and **8** formed.

3.5.9 Reaction of $[Ru_3(\mu\text{-H})_2(\mu_3\text{-NTs})(CO)_8(MeCN)]$ 20 with CH≡CH

The compound **20** (51 mg, 0.070 mmol) was dissolved in CH_2Cl_2 (50 cm^3) and placed in a 3-necked 250cm^3 round-bottomed flask, equipped with an oil bubbler, a stopper, a rubber septum and a magnetic stirrer bar. Acetylene was bubbled through this yellow/orange solution *via* a filter cannula at room temperature while monitoring by IR spectroscopy. After 45 min all **20** was consumed and the solution turned dark red. The solvent was then removed under reduced pressure to leave a dark red/brown solid. This crude mixture was purified by TLC using 45% CH_2Cl_2: 55% hexane as

eluent. The polarity of the eluent was then increased to 60% CH_2Cl_2: 40% hexane. This yielded 4 bands that were each extracted with CH_2Cl_2, which was then removed under reduced pressure. A yellow band gave a yellow/brown oil (trace amount), a yellow band yielded **8** (1 mg), a bright yellow band yielded $[Ru_3(\mu\text{-}\eta^2,\eta^2\text{-}C_4H_6)(\mu_3\text{-}NTs)(\mu_3\text{-}CO)(CO)_7]$ **24** as a yellow crystalline solid (4 mg, 8%) and a pale orange band to give a yellow solid (trace amount). Dissolving the solid in the minimum amount of CH_2Cl_2 and layering with heptane and allowing the solvent mixture to diffuse grew crystallographic quality crystals of **24**.

Yellow/brown oil: IR ν(CO): 2097 (w), 2069 (m), 2063 (w, sh), 2035 (s), 2020 (m), 2008 (m), 2003 (w), 2000 (w), 1991 (w), 1982 (w), 1978 (w, sh), 1970 (w), 1961 (w), 1952 (w), 1750 (m), 1747 (m), 1743 (m), 1735 (m) cm^{-1}.

$[Ru_3(\mu\text{-}\eta^2,\eta^2\text{-}C_4H_6)(\mu_3\text{-}NTs)(\mu_3\text{-}CO)(CO)_7]$ 24: IR ν(CO): 2093 (m), 2054 (s), 2044 (s), 2029 (m), 2019 (m), 2006 (m), 1990 (w), 1758 (w) cm^{-1}. ^1H NMR: δ 2.43 (s, 3H, CH_3), 2.91 (d, 2H, J = 13.4 Hz, $CH_aH_bCH_cCH_c{\cdot}CH_a{\cdot}H_b{\cdot}$), 3.98 (d, 2H, J = 9.5 Hz, $CH_aH_bCH_cCH_c{\cdot}CH_a{\cdot}H_b{\cdot}$), 4.58 (m, 2H, $CH_aH_bCH_cCH_c{\cdot}CH_a{\cdot}H_b{\cdot}$), 7.27 (d, 2H, J = 7.9 Hz, Ar), 7.60 (d, 2H, J = 8.2 Hz, Ar). MS (FAB): *m/z* 752 (M^+). Anal. Calcd for $C_{19}H_{13}NO_{10}SRu_3$: C, 30.40, H, 1.75, N, 1.87%. Found: C, 31.96, H, 1.92, N, 1.72%.

Yellow solid: IR ν(CO): 2113 (w), 2104 (w), 2084 (s), 2080 (w, sh), 2072 (s), 2031 (m), 2023 (w), 2010 (s), 1987 (w), 1972 (w), 1967 (w) cm^{-1}.

3.5.10 Reaction of $[Ru_3(\mu\text{-}H)_2(\mu_3\text{-}NTs)(CO)_8(MeCN)]$ 20 with PhC≡CH

The compound **20** (51 mg, 0.070 mmol) was dissolved in CH_2Cl_2 (25 cm^3). To this was added a solution of PhC≡CH (21 mg, 0.206 mmol) in CH_2Cl_2 (5 cm^3). The

solution was stirred at room temperature while monitoring by IR spectroscopy. After 45 min all **20** was consumed and the yellow/orange solution turned orange. The CH_2Cl_2 was removed under reduced pressure to leave a dark red oily solid. This crude mixture was purified by TLC using 50% CH_2Cl_2: 50% light petroleum as eluent. This yielded 8 bands that were each extracted with CH_2Cl_2, which was then removed under reduced pressure. A yellow/orange band gave an orange oily solid (7 mg); a pale red band gave a pale red solid (trace amount); a yellow band gave an orange oil (8 mg); a yellow/orange band gave an orange oily solid (7 mg); a yellow band yielded $[Ru_3(\mu\text{-}\eta^2,\eta^2\text{-}C_4H_4Ph_2)(\mu_3\text{-}NTs)(\mu_3\text{-}CO)(CO)_7]$ **25** as a yellow crystalline solid (9 mg, 16%); a green/yellow band yielded **8** (5 mg); a pale yellow band gave an orange solid (7 mg) and a red band to give a red solid (6 mg). Compound **25** was recrystallised by dissolving in the minimum amount of CH_2Cl_2, adding hexane (~ 5 cm^3), removing solvent under reduced pressure until precipitation occurred and isolating the solid by filtration.

1st orange oily solid: IR ν(CO): 2089 (m), 2083 (m, sh), 2067 (w), 2054 (s), 2033 (m), 2021 (m), 2014 (s), 2000 (m), 1984 (m), 1971 (m) cm^{-1}.

1st red solid: IR ν(CO): 2100 (w), 2082 (s), 2054 (s), 2031 (m), 2017 (m), 2009 (w, sh), 1989 (w), 1977 (w), 1735 (m) cm^{-1}.

Orange oil: IR ν(CO): 2096 (w), 2048 (w), 2033 (s), 2021 (m), 2010 (w), 1997 (w), 1989 (w), 1984 (w, sh), 1967 (w), 1960 (w), 1948 (w), 1735 (s) cm^{-1}. ^1H NMR: δ 4.32 (m, 4H), 7.54 (m, 2H, Ar), 7.71 (m, 2H, Ar). MS (FAB): *m/z* 984 (M^+).

2nd orange oily solid: IR ν(CO): 2068 (s), 2064 (w, sh), 2033 (w), 2020 (w), 2015 (m), 2005 (s), 1995 (s), 1735 (s) cm^{-1}.

$[Ru_3(\mu\text{-}\eta^2,\eta^2\text{-}C_4H_4Ph_2)(\mu_3\text{-}NTs)(\mu_3\text{-}CO)(CO)_7]$ 25: IR ν(CO): 2090 (s), 2083 (m, sh), 2064 (w), 2053 (s), 2043 (s, sh), 2027 (m), 2018 (m, sh), 2010 (m), 2004 (m, sh),

1997 (w), 1990 (w), 1960 (w), 1948 (w), 1752 (m) cm^{-1}. ^1H NMR: δ 2.44 (s, 3H, CH_3), 2.98 (d, 1H, J = 1.0 Hz, PhCHHCPhCH^aH^b), 4.72 (s, 1H, PhCHCHCPhCH^aH^b), 5.53 (d, 1H, J = 13.5 Hz, PhCHCHCPhCH^{a}H^b), 5.82 (dd, 1H, J = 1.5, 13.4 Hz, PhCHCHCPhCH^{a}H^b) 7.20 – 7.90 (m, 14H, Ph, Ar). MS (FAB): *m/z* 904 (M^+). Anal. Calcd for $C_{31}H_{21}NO_{10}SRu_3$: C, 41.24, H, 2.34, N, 1.55%. Found: C, 40.98, H, 2.60, N, 1.61%.

Orange solid: IR ν(CO): 2110 (w), 2082 (s), 2077 (m, sh), 2055 (w), 2050 (w), 2042 (m), 2036 (w), 2029 (m), 2017 (s), 2008 (s), 1996 (w), 1957 (w), 1950 (w) cm^{-1}.

2nd red solid: IR ν(CO): 2119 (w), 2110 (w), 2106 (w), 2087 (m), 2082 (m), 2078 (m), 2065 (m), 2049 (m), 2043 (m), 2035 (m), 2024 (s), 2019 (m, sh), 2009 (m), 1996 (w), 1990 (w), 1981 (w), 1969 (w), 1958 (w) cm^{-1}.

3.5.11 Reaction of [Ru$_3$(μ-H)$_2$(μ$_3$-NTs)(CO)$_8$(MeCN)] 20 with PhC≡CD

The compound **20** (55 mg, 0.074 mmol) was dissolved in CH_2Cl_2 (25 cm^3) and a solution of PhC≡CD (33 mg, 0.316 mmol) in CH_2Cl_2 (5 cm^3) was added. This solution was stirred at room temperature while monitoring by IR spectroscopy. After 1^1/$_2$ h all **20** was consumed and the yellow/orange solution turned orange. The CH_2Cl_2 was removed under reduced pressure to leave a dark red/orange oily solid. This crude mixture was purified by TLC using 50% CH_2Cl_2: 50% light petroleum as eluent. This yielded 5 bands that were each extracted with CH_2Cl_2, which was then removed under reduced pressure. A yellow/orange band gave an orange solid (9 mg), an orange band gave an orange solid (4 mg), a yellow band yielded two isomers of [Ru$_3$(μ-η^2,η^2-C$_4$H$_2$D$_2$Ph$_2$)(μ$_3$-NTs)(μ$_3$-CO)(CO)$_7$] **26a** and **26b** as a yellow crystalline

solid (13 mg, 21 %), a green band yielded **8** (5 mg) and a red band gave a red solid (5 mg). Compound **26a** and **26b** was recrystallised by dissolving in the minimum amount of CH_2Cl_2, adding hexane (~ 5 cm^3), removing solvent under reduced pressure until precipitation occurred and isolating the solid by filtration.

1st orange solid: IR ν(CO): 2089 (m), 2083 (m, sh), 2067 (w), 2054 (s), 2033 (m), 2021 (m), 2014 (s), 2000 (m), 1984 (m), 1971 (m) cm^{-1}.

2nd orange solid: IR ν(CO): 2096 (w), 2068 (m), 2064 (m), 2049 (m), 2033 (s), 2016 (m), 2010 (m), 1995 (m), 1985 (w, sh), 1964 (w), 1960 (w, sh), 1907 (w) cm^{-1}.

$[Ru_3(\mu\text{-}\eta^2,\eta^2\text{-}C_4H_2D_2Ph_2)(\mu_3\text{-}NTs)(\mu_3\text{-}CO)(CO)_7]$ 26a and 26b: IR ν(CO): 2090 (s), 2083 (m, sh), 2064 (w), 2053 (s), 2043 (s, sh), 2026 (m), 2018 (m, sh), 2009 (m), 2004 (m, sh), 1997 (w), 1990 (m), 1959 (w), 1949 (w), 1752 (m) cm^{-1}. ^1H NMR: δ 2.43 (s, 3H, CH_3), 2.97 (s, 0.9H, PhCHCDCPhCH^aD), 4.70 (s, 0.1H, PhCHCDCPhCDH^b), 5.51 (s, 1H, PhC*H*CDCPhCHD), 7.10 – 7.90 (m, 14H, Ph, Ar). MS (FAB): *m z* 904 (M^+). Anal. Calcd for $C_{31}H_{19}NO_{10}SRu_3D_2$: C, 41.15, H, 2.12, N, 1.55%. Found: C, 41.13, H, 2.31, N, 1.44%.

Red solid: IR ν(CO): 2110 (w), 2087 (m), 2083 (m), 2077 (w), 2065 (s), 2049 (w), 2042 (w), 2035 (m), 2024 (s), 2008 (s), 1996 (w), 1981 (w), 1970 (w), 1957 (w), 1949 (w) cm^{-1}.

3.5.12 Reaction of $[Ru_3(\mu\text{-}H)_2(\mu_3\text{-}NTs)(CO)_8(MeCN)]$ 20 with 1,3-Butadiene

The compound **20** (46 mg, 0.062 mmol) was dissolved in CH_2Cl_2 (40 cm^3) and placed in a 3-necked 250cm^3 round bottomed flask, equipped with a rubber balloon, a stopper, a rubber septum and a magnetic stirrer bar. The yellow/orange solution was left under an atmosphere of 1,3-butadiene at room temperature while monitoring by

IR spectroscopy. After 7 h all **20** was consumed. The CH_2Cl_2 was removed under reduced pressure to leave a yellow/orange solid. This crude mixture was purified by TLC using 60% CH_2Cl_2: 40% light petroleum as eluent. This yielded 5 bands that were each extracted with CH_2Cl_2, which was then removed under reduced pressure. An orange band gave a yellow solid (trace amount), a yellow band yielded **24** (9 mg, 22 %), a purple band gave a yellow solid (4 mg), a pale yellow band gave a yellow solid (6 mg) and an orange band yielded **8** (7 mg). Compound **24** was recrystallised by dissolving in the minimum amount of CH_2Cl_2, adding hexane (~ 5 cm^3), removing solvent under reduced pressure until precipitation occurred and isolating the solid by filtration.

1st yellow solid (from purple band): IR ν(CO): 2128 (w), 2092 (m), 2066 (m), 2048 (m), 2022 (w), 1999 (w) cm^{-1}.

2nd yellow solid (from pale yellow band): IR (CH_2Cl_2) ν(CO): 2094 (w), 2057 (s), 2024 (m), 1997 (s) cm^{-1}. ^1H NMR: δ 2.39 (s, 3H, CH_3), 2.75 (d, 2H, J = 14.1 Hz), 2.96 (d, 2H, J = 13.8 Hz), 4.13 (d, 2H, 7.0 Hz), 4.33 (d, 2H, 8.8 Hz), 7.18 (d, 2H, J = 7.7 Hz, Ar), 7.30 (d, 2H, Ar). MS (EI): *m/z* 751 (M^+).

3.5.13 Reaction of $[Os_3(\mu\text{-}H)_2(\mu_3\text{-}NTs)(CO)_8(MeCN)]$ 21 with $Bu^tC{\equiv}CH$

The compound **21** (53 mg, 0.052 mmol) was dissolved in THF (20 cm^3) and placed in a Young's ampoule. To this solution was added a solution of $Bu^tC{\equiv}CH$ (19 mg, 0.231 mmol) in THF (5 cm^3). The ampoule was then sealed and placed in an oven at 65 °C for 12 h, during which time the solution turned from pale yellow to a darker yellow. After cooling the THF was removed under reduced pressure to leave a dark orange/brown oil. This crude mixture was purified by TLC using 50% CH_2Cl_2: 50%

light petroleum as eluent. This yielded 3 bands that were each extracted with CH_2Cl_2, which was removed under reduced pressure. An orange band yielded $[Os_3(\mu\text{-H})(\mu\text{-}trans\text{-CH=CHBu}^t)(\mu_3\text{-NTs})(CO)_8]$ **27** as a yellow solid (40 mg, 73%) as the major product. Dissolving the solid in the minimum amount of hexane and allowing the hexane to slowly evaporate at room temperature grew crystallographic quality crystals of **27**.

27: IR ν(CO): 2104(s), 2078 (s), 2060 (w, sh), 2039 (s), 2033 (s), 2021 (s, sh), 2008 (m, sh), 1996 (m), 1982 (m), 1972 (s), 1950 (w), 1945 (w) cm^{-1}. ^1H NMR: δ -12.89 (s, 1H, Os-*H*), 1.28 (s, 9H, $C(CH_3)_3$), 2.42 (s, 3H, CH_3), 5.99 (d, 1H, J = 12.4 Hz, CH=C*H*Bu^t), 7.27 (d, 2H, J = 8.1 Hz, Ar), 7.55 (d, 2H, J = 8.2 Hz, Ar), 9.48 (d, 1H, J = 12.4 Hz, C*H*=CHBu^t). MS (FAB): *m/z* 1049 (M^+).

3.5.14 Reaction of $[Os_3(\mu\text{-H})_2(\mu_3\text{-NTs})(CO)_8(MeCN)]$ 21 with PhC≡CH

The compound **21** (52 mg, 0.053 mmol) was dissolved in THF (40 cm^3) and to this solution was added a solution of PhC≡CH (21 mg, 0.207 mmol) in THF (5 cm^3). The solution was refluxed while monitoring by IR spectroscopy until no **21** remained (10 h) during which time the solution turned from pale yellow to a darker yellow. After cooling THF was removed under reduced pressure to leave a dark yellow oily mixture of $[Os_3(\mu\text{-H})(\mu\text{-}trans\text{-CH=CHPh})(\mu_3\text{-NTs})(CO)_8]$ **28** and $[Os_3(\mu\text{-H})_2(\mu_3\text{-NTs})(CO)_9]$ **11**.

$[Os_3(\mu\text{-H})(\mu\text{-}trans\text{-CH=CHPh})(\mu_3\text{-NTs})(CO)_8]$ 28: Crude IR (THF) ν(CO): 2106 (m), 2078 (m), 2035 (s), 2024 (s, sh) cm^{-1}. Crude ^1H NMR: δ –12.82 (s, 1H, Os-*H*), 2.43 (s, 3H, CH_3), 6.63 (d, 1H, J = 12.1 Hz, CH=C*H*Ph), 7.00 – 7.85 (m, 9H, Ph, Ar), 9.97 (d, 1H, J = 12.1 Hz, C*H*=CHPh).

Chapter 4:

Alkyne insertion into metal-hydrogen bonds of sulfido capped clusters

4.1 INTRODUCTION

Like the imido ligand, the sulfido ligand can adopt various modes of coordination, and in clusters the μ_3- and μ_4-modes predominate (Figs. 4.1a - d).[43,132] The μ_3-sulfido

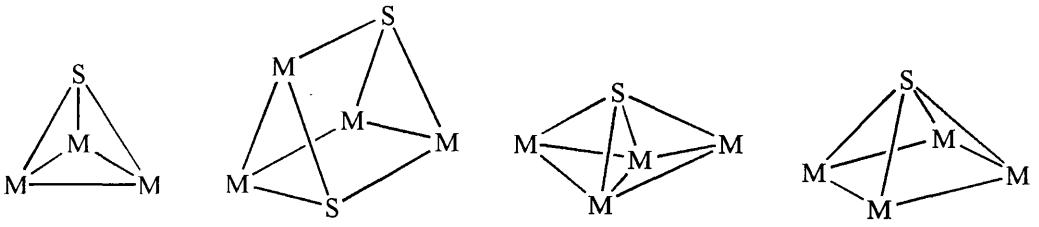

Fig. 4.1 Common coordination modes of the sulfido ligand in clusters

cap acts as a 4-electron donor with a lone pair of electrons and it can stabilise both early and late transition metals. Clusters analogous to the phenylimido-capped, clusters described in Chapter 2, can be formed by treating $[Ru_3(CO)_{12}]$ and $[Os_3(CO)_{12}]$ with elemental sulfur or hydrogen sulfide, to give trinuclear μ_3-sulfido-capped clusters such as $[M_3(\mu\text{-}H)_2(\mu_3\text{-}S)(CO)_9]$,[133-136] $[M_3(\mu_3\text{-}S)_2(CO)_9]$[137-139] and $[M_3(\mu_3\text{-}S)(\mu_3\text{-}CO)(CO)_{10}]$[140,141] (where M = Ru or Os) (Figs. 4.2a - c).

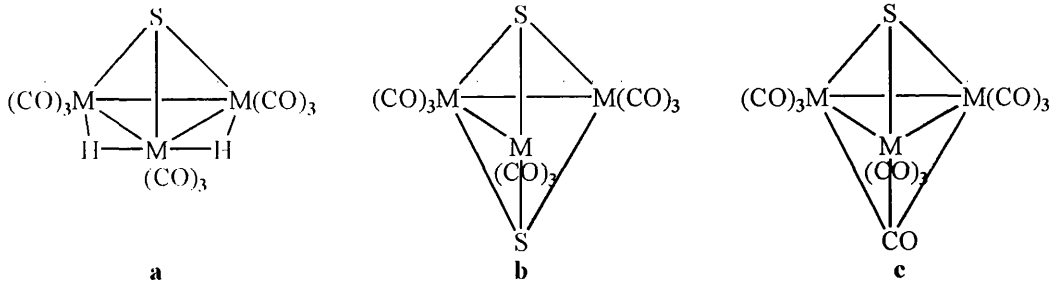

Fig. 4.2 Some common μ_3-sulfido clusters

Another useful source of sulfur is CS_2 which, when reacted with $[Os_3(CO)_{12}]$ forms $[Os_3(\mu_3\text{-}S)_2(CO)_8(CS)]$.[142] As with nitrogen-containing clusters, the use of the precursors $[M_3(\mu\text{-}H)(\mu\text{-}SPh)(CO)_{10}]$ (where M = Ru or Os), which are analogous to

amido clusters such as $[Os_3(\mu\text{-}H)(\mu\text{-}NHPh)(CO)_{10}]$ **5**, results in the formation of further sulfur-capped clusters.[140,141,143]

The cluster $[Ru_3(\mu\text{-}H)_2(\mu_3\text{-}S)(CO)_9]$ **29** protonates at a metal-metal bond rather than at the sulfur atom, which has reduced Lewis basicity relative to oxygen, to form $[Ru_3(\mu\text{-}H)_3(\mu_3\text{-}S)(CO)_9]^+$.[133] However, despite this apparent unavailability of the lone pair on the sulfido cap, **29** can trimerise to produce $[Ru_3(\mu\text{-}H)_2(\mu_4\text{-}S)(CO)_8]_3$ (Fig. 4.3).[144]

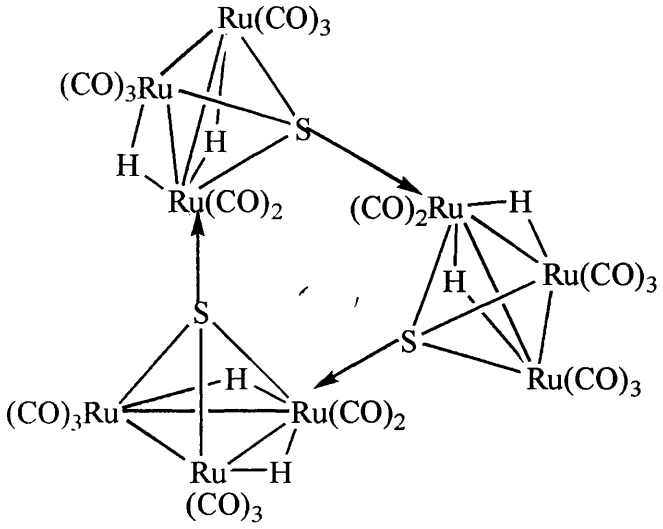

Fig. 4.3 The structure of $[Ru_3(\mu\text{-}H)_2(\mu_4\text{-}S)(CO)_8]_3$

Previous work has been carried out on the reactions of sulfur-capped clusters with alkynes. An example of this is the thermal reaction of $[Ru_3(\mu_3\text{-}S)(\mu_3\text{-}CO)(CO)_9]$ with phenylethyne, resulting in the formation of the insertion product shown in Scheme 4.1. Tetraruthenium clusters can then subsequently be formed by employing the lone pair of electrons on the sulfur atom (Scheme 4.1).[145]

The cluster $[Os_4(\mu_3\text{-}S)(CO)_{12}]$ reacts with terminal alkynes RC≡CH to initially form the compounds $[Os_4(\mu_4\text{-}\eta^3\text{-}SC(R)=CH)(CO)_{12}]$, by coupling of the alkyne with the

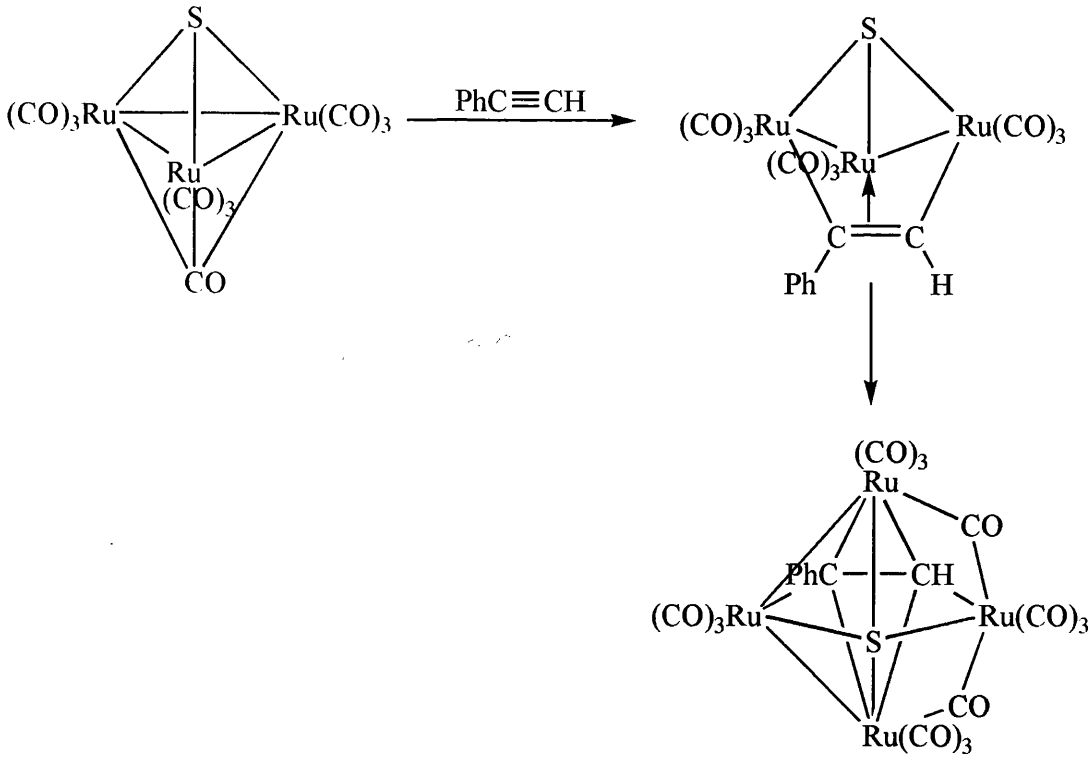

Scheme 4.1 Insertion of phenylethyne into $[Ru_3(\mu_3\text{-}S)(\mu_3\text{-}CO)(CO)_9]$

bridging sulfido ligand (Scheme 4.2) and the vinylidene cluster $[Os_4(\mu_3\text{-}S)(\mu_4\text{-}C{=}CHR)(CO)_{12}]$.[43,146,147] The latter is formed by a 1,2-shift of the acetylenic

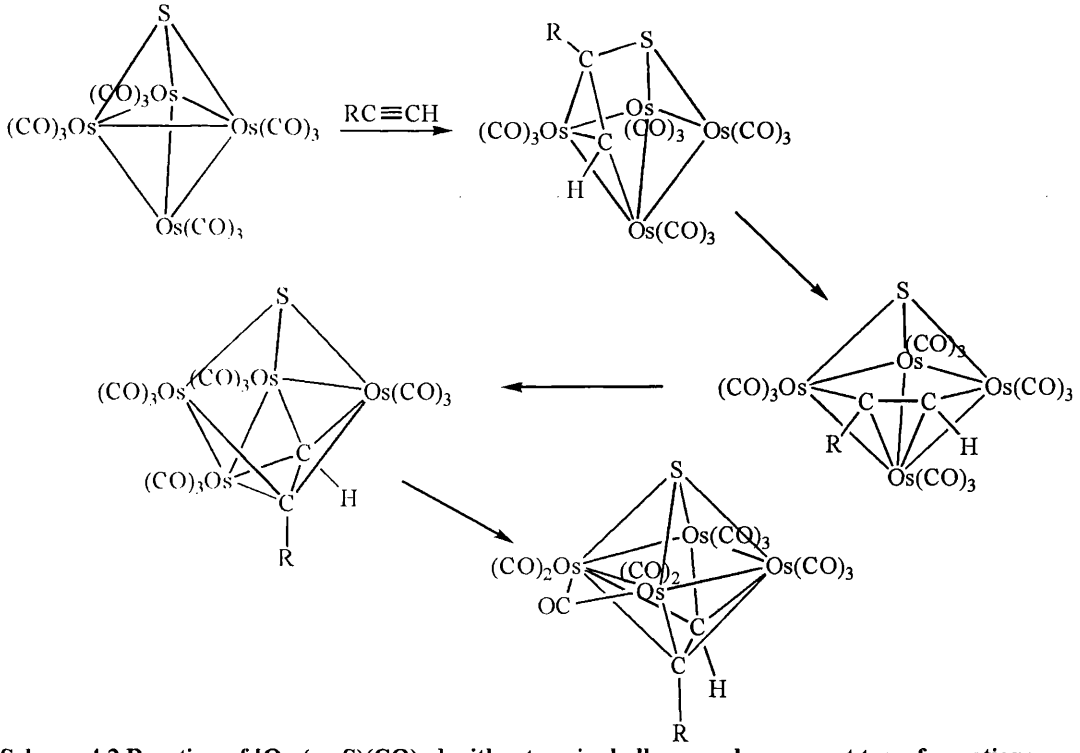

Scheme 4.2 Reaction of $[Os_4(\mu_3\text{-}S)(CO)_{12}]$ with a terminal alkyne and susequent transformations

hydrogen atom. The former species can then undergo S-C cleavage to $[Os_4(\mu_3\text{-}S)(\mu_3\text{-}CH{=}CR)(CO)_{12}]$, which has a butterfly framework of metal atoms.[148] This rearranges to a chain of metal atoms in the compound $[Os_4(\mu_3\text{-}S)(\mu_4\text{-}CH{=}CR)(CO)_{12}]$. Finally CO loss and cyclisation produces the unsaturated cluster $[Os_4(\mu_4\text{-}CH{=}CR)(\mu_4\text{-}S)(CO)_{11}]$ (Scheme 4.2). This sequence of steps gives an insight into the reversible coupling of alkyne with sulfur in a sulfido-bridged cluster.

The tetraosmium cluster $[Os_4(\mu_4\text{-}CR{=}CR')(\mu_4\text{-}S)(CO)_{11}]$ (where R = H or CO_2Me, R' = CO_2Me) further reacts with PhC≡CH (Scheme 4.3), the product formed being dependent on the substituents.[132,149]

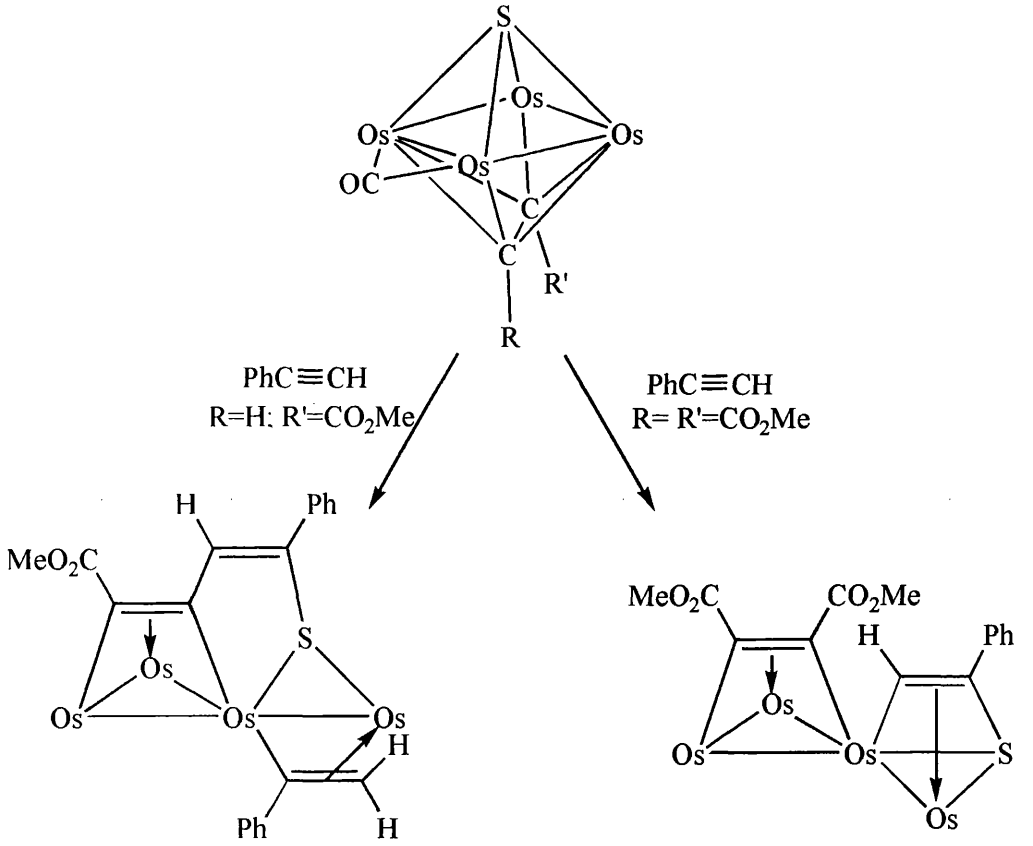

Scheme 4.3 Reaction of $[Os_4\{\mu_4\text{-}C(R)C(R')\}(\mu_4\text{-}S)(CO)_{11}]$ with phenylethyne (some CO ligands have been omitted for clarity)

Sulfido trimetal clusters can promote the stoichiometric oligomerisation of alkynes, such as the formation of 1,3,5-triphenylbenzene from phenylethyne, using the mixed-metal sulfido-capped cluster $[RuMo_2Cp_2(\mu_3\text{-}S)(CO)_7]$ (Scheme 4.4).[43,132,150,151]

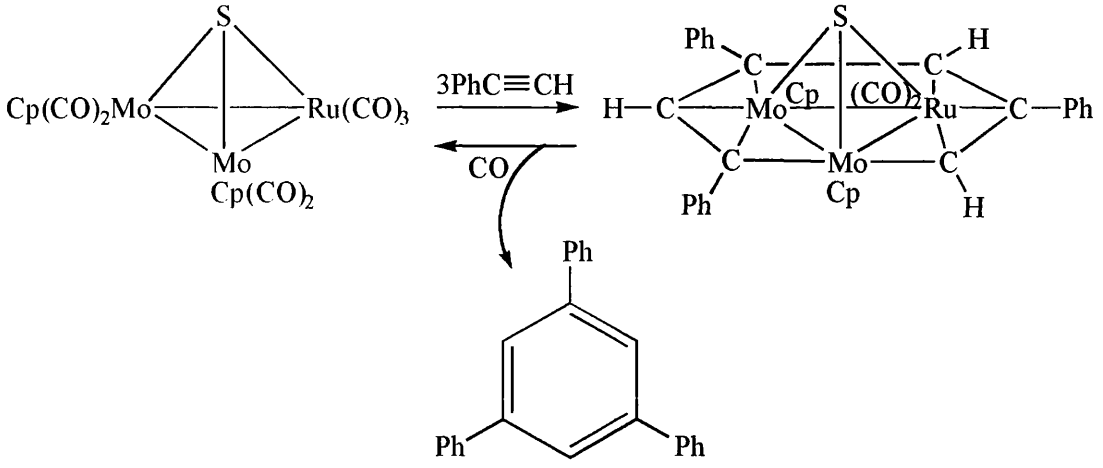

Scheme 4.4 The oligomerisation of phenylethyne to 1,3,5-triphenylbenzene

4.2 TARGETS, AIMS AND OBJECTIVES IN THIS CHAPTER

As described above, thermal reaction of sulfur-capped clusters with alkynes have been carried out previously, resulting in coupling of the alkyne with the sulfur cap. However, very little chemistry of this type has been carried with the hydrido clusters $[M_3(\mu\text{-}H)_2(\mu_3\text{-}S)(CO)_9]$ where we believe insertion of an alkyne into the M-H bond will be favoured. The targets, aims and objectives in this chapter are:

- To compare the reactivity of $[M_3(\mu\text{-}H)_2(\mu_3\text{-}S)(CO)_9]$ with that of $[M_3(\mu\text{-}H_2)(\mu_3\text{-}NTs)(CO)_9]$ (where M = Ru or Os) and the effects of increased electron donation on going from NTs (see Chapter 3) to S.
- To insert alkynes into the M-H bonds of sulfur-capped clusters using the same methodology as for the tosylimido-capped clusters.
- To further investigate the mechanism of the formation of butadiene from terminal alkynes.

4.3 RESULTS AND DISCUSSION

4.3.1 Preparation of $[Os_3(\mu\text{-}H)_2(\mu_3\text{-}S)(CO)_8(MeCN)]$ 31

The compound $[Os_3(\mu\text{-}H)_2(\mu_3\text{-}S)(CO)_9]$ **30** was prepared in quantitative yield using literature procedures,[135] by treating a refluxing solution of $[Os_3(CO)_{12}]$ in petroleum spirit (b.p. 120-160 °C) with hydrogen sulfide gas for 6 hours. Treatment of **30** in CH_2Cl_2 with a $Me_3NO.2H_2O$/MeCN solution at room temperature resulted in an immediate reaction, as shown by IR spectroscopy, to form $[Os_3(\mu\text{-}H)_2(\mu_3\text{-}S)(CO)_8(MeCN)]$ **31**. The solution was filtered through silica gel to remove any unreacted $Me_3NO.2H_2O$. This compound has been reported previously by Johnson *et al.*[152,153] but there was no mention of the method of preparation nor were any analytical data provided. The room temperature ^1H NMR spectrum of **31** shows a sharp singlet at δ -24.69 and a sharp doublet at δ -19.65 (J = 1.2 Hz) due to the hydride ligands. There is also a singlet at δ 2.54 for the MeCN ligand. As with $[Ru_3(\mu\text{-}H)_2(\mu_3\text{-}NTs)(CO)_8(MeCN)]$ **20** and $[Os_3(\mu\text{-}H)_2(\mu_3\text{-}NTs)(CO)_8(MeCN)]$ **21**, cluster **31** is also formed with the MeCN ligand *cis* to the capping ligand and bound to the metal atom which is bonded to both hydride ligands. Again there is also a small peak in the ^1H NMR spectrum due to a small amount of starting material and further peaks, possibly for isomers of **31** or the complex containing two MeCN ligands. The EI mass spectrum of **31**, however, was consistent with **30**, which could be attributed to the decomposition and re-conversion back to **30** in the inlet system of the mass spectrometer.

4.3.2 Reaction of $[Os_3(\mu\text{-}H)_2(\mu_3\text{-}S)(CO)_8(MeCN)]$ 31 with PhC≡CH

The cluster **31** was treated with five equivalents of PhC≡CH in refluxing THF for $16^1/_2$ hours. After purification six compounds were isolated: two bright yellow solids, a red solid, a dark yellow solid, a yellow solid and one brown solid. It was found the two bright yellow solids were regioisomers resulting from the single insertion of PhC≡CH into an M-H bond. Their IR spectra were very similar to each other and their structures were deduced from their ^{1}H NMR spectra. One of these compounds was found to be the α-isomer (as described in Chapter 3) of the hydrido-alkenyl cluster, the product of Markovnikov addition, which could only be obtained as an inseparable mixture with **30**. The ^{1}H NMR spectrum of this compound $[Os_3(\mu\text{-}H)(\mu\text{-}PhC{=}CH_2)(\mu_3\text{-}S)(CO)_8]$ **32** showed a singlet at δ -13.52 due to the hydride ligand, doublets at δ 4.29 and 4.59 (with small coupling constants for coupling between the protons on the β-carbon) and signals due to the Ph group. The EI mass spectrum displayed a molecular ion peak at *m/z* 932 and daughter ion peaks due to the successive loss of eight carbonyl ligands along with peaks for **30**. The second bright yellow compound was found to be the β-isomer $[Os_3(\mu\text{-}H)(\mu\text{-}CH{=}CHPh)(\mu_3\text{-}S)(CO)_8]$ **33**, obtained in 14% yield. The ^{1}H NMR spectrum of this compound showed a singlet at δ -14.07 due to the hydride ligand, a doublet at δ 5.91 due to the proton on the β-carbon and another doublet at δ 9.46 due to the proton on the α-carbon and a multiplet at δ 7.21-7.46 due to the Ph group. The coupling constant (11.5 Hz) is consistent with a *trans* geometry for the CH=CHPh group. The EI mass spectrum displayed a molecular ion peak at *m/z* 932 and daughter ions due to the successive loss of eight carbonyl ligands. There were also peaks consistent with **30**. The red solid (9% yield) was found to be an inseparable mixture of isomers of dialkenyl clusters formed by

double insertion of PhC≡CH into the M-H bonds. The IR spectrum was very similar to that for $[Os_3(\mu\text{-PhC=CHPh})_2(\mu_3\text{-}C_6H_4)(CO)_7]$[114] although the ν(CO) absorptions for this compound were at lower wavenumbers than those for the sulfur-capped dialkenyl cluster, as the C_6H_4 ligand donates more electron density to the metal core which in turn lowers the ν(CO) wavenumbers. From the ^{1}H NMR spectrum it appears that the mixed α and β dialkenyl cluster $[Os_3(\mu\text{-CH=CHPh})(\mu\text{-PhC=CH}_2)(\mu_3\text{-S})(CO)_7]$ **34** is the major isomer (Figs. 4.4a and b). Apart from the signals for the Ph group there

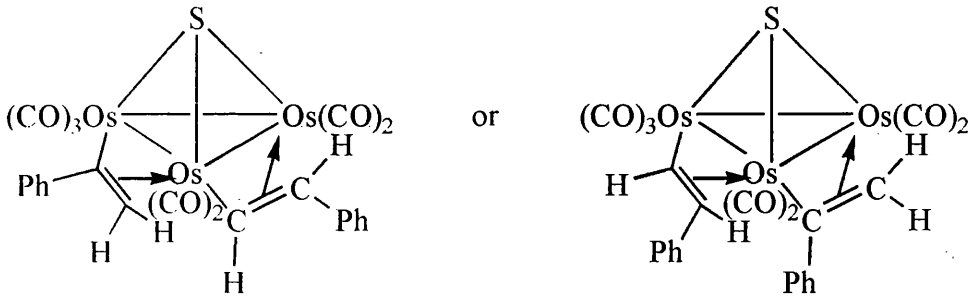

a **b**

Fig. 4.4 The two possible isomers of 34

are also two singlets at δ 3.78 and 4.13 due to the two protons on the α-isomer and two doublets at δ 5.63 (J = 12.2 Hz) and 9.77 (J = 12.5 Hz) due to the protons on the β-isomer present in the ^{1}H NMR spectrum. There is also evidence for the formation of the isomer where both alkenyl fragments are present as the α-form in the compound $[Os_3(\mu\text{-PhC=CH}_2)_2(\mu_3\text{-S})(CO)_7]$ **35** (Fig. 4.5).

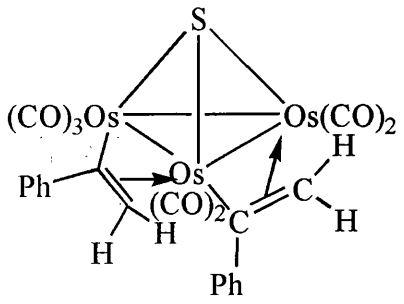

Fig. 4.5 The dialkenyl cluster 35

The ^{1}H NMR spectrum for this compound shows singlets at δ 3.81, 3.90, 4.10 and 5.61 along with signals for the Ph group. The EI mass spectrum displayed a molecular ion peak at *m/z* 1006 which would be consistent with the dialkenyl cluster. Additionally a peak was observed with a CO ligand in excess of this formula, which might be a butadiene cluster (see below). The dark yellow solid was indeed a butadiene cluster formed in 10% yield. The structure of the butadiene ligand was deduced from the ^{1}H NMR spectrum and was found to be the product of head-to-tail coupling to give $[Os_3(PhCH^a{=}CH^bCPh{=}CH^cH^d)(\mu_3\text{-}S)(CO)_8]$ **36**. The ^{1}H NMR spectrum shows doublets at δ 1.55 and 2.43 (J = 3.5 and 3.4 Hz respectively) for H^c and H^d, a doublet at δ 3.58 (J = 9.2 Hz) for H^a and a doublet at δ 6.79 (J = 9.0 Hz) for H^b along with signals for the Ph group. The EI mass spectrum displayed a molecular ion peak at *m/z* 1034 and daughter ions due to the successive loss of eight carbonyl ligands. There is also a peak at *m/z* 776 which would be consistent with the loss of the butadiene ligand and two carbonyl ligands, along with peaks for the successive loss of a further six carbonyl ligands. The IR spectrum of **36** is very different to those for $[Ru_3(\mu\text{-}\eta^2,\eta^2\text{-}C_4H_6)(\mu_3\text{-}NTs)(\mu_3\text{-}CO)(CO)_7]$ **24** and $[Ru_3(\mu\text{-}\eta^2,\eta^2\text{-}C_4H_4Ph_2)(\mu_3\text{-}NTs)(\mu_3\text{-}CO)(CO)_7]$ **25** with no evidence for a μ_3-CO ligand. The chemical shifts for the four vinylic hydrogen atoms in **36** are also very different from those for **25**, although this could be accounted for by the use of different metals and capping groups. To elucidate the structure of **36** single crystals were grown by allowing heptane to diffuse into a solution of **36** in CH_2Cl_2. The X-ray structure confirms that **36** has a different structure from **24** and **25** (Fig. 4.6). Selected bond lengths and angles are given in Table 4.1. The three osmium atoms form a closed isosceles triangle [Os(1)-Os(2) 2.8696(12); Os(1)-Os(3) 2.8524 (10); Os(2)-Os(3) 2.7339(9) Å] with all three osmium atoms bonded to the sulfur cap. Two osmium atoms, Os(2) and

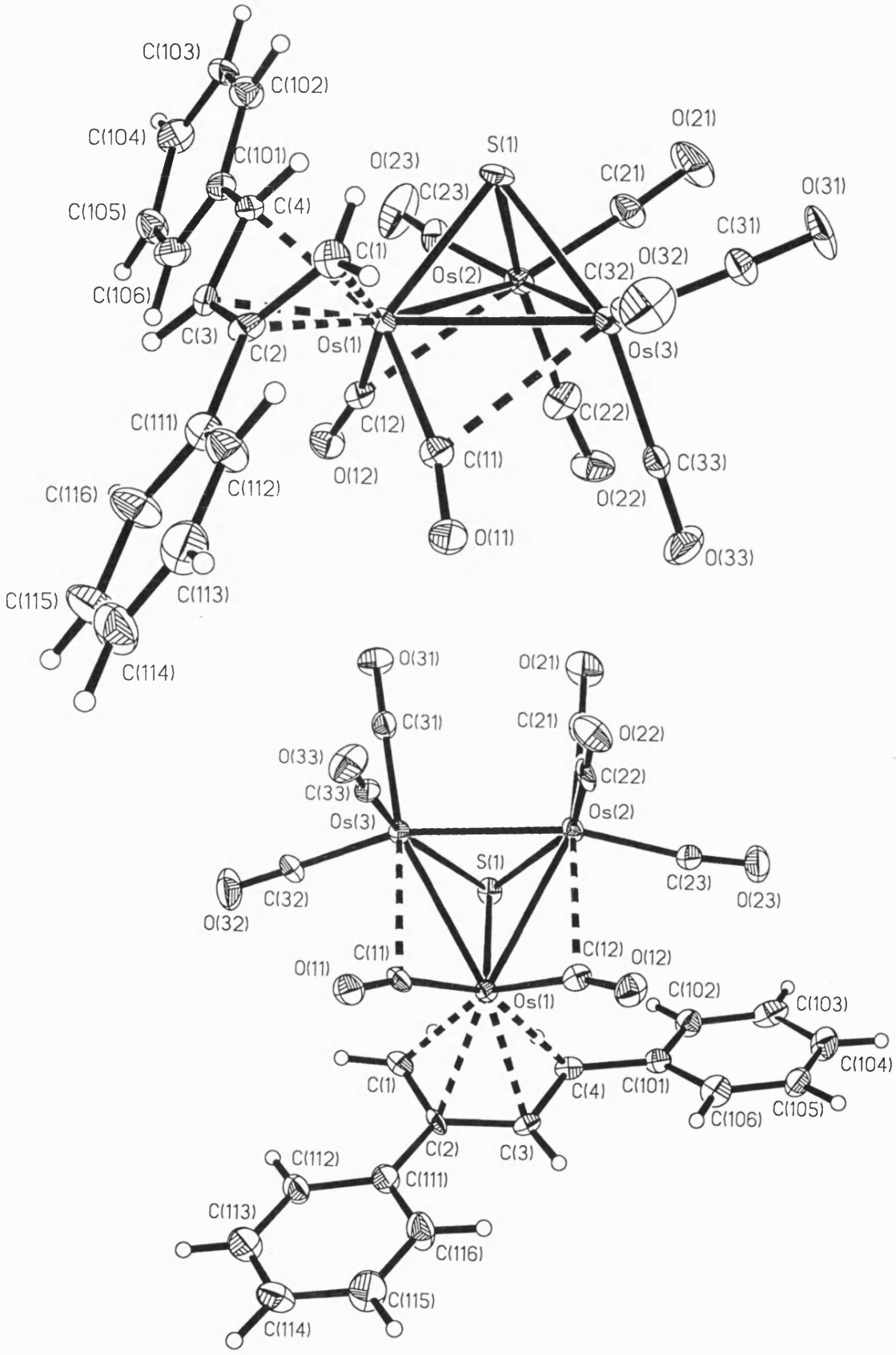

Fig. 4.6 Two views of the X-ray structure of $[Os_3(\eta^4\text{-}cis\text{-}CHPh{=}CHCPh{=}CH_2)(\mu_3\text{-}S)(CO)_8]$ 36

Table 4.1 Selected bond lengths [Å] and angles [°] for 36

Os(1)-Os(2)	2.8696(12)	Os(1)-S(1)	2.374(3)
Os(1)-Os(3)	2.8524(10)	Os(2)-S(1)	2.366(3)
Os(2)-Os(3)	2.7339(9)	Os(3)-S(1)	2.373(3)
Os(1)-C(1)	2.214(13)	C(1)-C(2)	1.40(2)
Os(1)-C(2)	2.252(12)	C(2)-C(3)	1.44(2)
Os(1)-C(3)	2.252(12)	C(3)-C(4)	1.46(2)
Os(1)-C(4)	2.267(12)		
C(1)-C(2)-C(3)	116.9(12)	C(2)-(C3)-C(4)	118.0(12)

Os(3) associated with the shortest Os-Os bond, are bonded to three terminal CO ligands while the two CO ligands at Os(1) are semi-bridging to Os(2) and Os(3). The structure confirms the IR spectroscopy evidence for no μ_3-CO ligand being present. The termini of the butadiene ligand are pointing up towards the sulfido cap, and more importantly this structure shows the 1,3-butadiene is η^4 coordinated to Os(1) rather than bridging as in **24** and **25**. The Os(1)-C(4) bond at 2.267(12) Å is longer than the Os(1)-C(1) bond at 2.214(13) Å because of the bulky Ph group being pushed away by the sulfur cap. The relatively long and similar C-C distances in the butadiene ligand [C(1)-C(2) 1.40(2); C(2)-C(3) 1.44(2); C(3)-C(4) 1.46(2) Å] could be due to donation of electron density from the metal into the π-acceptor orbital of the butadiene ligand, thereby lengthening the C-C double bonds and shortening the C-C single bond. The mode of coordination of the butadiene ligand could be affected by the electronic effects of the capping ligand involved or the choice of metal, that is ruthenium *versus* osmium. However, the results presented later in Section 4.3.4 would suggest the choice of capping ligand is the determining factor. The sulfido cap is more electron donating than the tosylimido cap, this could lead to a different distribution of CO ligands or the possibility that two different mechanisms for the formation of the butadiene clusters are taking place. One, which results in the formation of a butadiene

that bridges two metal atoms as in **24** and **25** and the other forming an η^4 butadiene as in **36**.

The yellow compound will be discussed in the next section. The brown solid appears to be a mixture of compounds. The IR spectrum is very similar to **34** suggesting other isomers of the butadiene clusters have been formed. The ^{1}H NMR spectrum showed two singlets at δ 3.26 and 3.38 and two multiplets at δ 3.50 and 6.35 along with signals for the Ph groups. It is speculated that the two singlets could be due to $[Os_3(\eta^4\text{-}CH_2{=}CPhCPh{=}CH_2)(\mu_3\text{-}S)(CO)_8]$ (Fig 4.7a) and the multiplets due to the compound $[Os_3(\eta^4\text{-}PhCH{=}CHCH{=}CHPh)(\mu_3\text{-}S)(CO)_8]$ where the hydrogen atoms are *trans* to each other (Fig. 4.7b). The multiplets were satisfactorily simulated by an

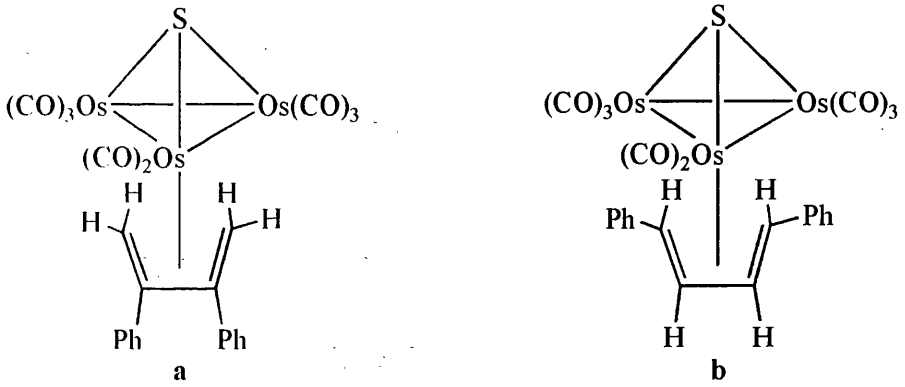

Fig. 4.7 Two other isomers of $[Os_3(\eta^4\text{-}C_4H_4Ph_2)(\mu_3\text{-}S)(CO)_8]$ that may have been formed

AA'BB' spectrum with J_{AB} = 7.4 Hz and $J_{BB'}$ = 5 to 7 Hz. The latter coupling corresponds to coupling within the central CHCH component. Unfortunately the EI mass spectrum showed a mixture of compounds, which, due to the small amount of compound available, could not be separated, and attempts to grow single crystals were also unsuccessful.

4.3.3 Reaction of $[Os_3(\mu\text{-}H)_2(\mu_3\text{-}S)(CO)_8(MeCN)]$ 31 with CH≡CH

Johnson *et al.* have reported a similar reaction,[153] however the method of preparation has not been given. This reaction was carried out by myself as a preliminary study, the results of which are presented in this section. Some interesting results were obtained which could not be explored in depth. Therefore, Caroline Forth in our group is continuing this work in more detail. A solution of **31** in THF was treated with CH≡CH in an ampoule at 55 °C for 16 hours. After purification, five compounds were isolated: two yellow solids, an orange solid and two yellow/orange solids. The first yellow solid was found to be the hydrido alkenyl compound $[Os_3(\mu\text{-}H)(\mu\text{-}CH{=}CH_2)(\mu_3\text{-}S)(CO_8)]$ **37** formed in 3% yield. This compound was also reported by Johnson *et al.* but no analytical data were given.[153] The IR spectrum of **37** is very similar to those for $[Os_3(\mu\text{-}H)(\mu\text{-}CPh{=}CH_2)(\mu_3\text{-}S)(CO)_8]$ **32** and $[Os_3(\mu\text{-}H)(\mu\text{-}\textit{trans}\text{-}CH{=}CHPh)(\mu_3\text{-}S)(CO)_8]$ **33** described in the previous section. Due to the small quantity of sample available the ^1H NMR spectrum was very weak. However, it showed a singlet at δ -13.48 for the hydride ligand, as well as doublets at δ 4.42 (J = 12.1 Hz) and 4.92 (J = 8.1 Hz) for *trans* and *cis* coupling, respectively, between the protons on the β- and α-carbons of the alkenyl ligand. There is also a doublet of doublets at δ 9.18 (J = 8.2 and 11.9 Hz) for the α-carbon proton. The EI mass spectrum displayed a molecular ion peak at *m/z* 856 with daughter ions due to the successive loss of eight carbonyl ligands. There was also a peak at *m/z* 910 which would be equivalent to the cluster **37** with an additional two carbonyl ligands.

The orange solid was formed in 6% yield, but the IR and NMR spectra showed it could not be obtained free from contamination by $[Os_3(\mu\text{-}H)_2(\mu_3\text{-}S)(CO)_9]$ **30**. The ^1H

NMR (Fig. 4.8) spectrum shows a doublet at δ 2.10 (J = 6.0 Hz) due to three protons indicating coupling between a methyl group and a CH group. A doublet of quartets at δ 2.72 (J = 6.5 Hz) due to one proton is consistent with a CH group coupling with the methyl group and a further CH group. A doublet of doublets at δ 7.07 (J = 7.2 Hz) due to one proton indicates coupling with the previous CH group and also another CH group. Finally there is a doublet at δ 9.66 (J = 6.0 Hz) due to one proton that couples only with the previous CH group.

From this spectrum the structure of the ligand can be deduced to be a $CHCHCHCH_3$ chain, an isomer of the 1,3-butadiene ligand. The spectrum also showed the presence of an AA'BB' pattern of signals at δ 6.72 and 7.30 for a minor impurity which could be a metallacyclopentadiene compound. The EI mass spectrum displayed a molecular ion peak at *m z* 880 with daughter ions due to the successive loss of eight carbonyl ligands as the main species. There are also peaks at *m/z* 630 and 604 consistent with the loss of the $CHCHCHCH_3$ ligand and seven and eight carbonyl ligands respectively. Impurities were also present with envelopes of peaks between *m/z* 908 and 1433. A molecular mass of 880 is consistent with the cluster $[Os_3(\mu\text{-}CHCHCHCH_3)(\mu_3\text{-}S)(CO)_8]$ **38**. The $CHCHCHCH_3$ ligand could bind to the metal atoms in different ways (Figs. 4.9a-d). All are four-electron donors, the first form in Fig 4.9a shows the ligand bridging two metals and bound in an η^1,η^2,η^1 manner. In Fig. 4.9b the ligand is bridging two metals with an η^1,η^1-alkylidene fragment and an η^2-alkene fragment. Fig. 4.9c is a variation of this with the ligand bridging all three metals atoms with an η^1,η^1- alkylidene fragment and an η^2-alkene fragment. The form shown in Fig. 4.9d has η^1,η^3-allyl coordination. To deduce conclusively the

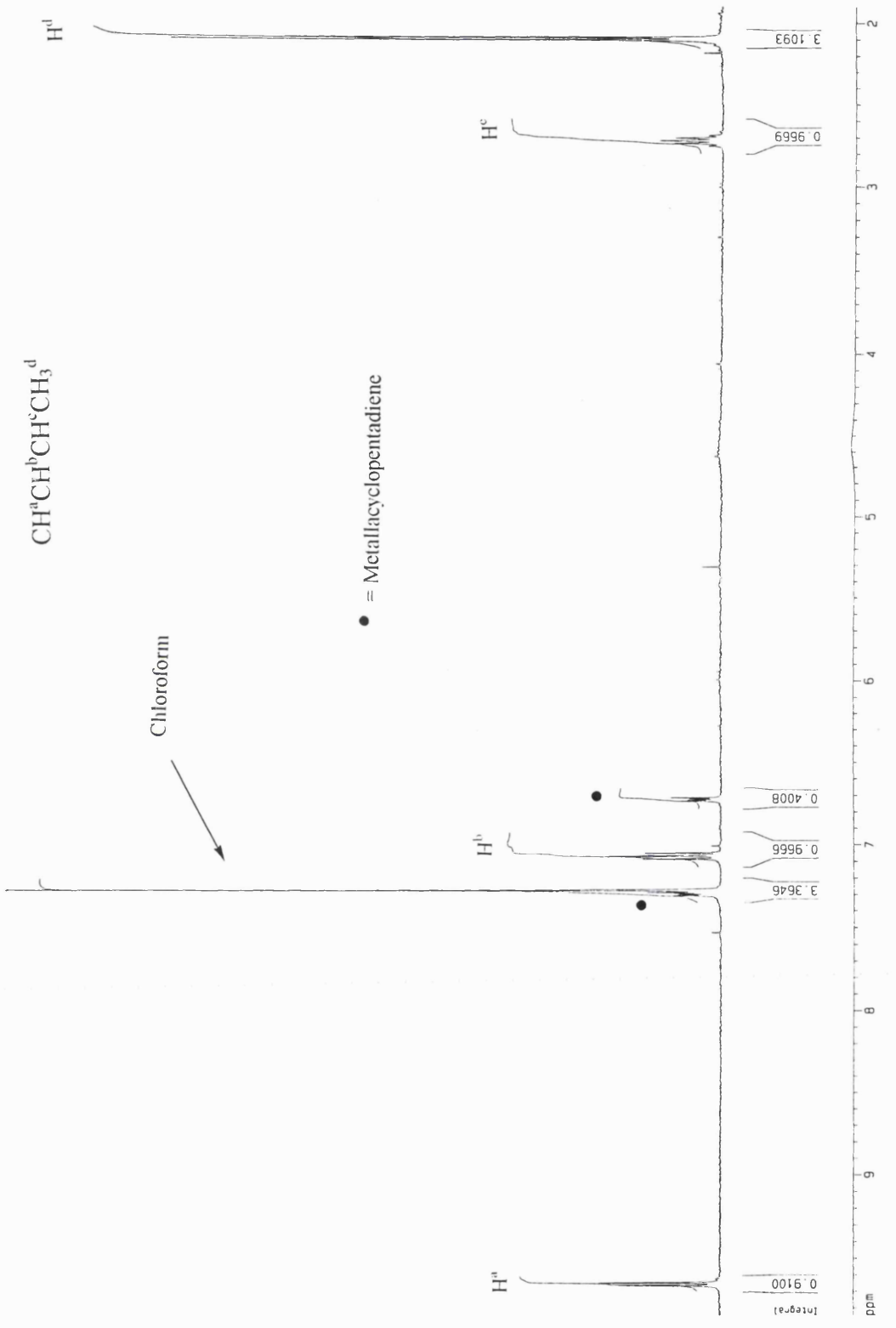

Fig. 4.8 The ^{1}H NMR spectrum of 38

structure of **38** an X-ray crystallographic determination needs to be carried out and Caroline Forth in our research group is working towards this end.

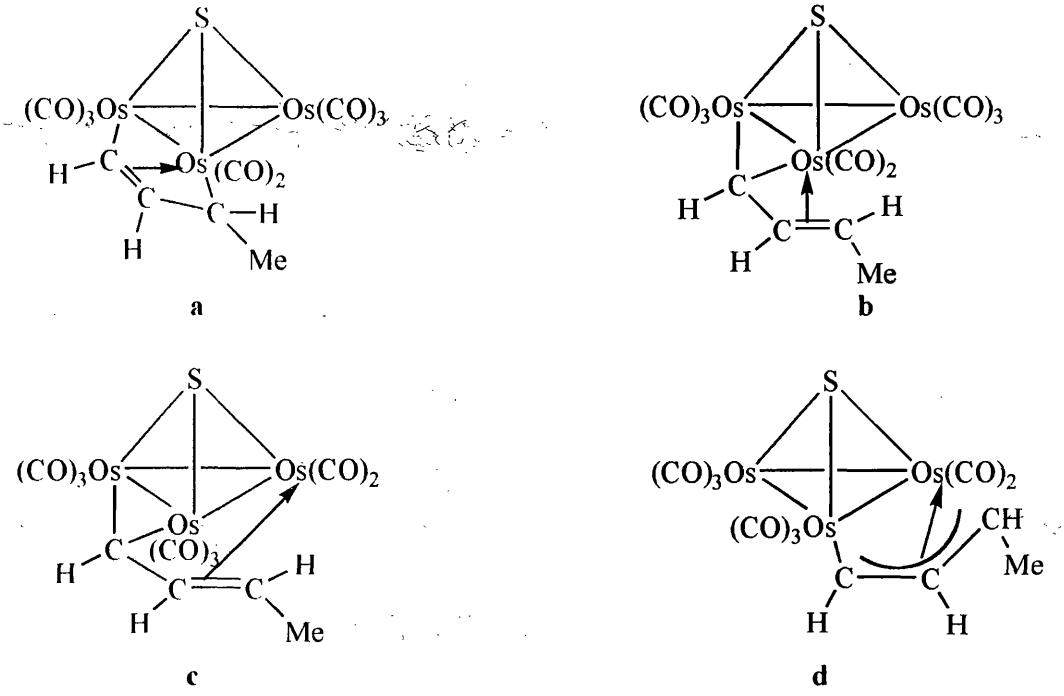

Fig. 4.9 The possible isomers of 38

The first yellow/orange product formed in 2% yield gave the ^{1}H NMR spectrum leading to a speculated structure shown in Fig. 4.10. The ^{1}H NMR spectrum

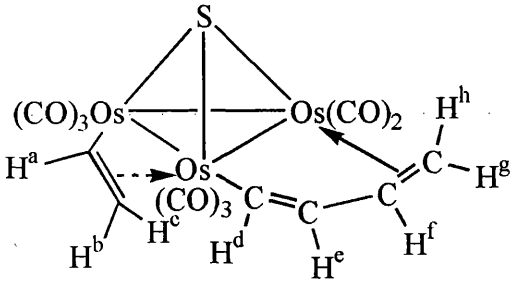

Fig. 4.10 The possible structure of 39

(Fig. 4.11) showed a doublet of doublet of doublets at δ 1.15 (J = 7.3, 9.9 and 12.0 Hz) for H^f, a doublet of doublets at δ 2.13 (J = 7.1 and 9.7 Hz) for H^e, a doublet at δ 3.44 (J = 12.3 Hz) for H^h, a doublet at δ 4.51 (J = 7.2 Hz) for H^g, a doublet at δ 6.02 (J = 14.1 Hz) for H^c, a doublet at δ 6.12 (J 9.2 Hz) for H^b, a doublet at δ 8.30 (J = 7.1

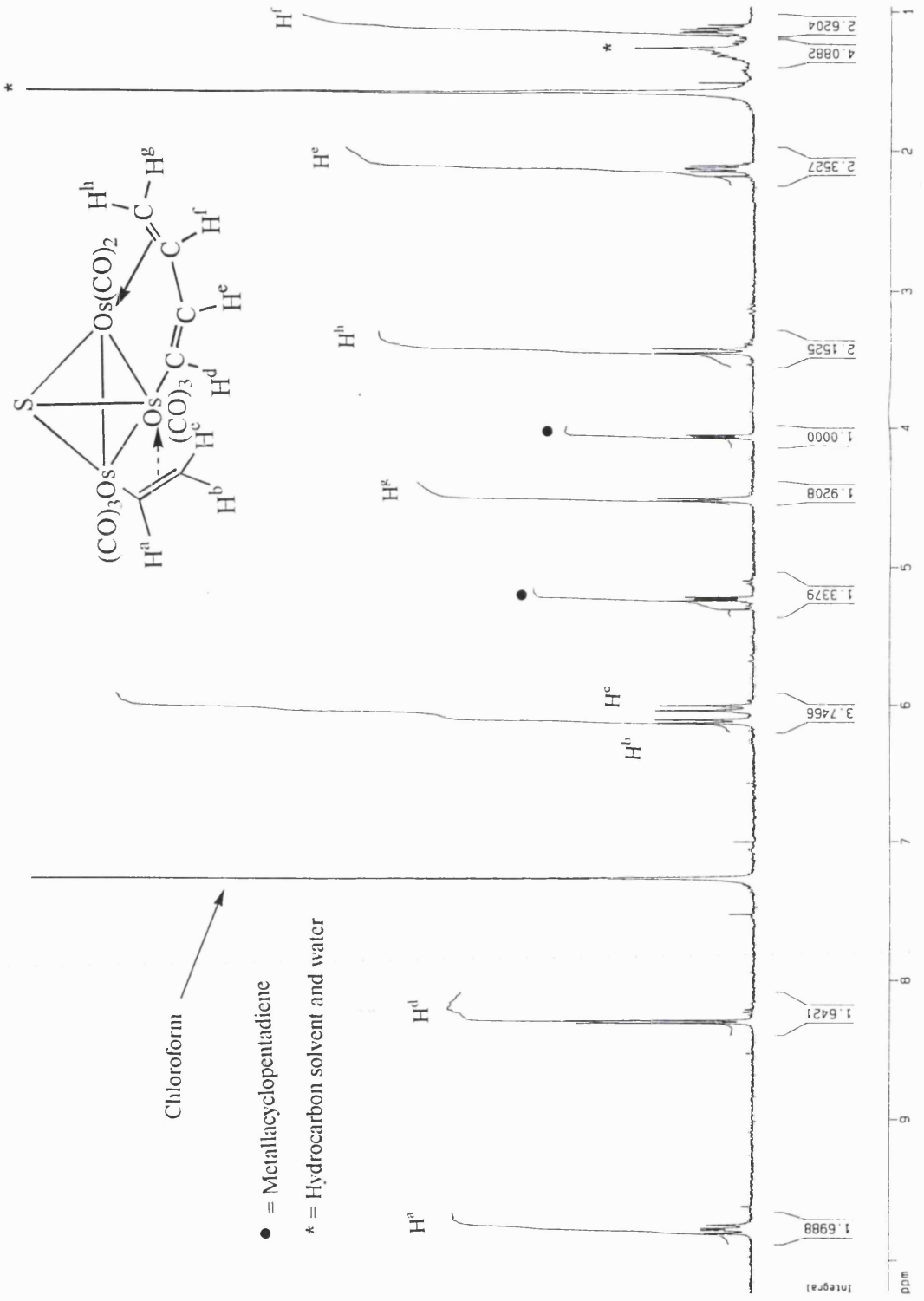

Fig. 4.11 The ^{1}H NMR spectrum of 39

Hz) for H^d and a doublet of doublets at δ 9.79 (J = 9.3 and 14.2 Hz) for H^a. The lack of coupling between H^a and H^d is consistent with there being two rather than one hydrocarbon ligand in the cluster. A minor impurity was also present with an AA'BB' pattern observed in the ^{1}H NMR spectrum at δ 4.07 and 5.23 which may again be attributed to a metallacyclopentadiene compound. This time the ring may also be π-coordinated to another osmium atom, resulting in the difference in chemical shift from the metallacyclopentadiene compound mentioned earlier.

The EI mass spectrum of this mixture showed a molecular ion peak at *m/z* 906 with daughter ions due to the successive loss of eight carbonyl ligands and also a peak at *m z* 628 consistent with the fragment '$[Os_3(\mu\text{-}CH{=}CH_2)(\mu_3\text{-}S)]$'. A molecular mass of 906 would be consistent with a compound of formula $[Os_3(\mu\text{-}CH{=}CH_2)(\mu\text{-}CH{=}CHCH{=}CH_2)(\mu_3\text{-}S)(CO)_8]$ **39** as shown in Fig. 4.10 above. For **39** to obey the 18-electron rule the alkenyl ligand would have to be η^1 coordinated instead of η^3 coordinated. The ^{1}H NMR spectrum appears to support this assumption, as the coupling constants (J = 9.3 and 14.2 Hz) are closer to the values for a free alkene. The $CH{=}CHCH{=}CH_2$ ligand is presumed to coordinate through the C=C bond shown but this has not been confirmed.

The second yellow/orange solid was found to be $[Os_3(\eta^4\text{-}C_4H_6)(\mu_3\text{-}S)(CO)_8]$ **40** obtained in 20% yield. The IR spectrum of **40** was similar to $[Os_3(\eta^4\text{-}PhCH{=}CHCPhCH_2)(\mu_3\text{-}S)(CO)_8]$ **36** implying the mode of coordination is the same as for **36** with a peak at 1924 cm^{-1} in the IR spectrum for the semi-bridging carbonyl ligands (Fig. 4.12). The ^{1}H NMR showed a doublet of doublets at δ 1.43 (J = 2.7 and 7.4 Hz) for H^c and $H^{c'}$, a broad signal at δ 2.05 for H^b and $H^{b'}$ and another broad

signal at δ 5.97 for H^a and $H^{a'}$. It should be noted that the chemical shifts in this case are very different to those observed for **36**. The EI mass spectrum displayed a molecular ion peak at *m/z* 882 with daughter ions for the successive loss of eight carbonyl ligands. Unfortunately there appear to be impurities in this spectrum with peaks between *m/z* 906-1068.

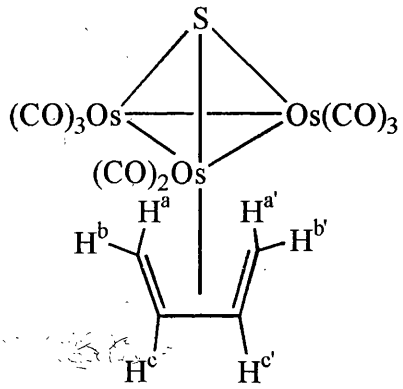

Fig. 4.12 $[Os_3(\eta^4\text{-}C_4H_6)(\mu_3\text{-}S)(CO)_8]$ 40

The second yellow solid, obtained in 4% yield, was also observed in the reaction of $[Os_3(\mu\text{-}H)_2(\mu_3\text{-}S)(CO)_8(MeCN)]$ **31** with PhC≡CH and will now be discussed in more detail. It does not appear to contain any ligands derived from phenylethyne or ethyne. The ^1H NMR spectrum shows singlets at δ -25.53 and −18.81 for two inequivalent hydride ligands and a singlet at δ 3.26 with an integral ratio of 9 protons. Consistent with the alkyne not being incorporated, this compound is formed irrespective of the alkyne used. The EI mass spectrum shows a molecular ion peak at *m/z* 888, which if the compound is of the form $[Os_3(\mu\text{-}H)_2(\mu_3\text{-}S)(CO)_8(L)]$, L should have a molecular mass of 59. These results are consistent with the compound $[Os_3(\mu\text{-}H)_2(\mu_3\text{-}S)(CO)_8(Me_3N)]$ **41** being formed, the Me_3N ligand coming from $Me_3NO.2H_2O$ used in the removal of a CO ligand. The isolation of **41** could partly account for the low yields obtained.

4.3.4 Reaction of $[Ru_3(\mu\text{-}H)_2(\mu_3\text{-}S)(CO)_9]$ 29 with $Me_3NO.2H_2O$ and PhC≡CH

The compound $[Ru_3(\mu\text{-}H)_2(\mu_3\text{-}S)(CO)_9]$ was prepared in quantitative yield using literature procedures,[134] by treating a refluxing solution of $[Ru_3(CO)_{12}]$ in petroleum spirit (b.p. 120-160 °C) with hydrogen sulfide gas for 30 minutes. A preliminary study was carried out by treating the cluster **29** with $Me_3NO.2H_2O$ and five equivalents of PhC≡CH in CH_2Cl_2 for two hours at room temperature. This resulted in a mixture of six compounds including **29**. The remaining five compounds, a yellow solid, a yellow/orange solid and three orange solids were found to be of the type $[Ru_3(\eta^4\text{-}C_4H_4Ph_2)(\mu_3\text{-}S)(CO)_8]$ isolated in a total of 17% yield. Their IR spectra were all very similar to each other and to those of $[Os_3(\eta^4\text{-}cis\text{-}CHPh{=}CH\text{-}CPh{=}CH_2)(\mu_3\text{-}S)(CO)_8]$ **36** and $[Os_3(\eta^4\text{-}cis\text{-}C_4H_6)(\mu_3\text{-}S)(CO)_8]$ **40**. Unfortunately the yellow solid and the yellow/orange solid were obtained in very small quantities. Hence the configurations of the butadiene ligands could not be deduced from their ^1H NMR spectra, which were too weak. The EI mass spectrum of the yellow solid displayed a molecular ion peak at *m/z* 735, which would be consistent with the fragment '$[Ru_3(\eta^4\text{-}C_4H_4Ph_2)(\mu_3\text{-}S)(CO)_7]$' with daughter ions due to the loss of a further seven carbonyl ligands. However there are also impurities present with peaks at *m/z* 847 and 791. The EI mass spectrum of the yellow/orange solid displayed molecular ion peaks at *m/z* 596 and 540 which would be consistent with the fragments '$[Ru_3(\eta^4\text{-}C_4H_4Ph_2)(\mu_3\text{-}S)(CO)_2]$' and '$[Ru_3(\eta^4\text{-}C_4H_4Ph_2)(\mu_3\text{-}S)]$' respectively.

The first of three orange solids had a ^1H NMR spectrum very similar to that for **36** indicating the compound $[Ru_3(\eta^4\text{-}PhCH^a{=}CH^bCPh{=}CH^cH^d)(\mu_3\text{-}S)(CO)_8]$ **42** had been

formed. The spectrum showed broad signals at δ 1.46 and 2.17 for H^c and H^d, a doublet at δ 3.43 (J = 9.6 Hz) for H^a and a doublet at δ 6.91 (J = 9.6 Hz) for H^b along with signals for the Ph group. The EI mass spectrum showed a molecular ion peak at *m z* 739, consistent with the fragment '$[Ru_3(\eta^4\text{-}C_4H_4Ph_2)(\mu_3\text{-}S)(CO)_7]$' with daughter ions due to the loss of a further seven carbonyl ligands. The second orange solid was a mixture of compounds, the major component from the ^1H NMR spectrum being $[Ru_3(\eta^4\text{-}PhCH{=}CHCH{=}CPhH)(\mu_3\text{-}S)(CO)_8]$ **43** (Fig. 4.13a). The spectrum showed a doublet at δ 3.87 (J = 10.5 Hz) for H^a, a doublet at δ 4.20 (J = 7.1 Hz) for H^d, a doublet of doublets at δ 5.87 (J = 5.7 and 6.7 Hz) for H^c and a doublet of doublets at δ 6.73 (J = 5.3 and 10.5 Hz) for H^b along with signals for the Ph group.

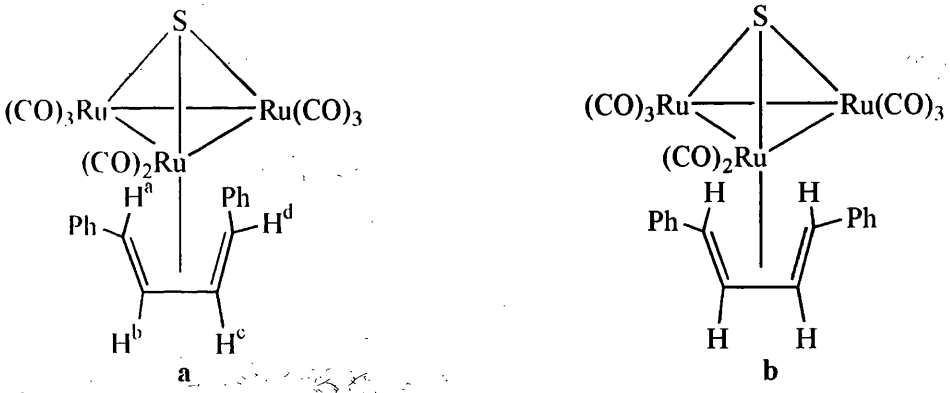

Fig. 4.13 The isomers 43 and 44

Unfortunately the EI mass spectrum was very weak and inconclusive. The third orange solid gave a ^1H NMR spectrum with an AA'BB' pattern at δ 3.45 and 6.46 (J = 4.7 and 12.7 Hz) and is consistent with the compound $[Ru_3(\eta^4\text{-}PhCH{=}CHCH{=}CHPh)(\mu_3\text{-}S)(CO)_8]$ **44** (Fig.4.13b). Again though, the EI mass spectrum was inconclusive.

Clearly we have good evidence for the formation of $Ph_2C_4H_4$ complexes but difficulties in obtaining sufficient quantities of pure products has prevented us from making a proper analysis of the isomers formed.

4.4 COMPARISON OF THE TOSYLIMIDO CAP WITH THE SULFIDO CAP IN THEIR REACTIONS WITH ALKYNES

The sulfido cap is a better electron donor than the tosylimido cap and this is evident in their IR spectra (Table 4.2). This difference could also result in different reactivities

Table 4.2 A comparison of ν(CO) between sulfido capped clusters and tosylimido capped clusters.

Compound	*ν(CO)/cm^{-1}*
$[Ru_3(\mu\text{-}H)_2(\mu_3\text{-}NTs)(CO)_9]$	2128 (m), 2089 (s), 2078 (s), 2071 (m), 2063 (m), 2052 (s), 2029 (m), 2021 (m) 2015 (s), 2008 (m), 2000 (w).
$[Ru_3(\mu\text{-}H)_2(\mu_3\text{-}S)(CO)_9]$	2119 (m), 2085 (s), 2063 (s), 2049 (m, sh), 2019 (s), 2011 (m, sh), 2000 (m, sh), 1969 (w).
$[Os_3(\mu\text{-}H)_2(\mu_3\text{-}NTs)(CO)_9]$	2128 (m), 2089 (m), 2068 (s), 2041 (m), 2021 (w), 2012 (m), 2005 (m), 1997 (w), 1989 (w, br).
$[Os_3(\mu\text{-}H)_2(\mu_3\text{-}S)(CO)_9]$	2120 (m), 2087 (s), 2060 (s), 2037 (s), 2014 (s), 1999 (m), 1986 (m).

for the two series of clusters. In their reactions with alkynes under mild conditions, there are a number of distinctions in the products that are formed. The sulfido-capped clusters undergo less regioselective insertion of alkynes into the M-H bonds than the

tosylimido analogues. This was observed in the formation of both the α- and β-alkenyl clusters $[Os_3(\mu\text{-}H)(\mu_3\text{-}S)(\mu\text{-}PhC{=}CH_2)(CO)_8]$ **32** and $[Os_3(\mu\text{-}H)(\mu_3\text{-}S)(\mu\text{-}CH{=}CHPh)(CO)_8]$ **33** and also different isomers of the substituted butadiene ligand $C_4H_4Ph_2$ when using the sulfido cap. Using the tosylimido cap only β-alkenyl compounds and the 1,3-butadiene ligand formed by head-to-tail coupling have been identified. The sulfido cap has also given an insight into the mechanism of butadiene formation, as a dialkenyl cluster has also been isolated. The dialkenyl cluster $[Os_3(\mu\text{-}CH{=}CHPh)(\mu\text{-}PhC{=}CH_2)(\mu_3\text{-}S)(CO)_7]$ **34** was treated with CO in a simple experiment to see if the two alkenyl ligands would couple to form the 1,3-butadiene cluster.[154] The IR spectrum after treatment showed the formation of the butadiene cluster $[Os_3(\eta^4\text{-}PhCH{=}CHCPh{=}CH_2)(\mu_3\text{-}S)(CO)_8]$ **36**. This experiment suggests that alkenyl and dialkenyl clusters are intermediates in the formation of butadiene clusters. With the mixed α,β-dialkenyl cluster being the major isomer, it would be expected that the 1,3-butadiene ligand formed by coupling of an α-alkenyl with a β-alkenyl ligand is favoured. Indeed this is the only isomer observed in the tosylimido clusters and the major product in the sulfido case. A speculative mechanism for alkenyl-alkenyl coupling and the formation of a 1,3-butadiene cluster from PhC≡CH is shown in Scheme 4.5. However, the different mode of coordination of the butadiene ligand in the tosylimido clusters $[Ru_3(\mu\text{-}\eta^2,\eta^2\text{-}C_4H_4R_2)(\mu_3\text{-}NTs)(CO)_8]$ **24** (R = H), and **25** (R = Ph) than in the sulfido clusters **36** and $[Os_3(\eta^4\text{-}CH_2{=}CHCH{=}CH_2)(\mu_3\text{-}S)(CO)_8]$ **40**, might reflect different alkenyl-alkenyl coupling mechanisms. If there is a mixture of isomers of the dialkenyl clusters and the alkenyl ligands couple, isomers of the butadiene ligand should reflect the composition of the isomeric mixture of dialkenyl clusters. This is what has been found for the ruthenium sulfur capped cluster in its reaction with PhC≡CH, although no intermediate compounds were isolated in this

case. The dialkenyl isomer **34** shown in Scheme 4.5 would require one of the alkenyl ligands to "flip" and then couple to form the butadiene ligand, since it is likely that both alkenyl ligands should be σ-bonded to the same metal atom to couple. Another interesting point to note is that butadiene clusters are isolated for osmium as well as ruthenium when using a sulfido cap. Whereas for the tosylimido cap, butadiene clusters are only seen for ruthenium. This indicates the sulfido-capped clusters are more reactive than the tosylimido capped clusters.

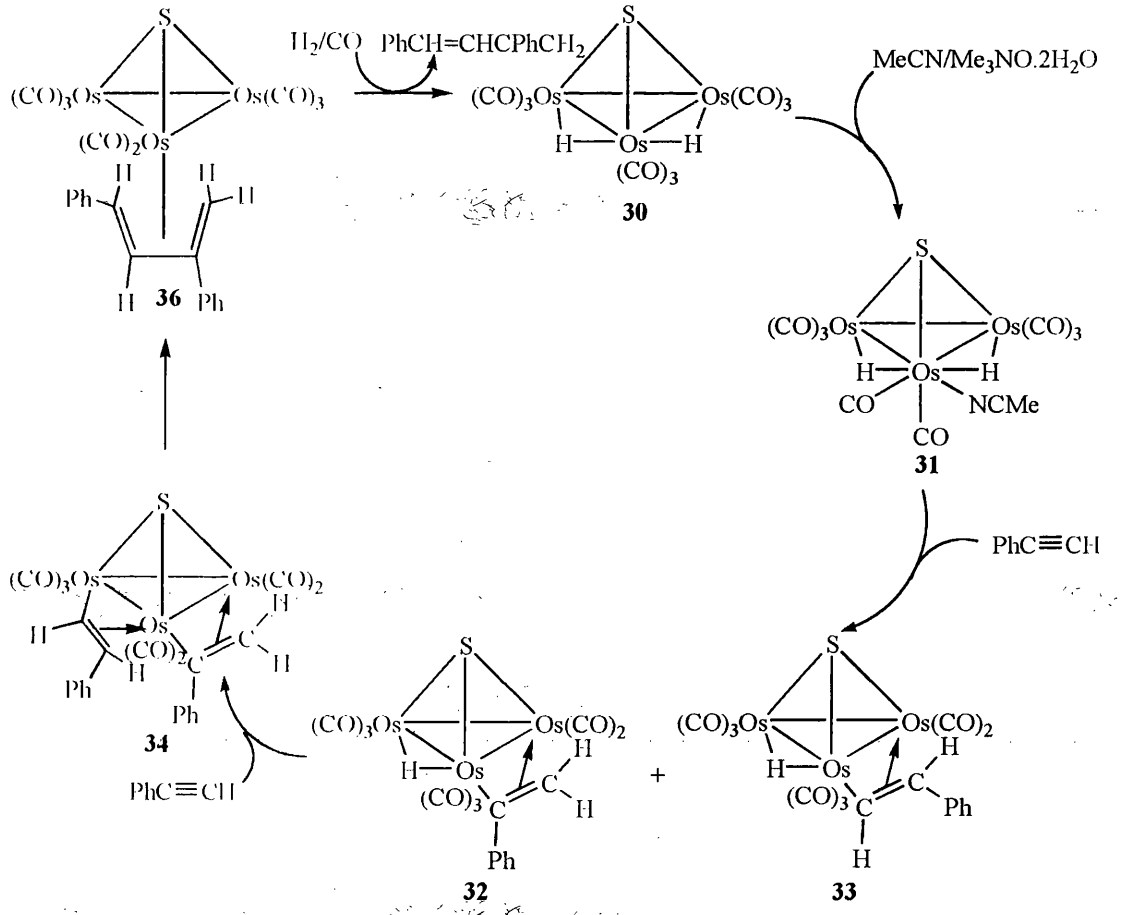

Scheme 4.5 A speculative mechanism for the formation of butadiene from an alkyne

The formation of $[Os_3(\mu\text{-}CHCHCHCH_3)(\mu_3\text{-}S)(CO)_8]$ **38**, an isomer of the 1,3-butadiene cluster **40**, and $[Os_3(\mu\text{-}CH{=}CH_2)(\mu\text{-}HC{=}CHCH{=}CH_2)(\mu_3\text{-}S)(CO)_8]$ **39** also suggests the possibility of other insertions and rearrangements taking place. Alkyne

insertion into one Os-CH=CH_2 bond could lead to **39** which presents the possibility of further alkyne insertions and alkyne oligomerisation or polymerisation (Scheme 4.6). All of these reactions appear to show that the mono-insertion compounds [$M_3(\mu$-H)(μ-alkenyl)(μ_3-X)$(CO)_8$] favour alkyne insertion into the second M-H bond rather than reductive elimination of alkene. This is almost certainly due to the hydride ligands being along separate M-M edges, and shows that hydrogenation reactions induced by clusters could follow a very different path to those catalysed by mononuclear species.

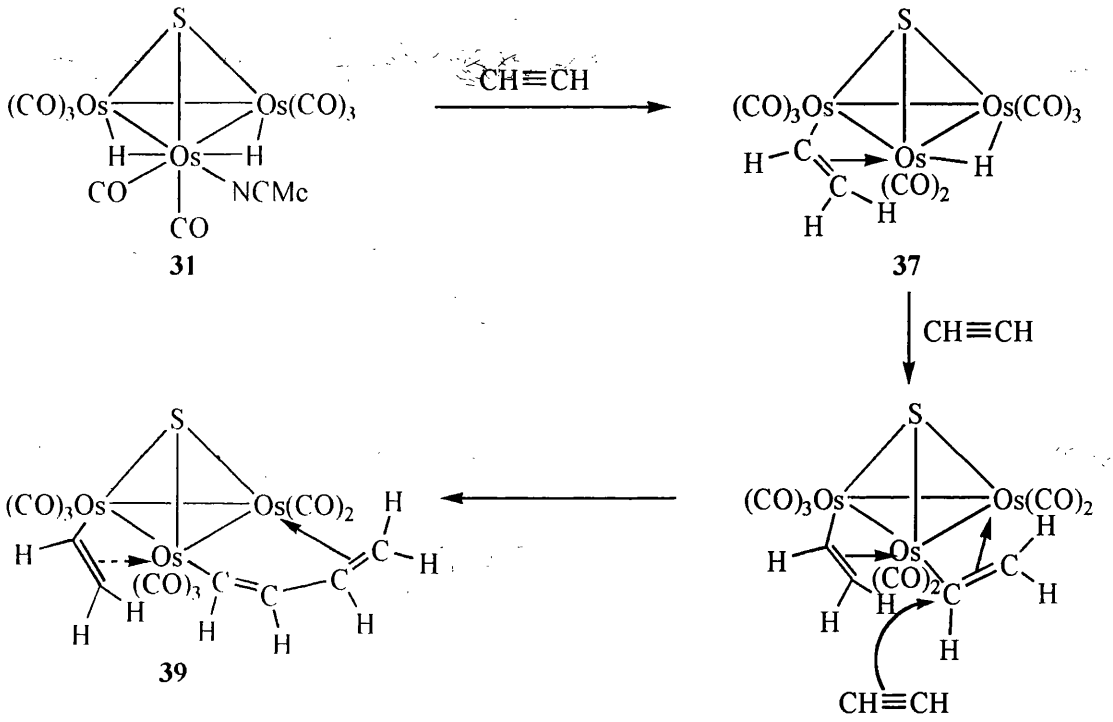

Scheme 4.6 A speculative mechanism for the formation of 39

4.5 FUTURE WORK

The conversion of an alkyne to give a butadiene could potentially be carried out catalytically (Scheme 4.7). Incoming alkyne, hydrogen and/or CO could then

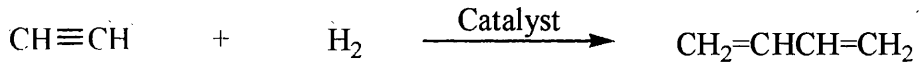

Scheme 4.7 Conversion of alkyne into butadiene

displace the butadiene. Other hydrogenative coupling processes involving alkenes and alkynes could also be possible. As detailed above, the choice of cap on the cluster could control the type of product formed. Greater electron donation appears to enhance reactivity and more strongly donating caps could be incorporated.

Establishing whether the two regioisomers **32** and **33** interconvert could give an insight into the factors controlling the isomeric form of the butadiene or other product isolated. As mentioned earlier, for the butadiene ligand to be formed by alkenyl-alkenyl coupling in a dialkenyl cluster, one alkenyl ligand would have to "flip", that is, interchange the σ- and the π-bonding across a M-M edge. Whether the alkenyl ligands are able to oscillate their μ-η^1,η^2 coordination between the metal centres can be established by dynamic NMR studies. Addition of CO induces coupling of the alkenyl ligands in $[Os_3(\mu\text{-}C_2H_2Ph)_2(\mu_3\text{-}S)(CO)_7]$,[154] whether the addition of hydrogen would achieve a similar result needs to be determined. Once these mechanistic features have been resolved a catalytic study of the hydrogenative coupling alkynes can then be carried out. For this a survey of the optimum conditions and reagents required would need to be ascertained. For instance whether or not the butadiene ligand can be displaced by incoming alkyne and/or hydrogen to complete the cycle shown in Scheme 4.5. A variety of alkynes can then be employed to investigate reactivity and to what extent hydrogenation *versus* hydrogenative coupling to butadienes can be controlled and whether alkenes or alkanes are produced.

4.6 CONCLUSIONS

- A carbonyl ligand in the cluster $[Os_3(\mu\text{-}H)_2(\mu_3\text{-}S)(CO)_9]$ can be easily displaced to form the acetonitrile cluster $[Os_3(\mu\text{-}H)_2(\mu_3\text{-}S)(CO)_8(MeCN)]$.

- Insertion of alkynes into the M-H bonds of the acetonitrile cluster can occur to give (a) single insertion hydrido-alkenyl clusters (b) double insertion dialkenyl clusters and (c) hydrogenative coupling of alkynes to give butadiene-containing clusters.
- The more electron-donating sulfido cap enhances reactivity towards alkyne hydrogenation relative to the tosylimido cap.
- The sulfido cap decreases the regioselectivity of the butadiene formed when compared to the tosylimido cap.
- The mode of coordination of the butadiene ligand is different in sulfido capped clusters than in the tosylimido-capped clusters. In the former the diene is chelating and the latter bridging.
- Coupling of the alkenyl ligands in a dialkenyl cluster may form the butadiene ligand.

4.7 EXPERIMENTAL

4.7.1 Materials and Instrumentation

All materials and instrumentation are as described in Chapters 2 and 3 (Sections 2.5.1 and 3.5.1). In addition to this the X-ray structure of $[Os_3(\eta^4\text{–PhCH=CH-CPh=CH}_2)(\mu_3\text{-S})(CO)_8]$ was obtained by Professor A. J. Deeming at UCL. X-ray data were collected at room temperature using a Nicolet R3v/m diffractometer, with crystals mounted in air (as described in Chapter 2).

4.7.2 Preparation of $[Os_3(\mu\text{–}H)_2(\mu_3\text{–}S)(CO)_9]$ 30

The compound **30** was prepared using literature procedures.[135] In a 2-neck 250 cm^3 round-bottomed flask, equipped with a condenser attached to an oil bubbler, a gas-inlet adaptor and a magnetic stirrer bar, was placed $[Os_3(CO)_{12}]$ (1 g, 1.103 mmol) and petroleum spirit (b.p. 120-160 °C) (100 cm^3). The solution was refluxed, while monitoring by IR spectroscopy, with H_2S (g) at 1 atm bubbling through the solution. After 6 h all $[Os_3(CO)_{12}]$ was consumed and the compound **30** had been formed quantitatively as a yellow solid as shown by IR and NMR spectroscopy. After cooling to room temperature, the solvent was removed under reduced pressure, to leave **30** as a yellow solid. The compound **30** was recrystallised by dissolving in the minimum amount of CH_2Cl_2, adding hexane (40 cm^3), removing solvent under reduced pressure until precipitation occurred and isolating the solid by filtration.

Compound 30: IR ν(CO) 2120 (m), 2087 (s), 2060 (s), 2037 (s), 2014 (s), 1999 (m), 1986 (m) cm^{-1}. ^1H NMR δ -20.95 (s, 2H, Os-*H*).

4.7.3 Preparation of $[Os_3(\mu\text{-}H)_2(\mu_3\text{-}S)(CO)_8(MeCN)]$ 31

Cluster **30** (153 mg, 0.179 mmol) was placed in a Schlenk tube, and dry CH_2Cl_2 (25 cm^3) added. In another Schlenk tube was placed $Me_3NO.2H_2O$ (20 mg, 0.175 mmol), and dry MeCN (25 cm^3) was added. The $Me_3NO.2H_2O$/MeCN solution was then added, dropwise, to the solution of **30** in CH_2Cl_2 *via* a cannula. The resulting pale yellow solution was left to stir at room temperature, while monitoring by IR spectroscopy until all **30** had been consumed (10 min). Silica gel was added to the stirring solution, which was then filtered into another Schlenk tube. The silica gel was washed with dry CH_2Cl_2 (3 × 15 cm^3) and the washings added to the filtrate. The

solvent was then removed from the filtrate, under reduced pressure, to leave an oily yellow solid of $[Os_3(\mu\text{-}H)_2(\mu_3\text{-}S)(CO)_8(MeCN)]$ **31.**

Compound 31: IR (CH_2Cl_2) ν(CO): 2121 (w), 2085 (m), 2049 (s), 1996 (s) cm^{-1}. ^1H NMR: δ -24.69 (s, 1H, Os-*H*), 19.65 (d, 1H, *J* = 1.2 Hz, Os-*H*), 2.54 (s, 3H, CH_3CN).

4.7.4 Reaction of $[Os_3(\mu\text{-}H)_2(\mu_3\text{-}S)(CO)_8(MeCN)]$ 31 with PhC≡CH

The compound **31** (153 mg, 0.179 mmol) was dissolved in dry THF (50 cm^3), and to this solution was added a solution of PhC≡CH (93 mg, 0.911 mmol) in dry THF (5 cm^3). The solution was refluxed while monitoring by IR spectroscopy. After $16\frac{1}{2}$ h all **31** was consumed and the yellow solution had turned dark red/orange. After cooling to room temperature the solvent was removed under reduced pressure. Flash chromatography on silica gel [light petroleum/CH_2Cl_2 eluent with a gradual increase in CH_2Cl_2 from 0% to ~ 20%] followed by removal of solvent under reduced pressure and then further purification by TLC yielded six bands. A yellow band yielded a mixture of $[Os_3(\mu\text{-}H)(\mu\text{-}PhC{=}CH_2)(\mu_3\text{-}S)(CO)_8]$ **32** and **30** as a bright yellow solid (45 mg, 27%), a yellow band yielded $[Os_3(\mu\text{-}H)(\mu\text{-}\textit{trans}\text{-}PhCH{=}CH)(\mu_3\text{-}S)(CO)_8]$ **33** as a bright yellow solid (24 mg, 14%), a pale red band yielded an inseparable mixture of isomers of $[Os_3(\mu\text{-}\textit{trans}\text{-}CH{=}CHPh)(\mu\text{-}PhC{=}CH_2)(\mu_3\text{-}S)(CO)_7]$ **34** and $[Os_3(\mu\text{-}PhC{=}CH_2)_2(\mu_3\text{-}S)(CO)_7]$ **35** as a red solid (17 mg, 9%), a pale yellow band yielded $[Os_3(\eta^4\text{-}PhCH{=}CHCPh{=}CH_2)(\mu_3\text{-}S)(CO)_8]$ **36** as a dark yellow solid (19 mg, 10%), a yellow/brown band gave a yellow solid (30 mg) and a pale yellow band yielded a mixture of $[Os_3(\eta^4\text{-}CH_2{=}CPhCPh{=}CH_2)(\mu_3\text{-}S)(CO)_8]$ and $[Os_3(\eta^4\text{-}PhCH{=}CHCH{=}CHPh)(\mu_3\text{-}S)(CO)_8]$ as a brown solid (13 mg). Dissolving **36** in the

minimum amount of CH_2Cl_2 in a small sample vial and placing this in a bigger sample vial containing heptane and allowing the solvents to diffuse, led to crystallographic quality crystals.

$[Os_3(\mu\text{-}H)(\mu\text{-}CPh{=}CH_2)(\mu_3\text{-}S)(CO)_8]$ 32: IR ν(CO): 2097 (m), 2063 (s), 2037 (s), 2022 (m), 2013 (s), 2000 (m), 1990 (w), 1980 (m) cm^{-1}. ^1H NMR: δ –13.52 (s, 1H, Os-*H*), 4.29 (d, 1H, *J* = 1.5 Hz, PhC=C*H*^{a}H^b), 4.59 (d, 1H, *J* = 1.4 Hz, PhC=CH^a*H*^{b}), 7.23-7.50 (m, 5H, Ph). MS (EI): *m/z* 932 (M^+).

$[Os_3(\mu\text{-}H)(\mu\text{-}$*trans*$\text{-}PhCH{=}CH)(\mu_3\text{-}S)(CO)_8]$ 33: IR ν(CO): 2099 (m), 2067 (s), 2035 (s), 2022 (m), 2017 (s), 2004 (w), 1992 (w), 1978 (m) cm^{-1}. ^1H NMR: δ –14.07 (s, 1H, Os-*H*), 5.91 (d, 1H, *J* = 11.6 Hz, CH=C*H*Ph), 7.21-7.46 (m, 5H, Ph), 9.46 (d, 1H, *J* = 11.5 Hz, C*H*=CHPh). MS (EI): *m/z* 932 (M^+). Anal. Calcd for $C_{16}H_8O_8Os_3S$: C, 20.64, H, 0.87, N, 0.00%. Found: C, 20.80, H, 0.74, N, 0.00%.

$[Os_3(\mu\text{-}$*trans*$\text{-}CH{=}CHPh)(\mu\text{-}PhC{=}CH_2)(\mu_3\text{-}S)(CO)_7]$ 34: IR ν(CO): 2077 (m), 2044 (s), 2026 (s), 2009 (s), 1980 (m), 1969 (m). ^1H NMR: δ 3.78 (s, 1H, PhC=C*H*^{a}H^b), 4.13 (s, 1H, PhC=CH^a*H*^{b}), 5.63 (d, 1H, *J* = 12.2 Hz, CH=C*H*Ph), 7.00-7.80 (m, 5H, Ph), 9.77 (d, 1H, *J* = 12.5 Hz, C*H*=CHPh). MS (EI): *m/z* 1034 (M+CO).

$[Os_3(\mu\text{-}PhC{=}CH_2)_2(\mu_3\text{-}S)(CO)_7]$ 35: ^1H NMR: δ 3.81 (s, 1H, PhC=C*H*^{a}H^b), 3.90 (s, 1H, PhC=CH^a*H*^{b}), 4.10 (s, 1H, PhC=C*H*^{c}H^d), 5.61 (s, 1H, PhC=CH^c*H*^{d}), 7.00-7.80 (m, 5H, Ph).

$[Os_3(\eta^4\text{-}PhCH{=}CHCPh{=}CH_2)(\mu_3\text{-}S)(CO)_8]$ 36: IR ν(CO): 2082 (m), 2049 (s), 2025 (m), 2006 (s), 1996 (m), 1979 (m), 1963 (w), 1918 (w) cm^{-1}. ^1H NMR: δ 1.55 (d, 1H, *J* = 3.5 Hz, PhCH=CHCPh=C*H*^{a}H^b), 2.43 (d, 1H, *J* = 3.4 Hz, PhCH=CHCPh=CH^a*H*^{b}), 3.58 (d, 1H, *J* = 9.2 Hz, PhC*H*=CHCPh=CH^{a}H^b), 6.79 (d, 1H, *J* = 9.0 Hz, PhCH=C*H*CPh=CH^{a}H^b), 7.22-7.72 (m, 5H, Ph). MS (EI): *m/z* 1034

(M$^+$). Anal. Calcd for $C_{24}H_{14}O_8Os_3S$: C, 27.90, H, 1.37, N, 0.00%. Found: C, 28.00, H, 1.21, N, 0.00%.

$[Os_3(\eta^4\text{-}CH_2{=}CPhCPh{=}CH_2)(\mu_3\text{-}S)(CO)_8]$: IR ν(CO) 2083 (m), 2069 (w), 2050 (s), 2037 (m), 2032 (m), 2024 (m), 2017 (m), 2006 (s), 1998 (m), 1985 (m), 1968 (w) cm^{-1}. ^{1}H NMR: δ 3.26 (s, 2H, CH^aH^b=CPhCPh=C$H^{a'}$H$^{b'}$), 3.38 (s, 2H, CH^aH^b=CPhCPh=CH$^{a'}$$H^{b'}$)

$[Os_3(\eta^4\text{-}PhCH{=}CHCH{=}CHPh)(\mu_3\text{-}S)(CO)_8]$: ^{1}H NMR δ 3.50 (m, 2H, J = 7.4, 5 to 7 Hz, PhCH^a=CH^{b}CH$^{b'}$=C$H^{a'}$Ph), 6.35 (m, 2H, J = 7.4, 5 to 7 Hz, PhCH^a=CH^bC$H^{b'}$=CH$^{a'}$Ph)

4.7.5 Reaction of $[Os(\mu\text{-}H)_2(\mu_3\text{-}S)(CO)_8(MeCN)]$ 31 with CH≡CH

The compound **31** (158 mg, 0.182 mmol) was placed in a Young's ampoule, which was flushed with CH≡CH, and dry THF (20 cm^3) was added. The ampoule was then sealed and placed in an oven at 55 °C for 16 h, during which time the solution turned from pale yellow/orange to a dark red/brown. After cooling the THF was removed under reduced pressure. Flash chromatography on silica gel [light petroleum/CH_2Cl_2 eluent with a gradual increase in CH_2Cl_2 from 0% to ~ 20%] followed by removal of solvent under reduced pressure and then further purification by TLC yielded five bands. A pale yellow band yielded $[Os_3(\mu\text{-}H)(\mu\text{-}CH{=}CH_2)(\mu_3\text{-}S)(CO)_8]$ **37** as a yellow solid (4 mg, 3%), a bright yellow band yielded a mixture of $[Os_3(\mu\text{-}CHCHCHCH_3)(\mu_3\text{-}S)(CO)_8]$ **38** and **30** as an orange solid (9 mg, 6%), a yellow band yielded $[Os_3(\mu\text{-}C{=}CH_2)(\mu\text{-}CH{=}CHCH{=}CH_2)(\mu_3\text{-}S)(CO)_8]$ **39** as a yellow/orange solid (4 mg, 2%), a pale yellow band yielded $[Os_3(\eta^4\text{-}H_2C{=}CHCH{=}CH_2)(\mu_3\text{-}S)(CO)_8]$ **40** as a yellow/orange solid (32 mg, 20%) and a yellow band yielded $[Os_3(\mu\text{-}H)_2(\mu_3\text{-}$

S)(CO)$_8$(Me$_3$N)] **41** as a yellow solid (7 mg, 4%). Compound **40** was recrystallised by dissolving in the minimum amount of CH_2Cl_2, adding hexane (~ 5 cm^3), removing solvent under reduced pressure until precipitation occurred and isolating the solid by filtration.

[Os$_3$(μ-H)(μ-CH=CH$_2$)(μ$_3$-S)(CO)$_8$] 37: IR ν(CO): 2100 (m), 2068 (s), 2036 (m), 2025 (m), 2017 (s), 2006 (m), 1993 (m), 1979 (m) cm^{-1}. ^{1}H NMR: δ -13.48 (s, 1H, Os-*H*), 4.42 (d, 1H, *J* = 12.1 Hz, CH=C*H*^{a}H^b), 4.92 (d, 1H, *J* = 8.1 Hz, CH=CH^a*H*^{b}), 9.18 (dd, 1H, *J* = 8.2, 11.9 Hz, C*H*=CH^{a}H^b). MS (EI): *m/z* 910 (M+2CO).

[Os$_3$(μ-CHCHCHCH$_3$)(μ$_3$-S)(CO)$_8$] 38: IR ν(CO): 2091 (m), 2070 (m), 2005 (s), 1978 (m), 1954 (m) cm^{-1}. ^{1}H NMR: δ 2.10 (d, 3H, *J* = 6.0 Hz, CHCHCHC*H*$_3$), 2.72 (dq, 1H, *J* = 6.5 Hz, CHCHC*H*CH$_3$), 7.07 (dd, 2H, *J* = 7.2 Hz, CHC*H*CHCH$_3$), 9.66 (d, 2H, *J* = 6.0 Hz, C*H*CHCHCH$_3$). MS (EI): *m/z* 880 (M$^+$).

[Os$_3$(μ-CH=CH$_2$)(μ-CH=CHCH=CH$_2$)(μ$_3$-S)(CO)$_8$] 39: IR ν(CO): 2097 (w), 2083 (m), 2075 (m), 2065 (w), 2059 (m), 2045 (s), 2016 (s), 2010 (s, sh), 1999 (m), 1991 (m), 1983 (m, sh), 1959 cm^{-1}. ^{1}H NMR: δ 1.15 (ddd, 1H, *J* = 7.3, 9.9, 12.0 Hz, CHCHC*H*CH^{a}H^b) 2.13 (dd, 2H, *J* = 7.1, 9.7 Hz, CHC*H*CHCH^{a}H^b), 3.44 (d, 2H, *J* = 12.3 Hz, CHCHCHC*H*^{a}H^b), 4.51 (d, 2H, *J* = 7.2 Hz, C*H*CHCHCH^{a}H^b), 6.02 (d, 2H, *J* = 14.1 Hz, CH=C*H*^{c}H^d), 6.12 (d, 2H, *J* = 9.2 Hz, CH=CH^c*H*^{d}), 8.30 (d, 1H, 7.1 Hz, CHCHCHCH^a*H*^{b}), 9.79 (dd, 1H, *J* = 9.3, 14.2 Hz, CH=CH^{c}H^d). MS (EI): *m/z* (906) (M$^+$).

[Os$_3$(η^4-CH$_2$=CHCH=CH$_2$)(μ$_3$-S)(CO)$_8$] 40: IR ν(CO): 2114 (w), 2084 (m), 2069 (w), 2059 (w), 2050 (s), 2036 (w), 2026 (w), 2008 (s), 1992 (m), 1980 (m), 1960 (w), 1924 (w) cm^{-1}. ^{1}H NMR: δ 1.43 (dd, 1H, *J* = 2.7, 7.4 Hz, CH^{a}H^{b}C*H*^{c}C*H*$^{c'}$CH$^{a'}$H$^{b'}$), 2.05 (s, br, 1H, C*H*^{a}H^{b}CH^{c}CH$^{c'}$C*H*$^{a'}$H$^{b'}$), 5.97 (s, br, 1H, CH^a*H*^{b}CH^{c}CH$^{c'}$CH$^{a'}$*H*$^{b'}$).

MS (EI): *m z* 882 (M^+). Anal. Calcd for $C_{12}H_6O_8SOs_3$: C, 16.36, H, 0.69, N, 0.00%. Found: C, 16.58, H, 0.58, N, 0.00%.

$[Os_3(\mu\text{-}H)_2(\mu_3\text{-}S)(CO)_8(Me_3N)]$ 41: IR ν(CO): 2086 (s), 2072 (w), 2050 (s), 2032 (s), 2017 (w), 2006 (s), 1989 (s), 1982 (w, sh), 1968 (s) cm^{-1}. ^1H NMR: δ -25.53 (s, 1H, Os-*H*), -18.77 (s, 1H, Os-*H*), 3.26 (s, 9H). MS (EI): *m/z* 888 (M^+).

4.7.6 Preparation of $[Ru_3(\mu\text{–}H)_2(\mu_3\text{–}S)(CO)_9]$ 29

The compound **29** was prepared using literature procedures.[134] In a 2-neck 250 cm^3 round bottom flask, equipped with a condenser attached to an oil bubbler, a gas-inlet adaptor and a magnetic stirrer bar, was placed $[Ru_3(CO)_{12}]$ (512 mg, 0.801 mmol) and petroleum spirit (b.p. 120-160 °C) (75 cm^3) added. The solution was refluxed, while monitoring by IR spectroscopy, with H_2S (g) bubbling through the solution. After 30 min all $[Ru_3(CO)_{12}]$ was consumed, and the compound **29** had been formed quantitatively as shown by IR and NMR spectroscopy. After cooling to room temperature, the solvent was removed under reduced pressure, to leave **29** as a dark red solid. The compound **29** was recrystallised by dissolving in the minimum amount of CH_2Cl_2, adding hexane (30 cm^3), removing solvent under reduced pressure until precipitation occurred and isolating the solid by filtration.

Compound 29: IR ν(CO): 2119 (m), 2085 (s), 2063 (s), 2049 (m, sh), 2019 (s), 2011 (m, sh), 2000 (m, sh), 1969 (w) cm^{-1}. ^1H NMR: δ –18.97 (s, 2H, Ru-*H*).

4.7.7 Reaction of $[Ru_3(\mu\text{-}H)_2(\mu_3\text{-}S)(CO)_9]$ 29 with $Me_3NO.2H_2O$ and PhC≡CH

In a Schlenk tube was placed **29** (151 mg, 0.256 mmol), dry CH_2Cl_2 (25 cm^3) and a solution of PhC≡CH (130 mg, 1.27 mmol) in dry CH_2Cl_2 (5 cm^3). To this solution

was added $Me_3NO.2H_2O$ (30 mg, 0.263 mmol). The resulting dark red solution was stirred at room temperature while monitoring by IR spectroscopy. After 2 h all **29** was consumed. Silica gel was added to the stirring solution, which was then filtered into another Schlenk tube. The silica gel was then washed with dry CH_2Cl_2 (3 × 10 cm^3) and the washings added to the filtrate. The solvent was then removed from the filtrate under reduced pressure. Flash chromatography on silica gel [light petroleum/CH_2Cl_2 eluent with a gradual increase in CH_2Cl_2 from 0 % to 20 %] followed by removal of solvent under reduced pressure and then further purification by TLC yielded six bands. A yellow band yielded **29** (15 mg), a yellow band gave a yellow solid (5 mg, 3%), a red band gave a yellow/orange solid (2 mg, 1%), a yellow/orange band yielded $[Ru_3(\eta^4\text{-}PhCH{=}CHCPh{=}CH_2)(\mu_3\text{-}S)(CO)_8]$ **42** as an orange solid (8 mg, 4%), a yellow/orange band yielded $[Ru_3(\eta^4\text{-}PhCH{=}CHCH{=}CPhH)(\mu_3\text{-}S)(CO)_8]$ **43** as an orange solid (9 mg, 5%) and a yellow/orange band yielded $[Ru_3(\eta^4\text{-}PhCH{=}CHCH{=}CHPh)(\mu_3\text{-}S)(CO)_8]$ **44** as an orange solid (9 mg, 5%).

Yellow solid: IR ν(CO): 2095 (w), 2088 (w), 2084 (m), 2076 (w), 2062 (m), 2055 (s, sh), 2042 (m), 2024 (w), 2016 (s), 2009 (m, sh), 2001 (m), 1993 (w), 1859 (w) cm^{-1}. MS (EI): *m z* 847 (M+3CO).

Yellow/orange solid: IR ν(CO): 2084 (m), 2052 (s), 2015 (s), 2006 (m, sh), 1993 (w), 1951 (w), 1910 (w), 1906 (w) cm^{-1}. MS (EI): *m/z* 596 (M-6CO).

$[Ru_3(\eta^4\text{-}PhCH{=}CHCPh{=}CH_2)(\mu_3\text{-}S)(CO)_8]$ 42: IR ν(CO): 2091 (w), 2083 (m), 2052 (s), 2035 (w), 2012 (s), 1993 (w), 1959 (w), 1916 (w) cm^{-1}. ^1H NMR: δ 1.46 (s, 1H, PhCH=CHCPh=C$H^q$$H^b$), 2.17 (s, 1H, PhCH=CHCPh=C$H^a$$H^b$), 3.43 (d, 1H, J = 9.6 Hz, PhC*H*=CHCPh=C$H^a$$H^b$), 6.91 (d, 1H, J = 9.6 Hz, PhCH=C*H*CPh=C$H^a$$H^b$), 7.12-7.77 (m, 10H, Ph). MS (EI): *m/z* 739 (M–CO).

$[Ru_3(\eta^4\text{-PhCH=CHCH=CPhH})(\mu_3\text{-S})(CO)_8]$ 43: IR ν(CO): 2090 (w), 2083 (m), 2071 (w), 2053 (s), 2045 (w), 2040 (w), 2034 (w), 2031 (w), 2014 (s), 1993 (w), 1946 (w), 1909 (w) cm^{-1}. ^1H NMR: δ 3.87 (d, 1H, J = 10.5 Hz, PhC*H*=CHCH=CHPh), 4.20 (d, 1H, J = 7.1 Hz PhCH=CHCH=C*H*Ph), 5.87 (dd, 1H, J = 5.7, 6.7 Hz, PhCH=CHC*H*=CHPh), 6.73 (dd, 1H, J = 5.3, 10.5 Hz, PhCH=C*H*CH=CHPh), 6.97-7.75 (m, 10H, Ph).

$[Ru_3(\eta^4\text{-PhCH=CHCH=CHPh})(\mu_3\text{-S})(CO)_8]$ 44: IR ν(CO): 2089 (w), 2083 (m), 2065 (w), 2053 (s), 2034 (w), 2029 (w), 2012 (s), 1997 (w), 1993 (w), 1950 (w), 1914 (w) cm^{-1}. ^1H NMR: δ 3.45 (dd, 2H, J = 4.7, 12.9 Hz, PhC*H*=CHCH=C*H*Ph), 6.46 (dd, 2H, J = 4.7, 12.7 Hz, PhCH=C*H*C*H*=CHPh).

Chapter 5:

High-low valent clusters

5.1 INTRODUCTION

The imido ligand bridging low-valent metal centres in clusters has already been discussed previously in this thesis. The main focus of this chapter is on the imido ligand bound in a terminal fashion to high-valent metal centres. Terminal organoimido complexes are known for all the metals of the titanium, vanadium, chromium, manganese and iron triads and also for iridium.[84,155,156]

The imido ligand forms multiple bonds with a metal centre involving one σ and either one or two π interactions. The π-bonds involve overlap of metal d-orbitals with ligand p-orbitals (Figs. 5.1a and b) to give d_π-p_π interactions.[84] By describing the

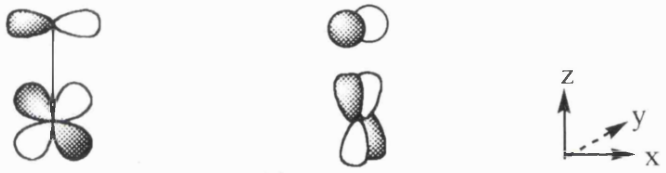

a **b**

Overlap of d_{xz} with p_x **Overlap of d_{yz} with p_y**

Fig. 5.1 d_π-p_π interactions

imido ligand as the closed shell anion NR^{2-} implies that the p-orbitals are filled. Hence, to form a π-bond with a metal centre requires the metal to be in a high oxidation state with empty metal d-orbitals. A valence bond description infers the nitrogen bond order from the position of the substituent. An sp^2 hybridised nitrogen results in a M=N double bond (1σ, 1π) and a bent M-N-R unit (Fig. 5.2a), with the lone pair residing in a N(sp^2) orbital. In this case the NR^{2-} ligand acts as a four-electron donor. An sp hybridised nitrogen forms a metal-ligand triple bond (Fig.

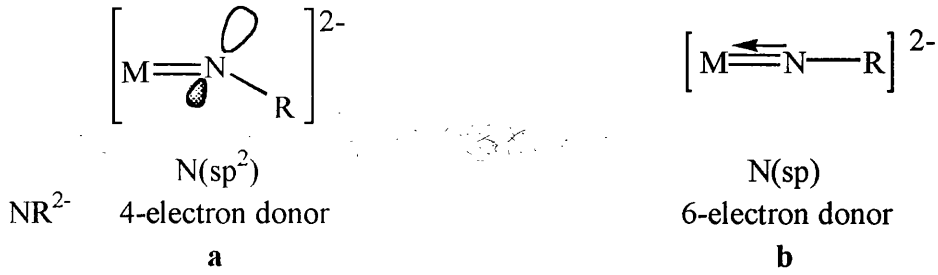

NR^{2-} $N(sp^2)$ 4-electron donor — **a**

N(sp) 6-electron donor — **b**

Fig. 5.2 A valence bond description of the M-N-R unit

5.2b) with a linear M-N-R unit. Here the NR^{2-} ligand acts as a 6-electron 1σ, 2π donor to the metal. The bent structure is only formed if the metal centre cannot form a bond with the nitrogen lone pair, for instance when a linear triply bonded imido ligand would cause the electron count of the complex to exceed 18-electrons.[155,156]

Molecular transition metal complexes can generally be classed as containing a metal centre with either a high or a low oxidation state. Although the chemistry of these two types of complexes can be very diverse, a common feature is the occurrence of metal-metal bonding. The interest in compounds with metal-metal bonds formed between high- and low-valent centres is growing. For example $[(\eta^5\text{-Cp*})W(CO)_3\text{-}WO_2(\eta^5\text{-Cp*})]$, the product of the air-oxidation of $[(\eta^5\text{Cp*})W(CO)_2]_2$ or $[(\eta^5\text{-Cp*W}(CO)_2(\mu\text{-H})]_2$, was synthesised by Alt and co-workers, and contains both W(V) and W(I) centres.[157] Bi- and trinuclear imido-containing complexes have been reported by Sundermeyer *et al.* (Figs. 5.3a and b), where metal-metal bonds are found between high- and low-valent centres.[158,159] However, in the trimolybdenum complex

a **b**

Fig. 5.3 The high-low valent compounds $[Re(NR)_3MoCp(CO)_3]$ and $[\{MoCp(CO)_3\}_2Mo(NR)_2]$

(Fig. 5.3b), there are no bonding interactions between the two low-valent centres and a linear complex is formed.

Group 6/8 mixed-metal clusters with imido ligands have been synthesised by Chi and co-workers. However, in these cases the imido ligand is only rarely bound in a monodentate fashion such as in the compound [(η^5-Cp*)$WRu_2(CO)_6$(NPh){C(Et)C(Et)C(CF_3)CH(CF_3)}] (Fig 5.4a),[160] and usually

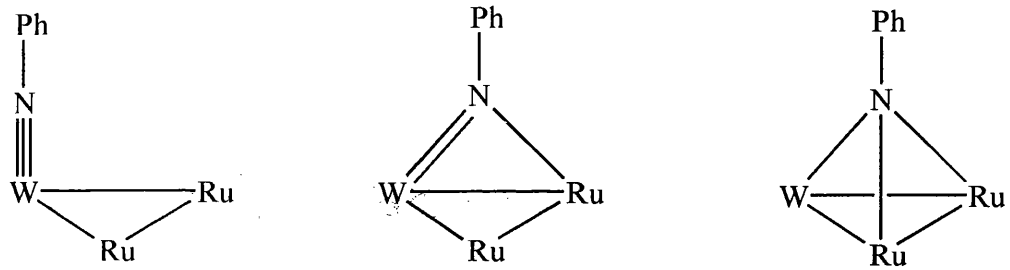

Fig. 5.4 The coordination modes of the NPh ligand in mixed group 6/8 clusters

bridges two or three metal centres as in [(η^5-Cp*)$WRu_2(CO)_6H(\mu$-NPh){μ_3-$C_2(CF_3)_2$}] (Fig. 5.4b)[41] and [(η^5-Cp*)$WRu_2(CO)_7(\mu_3$-NPh)(μ-*cis*-CF_3C=$CHCF_3$)] (Fig. 5.4c)[161] respectively. Thus, all the metal centres in these clusters can be regarded as having similar valency.

In contrast, Puddephatt *et al.* have shown the stepwise oxidation of [Pt_3{$Re(CO)_3$}(μ-dppm)$_3$]$^+$, which is a 54-electron coordinatively unsaturated tetrahedral cluster, gives the series of oxo clusters [Pt_3{$Re(CO)_3$}(μ_3-O)$_n$(μ-dppm)$_3$]$^+$ [n = 1-3] and finally [$Pt_3(ReO_3)(\mu_3$-O)$_3$(μ-dppm)$_3$]$^+$ (Scheme 5.1).[162,163] In these clusters, the electron count increases by up to 12-electrons (from 54 to 66 electrons) and the sum of the metal oxidation states increase by up to 12 units (from Pt_3Re^+ to Pt_3Re^{13+}) without cluster fragmentation or ligand redistribution.

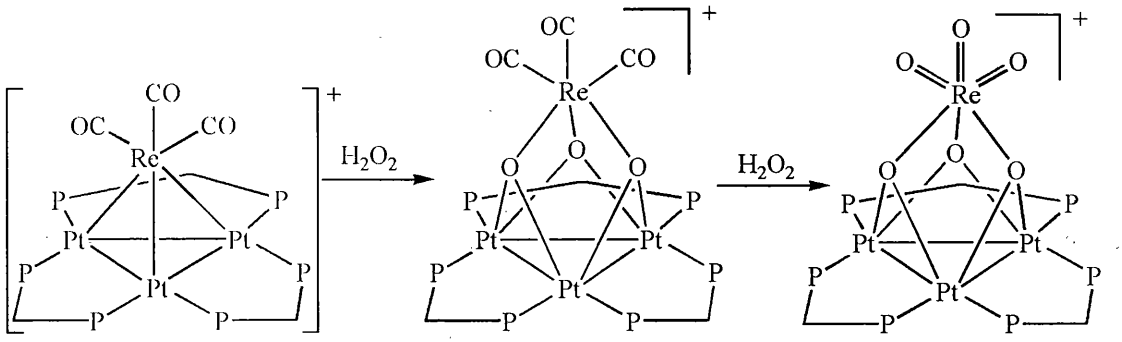

Scheme 5.1 The stepwise oxidation of $[Pt_3\{Re(CO)_3\}(\mu\text{-dppm})_3]^+$

At high temperature $[Pt_3(ReO_3)(\mu\text{-dppm})_3]^+$ was also formed (Scheme 5.2), where the formal metal oxidation states can be considered as Re(VII) and Pt(0) with strong Pt-Re interactions. This cluster represents a rare example of a cluster containing metals in widely different oxidation states.

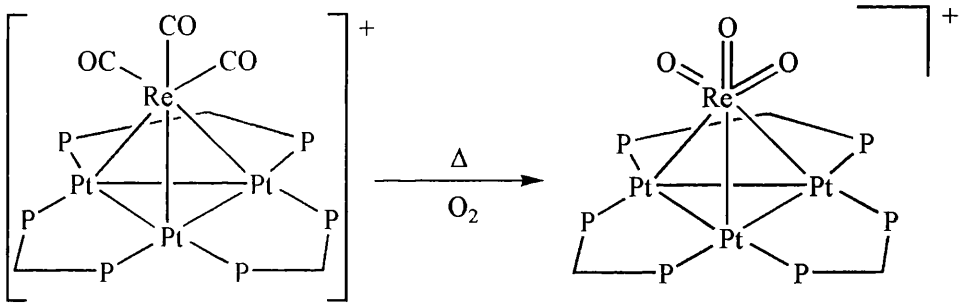

Scheme 5.2 Formation of a mixed-metal cluster with metals in widely different oxidation states

5.2 TARGETS, AIMS AND OBJECTIVES IN THIS CHAPTER

- To utilise the ability of low-valent carbonyl clusters to act as electron-sinks and to adopt different geometries.
- To combine these two properties and use a low-valent cluster, namely $[Ru_3(CO)_{11}]^{2-}$, as a ligand to a high-valent bis(imido) stabilised molybdenum centre to form high-low valent clusters.

5.3 RESULTS AND DISCUSSION

5.3.1 Preparation of $[Ru_3(CO)_{12}\{Mo(NAr)_2\}]$

The substitution reaction of a high-valent metal halide with a low-valent cluster ligand in order to form high-low valent mixed-metal clusters is now described (Scheme 5.3).

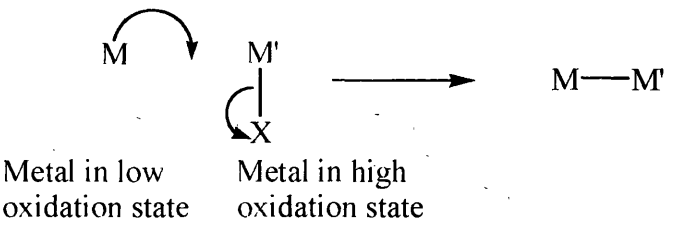

Scheme 5.3 Substitution reaction to form a high-low valent metal cluster

Although this approach appears to be very simple, and is utilised extensively in organic chemistry, in this case there is the potential for electron-transfer to occur instead. This is due to the large difference in metal oxidation states (Scheme 5.4).

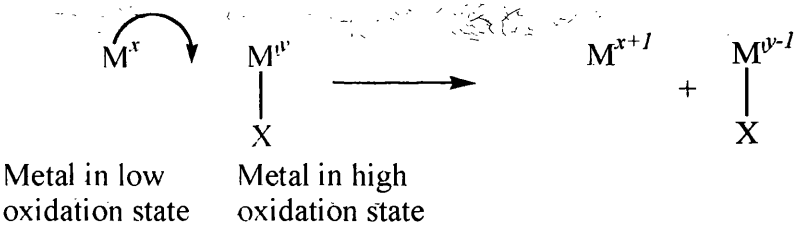

Scheme 5.4 The possible electron-transfer process that can take place

Ruthenium cluster anions have been prepared by Shore and co-workers through the reaction of alkali metal-benzophenone with $[Ru_3(CO)_{12}]$ in THF in an inert atmosphere.[164] For this work the cluster $K_2[Ru_3(CO)_{11}]$ **45** was employed, which was prepared by treating a solution of two equivalents of potassium-benzophenone in THF with one equivalent of $[Ru_3(CO)_{12}]$ (Scheme 5.5). $[Ru_3(CO)_{12}]$ was introduced in

small aliquots every 15-20 minutes to the potassium-benzophenone solution until the required amount had been added.

$$[Ru_3(CO)_{12}] + 2K^+[Ph_2CO]^- \xrightarrow{THF} \underset{\mathbf{45}}{K_2[Ru_3(CO)_{11}]} + CO + 2Ph_2CO$$

Scheme 5.5 The formation of the low-valent cluster anion 45

The molybdenum (VI) bis(imido) complexes, $[Mo(NAr)_2Cl_2(dme)]$ (Ar = 2,6-$Me_2C_6H_3$, **46**; 2,4,6-$Me_3C_6H_2$, **47**; and 2,6-Me_2-4-Br-C_6H_2, **48**) were prepared following a procedure reported by Schrock and co-workers.[165] Two equivalents of amine, $ArNH_2$, were treated with four equivalents of triethylamine and eight equivalents of chlorotrimethylsilane at 65 °C for 8–15 hours (Scheme 5.6). After purification all bis(imido) complexes were obtained in good yield (55-80%).

$$Na_2MoO_4 + 4Et_3N + 8TMSCl + 2RNH_2 \xrightarrow[65\ ^\circ C]{DME} [Mo(NAr_2)Cl_2(dme)]$$

Scheme 5.6 The formation of the high-valent imido complexes 46-48

The solution of **45** in THF was treated with a solution of the required bis(imido) complex also in THF at room temperature. Dark solutions were obtained in all cases, which were left to stir overnight. Purification by chromatography in an aerobic atmosphere, resulted in the isolation of $[Ru_3(CO)_{12}]$, $[H_2Ru_4(CO)_{13}]$[166] and the new clusters $[Ru_3(CO)_{12}\{Mo(NAr)_2\}]$ (Ar = 2,6-$Me_2C_6H_3$, **49**; 2,4,6-$Me_3C_6H_2$, **50**; and 2,6-Me_2-4-Br-C_6H_2, **51**) in yields of 20-40% as orange solids. Clusters **49**, **50** and **51** are soluble in hexane and are air-stable in this solvent. The ^1H NMR spectrum of **49** shows a singlet at δ 2.17 for the Me protons. A singlet is observed at δ 6.98 for the protons on the aromatic rings, although two sets of signals would be expected, as there are two different types of hydrogen atoms on the aromatic ring. It may be that the signals coincidentally overlap with each other. The positive ion FAB mass

spectrum for this cluster shows a molecular ion peak at *m/z* 945 consistent with M-CO, and daughter ions due to the successive loss of a further eleven carbonyl ligands.

IR and ^{1}H NMR spectroscopic techniques were inadequate with regard to determining the precise structure of the cluster and therefore X-ray crystallography was employed to do this. Cooling a saturated hexane solution to –20 °C afforded crystals of **49**. The structure determined is shown in Fig. 5.5 and selected bond lengths are given in Table 5.1. The molecule adopts a distorted butterfly shape of one molybdenum and three ruthenium atoms, with a fold angle of 25.4° about the hinge vector, Mo(1)-Ru(1). Each ruthenium atom is bonded to four terminal CO ligands and the imido ligands remain bonded in a terminal fashion to the molybdenum atom. Two of the three ruthenium-molybdenum interactions are very short [Mo(1)-Ru(2) 2.7165(5); Mo(1)-Ru(3) 2.7025(4) Å] the third, the hinge vector, is longer [Mo(1)-Ru(1) 3.1094(8) Å]. These bond lengths are within the range of molybdenum-ruthenium bonds in mixed metal clusters.[167] The short Mo-Ru distance could be attributed to the coulombic forces due to the electrostatic attraction in the dipolar heterometallic interaction $M^{\delta+}$-$M^{\delta-}$. The smaller radii of high-valent metal centres as compared low-valent one could also contribute to the shortening of the M-M bond as Sundermeyer *et al.* previously reported.[158,159] The hinge vector, Ru(1)-Mo(1), is associated with a dative bond, with the ruthenium tetracarbonyl unit acting as a donor to the high-valent molybdenum centre. The structure of **49** could be viewed as molybdenum (VI) bis(imido) centre bound to a chelating $[Ru_3(CO)_{12}]^{2-}$ ligand. The dianion would exist as $[Ru_3(CO)_{11}]^{2-}$ in the free state, which would be expected to contain one long and two short ruthenium-ruthenium bonds. As expected, due to the negative charge on the outer ruthenium atoms of **49**, the average ruthenium-ruthenium bond distance in

$[Ru_3(CO)_{12}]$ of 2.854 Å is *ca.* 0.1 Å shorter than the ruthenium-ruthenium bond lengths in **49** [Ru(1)-Ru(2) 2.9315(5); Ru(1)-Ru(3) 2.9556(5) Å].[168] The Ru(2)-Ru(3) distance of 4.593 Å is a non-bonding interaction. All these data are characteristic of a $[Ru_3(CO)_{12}]^{2-}$ unit.

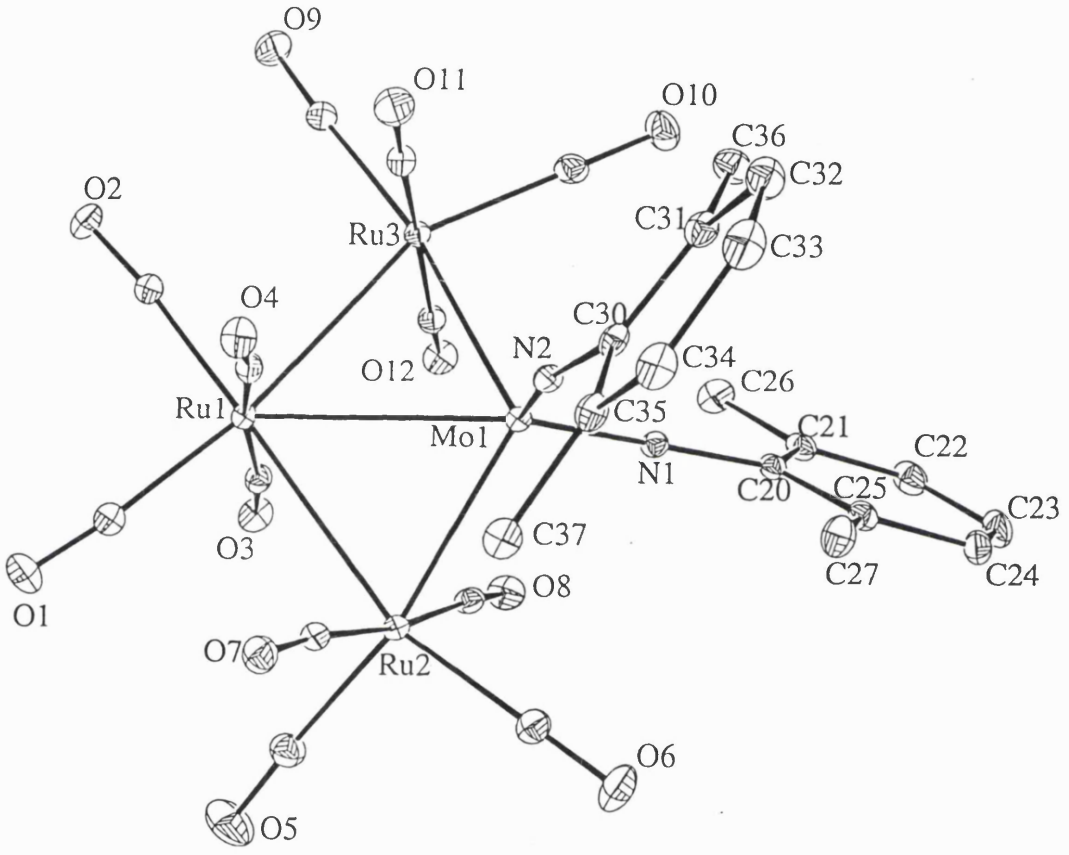

Fig. 5.5 The X-ray structure of $[Ru_3(CO)_{12}\{Mo(N\text{-}2,6\text{-}Me_2C_6H_3)_2\}]$ 49

Table 5.1 Selected bond lengths (Å) and angles (°) for 49

Mo(1)-Ru(1)	3.1094(8)	Ru(1)-Ru(3)	2.9556(5)
Mo(1)-Ru(2)	2.7165(5)	Mo(1)-N(1)	1.766(2)
Mo(1)-Ru(3)	2.7025(4)	Mo(1)-N(2)	1.761(2)
Ru(1)-Ru(2)	2.9315(5)		
Ru(2)-Mo(1)-Ru(3)	115.88(2)	N(1)-Mo(1)-N(2)	112.39(7)
Mo(1)-Ru(3)-Ru(1)	66.50(2)	Mo(1)-N(1)-C(20)	163.60(13)
Ru(3)-Ru(1)-Ru(2)	102.54(2)	Mo(1)-N(2)-C(30)	162.26(13)
Ru(1)-Ru(2)-Mo(1)	66.68(2)		

The molybdenum atom can be considered to be tetrahedral if the dative Ru-Mo interaction is ignored. Tetrahedral bis(imido) units are common for Mo(VI)[169-171] and known for Mo(IV),[172,174] although it is difficult to distinguish between the two as molybdenum-nitrogen distances are very similar. The molybdenum-nitrogen distances in **49** [Mo(1)-N(1) 1.766(2); Mo(1)-N(2) 1.761(2) Å] and the N(1)-Mo(1)-N(2) angle of 112.39(7)° are consistent with both Mo(VI) and Mo(IV) complexes.[156,169-174] As the imido ligands are linear [Mo(1)-N(1)-C(20) 163.60(13); Mo(1)-N(2)-C(30) 162.26(13)°] they could be considered as four-electron donors (neutral counting system) and would give a 62-electron cluster, consistent with a butterfly geometry. However, as there are only three d-orbitals of π-symmetry on the molybdenum, the maximum number of electrons that can be donated by the two imido ligands is six.[156] This would give the cluster an electron-count of 60-electrons, which would leave the molybdenum electron-deficient.

The IR spectra of all these compounds are very similar to each other indicating the structures are all the same. The ^{1}H NMR spectrum of the cluster $[Ru_3(CO)_{12}\{Mo(N\text{-}2,4,6\text{-}Me_3C_6H_2)_2\}]$ **50** showed a singlet at δ 2.14 for the Me groups in the *ortho* position, a singlet at δ 2.22 for the Me group in the *para* position and a singlet at δ 6.80 for the protons in the *meta* position of the aromatic rings. The positive ion FAB mass spectrum shows a molecular ion peak at *m/z* 1004 with daughter ions due to the successive loss of twelve carbonyl ligands.

The ^{1}H NMR spectrum of $[Ru_3(CO)_{12}\{Mo(N\text{-}2,6\text{-}Me\text{-}4\text{-}Br\text{-}C_6H_2)_2\}]$ **51** shows a singlet at δ 2.13 for the Me groups and a singlet at δ 7.15 for the protons on the

aromatic rings. The positive ion FAB mass spectrum shows a molecular ion peak at *m z* 1134 with other ions due to the successive loss of twelve carbonyl ligands.

5.3.2 Preparation of $[Ru_3(CO)_{12}\{MoO_2\}]$ 52

The cluster anion $K_2[Ru_3(CO)_{11}]$ **45** was treated with $[MoO_2Cl_2]$ in a similar fashion as with the imido complexes. Again $[Ru_3(CO)_{12}]$ and $[H_2Ru_4(CO)_{13}]$ were obtained along with a an orange solid that appeared to have the formulation of $[Ru_3(CO)_{12}\{MoO_2\}]$ **52** isolated in 49% yield. Unlike the imido counterparts, this cluster does not appear to be air-stable in hexane, as attempts at recrystallising it in this solvent resulted in decomposition to $[Ru_3(CO)_{12}]$. The IR spectrum in the CO region was very similar to those of the analogous imido clusters described above. The positive ion FAB mass spectrum showed a molecular ion peak at *m/z* 771 consistent with the formulation given, along with ions due to successive loss of eleven, possibly twelve, carbonyl ligands.

The solid-state IR spectrum displayed ν(Mo=O) peaks at 1097 and 1023 cm^{-1} for *cis* symmetric and asymmetric stretches respectively. On comparing this data with the *cis* Mo(VI) oxo complexes $[MoO_2X_2]$ (where X = F, Cl or Br)[175] and the Raman spectrum of the *trans* Mo(IV) complex $[MoO_2(CN)_4]^{4-}$ (Table 5.2),[176] the wavenumbers decrease with an increase in electron density at the metal. As **52** has the highest wavenumbers of all of these compounds, this data suggests that the molybdenum atom is in the +6 oxidation state.

The mechanism for the formation of the high-low valent clusters is not yet fully understood. Although it appears that CO scavenging occurs which would explain the

Table 5.2 A comparison of IR data for molybdenum oxo complexes

Compound	**52**	$[MoO_2F_2]$	$[MoO_2Cl_2]$	$[MoO_2Br_2]$	$[MoO_2(CN)_4]^{4-}$
ν(Mo O) cm^{-1}	1097, 1023.	1009, 987	994, 972	991, 969	826, 779

moderate yields obtained. As described above, electron-transfer competing with nucleophilic substitution could result in the isolation of $[Ru_3(CO)_{12}]$ as a by-product. It was also found that while the clusters **49**, **50** and **51** were stable indefinitely in hexane, a non-coordinating solvent, they decompose in THF, a coordinating solvent, over a period of hours under anaerobic conditions to give $[Ru_3(CO)_{12}]$, which may be due to the polarisation of the Mo-Ru bonds and the electron-deficiency at molybdenum. This would suggest that the high-low valent clusters could be decomposing in solution during synthesis, which could be another reason for the moderate yields. Attempts to synthesise further high-low valent clusters using other aryl imido ligands, namely NPh, N-2,6-Pr^i-C_6H_3, and NBu^t, and other high-valent metal complexes, such as $[TiCp_2Cl_2]$ and $[CrO_2Cl_2]$ were unsuccessful and yielded $[Ru_3(CO)_{12}]$ and $[H_2Ru_4(CO)_{13}]$ as the only tractable products. Again, this could be due to the solvent and the competing electron-transfer and nucleophilic substitution processes. It is possible that during the preparation of the cluster anion **45** there was some $K_2[Ru_4(CO)_{13}]$ formed as well, which can be synthesised by reacting two equivalents of $[Ru_3(CO)_{12}]$ with three equivalents of potassium-benzophenone. During purification by column chromatography, $K_2[Ru_4(CO)_{13}]$ could then be protonated to give $[H_2Ru_4(CO)_{13}]$.

5.3.3 Protonation of $[Ru_3(CO)_{12}\{Mo(N\text{-}2,6\text{-}Me_2C_6H_3)_2\}]$ 49

There are two possible sites for protonation in **49** (Scheme 5.7). One possibility is that H^+ can add onto the ruthenium cluster to form a hydride (Scheme 5.7a), or it can add onto one or even both of the nitrogen atoms (Scheme 5.7b). Studies by IR and ^1H NMR spectroscopy can show which situation occurs. If the situation in Scheme 5.7a occurs then in the IR spectrum the carbonyl peaks would shift to a higher wavenumber as the H^+ would remove electron density from the CO π^*-orbitals and a negative chemical shift would be observed in the ^1H NMR spectrum. Whereas, with the situation in Scheme 5.7b the carbonyl peaks in the IR spectrum should not shift significantly and an N-H signal would be observed in the ^1H NMR spectrum.

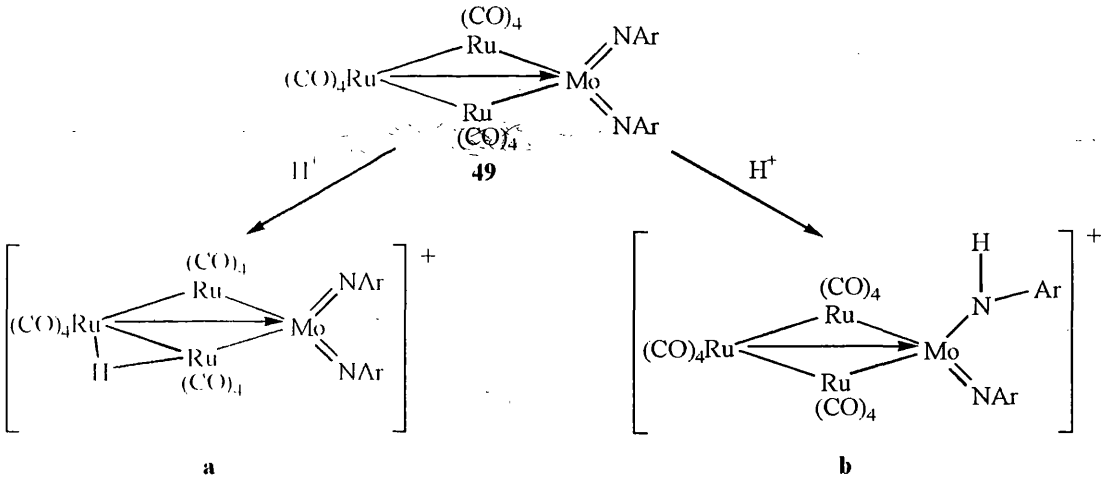

a b

Scheme 5.7 The two possible sites of protonation in 49

5.3.3.1 IR Study

The cluster **49** in a solution of dichloromethane was treated with an excess of tetrafluorboric acid ($HBF_4.Et_2O$). An immediate reaction occurred, the IR spectrum did not show a considerable shift which would be consistent with the situation in Scheme 5.7b occurring to form $[Ru_3(CO)_{12}\{Mo(HN\text{-}2,6\text{-}Me_2C_6H_3)(N\text{-}2,6\text{-}Me_2C_6H_3)\}][BF_4]$ **53a**. On leaving this solution over a period of time (4 days), it appeared that $[Ru_3(CO)_{12}]$ was formed.

5.3.3.2 ^{1}H NMR Study

The cluster **49** in a solution of $CDCl_3$ was treated with an excess of trifluroacetic acid. The reaction was monitored by ^{1}H NMR spectroscopy. The spectrum did not show a hydride signal, which would therefore be consistent with situation (b) occurring to form $[Ru_3(CO)_{12}\{Mo(HN\text{-}2,6\text{-}Me_2C_6H_3)(N\text{-}2,6\text{-}Me_2C_6H_3)\}][CF_3CO_2]$ **53b**. Initially peaks due to **49** were observed along with a small singlet at δ 2.43 for a new Me group and a broad signal at δ 7.85 due to an equilibrium between the free acid and the monocationic species, no aromatic signals for the monocation were visible. After 24 hours all the signals due to starting material had disappeared and a singlet at δ 2.43 for the Me groups, a singlet at δ 7.17 for the protons in the *para* position and a singlet at δ 7.19 for the protons in the *meta* position of the aromatic rings were observed, however, there did not appear to be any signal for an NH group. This combined with the fact that there are only one set of proton signals due to the aromatic group when two sets of signals would be expected, could mean there is a rapid exchange of the proton between the two nitrogen atoms (Scheme 5.8). Leaving the solution for a

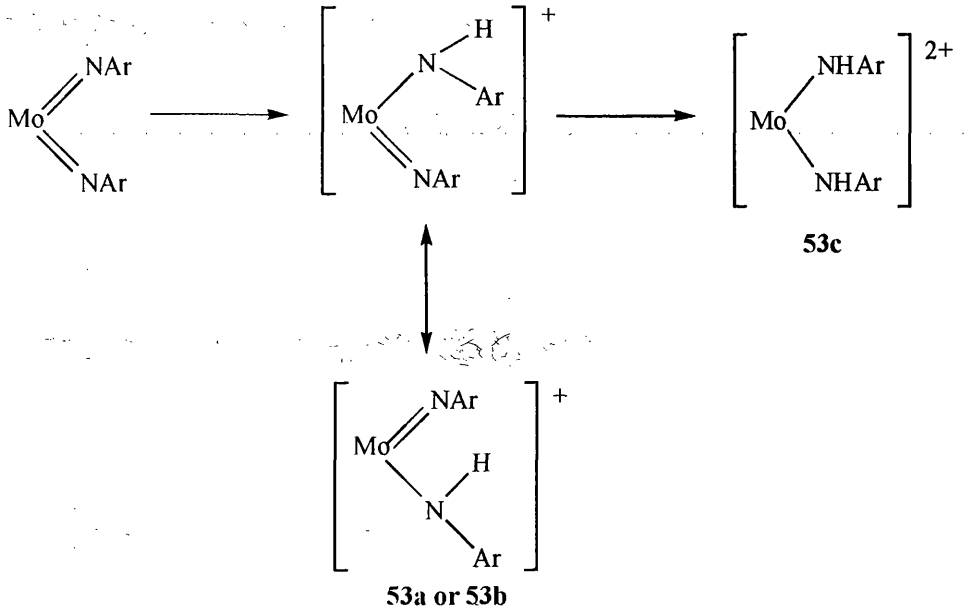

Scheme 5.8 The protonation of 49 to form two possible monocationic species and dication

further 7 days resulted in another singlet appearing at δ 2.29 along with the signal for the monocation. This additional signal could be due to the dicationic species $[Ru_3(CO)_{12}\{Mo(HN\text{-}2,6\text{-}Me_2C_6H_3)_2\}][CF_3CO_2]_2$ **53c** being formed (Scheme 5.8).

It should be noted that leaving the solution for a prolonged period of time in air resulted in it turning blue, indicative of molybdates being present. This could be caused by the hydrolysis of the protonated species (Scheme 5.9).

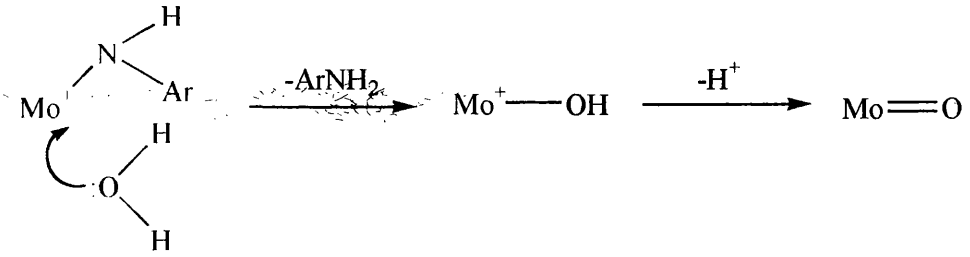

Scheme 5.9 Hydrolysis of the protonated complex

5.4 CONCLUSIONS

- It is possible to form high-low valent complexes of the type $[Ru_3(CO)_{12}\{MoX_2\}]$ where X = N-2,6-$Me_2C_6H_3$, N-2,4,6-$Me_3C_6H_2$, N-2,6-Me_2-4-BrC_6H_2 or O.
- The structure of $[Ru_3(CO)_{12}\{Mo(N\text{-}2,6\text{-}Me_2C_6H_3)_2\}]$ was elucidated by X-ray crystallography and was shown to have a distorted butterfly geometry with the imido ligands remaining bound to the molybdenum in a terminal fashion.
- Protonation of $[Ru_3(CO)_{12}\{Mo(N\text{-}2,6\text{-}Me_2C_6H_3)_2\}]$ occurred at the nitrogen atoms of the bis(imido) ligands, first forming the monocation and eventually the dication.

5.5 EXPERIMENTAL

5.5.1 Materials and Instrumentation

All materials and instrumentation are as described in Chapters 2 and 3 (Sections 2.5.1 and 3.5.1). In addition to this all reactions were carried out under N_2 using standard Schlenk line techniques or in a N_2 filled glove box unless otherwise specified. DME was distilled prior to use under an atmosphere of nitrogen over potassium.

Some NMR spectra were recorded on a Varian VXR-400 spectrometer using deuterated chloroform (δ 7.27) as an internal reference. The X-ray structure of $[Ru_3(CO)_{12}\{Mo(N\text{-}2,6\text{-}Me_2C_6H_3)_2\}]$ was obtained by Dr. G. Enright at The Steacie Institute for Molecular Sciences, NRC, Ottawa, Canada using a Siemens CCD diffractomer. X-ray data were collected at room temperature.

5.5.2 Preparation of $K_2[Ru_3(CO)_{11}]$ 45

The compound **45** was prepared using literature procedures.[164]

Potassium metal (30 mg, 0.782 mmol), benzophenone (143 mg, 0.782 mmol) and THF(~ 20 cm^3) were placed in a 50 cm^3 flask. The resulting blue solution was stirred until all the potassium had been consumed. Small aliquots (50-60 mg every 15-20 min) of $[Ru_3(CO)_{12}]$ (250 mg, 0.391 mmol) were added. The mixture was stirred until the last aliquot of $[Ru_3(CO)_{12}]$ was added and all the $[Ru_3(CO)_{12}]$ had dissolved, this yielded **45** as a brown/red solution.

5.5.3 Preparation of [Mo(NAr)$_2$Cl$_2$(dme)] compounds

The compounds [Mo(NAr)$_2$Cl$_2$(dme)] (Ar = 2,6-Me$_2$C$_6$H$_3$ **46**, 2,4,6-Me$_3$C$_6$H$_2$ **47** and 2,6-Me$_2$-4-Br-C$_6$H$_2$ **48**) were prepared using literature procedures.[165]

5.5.3.1 Preparation of [Mo(N-2,6-Me$_2$C$_6$H$_3$)$_2$Cl$_2$(dme)] 46

In a Schlenk tube equipped with an air condenser attached to an oil bubbler, was placed sodium molybdate (2.04 g, 9.907 mmol), DME (~ 40 cm^3), triethylamine (5.4 cm^3, 0.040 mol), chlorotrimethylsilane (10 cm^3, 0.080 mol) and distilled 2,6-dimethylaniline (2.5 cm^3, 0.020 mol). The opaque solution turned yellow and then deep red as some white precipitate was also formed. The mixture was then heated to ~ 65 °C for 15 h. The reaction mixture was cooled to room temperature and filtered to remove the sodium salts. The salts were washed with diethyl ether until the washings ran through colourless. The volatile components were removed under reduced pressure. The resulting solid was washed with light petroleum spirit (~ 35 cm^3) to yield **46** as a red/purple solid (3.91 g, 80%).

5.5.3.2 Preparation of [Mo(N-2,4,6-Me$_3$C$_6$H$_2$)$_2$Cl$_2$(dme)] 47

In a Schlenk tube equipped with an air condenser attached to an oil bubbler, was placed sodium molybdate (2.07 g, 0.010 mol), DME (~ 40 cm^3), triethylamine (5.4 cm^3, 0.040 mol), chlorotrimethylsilane (10 cm^3, 0.080 mol) and distilled 2,4,6-trimethylaniline (2.8 cm^3, 0.020 mol). The opaque solution turned yellow and then deep red as some white precipitate was also formed. The mixture was then heated to ~ 65 °C for 8 h. The reaction mixture was cooled to room temperature and filtered to remove the sodium salts. The salts were washed with diethyl ether until the washings

ran through colourless. The volatile components were removed under reduced pressure. The resulting solid was washed with light petroleum spirit (~ 35 cm^3) to yield **47** as a dark red solid (2.95 g, 57%).

5.5.3.3 Preparation of [Mo(N-2,6-Me_2-4-Br-C_6H_2)$_2$$Cl_2$(dme)] 48

In a Schlenk tube equipped with an air condenser attached to an oil bubbler, was placed sodium molybdate (500 mg, 2.428 mmol), DME (~ 10 cm^3), triethylamine (1.3 cm^3, 9.910 mmol), chlorotrimethylsilane (2.5 cm^3, 0.020 mol) and 2,6-dimethyl-4-bromoaniline (1.000 g, 4.998 mmol). The opaque solution turned brown/yellow and then deep red as some white precipitate was also formed. The mixture was then heated to ~ 65 °C for 15 h. The reaction mixture was cooled to room temperature and filtered to remove the sodium salts. The salts were washed with diethyl ether until the washings ran through colourless. The volatile components were removed under reduced pressure. The resulting solid was washed with light petroleum spirit (~ 35 cm^3) to yield **48** as a dark red solid (1.27 g, 79%).

5.5.4 Preparation of [$Ru_3(CO)_{12}${Mo(N-2,6-$Me_2C_6H_3$)$_2$}] 49

To a stirring solution of $K_2[Ru_3(CO)_{11}]$ **45** (539 mg, 0.782 mmol) was added a solution of [Mo(N-2,6-$Me_2C_6H_3$)$_2$$Cl_2$(dme)] **46** (387 mg, 0.782 mmol) in THF (~ 5 cm^3) dropwise. The dark brown/red solution was left to stir at room temperature for 16 h. The solution was removed from the glove box under N_2 and the THF removed under reduced pressure. Chromatography on silica gel [light petroleum spirit/CH_2Cl_2 eluent with a gradual increase in CH_2Cl_2 from 0% to 40%] yielded 3 bands. A yellow band yielded $[Ru_3(CO)_{12}]$ (70 mg, 14%, 0.109 mmol), a deep red/orange band yielded

$[H_2Ru_4(CO)_{13}]$[166] (90 mg, 17%) as an orange solid and a bright orange band which yielded **49** (210 mg, 36%) as a dark orange solid. The compound **49** was recrystallised from hexane.

Compound 49: IR ν(CO): 2106 (m), 2070 (s), 2055 (m), 2038 (m), 2030 (s), 2026 (m, sh), 2006 (m), 2003 (w, sh) cm^{-1}. IR (CH_2Cl_2) ν(CO): 2106 (m), 2071 (s), 2056 (m), 2028 (m), 2016 (w, sh), 2003 (w) cm^{-1}. ^1H NMR: δ 2.17 (s, 12H, CH_3), 6.98 (s, 6H, C_6H_3). MS (FAB): *m/z* 945 (M^+-CO). Anal. Calcd for $C_{28}H_{18}N_2O_{12}MoRu_3$: C, 34.54, H, 1.86, N, 2.88%. Found: C, 33.87, H, 1.70, N, 2.65%.

5.5.5 Preparation of $[Ru_3(CO)_{12}\{Mo(N\text{-}2,4,6\text{-}Me_3C_6H_2)_2\}]$ 50

To a stirring solution of **45** (270 mg, 0.391 mmol) was added a solution of [Mo(N-2,4,6-$Me_3C_6H_2)_2Cl_2$(dme)] **47** (205 mg, 0.391 mmol) in THF (~ 5 cm^3) dropwise. The dark brown/red solution was left to stir at room temperature for 16 h. The solution was removed from the glove box under N_2 and the THF removed under reduced pressure. Chromatography on silica gel [light petroleum spirit/CH_2Cl_2 eluent with a gradual increase in CH_2Cl_2 from 0% to 40%] yielded 3 bands. A yellow band yielded $[Ru_3(CO)_{12}]$ (60 mg, 24%, 0.094 mmol), a deep red/orange band yielded $[H_2Ru_4(CO)_{13}]$[166] (40 mg, 17%) as an orange solid and an orange band yielded **50** (70 mg, 23%) as an orange solid. The compound **50** was recrystallised from hexane.

Compound 50: IR ν(CO): 2104 (m), 2069 (s), 2054 (m), 2037 (m), 2029 (s), 2005 (m) cm^{-1}. ^1H NMR: δ 2.14 (s, 12H, CH_3), 2.22 (s, 6H, CH_3), 6.80 (s, 4H, C_6H_2). MS (FAB): *m/z* 1004 (M^+). Anal. Calcd for $C_{30}H_{22}N_2O_{12}MoRu_3$: C, 35.97, H, 2.21, N, 2.80%. Found: C, 36.01, H, 2.02, N, 2.69%.

5.5.6 Preparation of $[Ru_3(CO)_{12}\{Mo(N\text{-}2,6\text{-}Me_2\text{–}4\text{-}Br\text{-}C_6H_2)_2\}]$ 51

To a stirring solution of **45** (270 mg, 0.391 mmol) was added a solution of [Mo(N-2,6-Me_2–4Br-$C_6H_2)_2Cl_2$(dme)] **48** (256 mg, 0.391 mmol) in THF (~ 5 cm^3) dropwise. The dark brown/red solution was left to stir at room temperature for 16 h. The solution was removed from the glove box under N_2 and the THF removed under reduced pressure. Chromatography on silica gel [light petroleum spirit/CH_2Cl_2 eluent with a gradual increase in CH_2Cl_2 from 0% to 20%] yielded 3 bands. A yellow band yielded $[Ru_3(CO)_{12}]$ (90 mg, 36%, 0.140 mmol), a deep red/orange band yielded $[H_2Ru_4(CO)_{13}]$[166] (40 mg, 20%) as an orange solid and a yellow/orange band yielded **51** (60 mg, 21%) as an orange solid. The compound **51** was recrystallised from hexane.

Compound 51: IR ν(CO): 2107 (m), 2082 (w), 2072 (s), 2057 (m), 2040 (m), 2031 (s), 2017 (w), 2008 (m), 2004 (w, sh) cm^{-1}. ^1H NMR: δ 2.13 (s, 12H, CH_3), 7.15 (s, 4H, C_6H_2). MS (FAB): *m/z* 1134 (M^+). Anal. Calcd for $C_{28}H_{16}N_2O_{12}Br_2MoRu_3$: C, 29.72, H, 1.42, N, 2.48%. Found: C, 29.87, H, 1.31, N, 2.33%.

5.5.7 Preparation of $[Ru_3(CO)_{12}\{MoO_2\}]$ 52

To a stirring solution of **45** (270 mg, 0.391 mmol) was added a solution of $[MoO_2Cl_2]$ (78 mg, 0.391 mmol) in THF (~ 5 cm^3) dropwise. The dark brown/red solution was left to stir at room temperature for 16 h. The solution was removed from the glove box under N_2 and the THF removed under reduced pressure. Chromatography on silica gel [light petroleum spirit/CH_2Cl_2 eluent with a gradual increase in CH_2Cl_2 from 0% to 20%] yielded 3 bands. A yellow band yielded $[Ru_3(CO)_{12}]$ (130 mg, 52%, 0.203 mmol), a deep red/orange band which yielded $[H_2Ru_4(CO)_{13}]$[166] (60 mg, 41%)

as an orange solid and a bright orange band yielded **52** (70 mg, 49 %) as an orange solid. An attempt to recrystallised the compound **52** was made, however, the compound appeared to decompose to reform $[Ru_3(CO)_{12}]$ in solution.

Compound 52: IR ν(CO): 2106 (w), 2070 (s), 2057 (s), 2035 (m), 2026 (s), 2021 (s), 2003 (w, sh), 1993 (w) cm^{-1}. IR (KBr) ν(Mo=O): 1097 (s), 1023 (s) cm^{-1}. MS (FAB): *m/z* 771 (M^+).

5.5.8 Protonation of $[Ru_3(CO)_{12}\{Mo(N\text{-}2,6\text{-}Me_2C_6H_3)_2\}]$ 49

(a) IR Experiment: To a yellow/orange solution of **49** (~ 10 mg, 0.010 mmol) was added HBF_4 (1 drop) the solution turned yellow, and an IR spectrum was run, which was consistent with the formation of $[Ru_3(CO)_{12}Mo(HN\text{-}2,6\text{-}Me_2C_6H_3)(N\text{-}2,6\text{-}Me_2C_6H_3)][BF_4]$ **53a**.

$[Ru_3(CO)_{12}Mo(HN\text{-}2,6\text{-}Me_2C_6H_3)(N\text{-}2,6\text{-}Me_2C_6H_3)][BF_4]$ 53a: IR (CH_2Cl_2) ν(CO): 2108 (m), 2090 (m), 2074 (2), 2062 (s), 2049 (w), 2029 (m), 2015 (w) cm^{-1}.

(b) ^1H NMR Experiment: To a yellow/orange solution of **49** (~ 10 mg, 0.010 mmol) in $CDCl_3$ was added CF_3CO_2H (2 drops) and an NMR spectrum obtained, which was consistent with the formation of $[Ru_3(CO)_{12}Mo(HN\text{-}2,6\text{-}Me_2C_6H_3)(N\text{-}2,6\text{-}Me_2C_6H_3)]^+[CF_3CO_2]^-$ **53b**. The solution had turned dark brown.

$[Ru_3(CO)_{12}Mo(HN\text{-}2,6\text{-}Me_2C_6H_3)(N\text{-}2,6\text{-}Me_2C_6H_3)][CF_3CO_2]$ 53b: ^1H NMR: δ 2.43 (s, br, 12H, CH_3), 7.17 (s, 2H, C_6H_2H), 7.19 (s, 4H, C_6H_2H).

Appendices

APPENDIX I Crystallographic characterisation of $[Ru_3(\mu\text{-}H)_2(\mu_3\text{-}NTs)(CO)_9]$ 8

Crystal data and structure refinement for 8

Empirical formula	$C_{16}H_9NO_{11}Ru_3S$	
Formula weight	726.51	
Temperature	293(2) K	
Wavelength	0.71073 Å	
Crystal system	Monoclinic	
Space group	$P2_1/n$	
Unit cell dimensions	a = 14.236(3) Å	$\alpha = 90°$
	b = 15.167(3) Å	$\beta = 105.05(3)°$
	c = 23.305(5) Å	$\gamma = 90°$
Volume	4859(2) $Å^3$	
Z	8	
Density (calculated)	1.986 Mg/m^3	
Absorption coefficient	1.979 mm^{-1}	
F(000)	2784	
Crystal size	0.85 x 0.40 x 0.02 mm	
Theta range for data collection	2.69 to 24.00°	
Index ranges	0<=h<=16, 0<=k<=17, -26<=l<=25	
Reflections collected	7585	
Independent reflections	7265 [R(int) = 0.0717]	
Absorption correction	Psi-scans	
Max. and min. transmission	1.000 and 0.744	
Refinement method	Full-matrix least-squares on F^2	
Data / restraints / parameters	7260 / 0 / 577	
Goodness-of-fit on F^2	1.096	
Final R indices [I>2sigma(I)]	R1 = 0.0835, wR2 = 0.2177	
R indices (all data)	R1 = 0.1393, wR2 = 0.3102	
Largest difference peak and hole	1.719 and -1.426 $e.Å^{-3}$	

Bond lengths (Å) and angles (°) for $[Ru_3(\mu\text{-}H)_2(\mu_3\text{-}NTs)(CO)_9]$ 8

Ru(1)-C(13)	1.91(2)	S(1)-C(101)	1.78(2)
Ru(1)-C(12)	1.95(2)	C(101)-C(106)	1.38(3)
Ru(1)-C(11)	1.96(2)	C(101)-C(102)	1.43(2)
Ru(1)-N(1)	2.109(13)	C(102)-C(103)	1.40(3)
Ru(1)-Ru(3)	2.751(2)	C(103)-C(104)	1.36(3)
Ru(1)-Ru(2)	2.847(2)	C(104)-C(105)	1.39(3)
Ru(2)-C(21)	1.91(2)	C(104)-C(107)	1.52(3)
Ru(2)-C(23)	1.97(2)	C(105)-C(106)	1.36(3)
Ru(2)-C(22)	1.99(2)	C(11)-O(11)	1.14(2)
Ru(2)-N(1)	2.116(12)	C(12)-O(12)	1.14(2)
Ru(2)-Ru(3)	2.859(2)	C(13)-O(13)	1.14(2)
Ru(3)-C(32)	1.92(2)	C(21)-O(21)	1.18(2)
Ru(3)-C(33)	1.95(2)	C(22)-O(22)	1.14(2)
Ru(3)-C(31)	1.97(2)	C(23)-O(23)	1.13(2)
Ru(3)-N(1)	2.104(12)	C(31)-O(31)	1.11(2)
N(1)-S(1)	1.634(13)	C(32)-O(32)	1.18(2)
S(1)-O(2)	1.466(13)	C(33)-O(33)	1.16(2)
S(1)-O(1)	1.473(13)		

C(13)-Ru(1)-C(12)	89.2(7)	C(31)-Ru(3)-Ru(1)	92.7(6)
C(13)-Ru(1)-C(11)	95.3(7)	N(1)-Ru(3)-Ru(1)	49.3(4)
C(12)-Ru(1)-C(11)	97.9(9)	C(32)-Ru(3)-Ru(2)	117.4(7)
C(13)-Ru(1)-N(1)	104.1(6)	C(33)-Ru(3)-Ru(2)	100.1(6)
C(12)-Ru(1)-N(1)	153.6(8)	C(31)-Ru(3)-Ru(2)	147.5(5)
C(11)-Ru(1)-N(1)	103.4(6)	N(1)-Ru(3)-Ru(2)	47.5(3)
C(13)-Ru(1)-Ru(3)	94.0(5)	Ru(1)-Ru(3)-Ru(2)	60.97(5)
C(12)-Ru(1)-Ru(3)	108.1(7)	S(1)-N(1)-Ru(3)	133.3(7)
C(11)-Ru(1)-Ru(3)	152.5(5)	S(1)-N(1)-Ru(1)	133.4(7)
N(1)-Ru(1)-Ru(3)	49.2(3)	Ru(3)-N(1)-Ru(1)	81.5(5)
C(13)-Ru(1)-Ru(2)	150.2(5)	S(1)-N(1)-Ru(2)	121.6(7)
C(12)-Ru(1)-Ru(2)	113.2(6)	Ru(3)-N(1)-Ru(2)	85.3(5)
C(11)-Ru(1)-Ru(2)	100.4(5)	Ru(1)-N(1)-Ru(2)	84.8(5)
N(1)-Ru(1)-Ru(2)	47.7(3)	O(2)-S(1)-O(1)	118.5(8)
Ru(3)-Ru(1)-Ru(2)	61.38(5)	O(2)-S(1)-N(1)	107.6(7)
C(21)-Ru(2)-C(23)	91.8(9)	O(1)-S(1)-N(1)	108.7(7)
C(21)-Ru(2)-C(22)	94.3(9)	O(2)-S(1)-C(101)	108.8(8)
C(23)-Ru(2)-C(22)	91.4(7)	O(1)-S(1)-C(101)	109.1(8)
C(21)-Ru(2)-N(1)	99.4(7)	N(1)-S(1)-C(101)	103.1(7)
C(23)-Ru(2)-N(1)	163.8(6)	C(106)-C(101)-C(102)	117(2)
C(22)-Ru(2)-N(1)	99.4(6)	C(106)-C(101)-S(1)	123(2)
C(21)-Ru(2)-Ru(1)	145.7(7)	C(102)-C(101)-S(1)	120(2)
C(23)-Ru(2)-Ru(1)	118.9(5)	C(103)-C(102)-C(101)	121(2)
C(22)-Ru(2)-Ru(1)	99.5(6)	C(104)-C(103)-C(102)	120(2)
N(1)-Ru(2)-Ru(1)	47.5(3)	C(103)-C(104)-C(105)	120(2)
C(21)-Ru(2)-Ru(3)	94.8(6)	C(103)-C(104)-C(107)	119(2)
C(23)-Ru(2)-Ru(3)	120.5(5)	C(105)-C(104)-C(107)	121(2)
C(22)-Ru(2)-Ru(3)	146.4(5)	C(106)-C(105)-C(104)	122(2)
N(1)-Ru(2)-Ru(3)	47.2(3)	C(105)-C(106)-C(101)	121(2)
Ru(1)-Ru(2)-Ru(3)	57.65(5)	O(11)-C(11)-Ru(1)	176(2)
C(32)-Ru(3)-C(33)	93.7(10)	O(12)-C(12)-Ru(1)	178(2)
C(32)-Ru(3)-C(31)	89.2(8)	O(13)-C(13)-Ru(1)	178(2)
C(33)-Ru(3)-C(31)	96.2(8)	O(21)-C(21)-Ru(2)	177(2)
C(32)-Ru(3)-N(1)	158.8(8)	O(22)-C(22)-Ru(2)	176(2)
C(33)-Ru(3)-N(1)	103.3(8)	O(23)-C(23)-Ru(2)	170(2)
C(31)-Ru(3)-N(1)	101.4(6)	O(31)-C(31)-Ru(3)	178(2)
C(32)-Ru(3)-Ru(1)	112.5(7)	O(32)-C(32)-Ru(3)	172(2)
C(33)-Ru(3)-Ru(1)	152.5(7)	O(33)-C(33)-Ru(3)	177(2)

APPENDIX II Crystallographic characterisation of $[HNEt_3][Os_3(\mu\text{-}H)(\mu\text{-}NTs)(CO)_{10}]$ 19d

Crystal data and structure refinement for 19d

Empirical formula	$C_{23}H_{25}N_2O_{12}Os_3S$	
Formula weight	1124.11	
Temperature	100(2) K	
Wavelength	0.71070 Å	
Crystal system	Triclinic	
Space group	P-1	
Unit cell dimensions	a = 11.0537(4) Å	α = 88.9360(10)°
	b = 11.3426(6) Å	β = 77.8380(10)°
	c = 12.3793(6) Å	γ = 79.8090(10)°
Volume	1493.03(12) $Å^3$	
Z	2	
Density (calculated)	2.500 Mg/m^3	
Absorption coefficient	12.865 mm^{-1}	
F(000)	1034	
Crystal size	0.10 x 0.10 x 0.10 mm	
Theta range for data collection	3.37 to 26.00°	
Index ranges	-14<=h<=14, -14<=k<=14, -16<=l<=16	
Reflections collected	9267	
Independent reflections	5498 [R(int) = 0.0696]	
Refinement method	Full-matrix least-squares on F^2	
Data / restraints / parameters	5486 / 0 / 375	
Goodness-of-fit on F^2	1.080	
Final R indices [I>2sigma(I)]	R1 = 0.0292, wR2 = 0.0701	
R indices (all data)	R1 = 0.0341, wR2 = 0.1286	
Largest difference peak and hole	1.162 and -2.367 $e.A^{-3}$	

Bond lengths (Å) and angles (°) for $[Et_3NH][Os_3(\mu\text{-}H)(\mu\text{-}NTs)(CO)_{10}]$ 19d

Os(1)-C(2)	1.898(6)	O(3)-C(3)	1.147(8)
Os(1)-C(1)	1.909(7)	O(4)-C(4)	1.140(8)
Os(1)-C(3)	1.929(7)	O(5)-C(5)	1.157(8)
Os(1)-N(1)	2.118(5)	O(6)-C(6)	1.158(8)
Os(1)-Os(2)	2.8113(3)	O(7)-C(7)	1.152(8)
Os(1)-Os(3)	2.8437(4)	O(8)-C(8)	1.154(8)
Os(2)-C(5)	1.893(7)	O(9)-C(9)	1.147(8)
Os(2)-C(6)	1.895(7)	O(10)-C(10)	1.152(8)
Os(2)-C(4)	1.926(6)	C(11)-C(16)	1.374(8)
Os(2)-N(1)	2.106(5)	C(11)-C(12)	1.409(8)
Os(2)-Os(3)	2.8496(3)	C(12)-C(13)	1.378(9)
Os(3)-C(10)	1.915(6)	C(13)-C(14)	1.397(9)
Os(3)-C(8)	1.918(7)	C(14)-C(15)	1.394(9)
Os(3)-C(9)	1.944(6)	C(14)-C(17)	1.505(8)
Os(3)-C(7)	1.945(7)	C(15)-C(16)	1.398(8)
S(1)-O(11)	1.460(4)	N(1A)-C(5A)	1.493(7)
S(1)-O(12)	1.473(4)	N(1A)-C(1A)	1.508(8)
S(1)-N(1)	1.557(5)	N(1A)-C(3A)	1.525(8)
S(1)-C(11)	1.781(6)	C(1A)-C(2A)	1.512(8)
O(1)-C(1)	1.141(8)	C(3A)-C(4A)	1.500(10)
O(2)-C(2)	1.151(8)	C(5A)-C(6A)	1.518(9)

C(2)-Os(1)-C(1)	92.8(3)	C(10)-Os(3)-Os(2)	154.7(2)
C(2)-Os(1)-C(3)	97.3(3)	C(8)-Os(3)-Os(2)	102.8(2)
C(1)-Os(1)-C(3)	93.4(3)	C(9)-Os(3)-Os(2)	84.8(2)
C(2)-Os(1)-N(1)	93.2(2)	C(7)-Os(3)-Os(2)	84.7(2)
C(1)-Os(1)-N(1)	168.0(2)	Os(1)-Os(3)-Os(2)	59.179(8)
C(3)-Os(1)-N(1)	96.1(2)	O(11)-S(1)-O(12)	112.1(3)
C(2)-Os(1)-Os(2)	134.3(2)	O(11)-S(1)-N(1)	111.0(3)
C(1)-Os(1)-Os(2)	121.6(2)	O(12)-S(1)-N(1)	116.6(3)
C(3)-Os(1)-Os(2)	108.5(2)	O(11)-S(1)-C(11)	107.4(2)
N(1)-Os(1)-Os(2)	48.10(12)	O(12)-S(1)-C(11)	104.6(3)
C(2)-Os(1)-Os(3)	94.0(2)	N(1)-S(1)-C(11)	104.3(3)
C(1)-Os(1)-Os(3)	89.4(2)	S(1)-N(1)-Os(2)	125.5(3)
C(3)-Os(1)-Os(3)	168.2(2)	S(1)-N(1)-Os(1)	120.0(3)
N(1)-Os(1)-Os(3)	79.79(14)	Os(2)-N(1)-Os(1)	83.4(2)
Os(2)-Os(1)-Os(3)	60.514(8)	O(1)-C(1)-Os(1)	178.1(6)
C(5)-Os(2)-C(6)	91.3(3)	O(2)-C(2)-Os(1)	175.6(6)
C(5)-Os(2)-C(4)	95.6(2)	O(3)-C(3)-Os(1)	177.2(6)
C(6)-Os(2)-C(4)	93.5(3)	O(4)-C(4)-Os(2)	174.4(5)
C(5)-Os(2)-N(1)	95.6(2)	O(5)-C(5)-Os(2)	178.2(6)
C(6)-Os(2)-N(1)	167.0(2)	O(6)-C(6)-Os(2)	179.1(6)
C(4)-Os(2)-N(1)	96.7(2)	O(7)-C(7)-Os(3)	176.1(5)
C(5)-Os(2)-Os(1)	136.6(2)	O(8)-C(8)-Os(3)	179.2(6)
C(6)-Os(2)-Os(1)	120.2(2)	O(9)-C(9)-Os(3)	179.4(5)
C(4)-Os(2)-Os(1)	110.1(2)	O(10)-C(10)-Os(3)	179.6(7)
N(1)-Os(2)-Os(1)	48.46(13)	C(16)-C(11)-C(12)	120.4(5)
C(5)-Os(2)-Os(3)	94.5(2)	C(16)-C(11)-S(1)	121.3(4)
C(6)-Os(2)-Os(3)	88.7(2)	C(12)-C(11)-S(1)	118.3(4)
C(4)-Os(2)-Os(3)	169.6(2)	C(13)-C(12)-C(11)	119.1(5)
N(1)-Os(2)-Os(3)	79.83(14)	C(12)-C(13)-C(14)	121.7(6)
Os(1)-Os(2)-Os(3)	60.306(8)	C(15)-C(14)-C(13)	117.9(5)
C(10)-Os(3)-C(8)	102.4(3)	C(15)-C(14)-C(17)	121.3(5)
C(10)-Os(3)-C(9)	95.3(3)	C(13)-C(14)-C(17)	120.8(6)
C(8)-Os(3)-C(9)	92.8(3)	C(14)-C(15)-C(16)	121.4(5)
C(10)-Os(3)-C(7)	92.0(3)	C(11)-C(16)-C(15)	119.4(5)

C(8)-Os(3)-C(7)	94.4(3)	C(5A)-N(1A)-C(1A)	111.4(5)
C(9)-Os(3)-C(7)	168.4(3)	C(5A)-N(1A)-C(3A)	111.6(5)
C(10)-Os(3)-Os(1)	95.6(2)	C(1A)-N(1A)-C(3A)	113.5(5)
C(8)-Os(3)-Os(1)	162.0(2)	N(1A)-C(1A)-C(2A)	113.4(5)
C(9)-Os(3)-Os(1)	84.7(2)	C(4A)-C(3A)-N(1A)	114.6(5)
C(7)-Os(3)-Os(1)	85.7(2)	N(1A)-C(5A)-C(6A)	112.2(5)

APPENDIX III Crystallographic characterisation of $[Ru_3(\mu\text{-}\eta^2,\eta^2\text{-}C_4H_6)(\mu_3\text{-}NTs)(\mu_3\text{-}CO)(CO)_7]$ 24

Crystal data and structure refinement for 24

Empirical formula	$C_{19}H_{13}NO_{10}Ru_3S$	
Formula weight	750.57	
Temperature	100(2) K	
Wavelength	0.71070 Å	
Crystal system	Orthorhombic	
Space group	Pbc21	
Unit cell dimensions	a = 10.3720(2) Å	α = 90°
	b = 13.5883(2) Å	β = 90°
	c = 16.0282(3) Å	γ = 90°
Volume	2258.98(7) $Å^3$	
Z	4	
Density (calculated)	2.207 Mg/m^3	
Absorption coefficient	2.129 mm^{-1}	
F(000)	1448	
Crystal size	0.20 x 0.20 x 0.10 mm	
Theta range for data collection	3.80 to 26.00°	
Index ranges	-12<=h<=12, -16<=k<=16, -19<=l<=19	
Reflections collected	19655	
Independent reflections	4203 [R(int) = 0.0440]	
Absorption correction	Scalepack	
Max. and min. transmission	0.8153 and 0.6754	
Refinement method	Full-matrix least-squares on F^2	
Data / restraints / parameters	4203 / 1 / 309	
Goodness-of-fit on F^2	1.097	
Final R indices [I>2sigma(I)]	R1 = 0.0179, wR2 = 0.0455	
R indices (all data)	R1 = 0.0180, wR2 = 0.0456	
Largest difference peak and hole	0.735 and –0.683 e.$Å^{-3}$	

Bond lengths (Å) and angles (°) for $[Ru_3(\mu\text{-}\eta^2,\eta^2\text{-}C_4H_6)(\mu_3\text{-}NTs)(\mu_3\text{-}CO)(CO)_7]$ 24

Ru(1)-C(1)	1.898(3)	S(1)-O(10)	1.444(2)
Ru(1)-C(2)	1.904(4)	S(1)-N(1)	1.626(2)
Ru(1)-N(1)	2.080(3)	S(1)-C(13)	1.759(3)
Ru(1)C(5)	2.230(3)	O(1)-C(1)	1.141(4)
Ru(1)-C(9)	2.258(3)	O(2)-C(2)	1.134(4)
Ru(1)-C(10)	2.304(3)	O(3)-C(3)	1.147(4)
Ru(1)-Ru(3)	2.7416(4)	O(4)-C(4)	1.136(4)
Ru(1)-Ru(2)	2.7560(3)	O(5)-C(5)	1.174(4)
Ru(2)-C(3)	1.888(3)	O(6)-C(6)	1.138(4)
Ru(2)-C(4)	1.921(3)	O(7)-C(7)	1.138(4)
Ru(2)-N(1)	2.091(2)	O(8)-C(8)	1.137(4)
Ru(2)-C(5)	2.160(3)	C(9)-C(10)	1.393(5)
Ru(2)-C(12)	2.246(3)	C(10)-C(11)	1.461(4)
Ru(2)-C(11)	2.338(3)	C(11)-C(12)	1.393(5)
Ru(2)-Ru(3)	2.7554(3)	C(13)-C(18)	1.385(4)
Ru(3)-C(6)	1.926(3)	C(13)-C(14)	1.393(4)
Ru(3)-C(7)	1.938(3)	C(14)-C(15)	1.389(4)
Ru(3)-C(8)	1.945(4)	C(15)-C(16)	1.390(5)
Ru(3)-N(1)	2.073(2)	C(16)-C(17)	1.387(5)
Ru(3)-C(5)	2.162(3)	C(16)-C(19)	1.514(4)
S(1)-O(9)	1.444(2)	C(17)-C(18)	1.393(5)

C(1)-Ru(1)-C(2)	86.72(13)	C(7)-Ru(3)-N(1)	99.47(11)
C(1)-Ru(1)-N(1)	165.75(11)	C(8)-Ru(3)-N(1)	98.04(12)
C(2)Ru(1)-N(1)	100.24(12)	C(6)-Ru(3)-C(5)	81.60(12)
C(1)-Ru(1)-C(5)	83.52(13)	C(7)-Ru(3)-C(5)	128.54(12)
C(2)-Ru(1)-C(5)	130.22(12)	C(8)-Ru(3)-C(5)	129.86(12)
N(1)-Ru(1)-C(5)	82.49(10)	N(1)-Ru(3)-C(5)	84.33(10)
C(1)-Ru(1)-C(9)	100.04(12)	C(6)-Ru(3)-Ru(1)	119.91(11)
C(2)-Ru(1)-C(9)	91.84(13)	C(7)-Ru(3)-Ru(1)	92.33(9)
N(1)-Ru(1)-C(9)	92.21(11)	C(8)-Ru(3)-Ru(1)	146.27(10)
C(5)-Ru(1)-C(9)	137.93(11)	N(1)-Ru(3)-Ru(1)	48.81(7)
C(1)-Ru(1)-C(10)	86.39(12)	C(5)-Ru(3)-Ru(1)	52.49(8)
C(2)-Ru(1)-C(10)	123.84(13)	C(6)-Ru(3)-Ru(2)	120.34(9)
N(1)-Ru(1)-C(10)	99.69(10)	C(7)-Ru(3)-Ru(2)	146.67(9)
C(5)-Ru(1)-C(10)	104.12(11)	C(8)-Ru(3)-Ru(2)	94.86(10)
C(9)-Ru(1)-C(10)	35.54(12)	N(1)-Ru(3)-Ru(2)	48.85(7)
C(1)-Ru(1)-Ru(3)	118.84(9)	C(5)-Ru(3)-Ru(2)	50.35(8)
C(2)-Ru(1)-Ru(3)	95.01(10)	Ru(1)-Ru(3)-Ru(2)	60.181(8)
N(1)-Ru(1)-Ru(3)	48.59(6)	O(9)-S(1)-O(10)	117.45(13)
C(5)-Ru(1)-Ru(3)	50.28(8)	O(9)-S(1)-N(1)	108.92(13)
C(9)-Ru(1)-Ru(3)	140.80(9)	O(10)-S(1)-N(1)	108.90(13)
C(10)-Ru(1)-Ru(3)	135.88(8)	O(9)-S(1)-C(13)	107.53(13)
C(1)-Ru(1)-Ru(2)	121.78(9)	O(10)-S(1)-C(13)	107.34(13)
C(2)-Ru(1)-Ru(2)	148.13(10)	N(1)-S(1)-C(13)	106.12(13)
N(1)-Ru(1)-Ru(2)	48.81(7)	S(1)-N(1)-Ru(3)	124.92(14)
C(5)-Ru(1)-Ru(2)	49.98(8)	S(1)-N(1)-Ru(1)	140.27(14)
C(9)-Ru(1)-Ru(2)	96.26(8)	Ru(3)-N(1)-Ru(1)	82.60(8)
C(10)-Ru(1)-Ru(2)	75.89(8)	S(1)-N(1)-Ru(2)	124.65(13)
Ru(3)-Ru(1)-Ru(2)	60.158(8)	Ru(3)-N(1)-Ru(2)	82.85(9)
C(3)-Ru(2)-C(4)	87.09(14)	Ru(1)-N(1)-Ru(2)	82.71(9)
C(3)-Ru(2)-N(1)	167.66(12)	O(1)-C(1)-Ru(1)	178.0(3)
C(4)-Ru(2)-N(1)	97.97(11)	O(2)-C(2)-Ru(1)	177.6(3)
C(3)-Ru(2)-C(5)	84.31(13)	O(3)-C(3)-Ru(2)	177.4(3)
C(4)-Ru(2)-C(5)	132.34(12)	O(4)-C(4)-Ru(2)	175.9(3)
N(1)-Ru(2)-C(5)	83.98(10)	O(5)-C(5)-Ru(2)	134.6(2)
C(3)-Ru(2)-C(12)	98.16(12)	O(5)-C(5)-Ru(3)	133.7(2)

C(4)-Ru(2)-C(12)	91.69(12)	Ru(2)-C(5)-Ru(3)	79.22(11)
N(1)-Ru(2)-C(12)	92.95(10)	O(5)-C(5)-Ru(1)	131.6(3)
C(5)-Ru(2)-C(12)	135.92(12)	Ru(2)-C(5)-Ru(1)	77.77(9)
C(3)-Ru(2)-C(11)	88.72(12)	Ru(3)-C(5)-Ru(1)	77.23(10)
C(4)-Ru(2)-C(11)	125.27(12)	O(6)-C(6)-Ru(3)	176.9(3)
N(1)-Ru(2)-C(11)	97.37(10)	O(7)-C(7)-Ru(3)	176.7(3)
C(5)-Ru(2)-C(11)	101.33(11)	O(8)-C(8)-Ru(3)	178.9(3)
C(12)-Ru(2)-C(11)	35.30(11)	C(10)-C(9)-Ru(1)	74.06(17)
C(3)-Ru(2)-Ru(3)	120.11(10)	C(9)-C(10)-C(11)	127.5(3)
C(4)-Ru(2)-Ru(3)	96.64(9)	C(9)-C(10)-Ru(1)	70.41(17)
N(1)-Ru(2)-Ru(3)	48.30(6)	C(11)-C(10)-Ru(1)	103.49(19)
C(5)-Ru(2)-Ru(3)	50.43(9)	C(12)-C(11)-C(10)	127.6(3)
C(12)-Ru(2)-Ru(3)	141.09(8)	C(12)-C(11)-Ru(2)	68.72(17)
C(11)-Ru(2)-Ru(3)	131.29(8)	C(10)-C(11)-Ru(2)	108.86(19)
C(3)-Ru(2)-Ru(1)	124.85(10)	C(11)-C(12)-Ru(2)	75.98(17)
C(4)-Ru(2)-Ru(1)	146.19(9)	C(18)-C(13)-C(14)	120.6(3)
N(1)-Ru(2)-Ru(1)	48.48(7)	C(18)-C(13)-S(1)	120.8(2)
C(5)-Ru(2)-Ru(1)	52.26(8)	C(14)-C(13)-S(1)	118.6(2)
C(12)-Ru(2)-Ru(1)	93.95(8)	C(15)-C(14)-C(13)	119.1(3)
C(11)-Ru(2)-Ru(1)	71.69(8)	C(14)-C(15)-C(16)	120.9(3)
Ru(3)-Ru(2)-Ru(1)	59.661(8)	C(17)-C(16)-C(15)	119.2(3)
C(6)-Ru(3)-C(7)	88.72(13)	C(17)-C(16)-C(19)	121.0(3)
C(6)-Ru(3)-C(8)	91.62(14)	C(15)-C(16)-C(19)	119.8(3)
C(7)-Ru(3)-C(8)	100.65(14)	C(16)-C(17)-C(18)	120.6(3)
C(6)-Ru(3)-N(1)	165.91(13)	C(13)-C(18)-C(17)	119.5(3)

APPENDIX IV Crystallographic characterisation of $[Os_3(\mu\text{-}H)(\mu\text{-}trans\text{-}\sigma,\eta^2\text{-}CH{=}CHBu^t)(\mu_3\text{-}NTs)(CO)_8]$ 27

Crystal data and structure refinement for 27

Empirical formula	$C_{21}H_{17}NO_{10}Os_3S$	
Formula weight	1046.02	
Temperature	293(2) K	
Wavelength	0.71073 Å	
Crystal system	Triclinic	
Space group	P-1	
Unit cell dimensions	a = 8.065(2) Å	α = 95.89(3)°
	b = 9.757(2) Å	β = 94.27(3)°
	c = 18.187(4) Å	γ = 97.60(3)°
Volume	1405.4(5) $Å^3$	
Z	2	
Density (calculated)	2.472 Mg/m^3	
Absorption coefficient	13.651 mm^{-1}	
F(000)	948	
Theta range for data collection	2.51 to 25.05°	
Index ranges	0<=h<=9, -11<=k<=11, -21<=l<=21	
Reflections collected	5289	
Independent reflections	4842 [R(int) = 0.0420]	
Refinement method	Full-matrix least-squares on F^2	
Data / restraints / parameters	4838 / 0 / 325	
Goodness-of-fit on F^2	1.037	
Final R indices [I>2sigma(I)]	R1 = 0.0862, wR2 = 0.2266	
R indices (all data)	R1 = 0.0929, wR2 = 0.2481	
Largest difference peak and hole	8.462 and -6.948 $e.A^3$	

Bond lengths (Å) and angles (°) for $[Os_3(\mu\text{-}H)(\mu\text{-}trans\text{-}\eta,\eta^2\text{-}CH{=}CHBu^t)(\mu_3\text{-}NTs)(CO)_8]$ 27

Os(1)-C(12)	1.86(2)	C(100)-C(101)	1.40(3)
Os(1)-C(11)	1.90(2)	C(100)-C(105)	1.41(3)
Os(1)-C(1)	2.16(2)	C(101)-C(102)	1.40(3)
Os(1)-N(1)	2.184(12)	C(102)-C(103)	1.41(3)
Os(1)-C(2)	2.333(14)	C(103)-C(104)	1.42(3)
Os(1)-Os(2)	2.7513(11)	C(103)-C(106)	1.48(3)
Os(1)-Os(3)	2.7859(12)	C(104)-C(105)	1.41(3)
Os(2)-C(21)	1.92(2)	C(1)-C(2)	1.47(2)
Os(2)-C(23)	1.99(2)	C(2)-C(3)	1.58(2)
Os(2)-C(22)	2.014(14)	C(3)-C(5)	1.50(3)
Os(2)-N(1)	2.147(14)	C(3)-C(4)	1.51(3)
Os(2)-C(1)	2.203(14)	C(3)-C(6)	1.60(3)
Os(2)-Os(3)	2.8417(12)	C(11)-O(11)	1.17(2)
Os(3)-C(32)	1.91(2)	C(12)-O(12)	1.20(3)
Os(3)-C(33)	1.92(2)	C(21)-O(21)	1.17(2)
Os(3)-C(31)	1.97(2)	C(22)-O(22)	1.13(2)
Os(3)-N(1)	2.117(13)	C(23)-O(23)	1.11(3)
N(1)-S(1)	1.640(13)	C(31)-O(31)	1.13(3)
S(1)-O(2)	1.456(13)	C(32)-O(32)	1.18(2)
S(1)-O(1)	1.456(14)	C(33)-O(33)	1.15(3)
S(1)-C(100)	1.77(2)		

C(12)-Os(1)-C(11)	87.7(9)	C(31)-Os(3)-Os(1)	113.3(5)
C(12)-Os(1)-C(1)	86.0(7)	N(1)-Os(3)-Os(1)	50.7(3)
C(11)-Os(1)-C(1)	131.3(8)	C(32)-Os(3)-Os(2)	102.5(6)
C(12)-Os(1)-N(1)	159.9(7)	C(33)-Os(3)-Os(2)	154.6(8)
C(11)-Os(1)-N(1)	111.3(7)	C(31)-Os(3)-Os(2)	107.2(6)
C(1)-Os(1)-N(1)	86.0(5)	N(1)-Os(3)-Os(2)	48.7(4)
C(12)-Os(1)-C(2)	101.1(7)	Os(1)-Os(3)-Os(2)	58.53(3)
C(11)-Os(1)-C(2)	97.1(7)	S(1)-N(1)-Os(3)	126.8(7)
C(1)-Os(1)-C(2)	37.8(6)	S(1)-N(1)-Os(2)	124.1(7)
N(1)-Os(1)-C(2)	83.6(6)	Os(3)-N(1)-Os(2)	83.6(5)
C(12)-Os(1)-Os(2)	111.5(6)	S(1)-N(1)-Os(1)	142.5(8)
C(11)-Os(1)-Os(2)	160.6(6)	Os(3)-N(1)-Os(1)	80.7(4)
C(1)-Os(1)-Os(2)	51.6(4)	Os(2)-N(1)-Os(1)	78.9(4)
N(1)-Os(1)-Os(2)	50.0(4)	O(2)-S(1)-O(1)	114.8(9)
C(2)-Os(1)-Os(2)	77.4(4)	O(2)-S(1)-N(1)	107.6(7)
C(12)-Os(1)-Os(3)	119.4(6)	O(1)-S(1)-N(1)	108.9(7)
C(11)-Os(1)-Os(3)	111.7(6)	O(2)-S(1)-C(100)	110.2(8)
C(1)-Os(1)-Os(3)	113.3(4)	O(1)-S(1)-C(100)	109.6(9)
N(1)-Os(1)-Os(3)	48.6(3)	N(1)-S(1)-C(100)	105.3(8)
C(2)-Os(1)-Os(3)	130.0(4)	C(101)-C(100)-C(105)	120(2)
Os(2)-Os(1)-Os(3)	61.75(3)	C(101)-C(100)-S(1)	120(2)
C(21)-Os(2)-C(23)	99.0(9)	C(105)-C(100)-S(1)	119.5(13)
C(21)-Os(2)-C(22)	93.5(7)	C(100)-C(101)-C(102)	121(2)
C(23)-Os(2)-C(22)	91.8(7)	C(103)-C(102)-C(101)	120(2)
C(21)-Os(2)-N(1)	153.1(7)	C(102)-C(103)-C(104)	118(2)
C(23)-Os(2)-N(1)	106.3(7)	C(102)-C(103)-C(106)	122(2)
C(22)-Os(2)-N(1)	94.7(6)	C(104)-C(103)-C(106)	120(2)
C(21)-Os(2)-C(1)	89.5(7)	C(105)-C(104)-C(103)	122(2)
C(23)-Os(2)-C(1)	80.5(7)	C(104)-C(105)-C(100)	118(2)
C(22)-Os(2)-C(1)	172.1(6)	C(2)-C(1)-Os(1)	77.5(9)
N(1)-Os(2)-C(1)	85.9(5)	C(2)-C(1)-Os(2)	119.8(11)
C(21)-Os(2)-Os(1)	106.9(5)	Os(1)-C(1)-Os(2)	78.2(5)

C(23)-Os(2)-Os(1)	122.5(5)	C(1)-C(2)-C(3)	122(2)
C(22)-Os(2)-Os(1)	135.1(5)	C(1)-C(2)-Os(1)	64.7(8)
N(1)-Os(2)-Os(1)	51.2(3)	C(3)-C(2)-Os(1)	124.9(12)
C(1)-Os(2)-Os(1)	50.2(4)	C(5)-C(3)-C(4)	112(2)
C(21)-Os(2)-Os(3)	110.3(7)	C(5)-C(3)-C(2)	106(2)
C(23)-Os(2)-Os(3)	148.6(6)	C(4)-C(3)-C(2)	115(2)
C(22)-Os(2)-Os(3)	75.9(5)	C(5)-C(3)-C(6)	110(2)
N(1)-Os(2)-Os(3)	47.8(3)	C(4)-C(3)-C(6)	111(2)
C(1)-Os(2)-Os(3)	109.9(4)	C(2)-C(3)-C(6)	102(2)
Os(1)-Os(2)-Os(3)	59.72(3)	O(11)-C(11)-Os(1)	178(2)
C(32)-Os(3)-C(33)	89.7(8)	O(12)-C(12)-Os(1)	173(2)
C(32)-Os(3)-C(31)	90.8(9)	O(21)-C(21)-Os(2)	179(2)
C(33)-Os(3)-C(31)	94.7(10)	O(22)-C(22)-Os(2)	169(2)
C(32)-Os(3)-N(1)	101.8(7)	O(23)-C(23)-Os(2)	178(2)
C(33)-Os(3)-N(1)	107.3(9)	O(31)-C(31)-Os(3)	175(2)
C(31)-Os(3)-N(1)	154.5(7)	O(32)-C(32)-Os(3)	175(2)
C(32)-Os(3)-Os(1)	152.3(7)	O(33)-C(33)-Os(3)	177(2)
C(33)-Os(3)-Os(1)	101.3(8)		

APPENDIX V Crystallographic characterisation of $[Os_3(\mu^4\text{-}cis\text{-}CHPh{=}CHCPh{=}CH_2)(\mu_3\text{-}S)(CO)_8]$ 36

Crystal data and structure refinement for 36

Empirical formula	$C_{24}H_{14}O_8Os_3S$	
Formula weight	1033.01	
Temperature	291(2) K	
Wavelength	0.71073 Å	
Crystal system	Triclinic	
Space group	P-1	
Unit cell dimensions	a = 9.406(2) Å	α = 91.58(3)°
	b = 10.615(2) Å	β = 108.82(3)°
	c = 13.885(3) Å	γ = 104.51(3)°
Volume	1261.4(5) $Å^3$	
Z	2	
Density (calculated)	2.720 Mg/m^3	
Absorption coefficient	15.201 mm^{-1}	
F(000)	932	
Crystal size	0.42 x 0.40 x 0.16 mm	
Theta range for data collection	2.65 to 25.05°	
Index ranges	-11<=h<=0, -12<=k<=12, -15<=l<=16	
Reflections collected	4713	
Independent reflections	4421 [R(int) = 0.0271]	
Absorption correction	Psi-scans	
Max. and min. transmission	0.975 and 0.275	
Refinement method	Full-matrix least-squares on F^2	
Data / restraints / parameters	4417 / 0 / 325	
Goodness-of-fit on F^2	1.060	
Final R indices [I>2sigma(I)]	R1 = 0.0501, wR2 = 0.1344	
R indices (all data)	R1 = 0.0564, wR2 = 0.1453	
Largest difference peak and hole	3.176 and -4.835 $e.Å^{-3}$	

Bond lengths (Å) and angles (°) for $[Os_3(\mu^4\text{-}cis\text{-}CHPh{=}CHCPh{=}CH_2)(\mu_3\text{-}S)(CO)_8]$

36

Os(1)-C(11)	1.924(13)	C(4)-C(101)	1.46(2)
Os(1)-C(12)	1.941(14)	C(101)-C(106)	1.41(2)
Os(1)-C(1)	2.214(13)	C(101)-C(102)	1.41(2)
Os(1)-C(2)	2.252(12)	C(102)-C(103)	1.42(2)
Os(1)-C(3)	2.252(12)	C(103)-C(104)	1.38(2)
Os(1)-C(4)	2.267(12)	C(104)-C(105)	1.41(2)
Os(1)-S(1)	2.374(3)	C(105)-C(106)	1.35(2)
Os(1)-Os(3)	2.8524(10)	C(111)-C(116)	1.37(2)
Os(1)-Os(2)	2.8696(12)	C(111)-C(112)	1.41(2)
Os(2)-C(21)	1.87(2)	C(112)-C(113)	1.33(3)
Os(2)-C(23)	1.929(14)	C(113)-C(114)	1.36(3)
Os(2)-C(22)	1.94(2)	C(114)-C(115)	1.37(3)
Os(2)-S(1)	2.366(3)	C(115)-C(116)	1.40(2)
Os(2)-Os(3)	2.7339(9)	C(11)-O(11)	1.13(2)
Os(3)-C(31)	1.868(14)	C(12)-O(12)	1.14(2)
Os(3)-C(33)	1.909(14)	C(21)-O(21)	1.17(2)
Os(3)-C(32)	1.915(12)	C(22)-O(22)	1.13(2)
Os(3)-S(1)	2.373(3)	C(23)-O(23)	1.13(2)
C(1)-C(2)	1.40(2)	C(31)-O(31)	1.15(2)
C(2)-C(3)	1.44(2)	C(32)-O(32)	1.14(2)
C(2)-C(111)	1.50(2)	C(33)-O(33)	1.16(2)
C(3)-C(4)	1.46(2)		

C(11)-Os(1)-C(12)	88.3(6)	C(33)-Os(3)-C(32)	99.4(6)
C(11)-Os(1)-C(1)	90.4(5)	C(31)-Os(3)-S(1)	102.3(5)
C(12)-Os(1)-C(1)	153.0(6)	C(33)-Os(3)-S(1)	153.0(4)
C(11)-Os(1)-C(2)	87.0(5)	C(32)-Os(3)-S(1)	103.4(4)
C(12)-Os(1)-C(2)	116.4(5)	C(31)-Os(3)-Os(2)	98.0(4)
C(1)-Os(1)-C(2)	36.6(5)	C(33)-Os(3)-Os(2)	100.5(4)
C(11)-Os(1)-C(3)	113.3(5)	C(32)-Os(3)-Os(2)	157.0(4)
C(12)-Os(1)-C(3)	90.3(5)	S(1)-Os(3)-Os(2)	54.64(8)
C(1)-Os(1)-C(3)	65.6(5)	C(31)-Os(3)-Os(1)	153.8(5)
C(2)-Os(1)-C(3)	37.2(5)	C(33)-Os(3)-Os(1)	108.5(4)
C(11)-Os(1)-C(4)	151.0(5)	C(32)-Os(3)-Os(1)	100.8(4)
C(12)-Os(1)-C(4)	92.6(5)	S(1)-Os(3)-Os(1)	53.09(8)
C(1)-Os(1)-C(4)	76.0(5)	Os(2)-Os(3)-Os(1)	61.78(3)
C(2)-Os(1)-C(4)	66.8(4)	Os(2)-S(1)-Os(3)	70.46(9)
C(3)-Os(1)-C(4)	37.8(5)	Os(2)-S(1)-Os(1)	74.51(10)
C(11)-Os(1)-S(1)	118.4(4)	Os(3)-S(1)-Os(1)	73.85(9)
C(12)-Os(1)-S(1)	115.0(4)	C(2)-C(1)-Os(1)	73.2(7)
C(1)-Os(1)-S(1)	89.2(4)	C(1)-C(2)-C(3)	116.9(12)
C(2)-Os(1)-S(1)	122.6(4)	C(1)-C(2)-C(111)	122.9(12)
C(3)-Os(1)-S(1)	122.1(4)	C(3)-C(2)-C(111)	120.2(13)
C(4)-Os(1)-S(1)	87.3(3)	C(1)-C(2)-Os(1)	70.2(7)
C(11)-Os(1)-Os(3)	66.3(4)	C(3)-C(2)-Os(1)	71.4(6)
C(12)-Os(1)-Os(3)	105.2(4)	C(111)-C(2)-Os(1)	126.5(9)
C(1)-Os(1)-Os(3)	98.9(4)	C(2)-C(3)-C(4)	118.0(12)
C(2)-Os(1)-Os(3)	129.6(3)	C(2)-C(3)-Os(1)	71.4(7)
C(3)-Os(1)-Os(3)	164.4(3)	C(4)-C(3)-Os(1)	71.6(7)
C(4)-Os(1)-Os(3)	140.3(3)	C(101)-C(4)-C(3)	121.4(12)
S(1)-Os(1)-Os(3)	53.06(8)	C(101)-C(4)-Os(1)	123.2(8)
C(11)-Os(1)-Os(2)	103.5(4)	C(3)-C(4)-Os(1)	70.5(7)
C(12)-Os(1)-Os(2)	64.4(4)	C(106)-C(101)-C(102)	116.9(13)
C(1)-Os(1)-Os(2)	141.6(4)	C(106)-C(101)-C(4)	125.7(13)

C(2)-Os(1)-Os(2)	169.5(3)	C(102)-C(101)-C(4)	117.4(13)
C(3)-Os(1)-Os(2)	134.6(3)	C(101)-C(102)-C(103)	120.8(14)
C(4)-Os(1)-Os(2)	102.9(3)	C(104)-C(103)-C(102)	119.7(14)
S(1)-Os(1)-Os(2)	52.61(8)	C(103)-C(104)-C(105)	119(2)
Os(3)-Os(1)-Os(2)	57.08(3)	C(106)-C(105)-C(104)	121(2)
C(21)-Os(2)-C(23)	93.6(6)	C(105)-C(106)-C(101)	122(2)
C(21)-Os(2)-C(22)	92.0(7)	C(116)-C(111)-C(112)	117(2)
C(23)-Os(2)-C(22)	98.1(6)	C(116)-C(111)-C(2)	124.1(14)
C(21)-Os(2)-S(1)	95.7(5)	C(112)-C(111)-C(2)	119.3(14)
C(23)-Os(2)-S(1)	110.2(4)	C(113)-C(112)-C(111)	121(2)
C(22)-Os(2)-S(1)	150.1(4)	C(112)-C(113)-C(114)	123(2)
C(21)-Os(2)-Os(3)	95.2(4)	C(113)-C(114)-C(115)	119(2)
C(23)-Os(2)-Os(3)	163.4(4)	C(114)-C(115)-C(116)	119(2)
C(22)-Os(2)-Os(3)	95.6(4)	C(111)-C(116)-C(115)	122(2)
S(1)-Os(2)-Os(3)	54.90(8)	O(11)-C(11)-Os(1)	166.0(12)
C(21)-Os(2)-Os(1)	147.4(5)	O(12)-C(12)-Os(1)	164.4(12)
C(23)-Os(2)-Os(1)	104.9(4)	O(21)-C(21)-Os(2)	175(2)
C(22)-Os(2)-Os(1)	111.3(4)	O(22)-C(22)-Os(2)	175(2)
S(1)-Os(2)-Os(1)	52.88(8)	O(23)-C(23)-Os(2)	172.3(13)
Os(3)-Os(2)-Os(1)	61.14(2)	O(31)-C(31)-Os(3)	179(2)
C(31)-Os(3)-C(33)	90.7(6)	O(32)-C(32)-Os(3)	178.8(14)
C(31)-Os(3)-C(32)	93.2(6)	O(33)-C(33)-Os(3)	178.2(12)

APPENDIX VI Crystallographic characterisation of $[Ru_3(CO)_{12}\{Mo(N\text{-}2,6\text{-}Me_2C_6H_3)_2\}]$ 49

Crystal data and structure refinement for 49

Empirical formula	$C_{28}H_{18}MoN_2O_{12}Ru_3$	
Formula weight	973.59	
Temperature	293(2) K	
Wavelength	0.71073 Å	
Crystal system	Monoclinic	
Space group	$P2_1/c$	
Unit cell dimensions	a = 19.409(4) Å	α = 90°
	b = 9.887(2) Å	β = 109.98(3)°
	c = 17.947(4) Å	γ = 90°
Volume	3236.7(11) $Å^3$	
Z	4	
Density (calculated)	1.998 Mg/m^3	
Absorption coefficient	1.814 mm^{-1}	
F(000)	1880	
Theta range for data collection	2.23 to 29.20°	
Index ranges	-26<=h<=12, -13<=k<=13, -23<=l<=24	
Reflections collected	22977	
Independent reflections	8673 [R(int) = 0.0199]	
Absorption correction	None	
Refinement method	Full-matrix least-squares on F^2	
Data / restraints / parameters	8668 / 0 / 487	
Goodness-of-fit on F^2	1.020	
Final R indices [I>2sigma(I)]	R1 = 0.0192, wR2 = 0.0441	
R indices (all data)	R1 = 0.0244, wR2 = 0.0465	
Largest difference peak and hole	0.556 and –0.768 $e.Å^{-3}$	

Bond lengths (Å) and angles (°) for $[Ru_3(CO)_{12}\{Mo(N\text{-}2,6\text{-}Me_2C_6H_3)_2\}]$ 49

Ru(1)-C(1)	1.921(2)	O(5)-C(5)	1.130(3)
Ru(1)-C(2)	1.925(2)	O(6)-C(6)	1.127(2)
Ru(1)-C(3)	1.941(2)	O(7)-C(7)	1.134(2)
Ru(1)-C(4)	1.973(2)	O(8)-C(8)	1.136(2)
Ru(1)-Ru(2)	2.9315(5)	O(9)-C(9)	1.127(2)
Ru(1)-Ru(3)	2.9556(5)	O(10)-C(10)	1.134(2)
Ru(1)-Mo(1)	3.1094(8)	O(11)-C(11)	1.131(2)
Ru(2)-C(6)	1.907(2)	O(12)-C(12)	1.134(2)
Ru(2)-C(7)	1.948(2)	C(20)-C(25)	1.412(3)
Ru(2)-C(8)	1.956(2)	C(20)-C(21)	1.424(2)
Ru(2)-C(5)	1.979(2)	C(21)-C(22)	1.386(3)
Ru(2)-Mo(1)	2.7165(5)	C(21)-C(26)	1.496(3)
Ru(3)-C(10)	1.898(2)	C(22)-C(23)	1.380(3)
Ru(3)-C(12)	1.951(2)	C(23)-C(24)	1.390(3)
Ru(3)-C(11)	1.970(2)	C(24)-C(25)	1.392(3)
Ru(3)-C(9)	1.972(2)	C(25)-C(27)	1.510(3)
Ru(3)-Mo(1)	2.7025(4)	C(30)-C(31)	1.409(3)
Mo(1)-N(2)	1.761(2)	C(30)-C(35)	1.412(2)
Mo(1)-N(1)	1.766(2)	C(31)-C(32)	1.393(3)
N(1)-C(20)	1.388(2)	C(31)-C(36)	1.505(3)
N(2)-C(30)	1.394(2)	C(32)-C(33)	1.386(3)
O(1)-C(1)	1.134(2)	C(33)-C(34)	1.386(3)
O(2)-C(2)	1.130(2)	C(34)-C(35)	1.396(3)
O(3)-C(3)	1.139(2)	C(35)-C(37)	1.499(3)
O(4)-C(4)	1.133(2)		

C(1)-Ru(1)-C(2)	94.31(8)	Mo(1)-Ru(3)-Ru(1)	66.50(2)
C(1)-Ru(1)-C(3)	89.57(8)	N(2)-Mo(1)-N(1)	112.39(7)
C(2)-Ru(1)-C(3)	95.78(8)	N(2)-Mo(1)-Ru(3)	106.09(5)
C(1)-Ru(1)-C(4)	91.43(7)	N(1)-Mo(1)-Ru(3)	105.99(5)
C(2)-Ru(1)-C(4)	93.97(7)	N(2)-Mo(1)-Ru(2)	112.90(5)
C(3)-Ru(1)-C(4)	170.09(7)	N(1)-Mo(1)-Ru(2)	103.51(5)
C(1)-Ru(1)-Ru(2)	86.84(6)	Ru(3)-Mo(1)-Ru(2)	115.88(2)
C(2)-Ru(1)-Ru(2)	171.30(5)	N(2)-Mo(1)-Ru(1)	107.88(6)
C(3)-Ru(1)-Ru(2)	75.59(6)	N(1)-Mo(1)-Ru(1)	139.72(5)
C(4)-Ru(1)-Ru(2)	94.62(6)	Ru(3)-Mo(1)-Ru(1)	60.656(13)
C(1)-Ru(1)-Ru(3)	170.59(5)	Ru(2)-Mo(1)-Ru(1)	59.973(14)
C(2)-Ru(1)-Ru(3)	76.53(6)	C(20)-N(1)-Mo(1)	163.60(13)
C(3)-Ru(1)-Ru(3)	93.45(5)	C(30)-N(2)-Mo(1)	162.26(13)
C(4)-Ru(1)-Ru(3)	87.13(5)	O(1)-C(1)-Ru(1)	174.8(2)
Ru(2)-Ru(1)-Ru(3)	102.54(2)	O(2)-C(2)-Ru(1)	173.3(2)
C(1)-Ru(1)-Mo(1)	135.54(5)	O(3)-C(3)-Ru(1)	173.3(2)
C(2)-Ru(1)-Mo(1)	128.18(5)	O(4)-C(4)-Ru(1)	172.7(2)
C(3)-Ru(1)-Mo(1)	97.37(6)	O(5)-C(5)-Ru(2)	177.6(2)
C(4)-Ru(1)-Mo(1)	75.12(6)	O(6)-C(6)-Ru(2)	179.0(2)
Ru(2)-Ru(1)-Mo(1)	53.348(12)	O(7)-C(7)-Ru(2)	172.7(2)
Ru(3)-Ru(1)-Mo(1)	52.848(6)	O(8)-C(8)-Ru(2)	175.3(2)
C(6)-Ru(2)-C(7)	92.30(8)	O(9)-C(9)-Ru(3)	176.4(2)
C(6)-Ru(2)-C(8)	91.10(8)	O(10)-C(10)-Ru(3)	179.1(2)
C(7)-Ru(2)-C(8)	173.44(7)	O(11)-C(11)-Ru(3)	174.5(2)
C(6)-Ru(2)-C(5)	101.71(9)	O(12)-C(12)-Ru(3)	174.9(2)
C(7)-Ru(2)-C(5)	91.05(8)	N(1)-C(20)-C(25)	120.3(2)
C(8)-Ru(2)-C(5)	93.75(8)	N(1)-C(20)-C(21)	119.4(2)
C(6)-Ru(2)-Mo(1)	92.15(6)	C(25)-C(20)-C(21)	120.3(2)
C(7)-Ru(2)-Mo(1)	96.00(5)	C(22)-C(21)-C(20)	118.4(2)
C(8)-Ru(2)-Mo(1)	78.26(5)	C(22)-C(21)-C(26)	120.7(2)
C(5)-Ru(2)-Mo(1)	164.20(6)	C(20)-C(21)-C(26)	120.9(2)

C(6)-Ru(2)-Ru(1)	156.14(6)	C(23)-C(22)-C(21)	121.6(2)
C(7)-Ru(2)-Ru(1)	79.75(5)	C(22)-C(23)-C(24)	119.8(2)
C(8)-Ru(2)-Ru(1)	94.93(6)	C(23)-C(24)-C(25)	121.1(2)
C(5)-Ru(2)-Ru(1)	100.91(6)	C(24)-C(25)-C(20)	118.7(2)
Mo(1)-Ru(2)-Ru(1)	66.68(2)	C(24)-C(25)-C(27)	119.7(2)
C(10)-Ru(3)-C(12)	91.15(8)	C(20)-C(25)-C(27)	121.6(2)
C(10)-Ru(3)-C(11)	91.86(8)	N(2)-C(30)-C(31)	120.8(2)
C(12)-Ru(3)-C(11)	171.83(7)	N(2)-C(30)-C(35)	118.4(2)
C(10)-Ru(3)-C(9)	101.26(8)	C(31)-C(30)-C(35)	120.9(2)
C(12)-Ru(3)-C(9)	93.38(8)	C(32)-C(31)-C(30)	118.3(2)
C(11)-Ru(3)-C(9)	93.48(8)	C(32)-C(31)-C(36)	120.1(2)
C(10)-Ru(3)-Mo(1)	88.99(6)	C(30)-C(31)-C(36)	121.6(2)
C(12)-Ru(3)-Mo(1)	88.23(6)	C(33)-C(32)-C(31)	121.3(2)
C(11)-Ru(3)-Mo(1)	84.23(6)	C(34)-C(33)-C(32)	119.9(2)
C(9)-Ru(3)-Mo(1)	169.58(6)	C(33)-C(34)-C(35)	121.0(2)
C(10)-Ru(3)-Ru(1)	155.17(6)	C(34)-C(35)-C(30)	118.4(2)
C(12)-Ru(3)-Ru(1)	84.46(5)	C(34)-C(35)-C(37)	121.0(2)
C(11)-Ru(3)-Ru(1)	89.64(6)	C(30)-C(35)-C(37)	120.6(2)
C(9)-Ru(3)-Ru(1)	103.39(6)		

REFERENCES

1. F. A. Cotton, *J. Chem. Educ.*, 1983, 60, 713, *and references therein.*
2. F. A. Cotton in *Metal Clusters in Chemistry,* eds., P. Braunstein, L. A. Oro and P. R. Raithby, Vol. 1, Wiley-VCH, Weinheim, Germany, 1999, *and references therein.*
3. F. A. Cotton, *Inorg. Chem.*, 1964, **3**, 1217.
4. F. A. Cotton, *Quart. Rev.*, 1966, **20**, 389.
5. L. J. Farrugia, *J. Chem. Soc., Dalton Trans.*, 1997, 1783.
6. C. H. Wei and L. F. Dahl, *J. Am. Chem. Soc.*, 1966, **88**, 1821.
7. C. H. Wei and L. F. Dahl, *J. Am. Chem. Soc.*, 1969, **91**, 1351.
8. J. Lewis, in *Metal Clusters in Chemistry,* eds., P. Braunstein, L. A. Oro and P. R. Raithby, Vol. 3, Wiley-VCH, Weinheim, Germany, 1999, *and references therein.*
9. B. H. S. Thimmappa, *Coord. Chem.Rev.*, 1995, **143**, 1, *and references therein.*
10. D. M. P. Mingos and A. S. May, in *The chemistry of Metal Cluster Complexes*; eds., D. F. Shriver, H. D. Kaesz and R. D. Adams, VCH Publishers Inc., New York, 1990.
11. E. R. Corey, L. F. Dahl and W. Beck, *J. Am. Chem. Soc.*, 1963, **85**, 1202.
12. V. G. Albano, P. L. Bellon and M. Sansoni, *J. Chem. Soc. (A)*, 1971, 678.
13. G. Ciani, G. D'Alfonso, M. Freni, P. Romiti and A. Sironi, *J. Organomet. Chem.*, 1983, **244**, C27.
14. R. E. McCarley, in *Early Transition Metal Clusters with π-donor ligands,* ed., M. H. Chisholm, VCH Publishers Inc., New York, 1995, *and references therein.*

15. M. H. Chisholm, in *Early Transition Metal Clusters with π-donor ligands,* ed., M. H. Chisholm, VCH Publishers Inc., New York, 1995, *and references therein.*

16. B. F. G. Johnson and A. Bott, *J. Chem. Soc., Dalton Trans.,* 1990, 2437.

17. D. Braga, F. Grepioni, L. J. Farrugia and B. F. G. Johnson, *J. Chem. Soc., Dalton Trans.,* 1994, 2911.

18. L. Manojlović -Muir, K. W. Muir, B. R. Lloyd and R. J. Puddephatt *J. Chem. Soc. Chem. Commun.*, 1985, 536.

19. A. G. Orpen, A. V. Rivera, E. G. Bryan, D. Pippard and G. M. Sheldrick, *J. Chem. Soc. Chem. Commun.*, 1978, 723.

20. C. A. Ghilardi, S. Midollini and L. Sacconi, *Inorg. Chim. Acta,* 1978, **31**, L431.

21. H. Werner, W. Bertleff and U. Schubert, *Inorg. Chim. Acta,* 1980, 43, 199.

22. R. Havlin and G. R. Knox, *J. Organomet. Chem.,* 1965, **4**, 247.

23. W.-Y. Yeh, C. L. Stern and D. F. Shriver *Inorg. Chem.,* 1997, **36**, 4408.

24. W. T. Wong, *J. Chem. Soc., Dalton Trans.,* 1998, 1253, *and references therein.*

25. A. J. Deeming, in *Trinuclear Clusters of Ruthenium and Osmium, Comprehensive Organometallic Chemistry II,* Eds., E. W. Abel, F. G. A. Stone and G. Wilkinson, Vol. 7, Pergamon Press, Elsevier Science, Oxford, 1995, *and references therein.*

26. A. J. Deeming, *Adv. Organomet. Chem.,* 1986, **26**, 1, *and references therein.*

27. M. G. Richmond, *Coord. Chem. Rev.,* 1997, **160**, 237, *and references therein.*

28. G. Süss-Fink, I. Godefroy, V. Ferrand, A. Neels, H. Stœckli-Evans, S. Kahlal, J.-Y. Saillard and M. T. Garland, *J. Organomet. Chem.,* 1999, **579**, 285.

29. T. Beringhelli, G. D'Alfonso, M. Panigati, F. Porta, P. Mercandelli, M. Moret and A. Sironi, *J. Am. Chem. Soc.,* 1999, **121**, 2307.

30. Ch. Elschenbroich and A. Salzer, *Organometallics A Concise Introduction*, VCH, Weinheim, 1992.

31. K. K.-H. Lee and W.-T. Wong, *J. Organomet. Chem.*, 1999, **575**, 200.

32. A. R. Mannig, A. J. Palmer, J. McAdam, B. H. Robinson and J. Simpson, *J. Chem. Soc. Chem. Commun.*, 1998, 1577.

33. J. A. Krause Bauer, J.-H. Chung, E. P. Boyd, J. Liu, D. S. Strickland, H.-J. Kneuper, J. R. Shapley and S. G. Shore, *Inorg. Chem.*, 1996, **35**, 1405.

34. Y.-Y. Choi, W.-Y. Wong and W.-T. Wong, *J. Organomet. Chem.*, 1996, **518**, 227.

35. C. A. Collins, I. D. Salter, V. Šik, S. A. Williams and T. Adatia, *J. Chem. Soc., Dalton Trans.*, 1998, 1107.

36. W. G. Feighery, H. Yao, A. F. Hollenkamp, R. D. Allendoerfer and J. B. Keister, *Organometallics*, 1998, **17**, 872.

37. M. Akita, S. Sakurai and Y. Moro-oka, *J. Chem. Soc. Chem. Commun.*, 1999, 101.

38. J. H. Chung, E. P. Boyd, J. Liu and S. G. Shore, *Inorg. Chem.*, 1997, **36**, 4778.

39. M. Laing, P. Sommerville, Z. Dawoodi, M. J. Mays, *J. Chem. Soc. Chem. Commun.*, 1978, 1035.

40. Z. Dawoodi and M. J. Mays, *J. Chem. Soc., Dalton Trans.*, 1984, 1931.

41. R.-C. Lin, Y. Chi, S.-M. Peng and G.-H. Lee, *J. Chem. Soc., Dalton Trans.*, 1993, 227.

42. M. I. Bruce, M. P. Cifuentes and M. G. Humphrey, *Polyhedron*, 1991, **10**, 277, *and references therein.*

43. C. E. Housecroft, in *Inorganometallic Chemistry*, Ed., T. P. Fehlner, Plenum Press, New York, 1992, *and references therein.*

44. K. H. Whitmire, *Adv. Organomet. Chem.*, 1998, **42**, 1, *and references therein.*

45. K. K. H. Lee and W.-T. Wong, *J. Chem. Soc., Dalton Trans.*, 1996, 3911.

46. C.-W. Pin, Y. Chi, C. Chung, A. J. Carty, S.-M. Peng and G.-H. Lee, *Organometallics*, 1998, **17**, 4146.

47. C. Tejel, Y-M. Shi, M. A. Ciriano, A. J. Edwards, F. J. Lahoz, J. Modrego and L. A. Oro, *J. Am. Chem. Soc.*, 1997, **119**, 6678.

48. W.-Y. Yeh, C. Stern and D. F. Shriver, *Inorg. Chem.*, 1996, **35**, 7857.

49. K. K. H. Lee and W.-T. Wong, *J. Chem. Soc., Dalton Trans.*, 1996, 1707.

50. K. K. H. Lee and W.-T. Wong, *Inorg. Chem.*, 1996, **35**, 5393.

51. E. N.-M. Ho and W.-T. Wong, *J. Chem. Soc., Dalton Trans.*, 1998, 513.

52. E. N.-M. Ho and W.-T. Wong, *J. Chem. Soc., Dalton Trans.*, 1998, 4215.

53. G. Süss-Fink, G. Rheinwald, H. Stœckli-Evans, C. Bolm and D. Kaufmann, *Inorg. Chem.*, 1996, **35**, 3081.

54. V. Ferrand, K. Merzweiler, G. Rheinwald, H. Stœckli-Evans and G. Süss-Fink, *J. Organomet. Chem.*, 1997, **549**, 263.

55. V. Ferrand, C. Gambs, N. Derrien, C. Bolm, H. Stœckli-Evans and G. Süss-Fink, *J. Organomet. Chem.*, 1997, **549**, 275.

56. C. Bois, J. A. Cabeza, R. J. Franco, V. Riera and E. Saborit, *J. Organomet. Chem.*, 1998, **564**, 201.

57. W. Wang, J. F. Corrigan, G. D. Enright, N. J. Taylor and A. J. Carty, *Organometallics*, 1998, **17**, 427.

58. H.-C. Böttcher, M. Graf and K. Merzweiler, *J. Organomet. Chem.*, 1997, **531**, 107.

59. F. A. Ajulu, F. Mathey and J. F. Nixon, *J. Organomet. Chem.*, 1997, **543**, 245.

60. W. Wang, G. D. Enright, J. Driedigen and A. J. Carty, *J. Organomet. Chem.*, 1997, **541**, 461.

61. H.-G. Ang, K.-W. Ang, S.-G. Ang and A. L. Rheingold, *J. Chem. Soc., Dalton Trans.*, 1996, 3131.

62. M. Faure, M. Jahncke, A. Neels, H. Stœckli-Evans and G. Süss-Fink, *Polyhedron*, 1999, **18**, 2679.

63. T. M. Räsänen, S. Jääskeläinen and T. A. Pakkanen, *J. Organomet. Chem.*, 1998, **554**, 129.

64. J. W. van Hal and K. H. Whitmire, *Organometallics*, 1998, **17**, 5197.

65. D. Cauzzi, C. Graiff, G. Predieri, A. Tiripicchio and C. Vignali, *J. Chem. Soc., Dalton Trans.*, 1999, 237.

66. J. R. Shapley, D. S. Strickland, G. M. St. George, M. R. Churchill and C. Bueno, *Organometallics*, 1983, **2**, 185.

67. R. W. Eveland, C. C. Raymond and D. F. Shriver, *Organometallics*, 1999, **18**, 534.

68. T. Chihara, T. Tase, H. Ogawa and Y. Wakatsuki, *J. Chem. Soc. Chem. Commun.*, 1999, 279.

69. R. W. Eveland, C. C. Raymond, T. E. Albrecht-Schmitt and D. F. Shriver, *Inorg. Chem.*, 1999, **38**, 1282.

70. M. I. Bruce, B. W. Skelton, A. H. White and N. N. Zaitseva, *J. Chem. Soc., Dalton Trans.*, 1999, 13.

71. A. J. Deeming and M. Underhill, *J. Chem. Soc., Dalton Trans.*, 1974, 1415.

72. H.-J. Jeon, N. Rokopik, C. Stern, D. F. Shriver, *Inorg. Chim. Acta*, 1999, **286**, 142.

73. M. I. Bruce, P. A. Humphrey, B. W. Skelton, A. H. White, K. Costuas and J.-F. Halet, *J. Chem. Soc., Dalton Trans.*, 1999, 479.

74. L. A. Hoferkamp, G. Rheinwald, H. Stœckli-Evans and G. Süss-Fink, *Organometallics*, 1996, **15**, 704.

75. A. Inagaki, Y. Takaya, T. Takemori and H. Suzaki, *J. Am. Chem. Soc.*, 1997, **119**, 625.

76. H.-F. Hsu and J. R. Shapley, *J. Am. Chem. Soc.*, 1996, **118**, 9192.

77. R. J. Puddephatt, in *Metal Clusters in Chemistry*, Eds. P. Braunstein, L. A. Oro and P. R. Raithby, Vol. 2, Wiley-VCH, Weinheim, 1999, *and references therein.*

78. W. L. Gladfelter and K. J. Roesselet, in *The chemistry of Metal Cluster Complexes*; eds., D. F. Shriver, H. D. Kaesz and R. D. Adams, VCH Publishers Inc., New York, 1990.

79. E. L. Muetterties, *Bull. Soc. Chim. Belg.*, 1975, **84**, 959.

80. E. L. Muetterties, *Bull. Soc. Chim. Belg.*, 1976, **85**, 451.

81. J. A. Cabeza, in *Metal Clusters in Chemistry*, Eds. P. Braunstein, L. A. Oro and P. R. Raithby, Vol. 2, Wiley-VCH, Weinheim, 1999, *and references therein.*

82. J. A. Cabeza, I. del Río, J. M. Fernández-Colinas and V. Riera, *Organometallics*, 1996, **15**, 449.

83. S. H. Han and G. L. Geoffroy, *Polyhedron*, 1988, **7**, 2331.

84. W. A. Nugent and B. L. Haymore, *Coord. Chem. Rev.*, 1980, **31**, 123.

85. S. Cenini and G. La Monica, *Inorg. Chem., Chim. Acta*, 1976, **18**, 279.

86. M. L. Blohm and W. L. Gladfelter, *Organometallics*, 1986, **5**, 1049.

87. M. Pizotti, S. Cenini, C. Crotti and F. Demartin, *J. Organomet. Chem.*, 1989, **375**, 123.

88. S.-H. Han, G. L. Geoffroy and A. L. Rheingold, *Organometallics,* 1986, **5**, 2561.

89. S.-H. Han, G. L. Geoffroy and A. L. Rheingold, *Organometallics,* 1987, **6**, 2380.

90. G. D. Williams, G. L. Geoffroy, R. R. Whittle and A. L. Rheingold *J. Am. Chem. Soc.*, 1985, **107**, 729.

91. G. D. Williams, R. R. Whittle, G. L. Geoffroy and A. L. Rheingold, *J. Am. Chem. Soc.*, 1987, **109**, 3936.

92. F. Ragaini, S. Cenini and F. Demartin, *Organometallics,* 1994, **13**, 1178.

93. J. D. Gargulak and W. L. Gladfelter, *J. Am. Chem. Soc.*, 1994, **116**, 3792.

94. E. Sappa and L. Milone, *J. Organomet. Chem.*, 1973, **61**, 383.

95. C. Choo Yin and A. J. Deeming, *J. Chem. Soc., Dalton Trans.*, 1974, 1013.

96. S. S. Alam and A. J. Deeming, *Unpublished Results.*

97. J. A. Smieja and W. L. Gladfelter, *Inorg. Chem.*, 1986, **25**, 2667.

98. J. P. Mahy, P. Battioni and D. Mansuy, *J. Chem. Soc., Perkin Trans. 2,* 1988, 1517.

99. D. A. Evans, M. M. Faul and M. T. Bilodeau, *J. Am. Chem. Soc.*, 1994, **116**, 2742.

100. Z. Li, W. Quan and E. N. Jacobsen, *J. Am. Chem. Soc.*, 1995, **117**, 5889.

101. W.-H. Leung, M.-C. Wu, J. L. C. Chim and W.-T. Wong, *Polyhedron,* 1998, **17**, 457.

102. S.-M. Au, W.-H. Fung, M.-C. Cheng, C.-M. Che and S.-M. Peng, *J. Chem. Soc. Chem. Commun.*, 1997, 1655.

103. M. R. Churchill, F. J. Hollander, J. R. Shapley and J. B. Keister, *Inorg. Chem.*, 1980, **19**, 1272.

104. H. D. Kaesz, S. A. R. Knox, J. W. Koepke and R. B. Saillant, *Chem. Commun.*, 1971, 477.

105. S. R. Drake, B. F. G. Johnson and J. Lewis, *J. Chem. Soc., Dalton Trans.*, 1989, 243.

106. S. Bhaduri, K. S. Gopalkrishnan, W. Clegg, P. G. Jones, G. M. Sheldrick and D. Stalke, J. Chem. Soc., Dalton Trans., 1984, 1765.

107. S. Bhaduri, H. Khwaja and P. G. Jones, *J. Chem. Soc. Chem. Commun.*, 1988, 194.

108. M. L. H. Green, G. Hogarth, P. C. Konidaris and P. Mountford, *J. Chem. Soc.*, Dalton Trans., 1990, 3781.

109. A. J. Deeming, S. Hasso and M. Underhill, *J. Organomet. Chem.*, 1974, **80**, C53.

110. A. J. Deeming, S. Hasso and M. Underhill, *J. Chem. Soc., Dalton Trans.*, 1975, 1614.

111. S. C. Brown and J. Evans, *J. Chem. Soc., Dalton Trans.*, 1982, 1049.

112. D. H. Hamilton and J. R. Shapley, *Organometallics*, 1998, **17**, 3087.

113. M. Koike, D. H. Hamilton, S. R. Wilson and J. R. Shapley, *Organometallics*, 1996, **15**, 4930.

114. H. Chen, B. F. G. Johnson, J. Lewis and P. R. Raithby, *J. Organomet. Chem.*, 1989, **376**, C7.

115. K. Tani, K. Ueda, K. Arimitsu, T. Yamagata, Y. Kataoka, *J. Organomet. Chem.*, 1998, **560**, 253.

116. S. A. Rao and M. Periasamy, *J. Chem. Soc. Chem. Commun.*, 1987, 495.

117. I. Ryu, N. Kusumoto, A. Ogawa, N. Kambe and N. Sonoda, *Organometallics*, 1989, **8**, 2279.

118. N. Satyanarayana and M. Periasamy, *Tetrahedron Lett.*, 1986, **27**, 6253.

119. M. I. Bruce, G. A. Koutsantonis, E. R. T. Tiekink and B. K. Nicholson, *J. Organomet. Chem.*, 1991, **420**, 271.

120. P. M. Maitlis, H. C. Long, R. Quyoum, M. L. Turner and Z.-Q. Wang, *J. Chem. Soc. Chem. Commun.*, 1996, 1.

121. O. S. Mills and G. Robinson, *Acta Cystallogr.*, 1963, **16**, 758.

122. G. Erker, J. Wicher, K. Engel, F. Rosenfeldt, W. Dietrich, C. Kruger, *J. Am. Chem. Soc.*, 1980, **102**, 6346.

123. R. Benn, H. Grodney, G. Erker, R. Aul and R. Nolte, *Organometallics,* 1990, **9**, 2493.

124. C. G. Pierpoint, *Inorg. Chem.*, 1978, **17**, 1976.

125. M. Tachikawa, J. R. Shapley, R. C. Haltiwanger and C. G. Pierpoint, *J. Am. Chem. Soc.*, 1976, **98**, 4651.

126. T. Murahashi, N. Kanehisa, Y. Kai, T. Otani and H. Kurosawam, *J. Chem. Soc. Chem. Commun.*, 1996, 825.

127. V. C. Adam, J. A. J. Jarvis, B. T. Kilbourn and P. G. Owston, *Chem. Commun.*, 1971, 467.

128. A. Scholz, A. Smola, J. Scholz, J. Loebel, H. Schumann and K.-H. Thiele, *Angew. Chem. Int. Ed. Engl.*, 1991, **30**, 435.

129. J. T. Barry, J. C. Bollinger, M. H. Chisholm, K. C. Glasgow, J. C. Huffman, E. A. Lucas, E. B. Lubkovsky and W. E. Streib, *Organometallics,* 1999, **18**, 2300.

130. Y. Kaneko, T. Suzuki and K. Isobe, *Organometallics,* 1998, **17**, 996.

131. J. A. King, Jr and K. P. C. Vollhardt, *Organometallics,* 1983, **2**, 686.

132. R. D. Adams, *Polyhedron*, 1985, **4**, 2003, *and references therein.*

133. A. J. Deeming, R. Ettorre, B. F. G. Johnson and J. Lewis, *J. Chem. Soc. (A)*, 1971, 1797.

134. R. D. Adams and D. A. Katahira, *Organometallics*, 1982, **1**, 53.

135. A. J. Deeming and M. Underhill, *J. Organomet. Chem.*, 1972, **42**, C60.

136. B. F. G. Johnson, J. Lewis, D. Pippard, P. R. Raithby, G. M. Sheldrick and K. D. Rouse, *J. Chem. Soc., Dalton Trans.*, 1979, 616.

137. B. F. G. Johnson, J. Lewis, P. G. Lodge and P. R. Raithby, *J. Chem. Soc. Chem. Commun.*, 1979, 719.

138. R. D. Adams, I. T. Horváth, B. E. Segmüller, L.-W. Yang, *Organometallics*, 1983, **2**, 144.

139. E. Sappa, O. Gambino and G. Cetini, *J. Organomet. Chem.*, 1972, **35**, 1972.

140. R. D. Adams, I. T. Horváth, B. E. Segmüller, L.-W. Yang, *Organometallics*, 1983, **2**, 1301.

141. R. D. Adams, I. T. Horváth, H.-S. Kim, *Organometallics*, 1984, **3**, 548.

142. P. V. Broadhurst, B. F. G. Johnson, J. Lewis and P. R. Raithby, *J. Organomet. Chem.*, 1980, **194**, C35.

143. R. D. Adams, J. E. Babin and M. Tasi, *Inorg. Chem.*, 1986, **25**, 4514.

144. R. D. Adams, D. Männig and B. E. Segmüller, *Organometallics*, 1983, **2**, 149.

145. R. D. Adams, J. E. Babin M. Tasi, T. A. Wolfe, *Organometallics*, 1987, **6**, 2228.

146. G. Lavigne, in *The Chemistry of Metal Cluster Complexes*, eds., D. F. Shriver, H. D. Kaesz and R. D. Adams, VCH, New York, 1990, *and references therein.*

147. R. D. Adams and S. Wang, *Organometallics*, 1985, **4**, 1902.

148. R. D. Adams and S. Wang, *J. Am. Chem. Soc.*, 1987, **109**, 924.

149. R. D. Adams and S. Wang, *Organometallics*, 1987, **6**, 739.

150. R. D. Adams, J. E. Babin and M. Tasi, *Organometallics*, 1988, 7, 219.

151. R. D. Adams, J. E. Babin and M. Tasi, *Organometallics,* 1987, **6**, 2247.

152. P. V. Broadhurst, B. F. G. Johnson, J. Lewis, A. G. Orpen, P. R. Raithby and J. R. Thornback, *J. Organomet. Chem.*, 1980, **187**, 141.

153. B. F. G. Johnson, J. Lewis and D. Pippard, *J. Organomet. Chem.*, 1978, **160**, 263.

154. N. A. Mehta and A. J. Deeming, *Unpublished results.*

155. W. A. Nugent and J. Mayer, *Metal-Ligand Multiple Bonds*, John Wiley and Sons, Inc., New York, 1988, *and references therein.*

156. D. E. Wigley, *Prog. Inorg. Chem.*, 1994, **42**, 239, *and references therein.*

157. H. G. Alt, H. I. Hayen and R. D. Rodgers, *J. Chem. Soc. Chem. Commun.*, 1987, 1795.

158. J. Sundermeyer, D. Runge and J. S. Field, *Angew. Chem. Int. Ed. Engl.*, 1995, **33**, 678.

159. J. Sundermeyer and D. Runge, *Angew. Chem. Int. Ed. Engl.*, 1995, **33**, 1255.

160. R.-C. Lin, Y. Chi, S.-M. Peng and G. H. Lee, *J. Chem. Soc. Chem. Commun.*, 1992, 1705.

161. Y. Chi, H.-F. Hsu, L.-K. Liu, S.-M. Peng and G.-H. Lee, *Organometallics,* 1992, **11**, 1763.

162. J. Xiao, R. J. Puddephatt, L. Manojlović -Muir, K. W. Muir and A. A. Torabi, *J. Am. Chem. Soc.*, 1994, **116**, 1129.

163. J. Xiao, R. J. Puddephatt, L. Manojlović -Muir and K. W. Muir, *J. Am. Chem. Soc.*, 1995, **117**, 6316.

164. A. A. Bhattacharyya, C. C. Nagel and S. G. Shore, *Organometallics,* 1983, **2**, 1187.

165. H. H. Fox, K. B. Yap, J. Robbins, S. Cai and R. R. Schrock, *Inorg. Chem.*, 1992, **31**, 2287.

166. B. F. G. Johnson, J. Lewis and I. G. Williams, *J. Chem. Soc. (A)*, 1970, 901.

167. R. D. Adams, J. E. Babin and M. Tasi, *Polyhedron*, 1988, **7**, 2263 *and references therein.*

168. M. R. Churchill, F. J. Hollander and J. P. Hutchinson, *Inorg. Chem.*, 1977, **16**, 2655.

169. A. C. Sullivan, G. Wilkinson, M. Motevalli and M. B. Hursthouse, *J. Chem. Soc., Dalton Trans.*, 1988, 53.

170. N. Bryson, M.-T. Youinou and J. A. Osborn, *Organometallics*, 1991, **10**, 3389.

171. W. Clegg, M. R. Elsegood, P. W. Dyer, V. C. Gibson and E. L. Marshall, *Acta. Cryst., Sect. C.*, 1999, **55**, 916.

172. P. W. Dyer, V. C. Gibson, J. A. K. Howard, B. Whittle and C. Wilson, *J. Chem. Soc. Chem. Commun.*, 1992, 1666.

173. P. W. Dyer, V. C. Gibson, J. A. K. Howard, B. Whittle and C. Wilson, *J. Organomet. Chem.*, 1993, **462**, C15.

174. P. W. Dyer, V. C. Gibson and W. Clegg, *J. Chem. Soc., Dalton Trans.*, 1995, 3313.

175. B. G. Ward and F. E. Stafford, *Inorg. Chem.*, 1968, **7**, 569.

176. W. P. Griffith, *J. Chem. Soc. (A)*, 1969, 211.